INVESTIGATION ON SENSORLESS PMSM DRIVE

Ph.D. THESIS

by

AMBARISHA MISHRA

DEPARTMENT OF ELECTRICAL ENGINEERING
INDIAN INSTITUTE OF TECHNOLOGY ROORKEE
ROORKEE – 247 667 (INDIA)
February, 2015

INVESTIGATIONS ON SENSORLESS PMSM DRIVE

A THESIS

Submitted in partial fulfilment of the requirements for the award of the degree of

DOCTOR OF PHILOSOPHY
in
ELECTRICAL ENGINEERING

by

AMBARISHA MISHRA

DEPARTMENT OF ELECTRICAL ENGINEERING
INDIAN INSTITUTE OF TECHNOLOGY ROORKEE
ROORKEE – 247 667 (INDIA)
February, 2015

©INDIAN INSTITUTE OF TECHNOLOGY ROORKEE, ROORKEE−2015
ALL RIGHTS RESERVED

This work is dedicated to my respected
Lord Shiva,
Satya Prakash Srivastava,
Pramod Agarwal,
and
my Parents

ABSTRACT

Direct current, induction machine and synchronous machines are three basic electrical machines which serve daily requirements, small household equipments to large industrial applications, year after year. Electric motors are the largest consumer of electric energy including domestic and commercial applications which is 46% of global energy consumption according to the IEA statistic. The application demand of electric motors is increasing rapidly with the technological advancement. Due to the rising demands of electric drive, researchers are continuing their efforts to develop new kinds of machines as the Brushless dc (BLDC) Machine, Switched Reluctance Machine (SRM), Permanent Magnet Hysteresis Machine and Permanent Magnet Synchronous Machine (PMSM). After developing these new types of special machines, researchers are working on the control of these motors to optimize the design performance and cost. These developmental activities are now in a revolutionary stage due to the recent development in semiconductor and microprocessor technologies.

The separately excited dc motors are been used, for many decades, extensively for variable speed drives and high performance drives, as the separately excited dc motor can be controlled in a simple way which is attributed to the decoupled nature of its field and armature. However, the dc motor has some disadvantages, which include limited range of speed of operation, lack of overload capability, robustness, and frequent maintenance as well as high cost due to brush-gear, and commutators. These drawbacks of dc motors have motivated researchers to develop high-performance variable speed drive for ac motors like induction and synchronous motors, where robustness and maintenance free operations are the main concern.

Among the ac motors, induction motor has been widely used in the industries due to some of their beneficial features like low cost, good efficiency, reliability and ruggedness. However, it has some limitations like; it always runs at a lagging power factor. Another limitation is that due to slip-power loss the IM drive system is not highly efficient.

The above mentioned limitations diverted attention of researchers towards the synchronous motors for high performance variable speed drives. The advantages of synchronous motors are as; it always runs at synchronous speed, its control is less complex as compared to IM. It also removes the slip power loss. The wire wound excited synchronous motors have some drawbacks such as the prerequisite of the extra supply, slip ring and brush gears for the field excitation. Keeping in view limitations of the conventional wire-wound synchronous motors, more recently different kinds of special motors have been developed. Among them, the permanent magnet (PM) motor is becoming popular due to some of its advantageous features, which include high torque to current ratio, high power to weight ratio, higher efficiency, and robustness. The elimination of excitation winding reduces the cost and power loss. The advantages of PMSM over dc motor are compact size, less

maintenance and over induction motor are high efficiency, small size and wide range of power factor.

The popularity of PMSM comes from its enviable features such as; high efficiency, high torque-inertia ratio, high torque-volume ratio, high flux density, high power factor, lower maintenance requirements, ruggedness, compact size.

An extensive review is carried out which starts with the basic motor modelling and covers open loop control, speed control and current control in vector controlled drive, performance analysis, possible inverters & control techniques used including dynamic performance improvement, torque ripple minimization and different sensorless control of the PMSM drive. In high performance drive current controller plays a vital role as it directly affects the quality of current fed to motor and indirectly affects the performance of motor in terms of efficiency, dynamic response etc.

In vector controlled PMSM drive the proportional integral (PI) controller is widely used due to its simple execution. However, tuning of gains of PI controller is a challenging task, when there is a change in system parameter or change in load torque or speed command values. The design of PI controller is usually based on the mathematical model of plant. However, even if the plant model is known, building an accurate mathematical model is very difficult task due to the problem of parameter variation. Control of PM motor with fast dynamic response, good speed regulation and high efficiency necessitates information of the rotor position to implement the vector control.

Rapid development of microprocessors and controllers (μC) and DSP has facilitated the vector control to become a common technique for PMSM drives. Vector control has been widely used and is a successful technique for PMSM because of its excellent torque response with minimum stator current uses. Implementation of vector control algorithm needs to use stationary to synchronous rotational reference frame transformation to regulate the corresponding current component. The reference frame transformation requires rotor position information.

In present work performance of PMSM is investigated and evaluated for different speed-torque control algorithms and sensorless techniques. Mathematical modeling of PMSM with saliency and without saliency in different reference frames is presented.

The design of an accurate control system requires the mathematical model of actual system being controlled. The d-q model for PMSM is developed in MTALAB. This model consists of only dynamic equations of PMSM representing the actual PMSM in terms of parameters and load performance. A close loop operation is performed with modelled PMSM, PI controller as speed controller and sinusoidal pulse width modulated (SPWM) inverter. With this PMSM drive shows the regain capability of speed with change in load. The

controller parameters are tuned to get the fast dynamic response in speed. The simulation results show the effectiveness of controller and high dynamic performance of the drive.

In comparison to other speed controllers a fuzzy logic controller is a non-linear adaptive controller. The fuzzy logic controller uses a time varying gains for speed control according to system responses raised by different control rules. Moreover, the FLC is based on the experience and intuition of a human operator. Fuzzy logic can be considered as mathematical theory with multi-valued judgment, probability speculation, and artificial intelligence to simulate the human approach to solve the problem by using an approximate reasoning to share different data sets for decision making.

A fuzzy logic controller (FLC) with input and output scaling factor is proposed as speed controller in PMSM drive. Fuzzy speed controller (FSC) is proposed to overcome the demerits of conventional PI speed controller which produces current reference for current controllers. These scaling factors are tuned to achieve the desired performance of drive. The value of these scaling factors depends on motor parameter, load torque, reference speed, and fuzzy speed controller FSC parameter. As for as the FSC parameters are concerned, these constitute range of membership functions, type of membership functions, implication methods, rules and number of rules. The usefulness of proposed method is verified by computer simulation and experimental results. The performance of proposed controller is investigated for different operating conditions.

In order to conquer the coupling effect and the sluggish response with scalar control and to achieve the high performance the vector control is implemented. Two-axis mathematical modeling is presented for PMSM. The basic idea of the vector control is to decompose the three-phase stator current into a magnetic flux-generating component and a torque-generating component. After decomposition both currents components are separately controlled like dc machine. The vector controlled PMSM drive has two loops; outer speed control loop, and inner current control loop. The Inner loop is having two- current controllers (d-q), which play an essential role as they directly affects the quality of current fed to the motor and indirectly affects the performance of drive in terms of efficiency and dynamic response.

In order to overcome the problems associated with PI controllers, fuzzy based current controllers are employed for motor control which eliminates the controller parameter dependency on the system's mathematical model and load disturbances. Use of fuzzy logic algorithm, to reduce the torque ripples, has been proposed, it refines the voltage vectors. Use of space vector modulation (SVM) significantly reduces the torque and flux ripples. A fuzzy current controller (FCC) is proposed, which generates the reference signals for the inverter, to improve the quality of voltage and current fed to the motor, resulting in high performance of drive.

The designed vector controlled PMSM drive has three fuzzy logic controllers (FLC); one FSC and other two FCCs. This complete fuzzy logic based vector controller is termed here as Fuzzy Vector Controller (FVC).

The limitations reported in literature are addressed through a FVC is proposed for PMSM drive and its performance is investigated. Further, the effects of load variation and reference commands on the performance of drive are extensively studied. The enhanced performance is achieved through designing and tuning of FLC for each controller separately. Tuning is done by observing the values at input and output of individual controller using PI controller by keeping the interval of membership function ([-15 15] for FSC, and [-2 2] for FCC) in mind. This methodology resolves the problem of nonlinearity and parameter deviations of PMSM drive. Moreover, it achieves high dynamic performance and good speed regulation and torque control with superior steady-state characteristics. Simulation is done in MATLAB/Simulink to prove the efficacy of proposed FVC as compared with PI controllers based vector control, and performance of drive under various operating condition is demonstrated. Further, experimental results obtained from laboratory prototype validate the efficacy & robustness of the proposed controller.

Generally the rotor position information is obtained from a optical encoder, revolver or Hall Effect sensors for the implementation of vector control. Though, it is enviable to abolish these position sensors from PMSM to reduce overall cost of drive and hardware complexity, inertia, maintenance requirements and to increase the robustness and reliability, and to have noise immunity. Back-emf based methods offer adequate performance in the higher speed range, but at low or zero speed the magnitude of back-emf becomes negligible and difficult to measure. This makes speed estimation at low speed very difficult and this method is highly sensitive to motor parameters. A high frequency signal injection is used to extract the rotor position is reliable at zero speed but there is adverse effects of injected signal on motor dynamics and necessity of extra hardware.

Principles for sensorless control of electrical machines are generally based on the either advance observers or special characteristic of motor, e.g. the saliency. However, it is difficult to find general methods that are possible or suitable to apply to various drives. The estimation is possible by constructing a state observer based on motor electrical and mechanical equations. Then stability of the observer is key point position estimation. Adaptive control seems to be the most promising one of various modern control strategies. The MRAC approach is capable of compensating the variations of the system parameters, such as inertia and torque constant with reduced computation. The estimators based on the Model Reference Adaptive System (MRAS) provide the desired state from two different models, one is used as reference model and another one is as adjustable model. The error between reference model and adjustable model is used for estimation of the unknown

parameter (speed in this case). In MRAS only adjustable model is dependent on speed parameter, while, reference model is not dependent on speed. The error signal is fed into adaptation mechanism, which provides the estimated quantity and is used to tune the adjustable model. This method is simple and requires less computation.

Among the existing sensorless schemes, the sliding mode has been recognized as a prospective estimation methodology for the drives. Sliding mode observer (SMO) has remarkable advantages of robustness against external disturbances and less sensitivity to motor parameter deviations. This method is an algorithm that uses the sign of the error on the machine current to update the value of the estimated speed and position stored in the controller. The major advantage of SMO is no requirement of extra electronics. Furthermore, the variation of motor parameters has little impact on the results accuracy.

Increase in the mechanical robustness of drive and to reduce the cost of drive, eradication of the position sensor is encouraged. Sensors are not reliable in explosive environment viz. chemical industries and may cause the EMI problem. A speed estimator for PMSM drive has been proposed. In the algorithm the PMSM used as reference model. The adaptation mechanism uses a Fuzzy controller to process the error between reference model and adjustable model. The estimation method used is independent of stator winding resistance, computationally less complex, free from integrator problem because back-emf estimation is not used and provides stable operation of drive system. Thus, the performance at zero and low speed is also good. The proposed estimation algorithm is implemented in MATLAB. Simulations results show the validity of proposed fuzzy logic based MRAS and verified through experimental results.

Further, sliding mode observer based position estimation for PMSM without saliency is presented. An equivalent control in the feedback is applied to extend the operating range and improve the estimation performance. In comparison to conventional SMO, the proposed algorithm gives the flexibility in selecting observer parameters for a wide speed range operation. The observer convergence in the high speed range is guaranteed, and the estimation error is reduced with proper selection of feedback gain. The chattering problem existing due to large switching gain at low-speed is reduced. The proposed SMO with equivalent control verified through simulation and laboratory results.

In the experimentation dSPACE version DS1104 is used for prototyping. Three phase inverter, used here, is an intelligent power module (PEC16DSM01) make Vi Microsystems. This rapid control prototyping (RCP) consists of software and hardware. The hardware is consisting of DS1104 R&D controller board with digital and analogue, input-output facility. All signals in CPL1104 can be monitored by status LEDs. The software consists of real time interface (RTI) blocks which connect the simulink controller to the real-time hardware.

Moreover, Control Desk is used to conduct experiment, adjust the controller parameters, and to visualize the desired signals involved in the experimentation.

The motor used here is with inbuilt resolver, which provides the sine and cosine of rotor position at its two output windings. These sine and cosine signals are given to dSPACE through ADC channels. Then these signals are used to calculate rotor position in degrees. A square wave signal of 3 kHz, with -5V to +5V amplitude generated from dSPACE, and given to primary winding of resolver through DAC channel, these sine and cosine signals are generated at resolver two secondary windings. The voltage sensor using isolation amplifier AD202JN is used to sense motor terminal voltages. The input voltage to dSPACE is reduced in the range of ±10 V. The voltage sensors are calibrated to convert ±100 V to ±1 V. The current sensors are inbuilt with power module. These sensed voltages and currents are fed to software controller in dSPACE through ADC channel for further processing and calculations. The controller part of the drive system is implemented in MATLAB using RTI block sets, and appropriate signals are generated in real time.

Author's Contribution

- Mathematical model of PMSM is developed.
- Close loop control of PMSM drive is investigated.
- Vector control of PMSM is investigated with PI controllers.
- A fuzzy logic based speed controller is proposed for PMSM drive.
- Fuzzy Vector Controller is proposed for PMSM drive.
- Fuzzy logic based MRAS is proposed for speed estimation in sensorless PMSM drive.
- The estimation performance is improved by using feedback gain.
- A prototype drive is developed with three phase 8 pole 1 kW PMSM.
- dSPACE is used to implement the control action, variable calculations using measured variables, generation of firing pulses for inverter, and feedback using computer.
- Proposed controllers and estimations algorithms are carried out with simulation and experimental studies. Performance issues and scope of implementation is examined in detail.
- Proposed controllers and algorithms are implemented on prototype drive to evaluate the effectiveness of controllers and performance of drive in different operating conditions. `

ACKNOWLEDGEMENTS

Apart from personal efforts and loyalty to work, constant motivation and encouragement given by a number of individuals acted as the driving force in attaining this day in my life. To quote all of them may be a tedious task but direct and indirect assistance and guidance received is gratefully acknowledged. I would like to express my feelings of gratefulness and submit my acknowledgement for them further in the following lines.

I take this opportunity to express my sincere gratitude towards my noble and kind hearted supervisors Dr. Pramod Agarwal and Dr. S.P. Srivastava, Professors, Electrical Engineering Department, Indian Institute of Technology Roorkee, for their expert and keen guidance, valuable suggestions, discussions, continuous encouragement and constant inspiration throughout the course of this study and critically examining the thesis write-up. If I will get a chance I would like to come in this institute again to work with only these two personalities in the area of electrical machines, power electronics and microprocessor control of electric drives.

I also express my sincere gratitude towards my research committee members, namely Prof. G.K. Singh (EED), Prof. R.C. Mittal (Head of the Mathematics Department), Chairman, Department Research Committee (DRC), and my supervisors for their valuable suggestions and cooperation.

My thanks are due to the Head of the Electrical Engineering Department of this institute and all faculty members of the department for their help, moral support, and providing the sufficient infrastructure, laboratory and other technical facilities for research work carried out. I am thankful to Mr. Mohan Singh and other staff of the department.

I am thankful to the staff of the Electrical Engineering Department, Mr Gautam Singh and Mr Rakesh for their timely cooperation and needful help in the fabrication and assembly of the experimental prototypes.

I would like to give a special thanks to Mr. Mohd. Ameer Ahmad for his dedication and workaholic nature and technical support to research scholars of this department.

I acknowledge my sincere gratitude to the Ministry of Human Resources and Development (MHRD), Government of India for its financial support to carry out this research. I would also like to thank Department of Science and Technology, Govt of India for providing the financial support for international travel to attend international conferences in the area of my research.

I thankfully appreciate and acknowledge my indebtedness to my friends and research scholars for their instant help, cooperation, advice, suggestion, and moral support during my stay. The list may go long but some of them I would like to mention are Dr. Madhukar Waware, Dr. Subhash Dubey, Dr Giribabu, Dr Jayaram, Dr. Srinivas, Dr Rakesh Maurya, Mr. Aurobinda Panda Mr. Sukanta Halder, Mr. Atul Kumar, Mr. Ashish Dhara for their technical

and non technical help provided to complete this thesis. I extend my sincere thanks to Dr. Subhash Joshi and Dr. Vasundhara Mahajan for the editing and of corrections of research papers and thesis.

There are some special persons who helped me at personal and emotional level in good and bad times, Dr. Akshay Dvivedi, Dr. Jignesh Makwana, Mr, Nagendra H, Mrs and Mr Shiwanand Suryavanshi, Mrs A. Upadhyay, Mrs and Mr. Dinesh Chandra Mahajan.

Finally, I wish to express my deepest gratitude to my parents, Shri Ram Pravesh Mishra and Smt. Mira Mishra, brother, Piyush Mishra for their endless support, encouragement and patience.

At last want to say thanks to all my respected teachers, beloved friends and some of my respected mentors in this campus for made me to reach this level.

May all praise be to the Almighty, the most beneficent, and the most merciful.

(Ambarisha Mishra)

CONTENTS

LIST OF FIGURES

LIST OF TABLES

LIST OF ACRONYMS

ac, AC	Alternating Current
ANN	Artificial Neural Network
ASD	Adjustable Speed Drive
BLDC	Brushless DC Machine
dc, DC	Direct Current
DSO	Digital Storage Oscilloscope
DSP	Digital Signal Processor
EMF	Electromotive Force
EMI	Electro Magnetic Interference
EKF	Extended Kalman Filter
FCC	Fuzzy Current Controller
FLC	Fuzzy Logic Controller
FSC	Fuzzy Speed Controller
HF	High Frequency
IM	Induction Motor
IPM	Intelligent Power Module
IEA	International Energy Agency
IEEE	Institute of Electrical & Electronics Engineers
IGBT	Insulated Gate Bipolar Transistor
INFORM	Indirect Flux Measurement by Online Reactance Measurement
MF	Membership Function
MRAS	Model Reference Adaptive System
MOSFET	Metal Oxide Semiconductor Field-effect Transistor
PI	Proportional and Integral
PM	Permanent Magnet
PMSM	Permanent Magnet Synchronous Motor
PWM	Pulse width Modulation
RTI	Real-Time Interface
SMC	Sliding Mode Control
SMO	Sliding Mode Observer
SVM	Space Vector Modulation
VLSI	Very Large Scale Integrated
VSC	Variable Structure Control

LIST OF SYMBOLS

v_a, v_b, v_c	Three-phase inverter output voltages
i_a, i_b and i_c	Three-phase inverter output currents
L_d	Direct-axis Inductance
L_q	Quadrature-axis Inductance
J	Moment of Inertia
V_{sin}, V_{cos}	Secondary windings voltages of Resolver
ω_{ref}	Frequency of excitation signal to inverter
k	Turn ratio of Resolver
ω_r, ω_e	Rotor Electrical Speed
Ω_m, ω_m	Rotor Mechanical Speed
θ_r	Rotor Electrical Angle
θ_m	Rotor Mechanical Angle
B	Viscous Friction Coefficient
P	Number of Pole Pair
λ	Flux-Linkage
r, R	Stator Resistance
	Commutation inductance
p, q	Instantaneous real and reactive powers
	Subscripts and Superscripts
'd', 'q'	Quantities Referred to d-q Reference Frame
'α', 'β'	Quantities Referred to α-β Reference Frame
's'	Parameter Associated with Stator Side
'r'	Parameters Associated with Rotor Side
'm'	Permanent Magnets
'^'	Estimated Value
'*'	Reference Value

CHAPTER 1: INTRODUCTION

[The chapter begins with the motivation to carryout research in the field of permanent magnet synchronous motor drive. The permanent magnet synchronous motor is discussed in detail with its advantages. Then close loop vector control of drive, and requirement and the problems associated with use of position sensor are explained. The permanent magnet synchronous motor provides excellent compactness, high energy efficiency. In the recent years price of rare-earth magnet decreased considerably. With these reasons PM motors are available upto 300 kW for the drive applications. An extensive literature on sensorless permanent magnet synchronous motor drive is carried out. The possible solutions to the problems are discussed. At the end, scope of work, author's contribution and thesis outlines are highlighted].

1.1 Introduction

English physicist and chemist Michael Faraday created a primitive model of the electric motor a dc motor in 1821. In 1870s the Belgian electrical engineer Zenobe-Theophile Gramme created the first commercially feasible dc motor. The dc motor was widely used in street railways and industries by 1900. A book entitled "The Electric Motor and its Applications" published in 1887, was an indication of the extensive interest in the field of electric motors in those years. Faraday's discovery of electromagnetic induction in 1831 provided the way towards the invention of induction motor. Serbian-American engineer Nikolai Tesla invented the first ac induction motor in 1883. Tesla's motor is generally considered the sample of the present electric motor, and it was the first brushless motor. The synchronous motor, which is also a brushless motor, was invented by Tesla as well. The principles of operation of synchronous and induction motors were well known by 1900, but these motors were not widely used by those days as the ac power was not yet commercially accessible. The flexibility of ac power led to commercial success even though dc power was still economical by that time. The production, distribution and utilization of ac power were easier in comparison to dc power. The force competition between ac and dc power was finally resolved in favour of the ac power by 1890. AC motors have no commutators, and the speed is only limited by the physical constraints. These two major benefits of ac motors led to the wide spread utilization in the area of motion control applications in the following years.

The key characteristic of the drive system refers to the capability to operate within the given speed and torque limits. Other desirable features of variable speed drives include low space requirement, low maintenance, and capability of the speed or torque to follow the speed or torque command. Permanent magnet synchronous motors (PMSM) are being used gradually more due to its advantageous features over other motor, which include compactness, high efficiency, and well developed drives [1-3].

Direct current, induction machine and synchronous machines are basic electrical machines which serve daily requirements, small household equipments to large industrial applications, year after year. Due to growing demands of electric motors, the develop of new machines such as the brushless dc machine, the switched reluctance machine, the permanent magnet hysteresis machine and the permanent magnet synchronous machine [4, 5].

After developing these new types of special machines, researchers are working on the control of these motors to optimize in design performance and cost. These developmental activities are now in a revolutionary stage due to the recent development of semiconductor and microprocessor technologies. The dc motors have been used for variable speed drives, due to the decoupled field and armature.

However, the dc motor has some disadvantages, which include limited range of speed operation, lack of overload capability, robustness, the frequent maintenance requirement as well as high cost due to brush-gear, and commutators and power loss in the field circuit. Due to these drawbacks of dc motors, ac motors such as induction and synchronous motors were used for the adjustable speed, where robustness and maintenance free operations are the main concern.

The ac motors are suitable for constant speed operation, but due to recent development of power electronic devices, very large scale integrated (VLSI) technologies and efficient use of microprocessors, ac motors can also be used for variable speed drives. The ac motors used for high performance drive with vector control techniques [8]. Among the ac motors, induction motors considered as workhorse in the industrial applications due to some of its features such as good efficiency, low cost, reliability and ruggedness, yet it has few limitations like is that it always works at a lagging power factor. Another limitation is that the IM drive is not highly efficient due to slip dependent loss, as the IM always runs at less than synchronous speed. Moreover, the real time implementation of these motor drives needs accurate estimation of motor parameters and modeling with complex control circuitry.

The above restrictions were eliminated with synchronous motors (SM) for the drive applications. There are few advantages of SM over the IM. As the synchronous motor runs at synchronous speed, its control is less complex. It also removes the slip power loss. However, the conventional synchronous motors have few drawbacks like the necessity of extra power supply, slip rings and brush gears. Due to the limitations of the conventional wire-wound synchronous motors, more recently different kinds of special motors have been developed. Among those, the permanent magnet (PM) motor is becoming popular due to some of its features, which comprise high torque and high power density, higher efficiency, and robustness. Unlike in the wire-wound synchronous motor, the excitation is given by the permanent magnets in a PM synchronous motor. Thus, there is no need for any extra power

supply or field windings. Hence, the cost is reduced and the power loss due to the excitation windings is eliminated.

The transition in the field of variable speed dc motor drives and induction motor drives, which have been conquered by PMSM and BLDC for low power applications with the use of advanced power electronics. Low power is range considered for less than 10 kWatts. Some of the applications of power less than 10 kW are in household applications, electric tools and small pumps, fans and washing machines [6-8]. PMSM have the advantages over dc motor as follows−

- Compact structure
- Lower maintenance cost
- Less audible noise
- Longer life
- Better heat transfer
- Rotor losses are minimum due to absence of rotor winding
- Spark less due to absence of brush and commutator

Permanent magnet motor is advantageous over Induction motor as−

- Wide range of power factors both lagging and leading, as the power factor for PMSM is controlled by d-axis current while Induction motor can operate only in lagging power factor
- Higher efficiency
- Better heat transfer
- Higher power density
- Small size
- Starting current is low.

PMSM uses magnets for the production of air gap field instead of electromagnets. The advantages of PMSM over dc motor and induction motors as already discussed above. These advantages pull the interest of researchers and industry for various applications such as rolling mills, textiles industries and marine applications. Recent developments in digital electronics, DSPs and ASICs, are the motivation to the increasing attention towards use of PMSMs for high performance variable speed drive and servo drives. PMSM is becoming more popular in adjustable speed drive (ASD) applications [9] due to the development in high energy permanent magnets such as NdBFe.

1.2 Literature Survey

In PMSM direct control of torque becomes complicated due to inherent coupling effects. Decoupling between torque and flux producing components can be provided by vector control algorithm and it also makes the control easier [10, 11]. Vector control makes

the performance of ac drives similar to that of dc drives, and with the speed and current control, stability problem of ac machine does not arise. Many control techniques were suggested for vector control and parameter estimation [12], for the decoupling and online parameter tuning using EKF [13, 14], and MRAC [15]. For the wide speed range vector control, a universal method, where indirect vector control for low-speed range and direct vector for high-speed range is reported in the [16].

Traditionally PI controllers are employed in vector controlled drives as speed and current controllers which inherently cause the sluggish response due to saturation; especially when the dc bus voltage is not sufficient or when sudden load disturbance or sudden change in reference occurs.

The design characteristic and inherent coupling makes direct control of torque complicated. Decoupling between torque and flux producing components can be provided by vector control algorithm. Vector control PMSM drives decouples torque, flux and it also makes the control simple. Speed controller employed in PMSM drive plays an vital role in achieving high performance [17]. In motion control applications speed controller plays an important role as it affects the efficiency, dynamic response etc of motor [18, 19].

In such high performance drive current controller plays a vital role as it directly affects the quality of current fed to motor and indirectly affects the performance of motor in terms of efficiency, dynamic response etc[18, 20]. A comprehensive literature is reported dictating the merit and demerits of various current controllers such as hysteresis, PWM and predictive current controller [20].

The vector control needs instantaneous regulation of current [21] which reduces the torque ripples [22] and is realized PWM controller in (d-q) reference frame [10]. The aim of vector control is to drive the motor to precisely trace the reference value irrespective of the changes in the load, machine parameter and any external environment [11].

A comprehensive literature is reported by dictating the merit and demerits of various controllers such as hysteresis, PWM and predictive current controller[20]. Solution to the problems of nonlinearity and parameter variation needs different control algorithm to achieve a wide speed range operation of PMSM. Several control methods such as PI Control, FLC, adaptive control and neural network control have been reported for motion control in PMSM drive. The design and implementation of a PI controller is simple and provides wide stability margin, but requires meticulous tuning and unable to cope up with parameter variation. Latter an observer based self tuned PI controller is proposed [23], in which controller parameters are adjusted as per requirement. This method need fast enough processors and is time consuming. Adaptive control methods are able to adjust the controller parameter as per the variation in system parameter, but require a reference model. Neural network based controllers are able to operate with highly nonlinear systems but requirement of huge training

data, lengthy training process and large convergence time reduces the superiority of this method [24].

To obtain the optimized robust performance with parameter variation and load disturbances, the controller parameters need to be continuously adapted. There are many ways to achieve this, MRAC [25, 26], SMC [27]. Robustness is one of the important factors in servo drives. One of the techniques to accomplish the robustness in drive is SMC, however, chattering and high frequency oscillation in torque are the some limitations of SMC [28]. Various modern control techniques like; robust control, adaptive control, non-linear control, and intelligent control have been suggested by various researchers to overcome the problems of the system model uncertainties [25, 26]. Now a day's promising intelligent control techniques are being used to replace conventional complex control techniques to avoid the dependency of controller on system's model which may vary because of unknown load variation, unknown parameter variation due to saturation, temperature variation and system disturbance.

Among the various available computational techniques such as ANN, Fuzzy, Genetic Algorithm (GA), the fuzzy logic is found less complicated and easy to implement as compared to ANN and GA to achieve the same performance. The neural network control is a good choice for control applications. As in ANN controller the selection of size of network structure, number of neurons, number of hidden layers, weight coefficients are the major challenges [29]. Moreover the complexity of the ANN controller increases while achieving the robustness in overall system performance, and its real time implementation becomes difficult on given hardware platform where sampling time and processing speed is limited. Similarly in GA the mutation and selecting the new chromosomes are computationally complex and time consuming.

Conventional PMSM drives employ a shaft `mounted position sensor to provide the position of rotor flux which maintains the synchronism. To implement the vector control algorithm rotor position is required to implement the current control in rotor reference frame. To improve the robustness and to reduce the cost and complexity of drive elimination of the position sensor is required. Sensors are not reliable in explosive environment like in chemical industries and may cause the EMI problem. Further online parameter estimation techniques are to be used to make the drive robust and reliable with high dynamic performance [30].

Several sensorless control algorithms for PMSM have been broadly studied, which is be categorized as−

- Estimation of Flux by voltage equations
- Inductance variation due to saliency effects
- State observers
- Extended Kalman filters

- Model reference adaptive schemes (MRAS)
- Sliding mode observers
- Artificial intelligence-based estimators
- Low frequency signal injection
- High frequency carrier injection (rotating high frequency carrier injection, pulsating high frequency carrier injection)

Both Wu and Xu reported flux estimation with voltage equation, stator flux vector is obtained by two line voltages and two currents. Here the performance is affected by measurements at low speed [10-11]. The PMSM with saliency has a varying inductance, this feature is used estimation at low-speed and standstill. An “INFORM” (indirect flux measurement by direct reactance measurement) method was suggested by Schroedl, which uses a real-time reactance measurement for short period for estimation of flux [31]. A signal injection method investigated by Corley and Lorenz using heterodyne process to estimate the rotor position [32]. The signal injection methods suffers from increased complexity of control system, and limits the PWM frequency, and produce noise

The Kalman Filter is a mathematical model running parallel to the real system and gives estimations of the physical values of a linear system. The EKF has been derived from the classic Kalman Filter for non-linear system [13, 33-35]. Once the EKF method converges, the estimation error on the position and the estimation error on the speed are found to be very low, and insensitive to parameter variations.

However, the EKF method presents many drawbacks –

- The EKF estimation is very sensitive to the flux linkage .
- The EKF diverges at start-up and the direction of rotation can be incorrect.
- The gains of the EKF filters are difficult to tune.
- The EKF implies lots of matrix calculation, and thus computing time.
- Zero speed and low speed operation is extremely difficult.

The EKF is capable of optimum filtering along with estimation of desired quantity. It is stochastic observer which uses least square method for accurate estimation. The complexity of the EKF method, and its limitation towards low speeds, make this algorithm not suitable for low cost and high reliability applications.

Adaptive control appears as a promising technique, Cerruto and others reported a control methodology MRAS featuring reduced calculations, and is able to compensate system parameters. The adaptive control increases the robustness of system.

The SMO is able to improve the robustness and less sensitivity to parameter, and used for non linear systems. Sign of error is used for the estimation purpose. The advantage of SMO is that it does not require additional hardware.

The model of PMSM is in general identified with neglecting nonlinear issues like saturation. This approximation is acceptable in most industry applications [17, 36, 37]. At this point AI based estimators offer a substitute to the sensorless operation of PMSM. In order to implement intelligent estimators efficient for real-time execution, there are still many aspects to be considered. A multilayer feed-forward ANN (FANN) solves the static problems, naturally, general static training algorithm; back propagation (BP) harshly limits use for real-time adaptation [21]. Moreover, artificially intelligent estimators are moderately complex and necessitate large computation time, which has to be implemented in a very fast processor or DSP, which is not suitable for cost-effective applications.

The schemes based on high frequency carrier injection for sensorless control have been the schemes with the highest activity during the 90-ties. These schemes use saliency in the machine as the basis for the flux or position estimate. The saliency may be present due to saturation, slot variations, slot harmonics or inherent saliency due to machine geometry. The goal for this type schemes are to enable high performance control at all speeds including zero speed. Rotating high frequency carrier injection scheme is based on injection a balanced high frequency carrier superimposed on the fundamental excitation. The response to this carrier signal will contain saliency position information if the machine has a saliency. In early stage both current and voltage injection was evaluated. The scheme based on voltage injection vas preferred as the current based injection needed very high bandwidths for the current regulators (larger than the carrier frequency).

In 1996 Corley and Lorenz [32] used pulsating high frequency carrier (voltage) injection in the estimated q-axis on an IPMSM. The response in the d-axis current was demodulated by multiplication of sinus to the injected angle. The demodulated signal was proportional to the position error.

Transient excitation has been used for parameter estimation and initial position estimation for more than three decades. In [38] used voltage steps in the field winding on a salient pole synchronous machine and determined the rotor position from the response as early as 1975. The method was performed in the commissioning stage in order to determine the initial position of the rotor. The progress in power electronics and microcontrollers allow online realization of these principles [39-41]. Schroedl presented the inductance of a surface mounted PMSM was estimated online and used for position estimation. In the first implementation the INFORM-method (Indirect Flux detection by On-line Reactance Measurement) was implemented with a measurement sequence that included measurements in all three basis axis (a-b-c axis). The measurements where done by applying voltage pulses and measure the current change. The fundamental operation of the drive system had to be halted during the measurement sequence. This was a limiting factor as the measurements sequence used several hundred micro seconds. In order to have

sufficient torque production the intervals between the measurements had to be long. An alternative approach [27 was presented by Ogasawara and Akagi in 1998. The PWM modulator was rearranged and all six active vectors where active for a minimal time during each switching period. This enabled measurements of the derivative of the current at zero speed. A hardware sampling arrangement where presented in [28] that increased the effective resolution of the analogue to digital converter. The scheme was tested with a IPMSM and the performance where described as: 20 rad/s position response and 300 ms settling time. In from Robeischl and Schroedl [42] the measurement sequence was limited to one direction in each measurement sequence. This reduced the measurement time dramatically and the measurement sequence could be performed in all three axis (a,b,c) in intervals with 2 ms between the measurement sequences.

The MRAS based estimators provide the desired state from two different models, one is reference model and another one is used as adjustable model [15, 43-46]. The error between two models is used to estimate the unknown parameter (speed in this case). In MRAS only adjustable model depends on unknown parameter [47], the reference model is independent of speed. The error signal is fed into adaptation mechanism, which provides the estimated quantity which is used to tune the adjustable model. This method is simple and requires less computation. Many other estimation techniques like passivity based techniques, variable structure based techniques etc are reported in literature to estimate the speed and position of PMSM drives. The schemes based on artificial intelligence (fuzzy logic and neural network) are also in recent trends.

Among the various available computational intelligent techniques like ANN, Fuzzy, GA, the fuzzy logic is found less complicated and easy to implement as compared to others. The neural network control is a good choice for control applications. As in ANN controller, the selection of size of network structure, number of neurons, number of hidden layers, weight coefficients are the major challenges [29]. The complexity of the ANN controller increases, while achieving the robustness in overall system performance, and its real time implementation becomes difficult on given hardware platform where sampling time and processing speed is limited. Similarly in GA the mutation and selecting the new chromosomes are computationally complex and time consuming. In order to overcome the above limitations fuzzy based controllers are employed for motor control which eliminates the controller parameter dependency on the system mathematical model and load disturbances. A fuzzy logic controller (FLC) is basically a non-linear controller which gives robust performance for linear or non linear system with parameter deviation. Use of fuzzy logic algorithm, to reduce the torque ripples, has been proposed, it refines the voltage vectors [48]. Use of space vector modulation (SVM) significantly reduces the torque and flux ripples.

The following concluding remarks can be made after going through the literature review−

- To use the PMSM in high performance drive application using field oriented control, knowledge of rotor position is required.
- With the rapid development of fast DSPs vector control has become a effective technique in PMSM drive system in low cost application.
- The sensor increases cost and complexity of overall drive and reduces robustness.
- The constant torque operation of PM motor can be easily realized by vector control.
- Above base speed air-gap flux can be reduced with field weakening by applying negative d-axis current.
- most widely used method for estimating the rotor position of a PMSM is using back emf for low performance applications.
- The performance of the sensorless PMSM drive using back-emf has dependency on the accuracy of the measured voltages and currents, and the selected integration algorithm.
- An “INFORM” method reported by Schroedl, was based on real-time inductance measurements using saliency effects.
- Once EKF method converges estimation error in speed and position becomes very low and insensitivity to parameter variation. But it needs a lot of computation time, so fast DSP is required.
- The complexity of EKF method and its limitation towards low speed, and not appropriate for low cost applications.
- The MRAS has reduced computation, and has ability of compensation to variations of parameters like inertia.
- The main advantage of SMO is that it does not need extra electronics. Furthermore, the variation of motor parameters has little impact on the results accuracy.
- HF injection suits the position estimation at low-speed range.
- Compared to the back-emf based methods, the inductance variation method works well at low and zero speed.
- Due to modeling uncertainties, the adaptive techniques, which can estimate the motor parameter and state together, could be adapted to reduce parameter sensitivity.

1.3 Scope of the Work and Authors Contribution

An extensive review is carried out which starts with the basic motor modelling and covers open loop control, speed control and current control in vector controlled drive, performance analysis, possible inverters & control techniques used including dynamic

performance improvement, torque ripple minimization and different sensorless control of the PMSM drive.

In present work performance of PMSM is investigated and evaluated for different speed-torque control algorithms and sensorless techniques. Mathematical modeling of PMSM with saliency and without saliency in different reference frames is presented. The design of an accurate control system requires the mathematical model of actual system being controlled. The d-q model for PMSM is developed in MTALAB. This model consists of only dynamic equations of PMSM representing the actual PMSM in terms of parameters and load performance. The close loop operation is performed with modelled PMSM, PI controller as speed controller and sinusoidal pulse width modulated (SPWM) inverter. With this PMSM drive shows the regain capability of speed on changing load applied on machine initially speed decreases then it regains the original speed for new applied load. The controller parameters are tuned to get the fast dynamic response in speed. The simulation results show the effectiveness of controller and good dynamic performance.

The FLC with input and output scaling factor is proposed as speed controller in PMSM drive. Fuzzy speed controller (FSC) is proposed to overcome the demerits of conventional PI speed controller which produces current reference for current controllers. Proper values of these scaling factors are selected to achieve the desired dynamic and steady state performance of drive. The value of these scaling factors depends on motor parameter, load torque, reference speed, and fuzzy speed controller FSC parameter. As for as the FSC parameters are concerned, these constitute range of membership functions, type of membership functions, implication methods, rules and number of rules. The effectiveness of the proposed control method is verified by simulation and experimental results. The performance of proposed controller is investigated for different operating conditions.

The vector controlled PMSM drive has two control loops-inner current control loop, and outer speed control loop. The inner loop is having two- current controllers (d-q), which play an essential role as they directly affects the quality of current fed to the motor and indirectly affects the performance of drive in terms of efficiency and dynamic response [18, 20].

In order to overcome the problems associated with PI controllers, fuzzy based current controllers are employed for motor control which eliminates the controller parameter dependency on the system's mathematical model and load disturbances [49]. Use of fuzzy logic algorithm, to reduce the torque ripples, has been proposed, it refines the voltage vectors. Use of space vector modulation (SVM) significantly reduces the torque and flux ripples. A fuzzy current controller (FCC) is proposed, which generates the reference signals for the inverter, to improve the quality of voltage and current fed to the motor, resulting in high performance of drive. The designed vector controlled PMSM drive has three fuzzy logic controllers (FLC); one FSC, and other two FCCs, which is unique in its application while,

speed is controlled by using fuzzy logic in vector control. This complete fuzzy based vector controller is termed here as Fuzzy Vector Controller (FVC).

Above limitations reported in literature are addressed through a FVC is proposed for PMSM drive and its performance is investigated. Further, the effects of load variation and reference commands on the performance of drive are extensively studied. The enhanced performance is achieved through designing and tuning of FLC for each controller separately. Tuning is done by observing the values at input and output of individual controller using PI controller by keeping the interval of membership function ([-15 15] for FSC, and [-2 2] for FCC) in mind. This control approach solves the issues of nonlinearity and parameter deviations of PMSM drive. Moreover, it achieves high dynamic and steady-state performance and accurate speed regulation and torque control. Simulation is done in MATLAB/Simulink to prove the effectiveness of proposed FVC as compared with PI controllers based vector control, and performance of drive under various operating condition is demonstrated. Further, experimental results obtained from laboratory prototype validate the efficacy & robustness of the proposed controller.

The elimination of position sensor increases the robustness and reduces the overall cost of drive. A speed and position estimator for PMSM drive has been proposed. In the algorithm the PMSM used as reference model. The fuzzy controller used in adaptation mechanism to process the error between reference model and adjustable model. The performance of estimation algorithm used has no dependency on stator resistance, computationally less complex, free from integrator problem because the estimation of back-emf is not required and provides stable operation of drive system. Thus, the performance at low and zero speed is also good. The proposed estimation algorithm is implemented in MATLAB. Simulations results show the validity of proposed fuzzy based MRAS and verified through experimental results.

Further, sliding mode observer based position estimation for PMSM without saliency is presented. An equivalent control in the feedback is applied to extend the operating range of estimator and improve the system performance. As compared to conventional SMO, the proposed algorithm provides the flexibility in selecting observer parameters for a wide speed range operation. The observer convergence in the high speed range is guaranteed, and the estimation error is reduced with proper selection of feedback gain. The chattering phenomenon existing due to large switching gain at low-speed is reduced. The proposed SMO with equivalent control verified through simulation and laboratory results.

In the prototyping dSPACE version DS1104 is used for prototyping. The pulses to the inverter switches are given through digital I/O of dSPACE. The motor used here is with inbuilt resolver, which provides the sine and cosine of rotor position at its two output windings. These sine and cosine signals are given to dSPACE through ADC channels. Then these

signals are used to calculate rotor position in degrees. A square wave signal of 3 kHz, with -5V to +5V amplitude generated from dSPACE, and given to primary winding of resolver through DAC channel, these sine and cosine signals are generated at resolver two secondary windings. The proposed control and estimation algorithms verified from the laboratory results.

At last, the survey is conducted to explore the industrial acceptance of the sensorless vector control technology of PMSM to show its current application area.

1.4 Thesis organisation

Apart from this chapter, this thesis contains six more chapters and the work incorporated in each chapter is briefly outlined here as:

Chapter 2 describes the various reference frame transformations used in vector control. A mathematical model is presented in d-q reference frame and simulated in MATALAB/Simulink.

Chapter 3 presents speed and current control in vector controlled PMSM drive. In order to overcome the problems associated with PI controllers, fuzzy based speed and current controllers are employed for motor control which eliminates the controller parameter dependency on the system's mathematical model and load disturbances. The limitations reported in literature are addressed through a proposed FVC for PMSM drive and its performance is investigated. Further, the effects of load variation and reference commands on the performance of drive are extensively studied, and simulation results are verified through experimental results.

Chapter 4 gives a brief survey of various position sensorless control schemes for PMSM drive. A comprehensive analysis of different sensorless methods is presented, and performance wise comparison is done to select a suitable scheme for desired performance. Further a sliding mode observer with stability analysis and selection of feedback gain of equivalent control is presented. The simulation results of SMO with equivalent control are presented.

Chapter 5 presents MRAS based estimator for sensorless operation of PMSM drive. Speed estimation using MRAS with application of artificial intelligence is proposed. The performance of this method is presented for different operating condition.

The experimental implementation is presented in **Chapter 6**. The prototype development is illustrated in detail, and experimental results are given for the authentication of simulation results for different control schemes.

The conclusion from the work done in this thesis and the possible suggestions for future research work in this area is presented in **Chapter 7**.

Additionally the list of references is provided at the end.

[In this chapter the mathematical model of PMSM in different reference frames, resolver is presented. The mathematical model of a system is required for accurate design of controller for the system, and deciding the controller parameters. The changes in controller parameters are obtained for the given load variations. A developed model of PMSM in MATLAB is studied and simulation performance is analyzed].

2.1 Introduction

The mathematical model of PMSM in designing controllers and simulation analysis and implementation of digital control is needed. For example the EKF and other artificial intelligence technique based control needs the mathematical model. The reference frame plays an important role in the modeling of any machine, as they are like observer platforms in which each of the platforms gives a specific view of system at hand as well as the changes in the system equations. Before proceeding to design and control observation, system review of mathematical model of PMSM (IPMSM and SMPMSM) is presented. The variable transformation is used for the time-varying inductances, coefficients of differential equations to describe the performance behavior of the motor. There are two different reference frames for the modelling depending on which axis reference frame is locked on. The stationary frame is fixed with stator and the synchronously rotating reference frame is fixed to the rotor. In general the transient studies of drives are done in stationary reference frame; moreover the calculations are simple in stationary reference frame due to zero-speed of the fame. The small signal stability analysis at some operating point is done in rotating reference frame, which yields the steady-state values of currents and voltages under balanced conditions. The PMSM equations in all reference frames are presented in this chapter.

2.2 PMSM Drive System

The PMSM drive mainly consist of four major components, PM motor, inverter, position sensor and a controller connected as shown in Figure 2.1

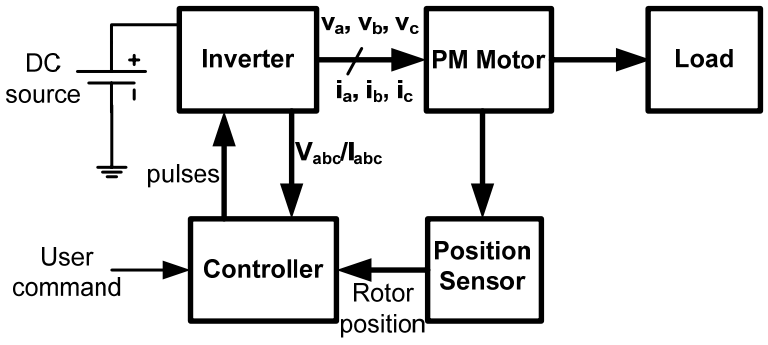

Figure 2.1 Schematic diagram of PMSM drive system

A PMSM is a three-phase synchronous motor, which produces the flux by permanent magnets. These motors have considerable advantages for developing the interest of researchers for use in household appliances and small/ medium power industry applications.

2.2.1 PM Motors

The PM motors can be broadly classified based on direction of flux, radial field motors (direction of flux is along the radius of motor), and axial field motors (direction of flux is perpendicular to radius of motor). In general the radial field motors are used except study and few applications. Depending on the flux density distribution, PM motors are PMSM and BLDC. PMSM has sinusoidal back-emf, whereas BLDC has the trapezoidal back-emf.

In the permanent magnet radial field motors, the magnets can be placed either on the surface of rotor or inside the rotor and so called surface mounted PM motor or interior PM motor. The surface mounted PM motors are easy to build and skewed poles are easily magnetized to reduce the cogging torque [50-52]. These types of motors are suitable only for low speed applications because at high speed magnets can be detached from the rotor as they are glued using adhesives on the rotor surface. These motors show very small saliency, practically equal inductances in both the axis L_d=L_q. The permeability of the magnet is equal to air, so for the magnetic flux reluctances in d-axis and q-axis are equal that is why these two inductances are equal.

In the interior PM motors, the magnets are buried inside the rotor core. The manufacturing cost of these motors is high so these motors are not as common as surface mounted PM motors, and are suitable for high speed operation. The interior PM motors show significant saliency because the magnets placed inside rotor creates the air gap which has more permeability than the rotor core. The reluctance in d-axis is higher than q-axis and so the inductance in d-axis is less as compared to q-axis L_q>L_d.

2.2.2 Position Sensor

The operation and control of PMSM requires the knowledge of rotor shaft position. There are four devices available for the position measurement, potentiometer, linear variable differential transformer, optical encoder and resolver. The most commonly used device for motor drives are optical encoders and resolvers. For the low cost applications like fans compressors etc. encoders are used, and for high performance drive applications like servo-drives resolvers are used where cost of resolver can be justified by the performance of drive.

2.2.2.1 Encoder

The most widely encoder used is optical encoders, which consist of rotating disk, light source and a light sensor. The encoders offer advantages in the digital interfaces. There are two categories of optical encoders, incremental encoders, and absolute encoders. The

incremental encoder has a very good precision and easy for implementation, but is unable to provide information when motor is at rest, which is always at starting point. The precision of absolute encoders are directly related to number of bits in the encoder. It rotates indefinitely and is able to provide the rotor position information even at rest position of the rotor. The absolute encoders can be used in the low speed application and devices which have to retains the information for a long period till power outage which is useful for the applications like telescopes, flood gate control, cranes etc.

2.2.2.2 Resolver

The resolver is a rotary transformer with one rotating winding (V_{ref}) and two stator windings. The reference winding rotates with the shaft passing the output windings [21]. Two stator windings referred as output windings are placed in quadrature to each other and generate the V_{sin}, V_{cos} respectively. As the excitation is applied on the reference winding and with the angular movement of the rotor θ, the respective voltages are generated by resolver output windings V_{sin} , V_{cos}. The frequency of the generated voltages is same as the excitation signal and their amplitudes vary according to the sine and cosine of the rotor angle θ. The resolver algorithm is presented here.

The relevant equations for rotor winding (V_0) and stator windings (V_1 as $V_{\sin}$, and V_2 as $V_{\cos}$) are defined as –

$$V_0(t) = \hat{V}_0 \bullet \sin \omega_{ref} t \tag{2.1}$$

$$V_1(\phi, t) = \hat{V}_0 \bullet k \bullet \sin \phi \bullet \sin \omega_{ref} t \tag{2.2}$$

$$V_2(\phi, t) = \hat{V}_0 \bullet k \bullet \cos \phi \bullet \sin \omega_{ref} t \tag{2.3}$$

Where, k= turn ratio of resolver

$\hat{V}_0$ = the peak value

ϕ = rotor position in rad.

ω_{ref} = frequency (rad. /sec.) of the excitation signal.

The control of an error between actual rotor angle (Φ) and the computed angle (θ) to close zero which provides the calculated angle is equal with the actual rotor angle by using the feedback loop and PI controller as shown in Figure 2.2. The output of PI controller is the motor speed. The rotor position is obtained by integration of the motor speed. The excitation signal given to rotor winding of resolver is +5 to -5 volt square wave signal, and the generated V_1 (sine) and V_2 (cosine) at stator windings are shown in Figure 2.3.

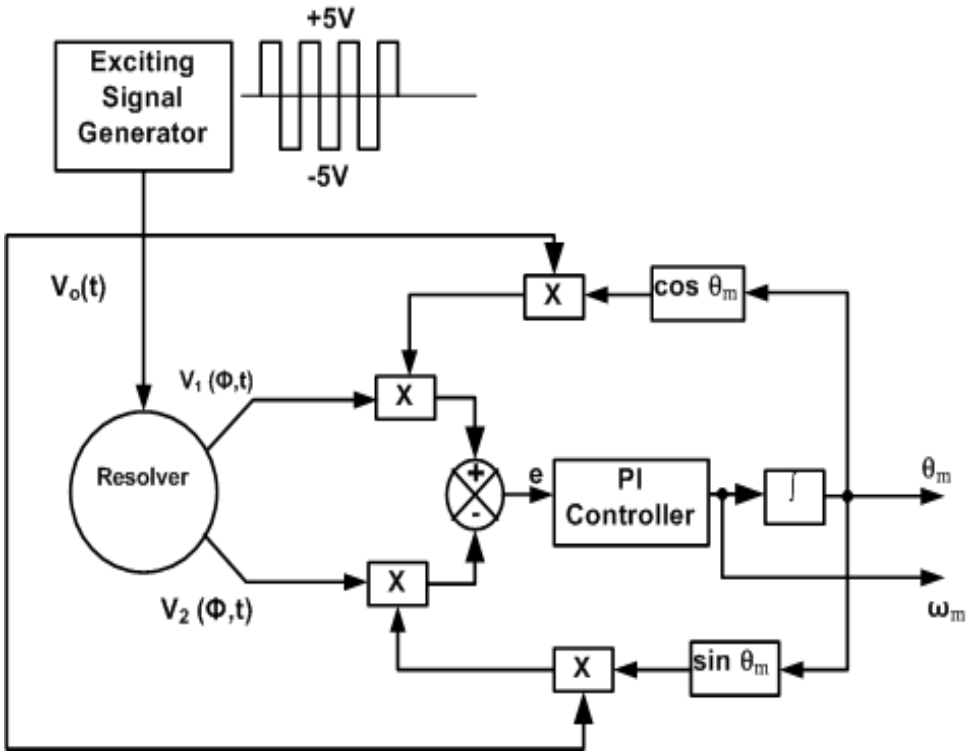

Figure 2.2 Block diagram of resolver algorithm

The error calculation is based on following trigonometric relation-

$$e = \left(V_0 \bullet \sin\omega_{ref} t \bullet \cos\theta\right)\left(V_0 \bullet k \bullet \sin\phi \bullet \sin\omega_{ref} t\right) - \left(\hat{V}_0 \bullet \sin\omega_{ref} t \bullet \sin\theta\right)\left(\hat{V}_0 \bullet k \bullet \cos\phi \bullet \sin\omega_{ref} t\right) \tag{2.4}$$

$$e = V_0(t) \bullet \left(\hat{V}_0 \bullet k \bullet \sin\omega_{ref} t\right)\left[\sin\phi\cos\theta - \cos\phi\sin\theta\right] \tag{2.5}$$

The above expression of (2.5) can be written in form of-

$$e = A \bullet \left[\sin(\phi - \theta)\right] \tag{2.6}$$

Where

$$A = V_0(t) \bullet \left(\hat{V}_0 \bullet k \bullet \sin\omega_{ref} t\right) \tag{2.7}$$

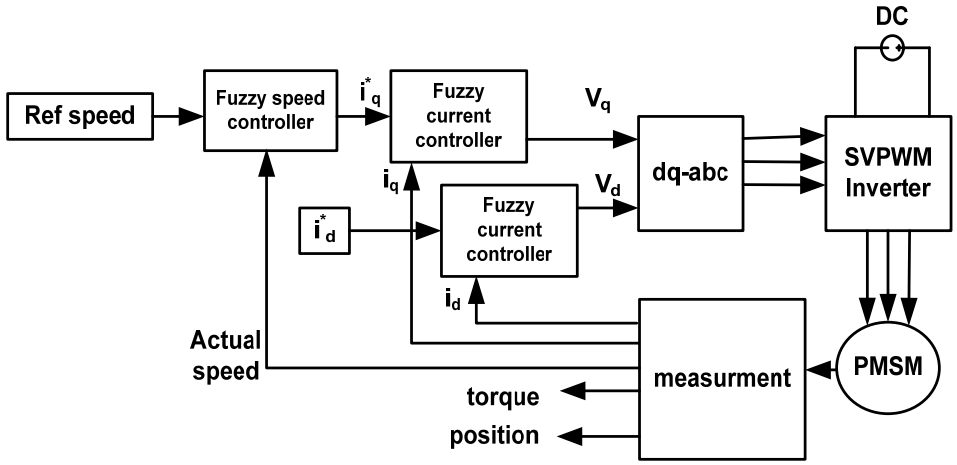

Figure 2.3 Measured rotor winding (excitation) signal and stator winding signals (V1: sine; V2: cosine) of Resolver

2.2.3 Load

The Mechanical load on the motor is generally put through its shaft. The mechanical equation the drive system is as-

$$T_e = T_l + B\omega_m + J\frac{d\omega_m}{dt} \tag{2.8}$$

This mechanical equation is used to obtain the rotor speed as-

$$\omega_m = \int\left(\frac{T_e - T_l - B\omega_m}{J}\right)dt \tag{2.9}$$

Here ω_m is the mechanical rotor speed; the electrical rotor speed ω_r can be obtained from this-

$$\omega_r = \frac{P}{2}\omega_m \tag{2.10}$$

2.3 Mathematical Model of PMSM in Stationary Reference Frame

Mathematical modeling of motor is required for simulation and analysis of drive system. The mathematical model of PMSM is required to design control schemes for PMSM drive. For the instantaneous deviation of current and voltage, and the transient and steady state performance of PMSM drive, the mathematical model is usually obtained by using space-phasor theory [12]. Figure 2.4 shows the different reference frames used in mathematical modeling of electrical ac machines. The stator windings are 120 electrical degrees apart from each other, θ_r is the rotor angle, which is the angle between magnetic axis of stator winding 'a' and rotor magnetic flux (i.e., d-axis). The positive direction is taken in anti-clockwise as shown in Figure 2.4, where angular velocity of rotor $\omega_r = d\theta_r / dt$ shown in positive direction. The permeability of iron parts in machine is assumed to be infinite, and the radial flux density in the air gap.

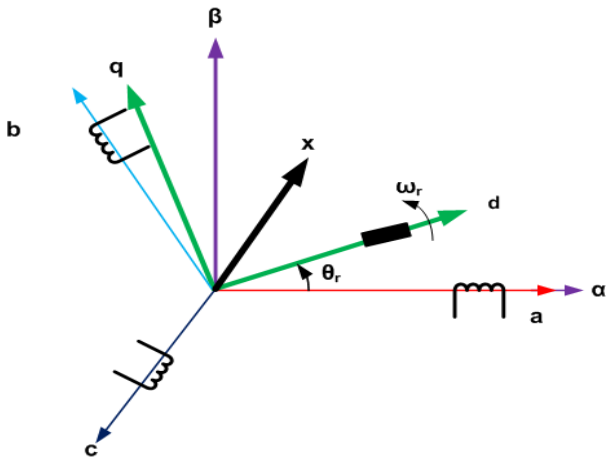

Figure 2.4 Different reference frames

Following assumptions are made for the modeling.

- Stator winding mmf distribution is sinusoidal.
- Space harmonics are neglected in air-gaps.
- The Air-gap reluctance has constant and sinusoidally varying components.
- supply voltage is considered to be balanced three phase.
- Saturation is neglected.
- The back emf is sinusoidal.
- Eddy currents and hysteresis losses are neglected.

2.3.1 PMSM with Saliency

The voltage equations of PMSM can be expressed in terms of instantaneous currents and flux linkages [12].

$$v_{abcs} = r_{abcs} \cdot i_{abcs} + p\lambda_{abcs} \tag{2.11}$$

$$\lambda_{abcs} = L_{abcs} \cdot i_{abcs} + \lambda_{abcm} \tag{2.12}$$

Where

$$v_{abcs} = \begin{bmatrix} v_{as} & v_{bs} & v_{cs} \end{bmatrix}^T \tag{2.13}$$

$$i_{abcs} = \begin{bmatrix} i_{as} & i_{bs} & i_{cs} \end{bmatrix}^T \tag{2.14}$$

$$r_{abcs} = diag\begin{bmatrix} R_s & R_s & R_s \end{bmatrix} \tag{2.15}$$

and

$$L_{abcs} = \begin{bmatrix} L_{aa} & L_{ab} & L_{ac} \\ L_{ba} & L_{bb} & L_{bc} \\ L_{ca} & L_{cb} & L_{cc} \end{bmatrix} \tag{2.16}$$

$$\lambda_{abcm} = \begin{bmatrix} \cos\theta_r \\ \cos(\theta_r - 2\pi/3) \\ \cos(\theta_r + 2\pi/3) \end{bmatrix} \tag{2.17}$$

In above equations subscript 's' represents the parameters and variables associated with stator circuit, and subscript 'r' represents the parameters and variables for rotor circuit and 'p' is a differential operator.

In equation (2.16) the winding inductances can be expressed as–

$$L_{aa} = L_{ls} + L_{0s} + L_{2s}\cos 2\theta_r \tag{2.18}$$

$$L_{bb} = L_{ls} + L_{0s} + L_{2s}\cos 2\left(\theta_r - \frac{2\pi}{3}\right) \tag{2.19}$$

$$L_{cc} = L_{ls} + L_{0s} + L_{2s}\cos 2\left(\theta_r + \frac{2\pi}{3}\right) \tag{2.20}$$

$$L_{ab} = L_{ba} = -\frac{1}{2}L_{0s} + L_{2s}\cos 2\left(\theta_r - \frac{\pi}{3}\right) \tag{2.21}$$

$$L_{ac} = L_{ca} = -\frac{1}{2}L_{0s} + L_{2s}\cos 2\left(\theta_r + \frac{\pi}{3}\right) \tag{2.22}$$

$$L_{bc} = L_{cb} = -\frac{1}{2}L_{0s} + L_{2s}\cos 2(\theta_r + \pi) \tag{2.23}$$

In equations (2.18)-(2.23), L_{ls} is the leakage inductance, L_{0s} and L_{2s} are the components of magnetizing inductance of stator winding, λ_m is rotor magnet flux. It is clear from the above equations that the magnetizing inductances are function of rotor position. In case of I interior PM motors L_{0s} while L_{2s} is negative due to the exclusive structure of its rotor, and quadrature-axis magnetizing inductance L_{mq} is larger than L_{md}.

The expression of flux linkage can be written as–

$$\begin{bmatrix} \lambda_{as} \\ \lambda_{bs} \\ \lambda_{cs} \end{bmatrix} = \begin{bmatrix} L_{aa} & L_{ab} & L_{ac} \\ L_{ba} & L_{bb} & L_{bc} \\ L_{ca} & L_{cb} & L_{cc} \end{bmatrix} \begin{bmatrix} i_{as} \\ i_{bs} \\ i_{cs} \end{bmatrix} + \lambda_m \begin{bmatrix} \cos\theta_r \\ \cos(\theta_r - 2\pi/3) \\ \cos(\theta_r + 2\pi/3) \end{bmatrix} \tag{2.24}$$

A three-phase machine can be represented in an equivalent quadrature-phase machine using two-axis theory, where direct and quadrature-axis currents are flowing in the virtual windings similar to actual three-phase currents flowing in the stator winding.

$$i_{\alpha\beta 0s} = T_{abc\to\alpha\beta 0} \cdot i_{abcs} \tag{2.25}$$

where

$$T_{abc\to\alpha\beta0} = \frac{2}{3}\begin{bmatrix} 1 & -1/2 & -1/2 \\ 0 & \sqrt{3}/2 & -\sqrt{3}/2 \\ 1/2 & 1/2 & 1/2 \end{bmatrix} \tag{2.26}$$

The transformation equation (2.26) called Clark transformation, and this new stationary reference frame representing quadrature-phase machine is known as $(\alpha-\beta)$ reference frame. The older stationary reference frame representing three-phase actual machine is called $(a-b-c)$ reference frame. Using equation (2.26) voltage and flux linkage also can be transformed to $(\alpha-\beta)$ reference frame in a similar way, and voltage equation becomes–

$$v_{\alpha\beta0} = r_{\alpha\beta0}\cdot i_{\alpha\beta0} + p\lambda_{\alpha\beta0} \tag{2.27}$$

where

$$\begin{aligned} v_{\alpha\beta0} &= \begin{bmatrix} v_\alpha & v_\beta & v_0 \end{bmatrix}^T \\ i_{\alpha\beta0} &= \begin{bmatrix} i_\alpha & i_\beta & i_0 \end{bmatrix}^T \\ \lambda_{\alpha\beta0} &= \begin{bmatrix} \lambda_\alpha & \lambda_\beta & \lambda_0 \end{bmatrix}^T \end{aligned} \tag{2.28}$$

and flux linkage equation becomes

$$\lambda_{\alpha\beta0s} = L_{\alpha\beta0s}\cdot i_{\alpha\beta0s} + \lambda_{\alpha\beta0m} \tag{2.29}$$

Where

$$L_{\alpha\beta0} = \begin{bmatrix} L_{ls} + \frac{3}{2}\left(L_{0s} + L_{2s}\cos 2\theta_r\right) & \frac{3}{2}L_{2s}\sin 2\theta_r & 0 \\ \frac{3}{2}L_{2s}\sin 2\theta_r & \frac{3}{2}\left(L_{0s} - L_{2s}\cos 2\theta_r\right) & 0 \\ 0 & 0 & L_{ls} \end{bmatrix} \tag{2.30}$$

$$\lambda_{\alpha\beta m} = \lambda_m \begin{bmatrix} \cos\theta_r \\ \sin\theta_r \end{bmatrix} \tag{2.31}$$

2.3.2 PMSM without Saliency

In case of surface mounted (magnetically symmetric) PMSM, the effective air gap is almost uniform which makes the saliency ratio (L_{mq}/L_{md}) approximately 1.0. So, inductance matrix expressed in (2.16) and (2.30) becomes–

$$L_{abcs} = \begin{bmatrix} L_s & 0 & 0 \\ 0 & L_s & 0 \\ 0 & 0 & L_s \end{bmatrix} \tag{2.32}$$

$$L_{\alpha\beta 0s} = \begin{bmatrix} L_{ls} + L_{ms} & -\frac{1}{2}L_{ms} & -\frac{1}{2}L_{ms} \\ -\frac{1}{2}L_{ms} & L_{ls} + L_{ms} & -\frac{1}{2}L_{ms} \\ -\frac{1}{2}L_{ms} & -\frac{1}{2}L_{ms} & L_{ls} + L_{ms} \end{bmatrix} \tag{2.33}$$

Where $L_s = L_{ls} + \frac{3}{2}L_{ms}$, L_s is stator magnetizing inductance.

It is important to note here that transformed inductance matrix by Park or Clark Transformation (discussed latter) reduces to a diagonal matrix, which, by effect decouples the variables in all reference frame other than (*a*-*b*-*c*) reference frame.

The voltage equations in (α–β) reference frame for star-connected PMSM without saliency-

$$v_{\alpha\beta s} = r_{\alpha\beta s} \cdot i_{\alpha\beta s} + L_{\alpha\beta s} \cdot i_{\alpha\beta s} + e_{\alpha\beta s} \tag{2.34}$$

Where

$$\begin{aligned} r_{\alpha\beta s} &= \begin{bmatrix} R_s & 0 \\ 0 & R_s \end{bmatrix} \\ L_{\alpha\beta s} &= \begin{bmatrix} L_s & 0 \\ 0 & L_s \end{bmatrix} \\ e_{\alpha\beta s} &= \begin{bmatrix} e_{\alpha s} \\ e_{\beta s} \end{bmatrix} = \omega_r \lambda_m \begin{bmatrix} -\sin\theta_r \\ \cos\theta_r \end{bmatrix} \end{aligned} \tag{2.35}$$

In (2.34) the term $e_{\alpha\beta s}$ represents the induced back-emf in the winding of fictitious phase-quadrature machine. This voltage equation can be written in state-space form by taking stator current as independent variable as–

$$\dot{i}_{\alpha\beta s} = -L_{\alpha\beta s}{}^{-1} r_{\alpha\beta s} \cdot i_{\alpha\beta s} + L_{\alpha\beta s}{}^{-1}\left(v_{\alpha\beta s} - e_{\alpha\beta s}\right) \tag{2.36}$$

In matrix form it can be written as–

$$\begin{bmatrix} \dot{i}_{\alpha s} \\ \dot{i}_{\beta s} \end{bmatrix} = \begin{bmatrix} -R_s/L_s & 0 \\ 0 & -R_s/L_s \end{bmatrix} \begin{bmatrix} i_{\alpha s} \\ i_{\beta s} \end{bmatrix} + \begin{bmatrix} 1/L_s & 0 \\ 0 & 1/L_s \end{bmatrix} \left(\begin{bmatrix} v_{\alpha s} \\ v_{\beta s} \end{bmatrix} - \begin{bmatrix} e_{\alpha s} \\ e_{\beta s} \end{bmatrix} \right) \tag{2.37}$$

This equation (2.37) is the dynamic model of PMSM mostly used in designing the different sensorless algorithms.

2.4 Mathematical Modeling of PMSM in Rotating Reference Frame

The control process is implemented here in d-q reference frame, because in d-q reference frame quantities are independent and can be controlled separately, which is the basic purpose of the vector control. R.H. Park established a new approach to implement the transformation of the variables which replace the time-variant variables (with respect to rotor side) referred to stator winding to time-invariant variables associated with fictitious winding with the rotor. The Park's transformation is expressed as–

$$f_{dq0s} = T_{abc\to dq0} \cdot f_{abcs} \tag{2.38}$$

$$T_{abc\to dq0} = T_{abc\to\alpha\beta0} T_{\alpha\beta0\to dq0} = \frac{2}{3}\begin{bmatrix} \cos\theta_r & \cos(\theta_r - 2\pi/3) & \cos(\theta_r - 4\pi/3) \\ -\sin\theta_r & -\sin(\theta_r - 2\pi/3) & -\sin(\theta_r - 4\pi/3) \\ 1/2 & 1/2 & 1/2 \end{bmatrix} \tag{2.39}$$

$$T_{\alpha\beta0\to dq0} = \begin{bmatrix} \cos\theta_r & \sin\theta_r & 0 \\ -\sin\theta_r & \cos\theta_r & 0 \\ 0 & 0 & 1 \end{bmatrix} \tag{2.40}$$

and inverse Park's transformation is expressed as–

$$f_{abc} = T_{dq0\to abc} \cdot f_{dq0} \tag{2.41}$$

Where

$$T_{dq0\to abc} = \left(T_{abc\to dq0}\right)^{-1} = \begin{bmatrix} \cos\theta_r & -\sin\theta_r & 1 \\ \cos(\theta_r - 2\pi/3) & -\sin(\theta_r - 2\pi/3) & 1 \\ \cos(\theta_r - 4\pi/3) & -\sin(\theta_r - 4\pi/3) & 1 \end{bmatrix} \tag{2.42}$$

In above transformation equations '*f*' denote a variable that may voltage, current or flux linkage. For a three-phase balanced system the transformation matrix of equation (2.38) reduces to–

$$Tabc \to dq = \frac{2}{3}\begin{bmatrix} \cos\theta_r & \cos(\theta_r - 2\pi/3) & \cos(\theta_r - 4\pi/3) \\ \sin\theta_r & \sin(\theta_r - 2\pi/3) & \sin(\theta_r - 4\pi/3) \end{bmatrix} \tag{2.43}$$

2.4.1 PMSM with Saliency

In rotor reference frame the voltage equation of (2.27) becomes–

$$v_{dq0s} = r_s \cdot i_{dq0s} + T_{abc\to dq0} \cdot p\left[\left(T_{abc\to dq0}\right)^{-1}\right]\lambda_{dq0s} + p\lambda_{dq0s} \tag{2.44}$$

$$\lambda_{dq0s} = L_{dq0s} \cdot i_{dq0s} + \lambda_{dq0m} \tag{2.45}$$

Where

$$\lambda_{dq0m} = \begin{bmatrix} \lambda_m & 0 & 0 \end{bmatrix}^T$$

$$L_{dq0} = \begin{bmatrix} L_d & 0 & 0 \\ 0 & L_q & 0 \\ 0 & 0 & L_0 \end{bmatrix}$$

$$L_d = L_{ls} + L_{md} = L_{ls} + \frac{3}{2}\left(L_{0s} + L_{2s}\right)$$

$$L_q = L_{ls} + L_{mq} = L_{ls} + \frac{3}{2}\left(L_{0s} - L_{2s}\right)$$

$$L_0 = L_{ls}$$

The L_{md} and L_{mq} can be obtained in terms of L_{0s} and L_{2s} as–

$$\begin{aligned} L_{md} &= \frac{3}{2}\left(L_{0s} + L_{2s}\right) \\ L_{mq} &= \frac{3}{2}\left(L_{0s} - L_{2s}\right) \end{aligned} \tag{2.46}$$

And the L_{0s} and L_{2s} can be obtained from L_{md} and L_{mq} as–

$$\begin{aligned} L_{0s} &= \frac{2}{3}\left[\frac{L_{md} + L_{mq}}{2}\right] = \frac{1}{3}\left(L_{md} + L_{mq}\right) \\ L_{0s} &= \frac{2}{3}\left[\frac{L_{md} - L_{mq}}{2}\right] = \frac{1}{3}\left(L_{md} - L_{mq}\right) \end{aligned} \tag{2.47}$$

In above L_d and L_q are direct-axis inductance and quadrature-axis inductance respectively. The second term of voltage equation of (2.44) can found as–

$$T_{abc\to dq0} \cdot p\left[\left(T_{abc\to dq0}\right)^{-1}\right] = \omega_r \begin{bmatrix} 0 & -1 & 0 \\ 1 & 0 & 0 \\ 0 & 0 & 0 \end{bmatrix} \tag{2.48}$$

Where

$$p\left[\left(T_{abc\to dq0}\right)^{-1}\right] = \omega_r \begin{bmatrix} -\sin\theta_r & -\cos\theta_r & 0 \\ -\sin\left(\theta_r - 2\pi/3\right) & -\sin\left(\theta_r - 2\pi/3\right) & 0 \\ -\sin\left(\theta_r - 4\pi/3\right) & -\sin\left(\theta_r - 42\pi/3\right) & 0 \end{bmatrix}$$

The voltage equation (2.44) is usually written in form of–

$$v_{ds} = R_s \cdot i_{ds} + L_d \frac{di_{ds}}{dt} - \omega_r L_q i_{qs} \tag{2.49}$$

$$v_{qs} = R_s \cdot i_{qs} + L_q \frac{di_{qs}}{dt} + \omega_r \left(L_d i_{ds} + \lambda_m\right) \tag{2.50}$$

$$v_{0s} = R_s i_{0s} + L_{0s} \frac{di_{0s}}{dt} \tag{2.51}$$

Under steady-state condition the speed of synchronously rotating reference frame is considered to be equal to speed of the rotor, in that case rate of change of flux is neglected and voltage equations ((2.49)-(2.51)) turns into form of–

$$V_{ds} = R_s \cdot I_{ds} - \omega_r L_q I_{qs} \tag{2.52}$$

$$V_{qs} = R_s \cdot I_{qs} + \omega_r \left(L_d I_{ds} + \lambda_m \right) \tag{2.53}$$

$$v_{0s} = R_s i_{0s} = 0 \tag{2.54}$$

The capital letters are used for quantities in steady-state.

In rotor reference frame the generated electromagnetic torque in terms of stator quantities is as–

$$T_e = \left(\frac{3}{2}\right)\left(\frac{P}{2}\right)\left(\lambda_{ds} i_{qs} - \lambda_{qs} i_{ds}\right) \tag{2.55}$$

By putting the values of λ_{ds} and λ_{qs} in above equation, it becomes in the form of–

$$T_e = \left(\frac{3}{2}\right)\left(\frac{P}{2}\right)\left[\lambda_m i_{qs} - \left(L_q - L_d\right) i_{qs} i_{ds}\right] \tag{2.56}$$

Where 'P' is the number of poles of machine.

2.4.2 PMSM without Saliency

For the PMSM without saliency $L_d = L_q = L_s$, so the inductance matrix in rotor reference frame becomes–

$$L_{dq0} = \begin{bmatrix} L_s & 0 & 0 \\ 0 & L_s & 0 \\ 0 & 0 & L_0 \end{bmatrix} \tag{2.57}$$

Similar to $(\alpha - \beta)$ reference frame, here in $(d - q)$ reference frame the voltage equations are obtained as–

$$v_{ds} = R_s \cdot i_{ds} + L_s \frac{di_{ds}}{dt} - \omega_r L_s i_{qs} \tag{2.58}$$

$$v_{qs} = R_s \cdot i_{qs} + L_s \frac{di_{qs}}{dt} + \omega_r \left(L_s i_{ds} + \lambda_m \right) \tag{2.59}$$

In the steady-state above equations becomes–

$$V_{ds} = R_s \cdot I_{ds} - \omega_r L_s I_{qs} \tag{2.60}$$

$$V_{qs} = R_s \cdot I_{qs} + \omega_r \left(L_s I_{ds} + \lambda_m \right) \tag{2.61}$$

And the generated electromagnetic torque is given by–

$$T_e = \left(\frac{3}{2}\right)\left(\frac{P}{2}\right)\lambda_m i_{qs} \tag{2.62}$$

It is clear from equations (2.56) and (2.62) that in case of PMSM with saliency both direct and quadrature-axis components of stator current are used, and in case of PMSM without saliency only quadrature-axis component of stator current is used for production of torque. This is the reason that field weakening is possible only case of PMSM with saliency.

2.5 Simulink Model of PMSM

The PMSM mathematical model is developed in MATLAB/Simulink. Figure 2.5 shows the individual blocks (processing wise) and the signal flow from user command (which is the reference speed here) through speed controller, reference frame transformation to inverter, which fed power to the motor. The mechanical load is connected to the motor and from the measurement block provides the voltage current drawn by the motor, and provides the speed and position information when the motor is running. The simulink view of the developed model is shown in Figure 2.6.

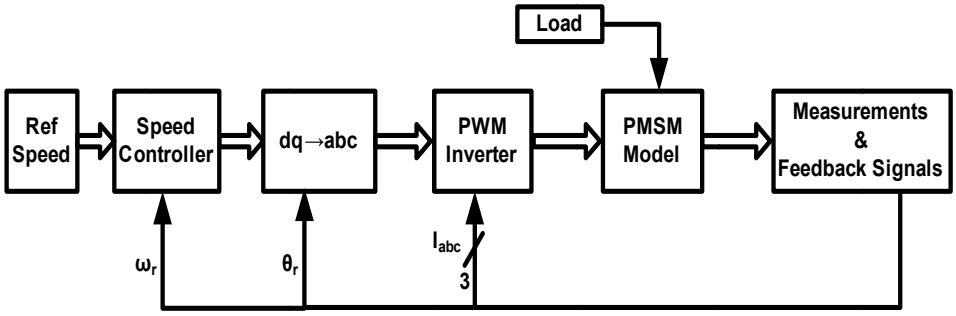

Figure 2.5 Block diagram of PMSM drive and individual blocks and signal flow

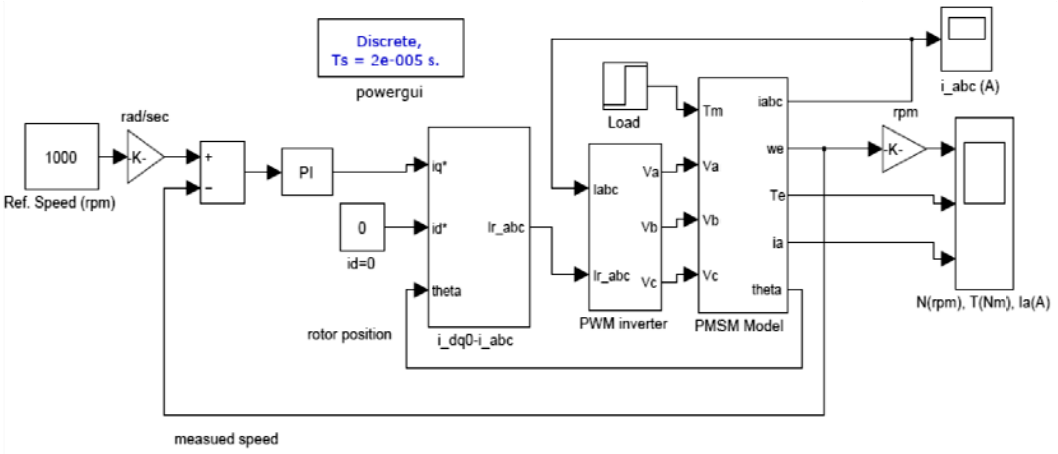

Figure 2.6 Simulink diagram of developed model

As shown in the simulink diagram the reference speed in given in rpm, and then converted to radian/sec. because in the mathematical processing speed in radian/sec. only is considered. Then speed error is obtained using measured speed, and then speed error is passed through a PI controller, which generates the q-axis current reference. For the maximum torque per ampere d-axis current reference is kept zero here, for the field-

weakening operation appropriate value of this d-axis current reference is to be chosen. The transformation block convert these d-q currents to a-b-c reference frame which act as the reference current for a three-phase PWM inverter, which is connected to developed mathematical model and after that there are measurement and feedback signals.

2.5.1 Transformation (dq0→abc)

The dq0 to abc transformation is already presented in this chapter, is rewritten here and as shown in Figure 2.7.

$$i_a = i_d \cos\theta_r - i_q \sin\theta_r \tag{2.63}$$

$$i_b = i_d \cos(\theta - 2\pi/3) - i_q \sin(\theta - 2\pi/3) \tag{2.64}$$

$$i_c = i_d \cos(\theta + 2\pi/3) - i_q \sin(\theta + 2\pi/3) \tag{2.65}$$

2.5.2 PWM Inverter

This generated reference currents and measured phase currents are used to find the errors in respective phase currents. These individual current errors are compared with a triangular signal of 2000 Hz frequency to generate the pulses for upper and lower leg of respective phases as given below.

- I_{ra}-I_a ≤ $I_{Triangular}$ S_1 ON else S_4 ON.
- I_{rb}-I_b ≤ $I_{Triangular}$ S_3 ON else S_6 ON
- I_{rc}-I_c ≤ $I_{Triangular}$ S_5 ON else S_2 ON

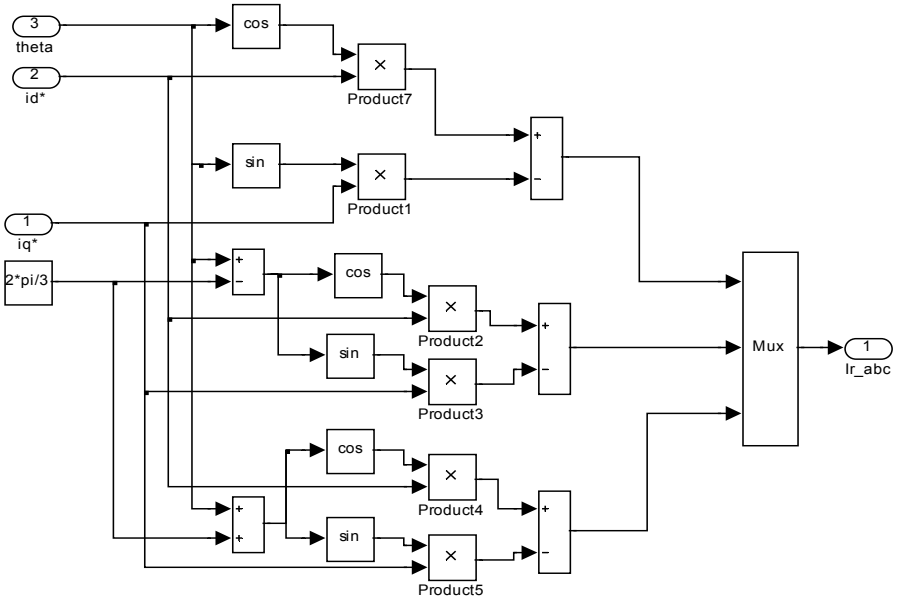

Figure 2.7 dq0 to abc transformation

2.5.3 PMSM Model

As shown in simulink diagram of Figure 2.6, PMSM model receives v_a , V_b and V_c from the inverter, the signal flow is shown in Figure 2.8.

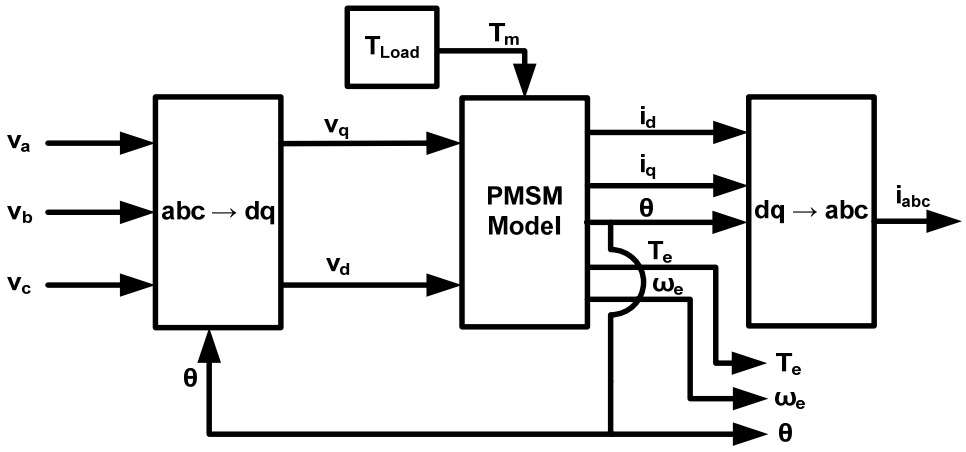

Figure 2.8 PMSM IN and OUT signals

For v_{abc} to v_{dqo} following transformation equation is used−

$$v_d = \frac{2}{3}\left[v_a \cos\theta + v_b \cos\left(\theta - 2\pi/3\right) + v_c \cos\left(\theta + 2\pi/3\right)\right] \qquad (2.66)$$

$$v_q = \frac{2}{3}\left[-v_a \sin\theta - v_b \sin\left(\theta - 2\pi/3\right) - v_c \sin\left(\theta + 2\pi/3\right)\right] \qquad (2.67)$$

Now coming to PMSM circuit, this consists of three inter-connected blocks, d-axis, q-axis and one for torque and speed having IN, OUT and Feedback signals as shown in Figure 2.9.

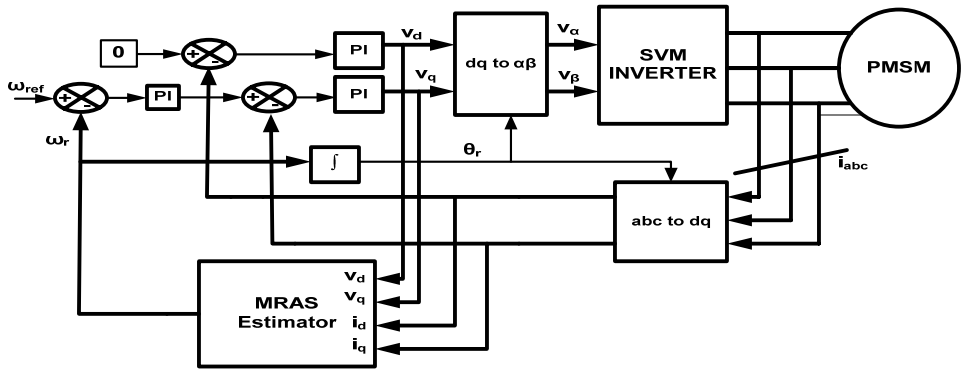

Figure 2.9 PMSM circuit with input, output and feedback signals

In q-axis circuit v_q is the input signal, i_d and ω_e are the feedback signals, and i_q is the output signals as per (2.68) if motor parameters are known.

$$i_q = \int \frac{1}{Lq}\left[v_q - i_d L_d \omega_e - \omega_e \lambda_m - i_q R_q\right] \qquad (2.68)$$

In the same way for d-axis circuit, v_d is the input signal, i_q and ω_e are the feedback signals, and i_d is the output signal as per (2.69).

$$i_d = \int \frac{1}{L_d}\left[v_d + i_q L_q \omega_e - i_d R_d \right] \tag{2.69}$$

For the torque production circuit mechanical load torque T_m is the input, i_d and i_q are already calculated, electromagnetic torque and speed (electrical) is calculated from−

$$T_e = P \cdot \frac{3}{4}\left[i_q \lambda_m + i_d i_q \left(L_d - L_q \right) \right] \tag{2.70}$$

$$\omega_e = \frac{T_e - T_m}{Js + B} \cdot \left(\frac{P}{2} \right) \tag{2.71}$$

And the rotor position is obtained electrical degree as−

$$\theta = \int \omega_e \tag{2.72}$$

2.6 Simulation Results and Analysis

The mathematical model is developed in MATLAB/SIMULINK and the simulation is performed for the different conditions. the PI controller is used and the performance is observed for the different values k_p and k_i. The parameters are given in Table 2-1.

Table 2-1 Parameters of PMSM

Parameters	Value
V_{dc}	1000 V
L_d	0.0066 H
L_q	0.0058 H
R_d=R_q	1.4 Ohm
λ	0.1546 Wb
P	6
J	0.00178 Kg.m^2
B	0.00038818 Nms

This mathematical model shows a very good regain capability of speed when the load torque is change from one value to other. The time taken to regain directly depends on controller parameter values k_p and k_i. As the k_i increases the regain time of speed reduces which is clear from simulation results. All the results have speed in rpm, torque in Nm and current Ia in ampere on Y-axis and time in seconds on X-axis. Figure 2.10 shows the speed, torque and phase 'a' current at reference speed 1000 rpm and load transition from 0-10 Nm for k_p=0.1 and k_i=2.0. At zero load torque the torque and current both are having more

ripples. At the load change the dip in speed at load changes goes below zero and time taken approximately 0.8 secs. Figure 2.11 shows the response for k_p=.0.5 and k_i=2.0, the time taken in 1.3 secs but it has less ripples as compared to Figure 2.10. The respose for k_p=1.0 and k_i=2.0 is taking more time and has large ripples in torque in the10 Nm region as shown in Figure 2.12. Now the k_p is kept constant at 1.0 and k_i is going to be varied. Figure 2.13 shows the response for k_p=1.0 and k_i=4.0 where time is reduced as compared to Figure 2.12. Figure 2.14 shows the response for k_p=1.0 and k_i=5.0, time is further reduced and torque ripples in the zero torque region is also reduced. In Figure 2.15 with k_p=1.0 and k_i=6.0 the time is around 0.9 and the ripples are less as compared to previous ones. Figure 2.16 shows the response with k_p=1.0 and k_i=7.0, after that k_p is reduced to 0.9 and start decreasing k_i shows the different responses in Figure 2.17, Figure 2.18 and Figure 2.19. In Figure 2.17 it clear from the response that the torque has significant ripples with k_p=0.9 and k_i=7.0, in Figure 2.18 response with k_p=0.9 and k_i=6.0 the torque becomes smoother after 1.2 secs. Further k_i is reduced with k_p=0.9 response goes worse as shown Figure 2.19 with k_p=0.9 and k_i=5.0.

So k_p=0.9 and k_i=6.0 selected as the controller parameter. The Figure 2.20 shows the speed, torque and current response k_p=0.9 and k_i=6.0 for reference speed 500 rpm.

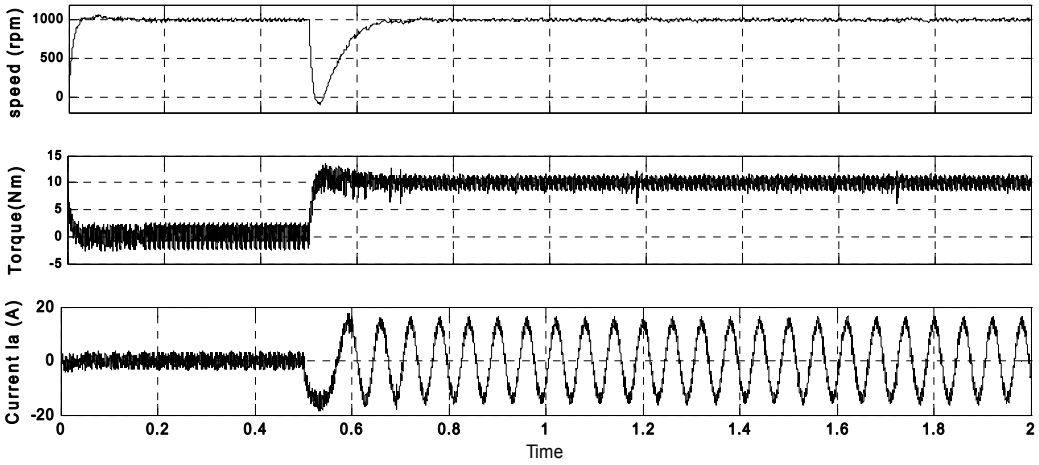

Figure 2.10 Speed, Torque and Current response for k_p=0.1 k_i=2.0 for N=1000rpm

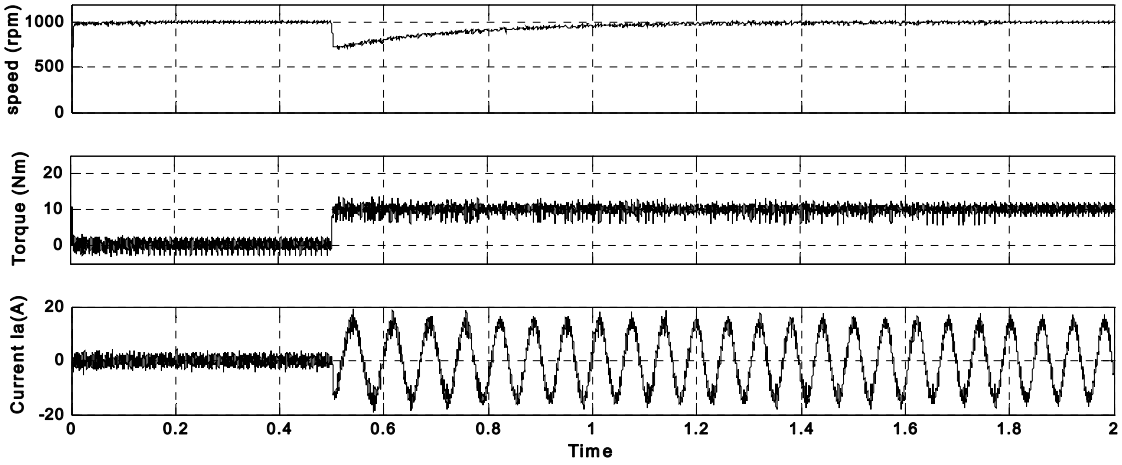

Figure 2.11 Speed, Torque and Current response for k_p=0.5 k_i=2.0 for N=1000rpm

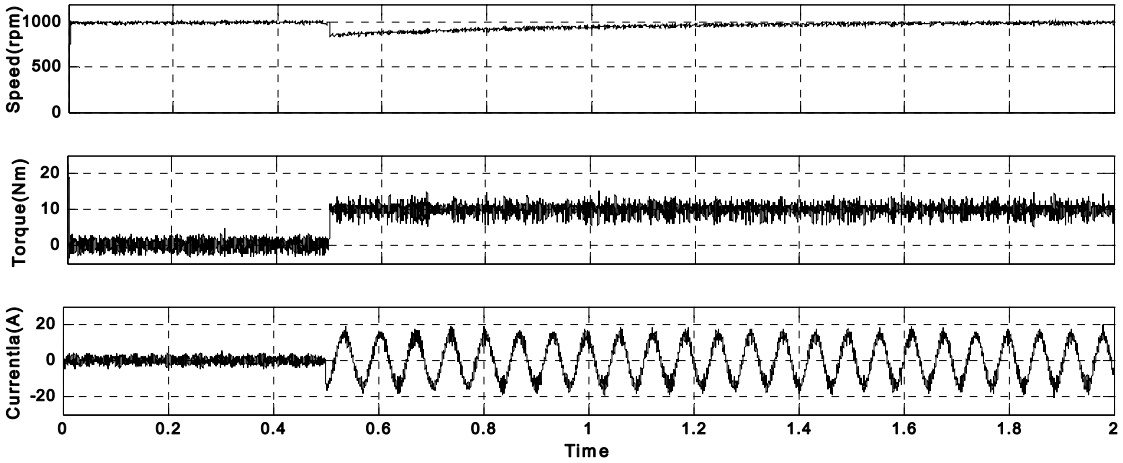

Figure 2.12 Speed, Torque and Current response for k_p=1.0 k_i=2.0 for N=1000rpm

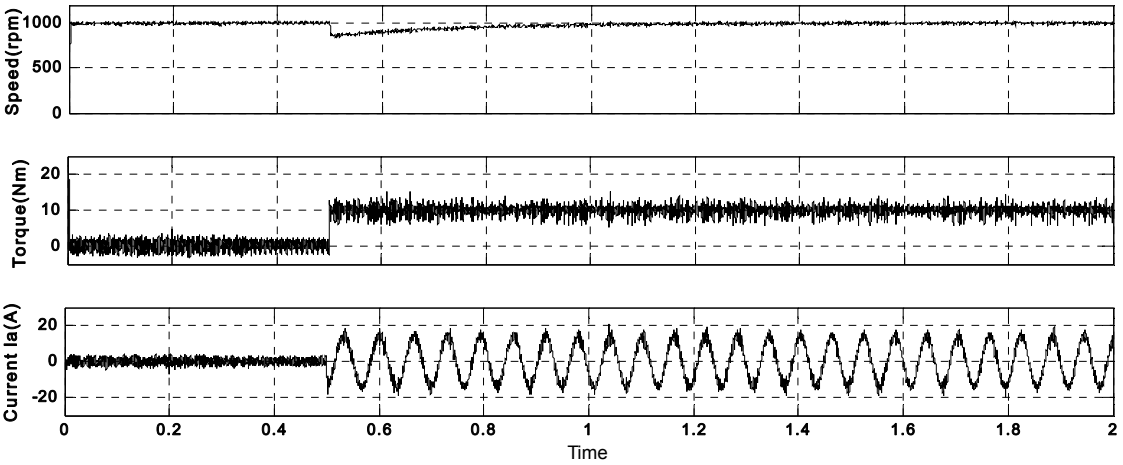

Figure 2.13 Speed, Torque and Current response for k_p=1.0 k_i=4.0 for N=1000rpm

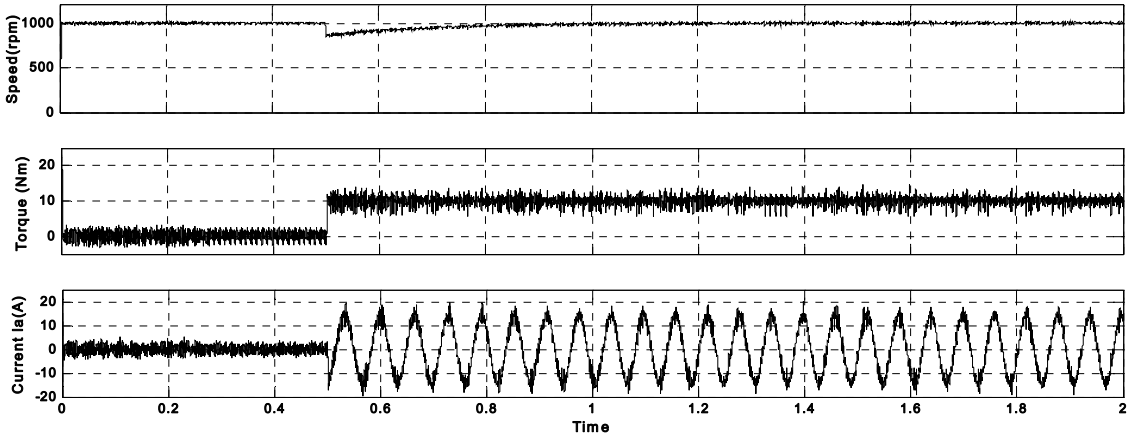

Figure 2.14 Speed, Torque and Current response for k_p=1.0 k_i=5.0 for N=1000rpm

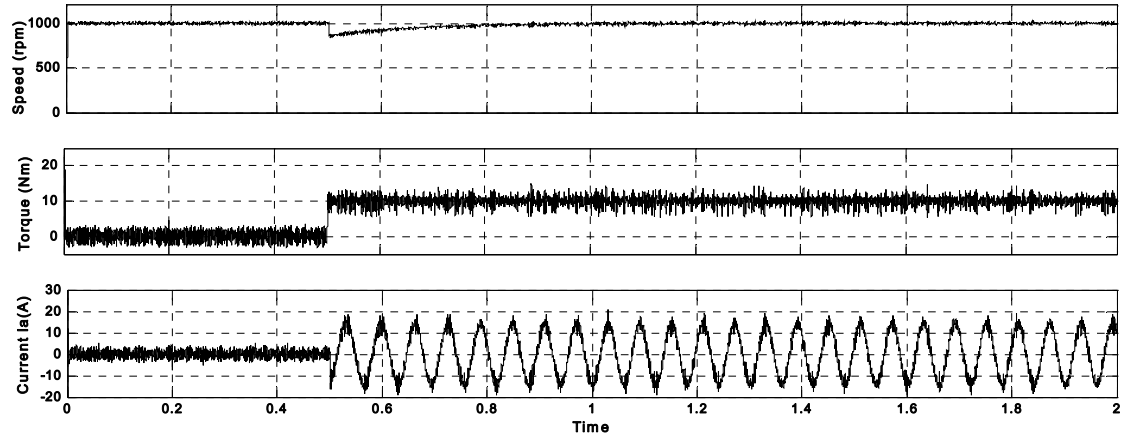

Figure 2.15 Speed, Torque and Current response for k_p=1.0 k_i=6.0 for N=1000rpm

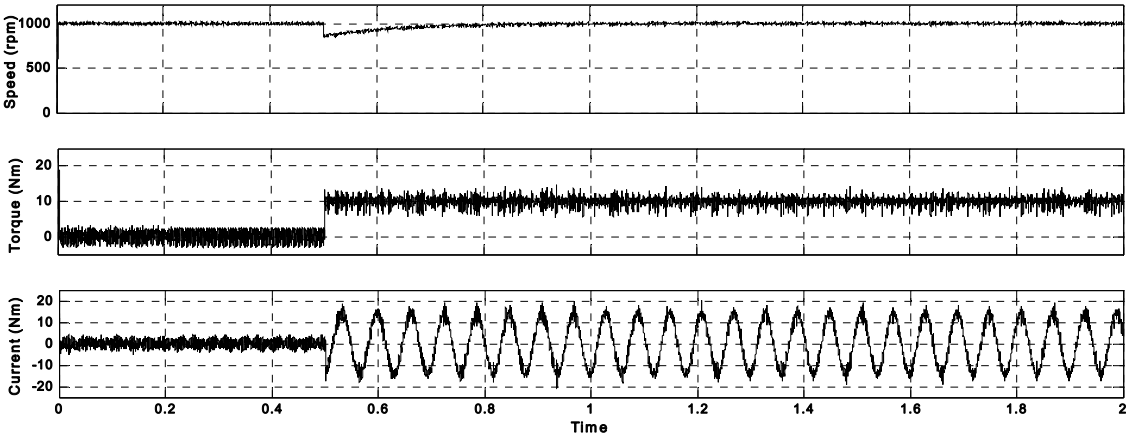

Figure 2.16 Speed, Torque and Current response for k_p=1.0 k_i=7.0 for N=1000rpm

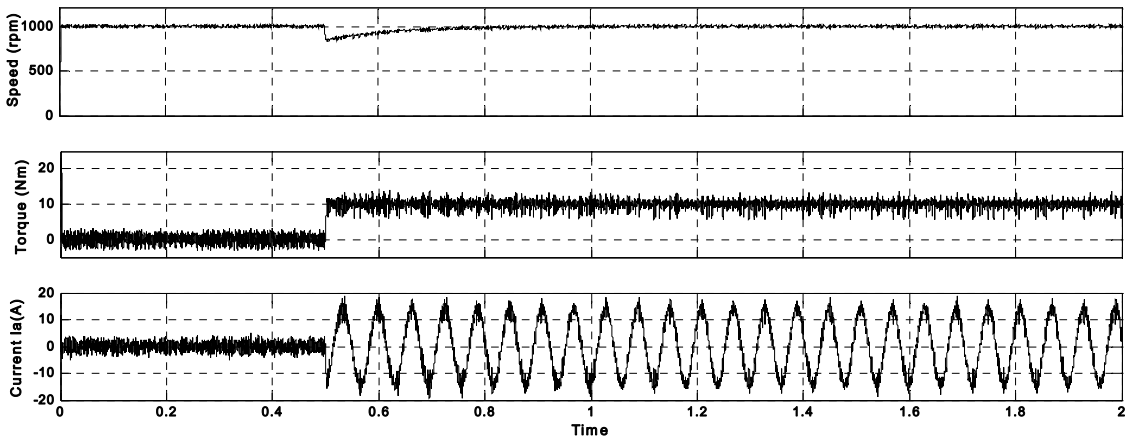

Figure 2.17 Speed, Torque and Current response for k_p=0.9 k_i=7.0 for N=1000rpm

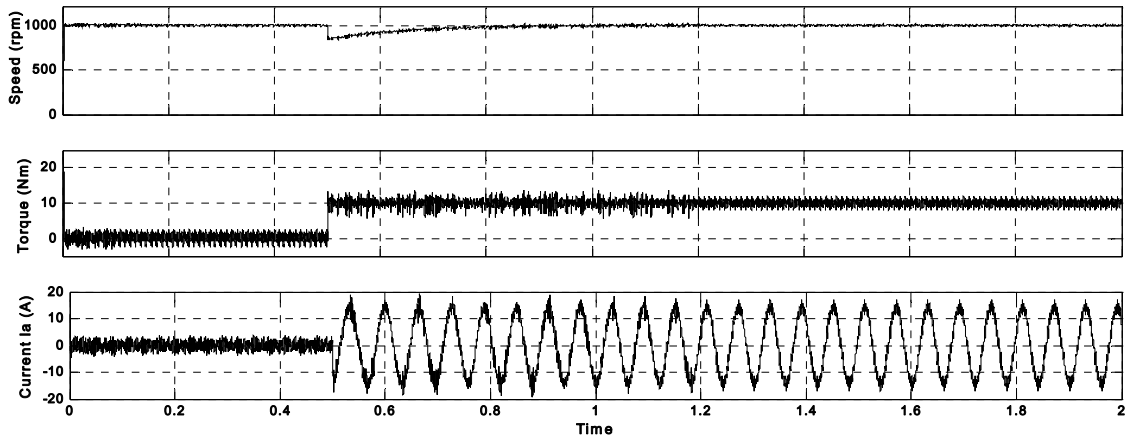

Figure 2.18 Speed, Torque and Current response for k_p=0.9 k_i=6.0 for N=1000rpm

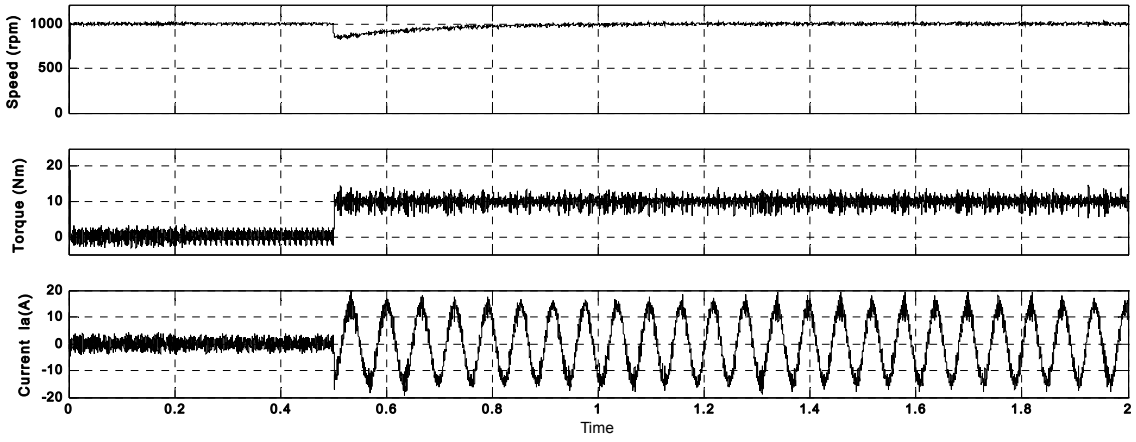

Figure 2.19 Speed, Torque and Current response for k_p=0.9 k_i=5.0 for N=1000rpm

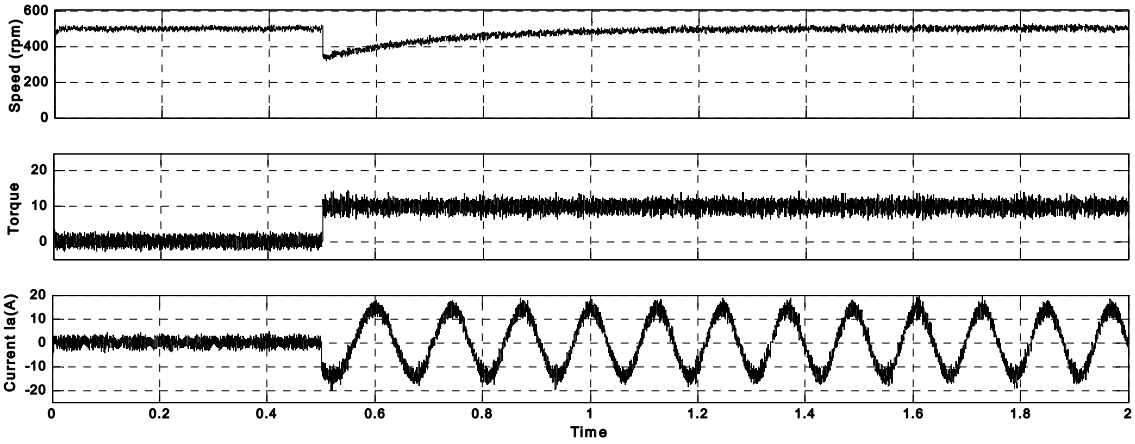

Figure 2.20 Speed, Torque and Current response for k_p=0.9 k_i=6.0 for N=500 rpm

Table 2-2 Performance for different controller parameters

K_p	K_i	Settling Time	Ripples/Overshoot
Kp=0.1	Ki=2.0	0.8s	More/ large deep
Kp=0.5	Ki=2.0	0.7s	Medium
Kp=1.0	Ki=2.0	0.7s	More
Kp=1.0	Ki=4.0	0.6s	More
Kp=1.0	Ki=5.0	0.4s	More
Kp=1.0	Ki=6.0	0.3s	Medium
Kp=1.0	Ki=7.0	0.25s	Medium
Kp=0.9	Ki=7.0	0.2s	Medium
Kp=0.9	**Ki=6.0**	**0.2s**	**less**
Kp=0.9	Ki=5.0	0.25	Medium

The PMSM drive is developed in MATLAB/Simulink and the performance evaluation is performed for different controller parameter of the used PI controller as given in Table 2-2. The gains K_p, K_i are selected by trial and error method with load variation. The speed and torque response with ripples and settling time is obtained, then based on the response the final value K_p=0.9, and K_i=6.0. The Table 2-2 gives the performance with 10.0 Nm load and 1000rpm speed reference. Figure 2.20 shows the response at 500 rpm.

The highlights of the chapter are as follows-

- The coordinate transformations make the computations easy and the simplification of electrical and mechanical differential equations.
- (a-b-c) to (α-β) (Clarke transformation) outputs a two coordinate time variant system.

- (a-b-c) to (d-q) outputs a two coordinate time invariant system.
- The (d-q) coordinate variables based models are mostly applicable to estimation of rotor position of PMSM drive.
- In case of SMO the (α-β) Clarke transformations and in case of MRAS (d-q) transformations are used as, each transformation has their own advantages and disadvantages.
- The d-q transformations are used, where no stator quantities used in computation, only the quantities of rotor side is used in control applications like in MRAS.
- The chosen mathematical model use mathematical in d-q reference frame, as it uses a rotor oriented control.
- The quantities in d-q reference frame are independent and can be controlled separately.

2.7 Conclusion

In this chapter the mathematical model of PMSM in stationary and rotating reference frame is presented. The selection of reference frame depends on the control requirement. The mathematical model is presented for both type of PMSM, with saliency (IPMSM) and without saliency (SMPMSM). As in this thesis PMSM is used with resolver, so the circuitry, mathematical equations and winding waveforms of the resolver is also presented. A MATLAB/SIMULINK based model of PMSM is developed and its simulation analysis for the different controller parameter is studied. The developed PMSM drive has a PI controller and PWM inverter. The performance of the drive for different reference speed with step change in the load torque is presented.

[In a PMSM to bestows the freedom of controlling not only magnitude and frequency of stator currents but also phase for having the control equivalent to that of DC machine control. In this chapter speed and current control in vector controlled PMSM drive. In order to overcome the problems associated with PI controllers, fuzzy based speed and current controllers are employed for motor control which eliminates the controller parameter dependency on the system's mathematical model and load disturbances. The limitations reported in literature are addressed through a proposed FVC for PMSM drive and its performance is investigated. Further, the effects of load variation and reference commands on the performance of drive are extensively studied, and simulation results are verified through experimental results].

3.1 Introduction

In the DC machines a completely decoupled and independent control of the field current forming flux and armature current forming torque is possible by the nature of machine. Because of this decoupled nature, very simple and less time computing time control algorithms were developed, due to this DC machine was preferred for high performance drive system in early stage of computerized feedback control. In contrast to this, in a 3-phase AC machine mathematically complicated structure with multi-phase phase winding and voltage system made it difficult to achieve the decoupling quality. Thus the purpose of vector control is to re-establish the decoupling of torque and flux producing components of stator current vector.

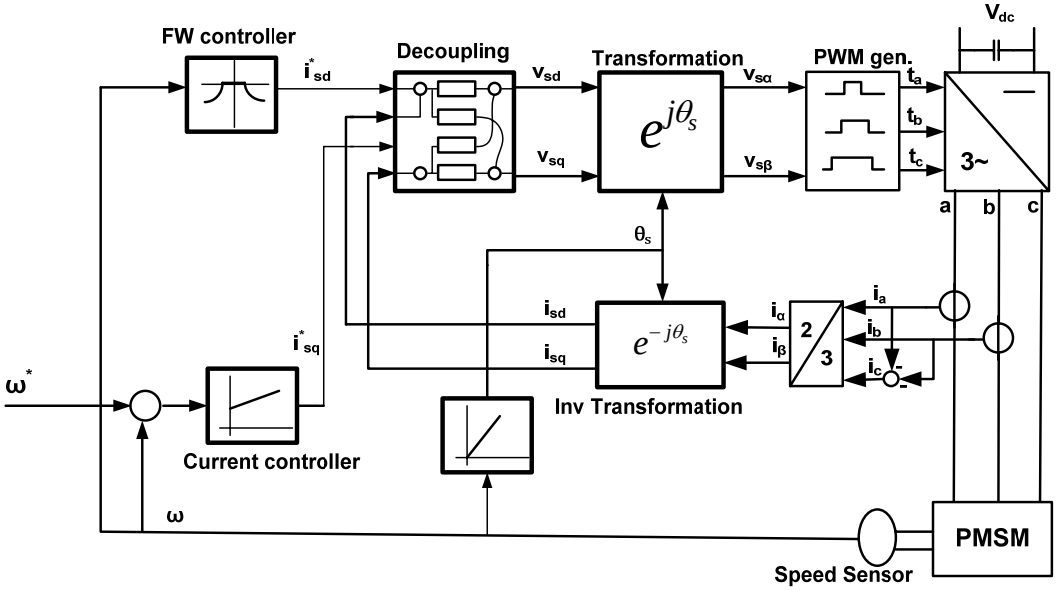

Figure 3.1 Schematic diagram for vector control of three-phase PMSM with VSI and current control

The torque generated by PMSM is given by−

$$T = \frac{3}{2}\frac{P}{2}\lambda_m I_{qs} \tag{3.1}$$

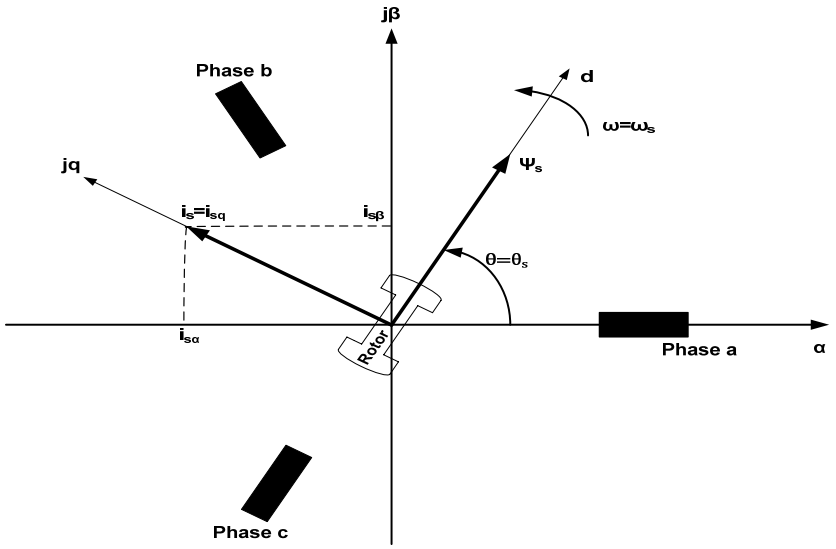

(a)

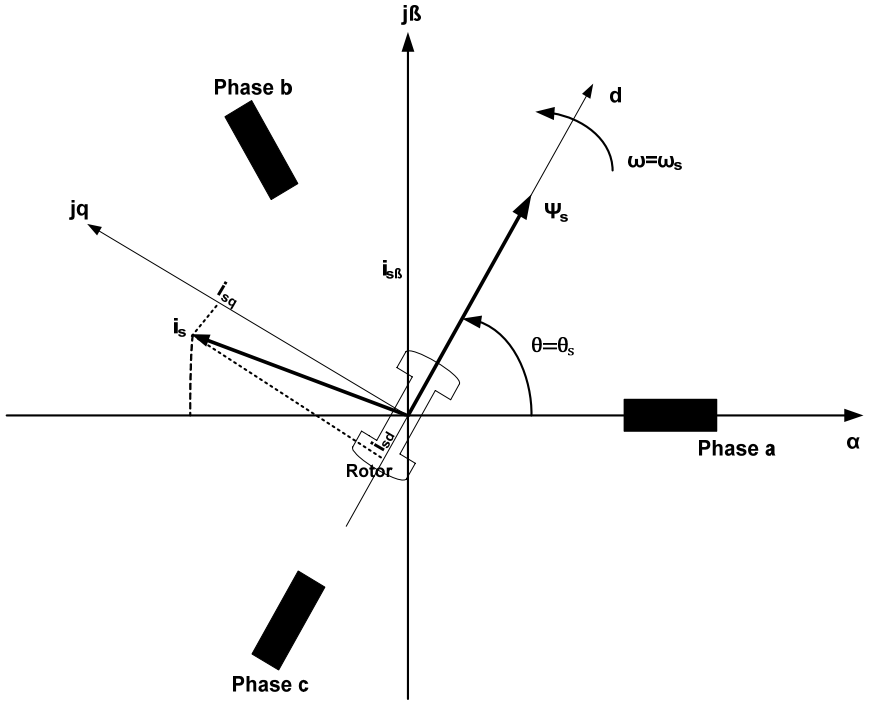

(b)

Figure 3.2 Stator current vector i_s of PMSM in (a) base speed region, and (b) field-weakening region

Vector controlled PMSM drive is widely used in practical applications. Because of constant rotor flux the torque generated by motor depends on current component i_{sq}, so stator current need not to build the flux which happens in case of IM. In the Figure 3.1, field-weakening controller is to inject the appropriate amount of negative d-axis current based on the speed. The inner loop is formed of two separate current controllers with PI behavior for flux producing component i_{sd} (similar to field current of dc motor) and torque producing component i_{sq} (similar to armature current of dc motor). If the angle θ_s between rotor d-axis and stator fixed reference axis (e.g. axis of phase 'a' or axis α) is known, the voltage vectors are transformed from rotor reference frame (d-q coordinate) to stator reference frame (α-β coordinate). After transformation and processing from vector modulation the voltage is finally applied on motor terminals with respective amplitude and phase through inverter. The outer loop consists of a speed controller, inv transformation also serves the same purpose as transformation but in an opposite way, it converts the quantities from stator reference frame to rotor reference frame.

The direct component of stator current i_{sd} has the value zero as shown in Figure 3.2 (a). To operate the drive above base speed field-weakening will be required and for this, a negative current will be fed into d-axis depending on speed Figure 3.2 (b). This injection of negative current becomes possible only because of modern magnets which do not easily get demagnetized.

3.1.1 Objective of Vector Control

The vector control technique brought on a new beginning in high-performance control of ac drives [12, 53-56]. This method has found a wide recognition in household and industrial applications. The vector control is based on transformation of a three phase time and speed dependent system into a two co-ordinate (d and q) time invariant system, which makes the PMSM performance same as that of a DC machine. Vector controlled machines need two components as input references: first is the torque component (with the q co-ordinate) and second is the flux components (with d co-ordinate). This makes the control accurate in every working operation (steady state and transient) and independent of the limited bandwidth of the mathematical model. It should be mentioned here that, the vector control can be applied to both IM and SM and, and can be applied for independent active and reactive power control[12].

3.1.2 Processing of Variables

The vector control processing block diagram is shown in Figure 3.3. As shown in block diagram first three phase quantities have to be converted to two phase using Clarke transformation, and then quantities are converted into d-q variables. The control process is

implemented here in d-q reference frame, because in d-q reference frame quantities are independent and can be controlled separately, which is the basic purpose of the vector control. These electrical quantities, in d-q reference frame, are again converted back to three phase stationary reference frame to feed power to three-phase PMSM. The three phase and two phase stationary and rotating reference frames are shown in Figure 3.4 and transformation equations are given in Table 3-1. Here as shown in diagram the electrical quantities may be voltage, current or frequency (x).

In real time all the electrical quantities are available to user in three phase stationary reference frame (i.e. a-b-c), but it becomes necessary to observe and control the thing with respect to rotor, because rotor is in motion with respect to stator. Thus, from stator side rotor quantities are not time invariant and vice versa, and hence it becomes difficult to implement the control algorithm or calculations. There are many ways to obtain the transformations between different reference frames as shown in Figure 3.5, which are compiled in Table 3-1.

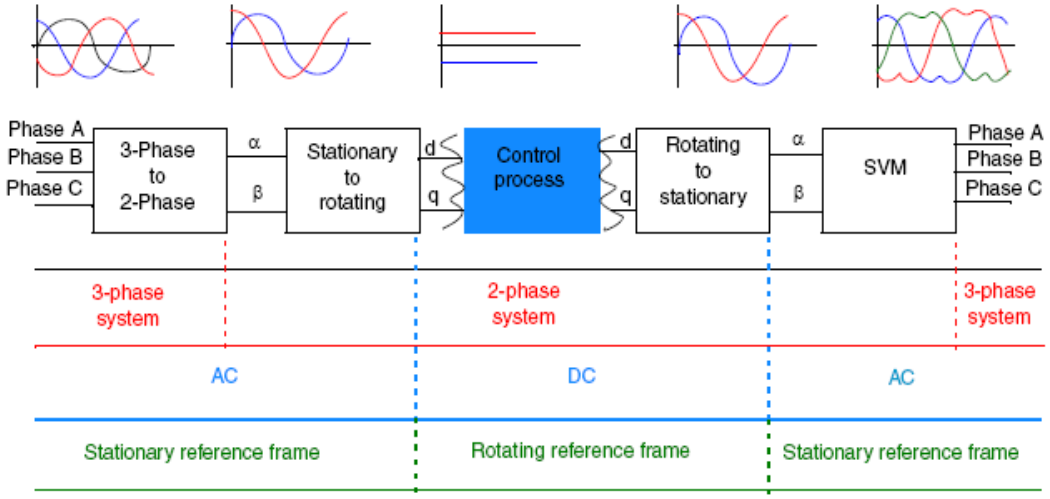

Figure 3.3 Vector control processing

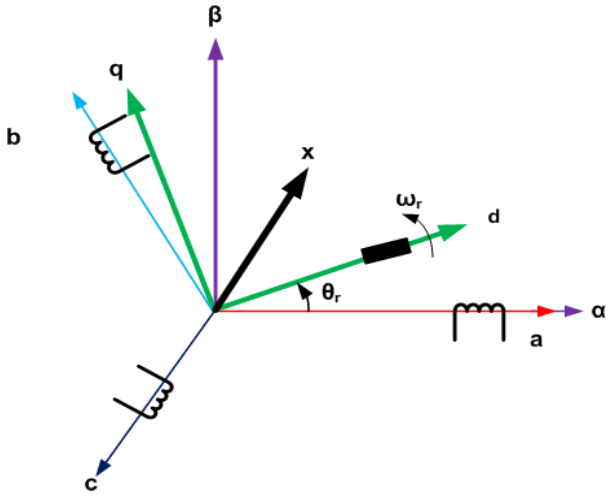

Figure 3.4 Different reference frames (a–b–c, α–β, d–q)

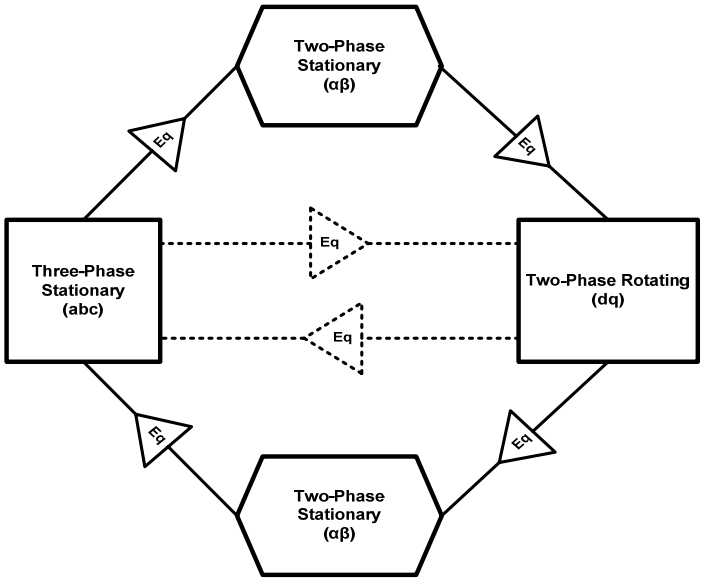

Figure 3.5 Flow chart for Transformation equations

The appropriate equation for Figure 3.5 can be selected from Table 3-1 for the required transformations

Table 3-1 Transformation equations

Stationary to Rotating co-ordinates		**Rotating to stationary co-ordinates**	
Through αβ (abc-αβ-dq)		**Through αβ (dq-αβ-abc)**	
abc→ αβ (3 stationary→ 2 stationary)	$\begin{bmatrix} x_\alpha \\ x_\beta \end{bmatrix} = \sqrt{\frac{2}{3}} \begin{bmatrix} 1 & -\frac{1}{2} & \frac{1}{2} \\ 0 & \frac{\sqrt{3}}{2} & -\frac{\sqrt{3}}{2} \end{bmatrix} \begin{bmatrix} x_a \\ x_b \\ x_c \end{bmatrix}$	dq→αβ (2 rotating→ 2 stationary)	$\begin{bmatrix} x_\alpha \\ x_\beta \end{bmatrix} = \begin{bmatrix} \cos\theta_r & -\sin\theta_r \\ \sin\theta_r & \cos\theta_r \end{bmatrix} \begin{bmatrix} x_d \\ x_q \end{bmatrix}$
αβ →dq (2 stationary→ 2 rotating)	$\begin{bmatrix} x_d \\ x_q \end{bmatrix} = \begin{bmatrix} \cos\theta_r & \sin\theta_r \\ -\sin\theta_r & \cos\theta_r \end{bmatrix} \begin{bmatrix} x_\alpha \\ x_\beta \end{bmatrix}$	αβ→abc (2 stationary→ 3 stationary)	$\begin{bmatrix} x_a \\ x_b \\ x_c \end{bmatrix} = \begin{bmatrix} 1 & 0 \\ -\frac{1}{2} & \frac{\sqrt{3}}{2} \\ -\frac{1}{2} & -\frac{\sqrt{3}}{2} \end{bmatrix} \begin{bmatrix} x_\alpha \\ x_\beta \end{bmatrix}$
Direct abc→dq		**Direct dq→abc**	
abc→dq (3 stationary→ 2 rotating)	$\begin{bmatrix} x_d \\ x_q \end{bmatrix} = \frac{2}{3} \begin{bmatrix} \sin\theta_r & \sin(\theta_r - 120) & \sin(\theta_r + 120) \\ \cos\theta_r & \cos(\theta_r - 120) & \cos(\theta_r + 120) \end{bmatrix} \begin{bmatrix} V_a \\ V_b \\ V_c \end{bmatrix}$	dq→abc (2 rotating→ 3 stationary)	$\begin{bmatrix} V_a \\ V_b \\ V_c \end{bmatrix} = \begin{bmatrix} \sin\theta_r & \cos\theta_r \\ \sin(\theta_r - 120) & \cos(\theta_r - 120) \\ \sin(\theta_r + 120) & \cos(\theta_r + 120) \end{bmatrix} \begin{bmatrix} x_d \\ x_q \end{bmatrix}$

Here some of the comparative remarks of vector control is necessary with its serious competitor i.e. direct torque control (DTC). The two major category of control schemes are vector control and DTC. The following Table 3-2 gives a comparative analysis of vector control and direct torque control.

Table 3-2 Contrast of direct torque control and vector control

issues	Direct Torque Control	Vector Control
Dynamics	Good	Good
Robustness	Good	Good
Transformation	Not required	Required
Speed/position sensor	Not necessary	Required
Decoupling	To achieve orientation	Automatic
Sensitivity to parameters	Average	High
Low speed response	Average	Good
Control	Not necessary PWM	PWM

3.2 Vector Control of PMSM Drive

The input excitation to machine from stator side is done to separate torque and flux channels by vector control. The vector control of a PMSM drive is achieved in similar way as for the induction motor drive. The vector control of PMSM is derived from the dynamic model of PMSM considering the currents as inputs. Three-phase currents are−

$$i_{as} = i_s \sin(\omega_r t + \delta) \tag{3.2}$$

$$i_{bs} = i_s \sin\left(\omega_r t + \delta - \frac{2\pi}{3}\right) \tag{3.3}$$

$$i_{cs} = i_s \sin\left(\omega_r t + \delta + \frac{2\pi}{3}\right) \tag{3.4}$$

Where ω_r, is the electrical rotor speed,

δ, is the angle between stator current phasor and rotor field and known as torque angle. The rotor field travels at speed same as rotor speed which is ω_r electrical rad/sec.

In PMSM direct control of torque becomes complicated due to inherent coupling effects. Decoupling between torque and flux producing components can be provided by vector control algorithm and it also makes the control easier [10, 11]. Vector or decoupling control makes the dynamics of ac drives similar to that of dc drives, and with current control, problems of the conventional stability limit of ac machine does not arise. The slip gain tuning has been attempted in order to have decoupling between the rotor flux and torque

component of current The stator currents in rotor reference frame are obtained as given in Table 3-1.

$$\begin{bmatrix} i_{ds} \\ i_{qs} \end{bmatrix} = \frac{2}{3}\begin{bmatrix} \sin\theta_r & \sin(\theta_r - 120) & \sin(\theta_r + 120) \\ \cos\theta_r & \cos(\theta_r - 120) & \cos(\theta_r + 120) \end{bmatrix}\begin{bmatrix} i_a \\ i_b \\ i_c \end{bmatrix} \tag{3.5}$$

The stator currents can be expressed as−

$$\begin{bmatrix} i_{ds} \\ i_{qs} \end{bmatrix} = i_s \begin{bmatrix} \cos\delta \\ \sin\delta \end{bmatrix} \tag{3.6}$$

It is to be observed that d-axis and q-axis currents are constant in rotor reference frame, as the torque angle δ is constant for a given load torque. The rotor flux is on the d-axis of machine, and which is on the rotor and rotating with the angular velocity ω_r electrical rad/sec from a stationary reference point termed as stator reference frame as shown in Figure 3.6. The stator current phasor, which is a combination of direct and quadrature axis in every reference frames (rotor reference frames are predominantly used in case of synchronous machine control), is applied at an angular frequency of rotor electrical speed, which is ω_r rad/sec with an angle of δ rad from rotor flux phasor (assuming initial rotor position is zero). One thing is to be noted here that the relative velocity between current phasor and rotor d-axis is zero, but it is δ rad from rotor flux phasor which is fixed for a specified load torque. The components of stator current phasor on rotating d-axis and q-axis (rotor reference frame) are constant for a given stator current phasor and given torque angle. The stator current component only along d-axis produces flux, and hence named as flux-producing component and can be denoted by i_f. This current partly contributes to d-axis flux and remaining part of rotor flux is contributed by permanent magnets (PMs). The generated PM flux can be assumed to be generated by an equivalent current source i_f.

The component of stator current which is in quadrature to rotor flux produces the torque in interaction with rotor flux, so called torque-producing component i_T, which is similar to armature current in case of DC machine. So the d-axis and q-axis components of stator current can be represented as−

$$i_{ds} = i_f \tag{3.7}$$

$$i_{qs} = i_T \tag{3.8}$$

To achieve the complete phasor diagram the voltage phase is assumed to be leading to current phasor by phase angle ϕ, and cosine of this angle is known as the power factor of machine.

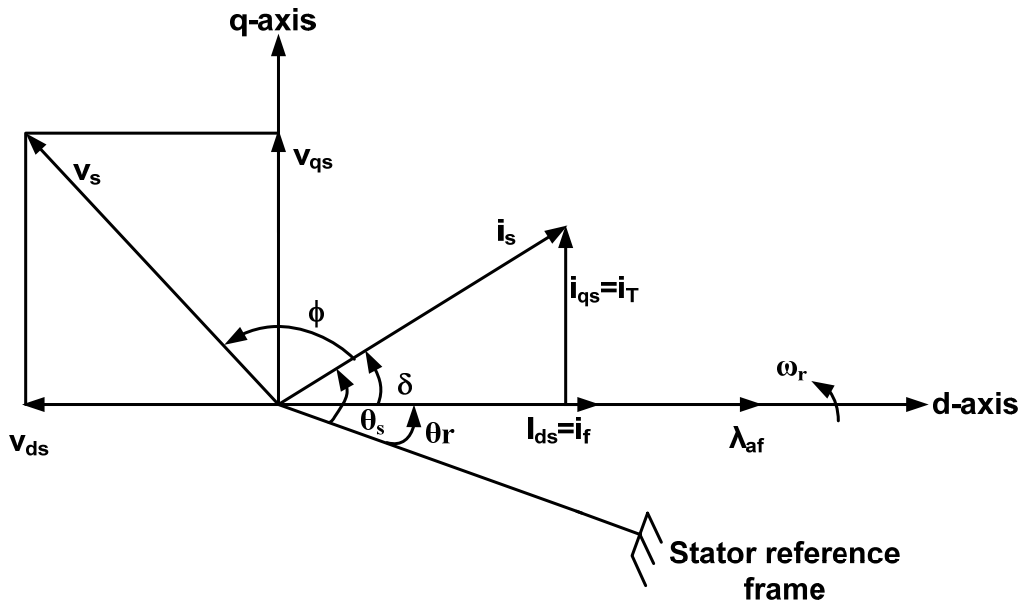

Figure 3.6 Phasor diagram of PMSM

The electromagnetic torque generated by PMSM is recalled from chapter 2, and is given by−

$$T_e = \frac{3}{2}\frac{P}{2}\left[\lambda_{af} i_{qs} + \left(L_d - L_q\right) i_{qs} i_{ds}\right] \quad (N.m) \tag{3.9}$$

For a surface mounted PMSM having no saliency, the torque angle is zero, i.e. i_{ds}=0, and torque expression becomes−

$$T_e = \frac{3}{2}\frac{P}{2}\lambda_{af} i_{qs} \tag{3.10}$$

In such case the torque-producing component of stator current becomes equal to magnitude of stator current, as the torque angle becomes equal to 90°. Then the PMSM behaves in the same manner as a separately excited DC machine, which is clear from torque expression. The toque generated by PMSM directly depends on i_{qs} for a constant otor flux linkage. The magnet rotor flux linkage is not usually a constant, due to temperature sensitivity of magnets.

Substituting the direct and quadrature-axis components of stator current in rotor reference frame into torque expression, torque is expressed in terms of stator current magnitude and torque angle as given by−

$$T_e = \frac{3}{2}\frac{P}{2}\left[\lambda_{af} i_s \sin\delta + \frac{1}{2}\left(L_d - L_q\right) i_s^2 \sin 2\delta\right] \tag{3.11}$$

Now it can be observed from torque expression that on R.H.S. the first part represents the synchronous torque generated by interaction between stator field generated by stator current and rotor field generated by permanent magnets. The second term depends on saliency due to reluctance variation of machine and is known as reluctance torque. It is to be

observed from the torque expression that, when torque angle δ is more than $\pi/2$, the i_{ds} becomes negative and total flux linkage decreases, it gives the key point for the field weakening operation of PMSM drives.

From the above discussion on control of PMSM drives following key points are found as−

- By controlling δ, magnitude and phase of stator current through inverter determines the torque control.
- Rotor speed (electrical rad/sec.) is controlled by controlling the angular frequency of stator current phasor.
- The PMSM drive is considered to be analogous to separately excited DC machine by finding the field and armature currents i_f and i_T (flux and torque producing components) for PMSM equivalent to field and armature currents of DC machines.
- In PMSM drive the independent control between torque and flux is achieved through torque and flux producing components is similar way to DC machine's field and armature current.

3.3 Controllers in Vector Controlled PMSM Drive

The implementation of vector control employ one speed controller which takes speed error and generates current reference for current controller, and two-current controllers for q-axis and d-axis respectively and a space vector pulse width modulated inverter [57, 58]. Traditionally PI controllers are used in drives as speed and current controllers which inherently causes the sluggish response due to saturation, especially when the dc bus voltage is not sufficient or when sudden load disturbance or sudden change in reference occurs.

3.3.1 Speed Control

In a vector controlled PMSM drive two control loops are required. Outer one is the speed control loop consists of one speed controller, which processes the speed error as shown in Figure 3.1. PI controller as a speed controller nullifies the steady state speed error $\left(\omega_r^* - \omega_r\right)$. The output of speed controller is basically torque reference, which multiplies by inverse of torque constant K_t. The speed error can be minimized only by changing the electromagnetic torque generated by motor, depending on whether speed error is negative or positive. Vector control for PMSM drives provides decoupling control between flux and torque components, and is able to achieve the good performance similar to dc motor in adjustable speed drive application. In such high performance drive speed controller plays a vital role

[59] as it directly affects the current reference input to current controllers and indirectly affects the performance of motor in terms of efficiency, dynamic response etc [18].

3.3.2 Current Control

A comprehensive literature is reported highlighting the merit and demerits of various controllers such as hysteresis, PWM and predictive current controller[20]. Similar to speed controllers, current controllers also affect the performance of drive as they directly affects the quality of current fed to the motor. Solution to the problems of nonlinearity and parameter variation needs different control algorithm to achieve a wide speed range operation of PMSM. Several control methods such as PI Control, FLC, adaptive control and neural network control have been reported for motion control in PMSM drive [60].

For the optimum operation below base speed d-axis reference is kept zero, the measured current i_a, i_b, and i_c, converted to i_d, and i_q, and the d-axis and q-axis current errors are processed through two separate current controllers as shown in Figure 3.7.

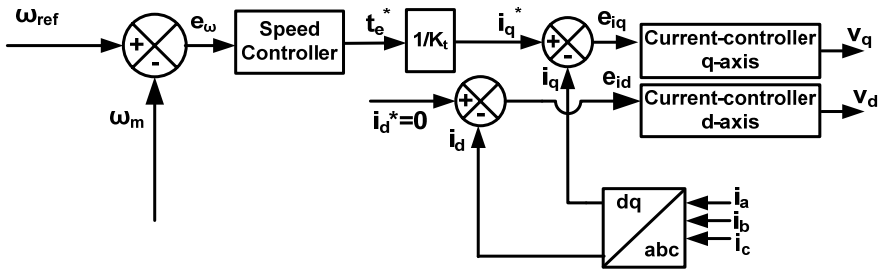

Figure 3.7 Speed and current-controllers in close loop drive

The design and implementation of a PI controller is simple and provides wide stability margin, but requires meticulous tuning and unable to cope up with parameter variation. So an observer based self tuning PI controller is proposed [23], in which the controller parameters are adjusted as per requirement [61, 62]. This method need fast enough processors and is time consuming. Adaptive control methods are able to adjust the controller parameter as per the variation in system parameter, but require a reference model. Neural network based controllers are able to operate with highly nonlinear systems but requirement of huge training data, lengthy training process and large convergence time reduces the superiority of this method [24].

To obtain the robustness performance with parameter variations and load disturbances, the controller parameters have to be continuously adapted on-line. This can be achieved by MRAC [25, 26], SMC [27], VSC, and self-tuning PI controllers and etc.

Among the various available computational intelligence techniques such as ANN, Fuzzy, Genetic Algorithm, the fuzzy logic is found less complicated and easy to implement as compared to others to achieve the same performance. The neural network control is a good choice for control applications. As in ANN controller the selection of size of network structure,

number of neurons, number of hidden layers, weight coefficients are the major challenges [29]. Moreover the complexity of the ANN controller increases while achieving the robustness in overall system performance, and its real time implementation becomes difficult on given hardware platform where sampling time and processing speed is limited. Similarly in GA the mutation and selecting the new chromosomes are computationally complex and time consuming.

3.4 Proposed Fuzzy Vector Control of PMSM Drive

The design and implementation of a PI controller is simple and provides wide stability margin, but requires meticulous tuning and unable to cope up with parameter variation. So an observer based self tuning PI controller is proposed [23], in which the controller parameters are adjusted as per requirement. This method need fast enough processors and is time consuming.

In order to overcome the above limitations fuzzy based controllers are employed for motor control which eliminates the controller parameter dependency on the system mathematical model and load disturbances. A FLC is basically a non linear and an adaptive controller which gives robust performance for a linear or non linear plant with parameter variation. Use of fuzzy logic algorithm, to reduce the torque ripples, has been proposed, it refines the voltage vectors[48]. Use of space vector modulation (SVM) significantly reduces the torque and flux ripples. Therefore, fuzzy speed controller (FSC) is proposed to overcome the demerits of conventional PI speed controller which produce current reference for current controllers. The proposed fuzzy current controller (FCC) generates the reference signals for the inverter [63], which directly improves the quality of voltage and current fed to the motor resulting in high performance of drives. The block diagram of FVC controlled PMSM drive is shown in Figure 3.8.

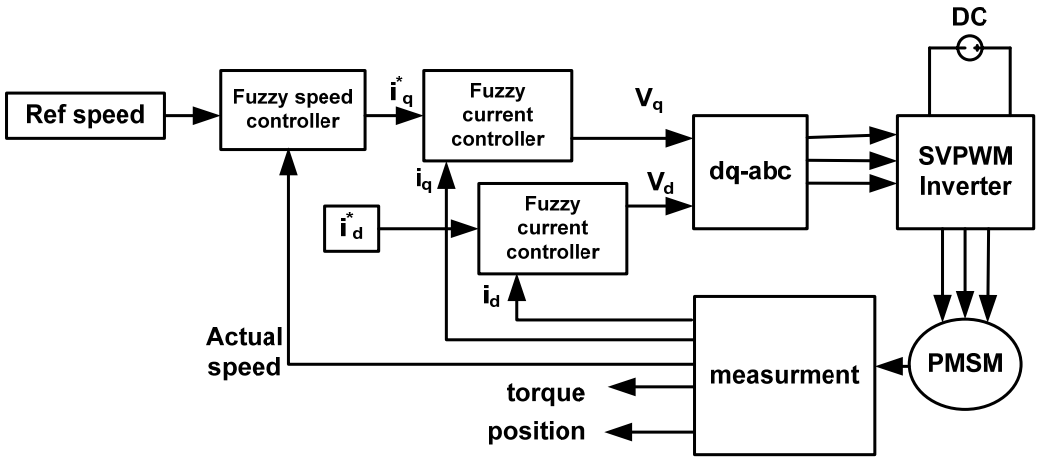

Figure 3.8 Schematic block diagram of FSC and FCCs controlled PMSM drive

To address the above limitations, a FVC is proposed for PMSM drive and its performance is investigated. Further, the effects of load variation and reference commands on the performance of drive are extensively studied. The proposed FVC based drive is simulated in MATLAB/Simulink and is validated through experimentation. The exhaustive results demonstrate the effectiveness and robustness of proposed controller.

In high performance drives speed controller and current controller both play an essential role as they directly affects the quality of current fed to the motor and indirectly affects the performance of drive in terms of efficiency and dynamic response [18, 20]. In view of this, by replacing these controllers with controllers based on fuzzy logic (FSC and FCC), an attempt has been made to improve the performance of drive and to overcome the problems associated with PI controllers. The block diagram of the proposed FVC based PMSM drive is shown in Figure 3.9.

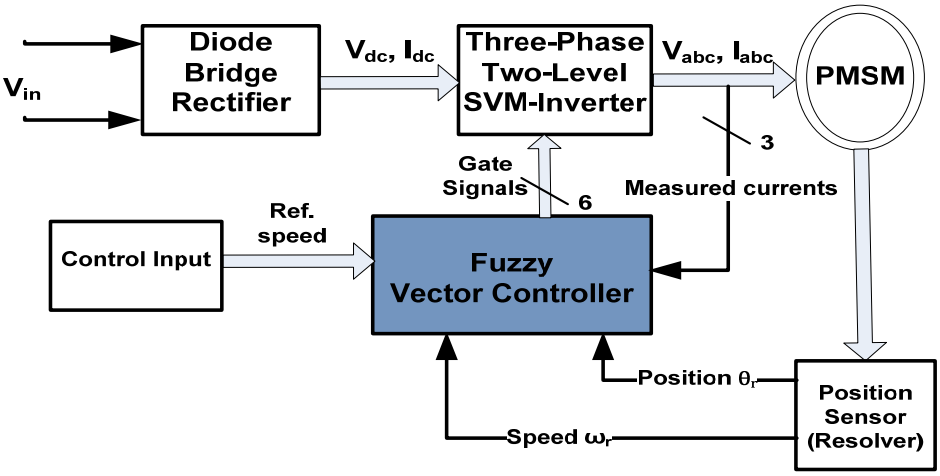

Figure 3.9 FVC based PMSM drive

The fuzzy vector controlled PMSM drive consists of four major components viz. PMSM, inverter, and the FVC and position sensor. The buildings blocks and signal flow is as shown in Figure 3.9. The PMSM used here is a surface mounted type and the resolver is internally mounted on the surface of rotor as a position sensing device. The PMSM is fed by a two-level, IGBT based intelligent power module inverter, which is getting gate signals from FVC, and dc power input from an uncontrolled diode bridge rectifier with a dc link capacitor. The FVC take rotor position information from resolver, measured phase currents of PMSM using current sensors, and control input from user as the reference speed. These components are explained in detail in further section.

The PMSM is a motor that uses permanent magnets to produce the air gap magnetic field. The most commonly used magnetic materials are rare earth magnets such as NdBFe, SmCo, Strontium Ferrite or Barium ferrite etc. The NdBFe is the magnet with highest flux density. PMSM stator is having three phase star connected winding and rotor is with

permanent magnets. In vector control mathematical modelling of motor in dq reference frame is required for simulation and analysis of drive system. In deriving the dq axis model of PMSM drives, the following assumptions are made:

- Back emf is sinusoidal
- Equal turns per phase
- Rotor flux is concentrated along d-axis
- No flux along q-axis
- Core loss is negligible
- Constant rotor flux

Rotor reference frame is used to express stator voltage equations. The d-q stator windings have fixed phase relationship with rotor magnet axis or d-axis. PMSM equations are presented in dq reference frame [12].

$$V_{ds} = i_{ds} r + l_d \frac{di_d}{dt} - \omega_e \lambda_q \tag{3.12}$$

$$V_{qs} = i_{qs} r + l_q \frac{di_q}{dt} + \omega_e \lambda_d \tag{3.13}$$

Above two equations are the voltage equations of PMSM used in vector control, based on that equivalent circuit of PMSM is obtained as shown in

The mechanical equations are given as -

$$J \frac{d\omega_m}{dt} = T_{em} - B\omega_m - T_{load} \tag{3.14}$$

$$\omega_e = \frac{P}{2} \omega_m \tag{3.15}$$

Where, B is a coefficient, which is calculated from moment of inertia J, and T_{load} is the toad torque.

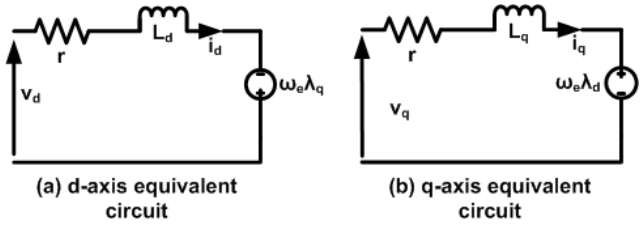

Figure 3.10 Equivalent circuit of PMSM

Then speed and torque generated by motor is calculated as -

$$T_e = P \cdot \frac{3}{4} \left[i_q \cdot \lambda_m + i_d i_q \left(L_d - L_q \right) \right] \tag{3.16}$$

$$\omega_e = \frac{T_e - T_{load}}{J_s + B} \tag{3.17}$$

$$\theta = \int \omega_e \tag{3.18}$$

In the proposed scheme surface mounted PMSM is used which has no saliency, so L_d is equal to L_q and hence second term (known as reluctance torque) in torque equation will not be present.

3.4.1 Inverter

The stator windings of the motor are fed by an inverter that generates a variable frequency variable voltage. In the proposed scheme space vector pulse width modulated (SVPWM) inverter is used. A three-phase two-level voltage source inverter has 8 distinct states, in which 6 are non-zero or active states and 2 are zero states which produce zero output voltage. The desired three phase voltages at the output of the inverter could be represented by an equivalent vector V rotating in the counter clock wise direction as shown in Figure 3.11.

In SVM for the rotating vector V first the sector is identified (1-6 each 60 degree span) then based on the sector the switching pattern (v1-v6 as shown in Figure 3.11) is selected and based on the switches conduction appropriate three-phase output voltage is generated.

The position is measured for the experimentation resolver is used for which detailed information and modeling is given in chapter 2.

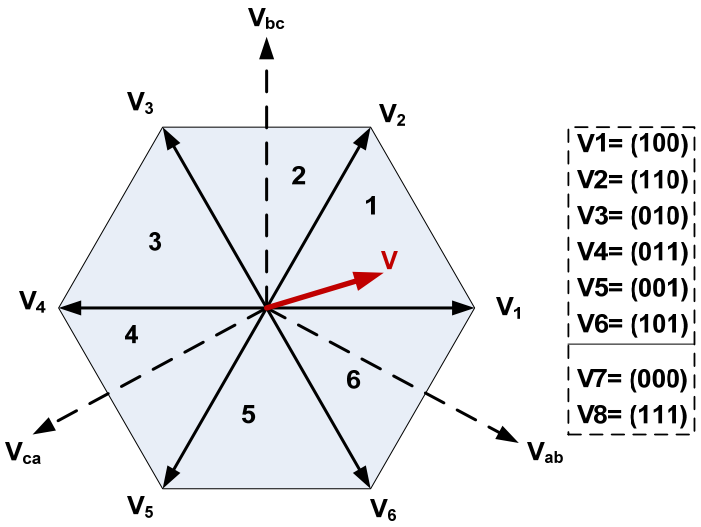

Figure 3.11 Output voltage vector in SVM

3.4.2 Fuzzy Logic Controller

As discussed earlier that performance of drive is affected by speed controller and current controllers. In view of this, by replacing these controllers with controllers based on fuzzy logic (FSC and FCC), an attempt has been made to improve the performance of drive

and to overcome the problems of non linearity, parameter dependency and problems associated with PI controllers, .

A fuzzy logic controller is basically a nonlinear and an adaptive controller which gives robust performance for a linear or non linear system with parameter variation [64]. Fuzzy logic is an approximate interpretation of multiple & diverse data sets and decisions by using linguistic variables similar to human analysis. Figure 3.12 shows a block diagram and signal flow of FLC.

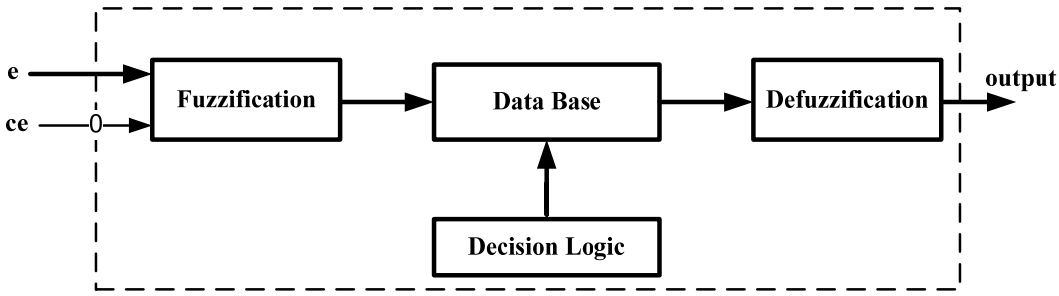

Figure 3.12 Block diagram of FLC structure

In the proposed controller, all control actions are entirely based on the fuzzy logic and is termed here as Fuzzy Vector Controller (FVC). The proposed FVC has input and output scaling factors. The values of these scaling factors are different for speed and current controllers based on their input range, required output range, and interval of membership function defined for that particular controller. Scaling factors are used to tune the controller without changing the controller data base, with system parameter to achieve high performance. As for as the controller parameters are concerned, these are the range of membership functions, type of membership function, implication methods, rules and number of rules. Initially, the scaling factors are selected based upon the approximate estimate of the input and output range for individual controller as PI controllers, and are tuned individually to achieve the desired performance.

3.5 Design of FSC and FCC

The FVC consists of three individual controllers based on fuzzy logic algorithm. The block diagram of FLC with scaling factors is shown in Figure 3.13. The structure of FLC for speed and controller is same only inputs and outputs for respective controllers are different.

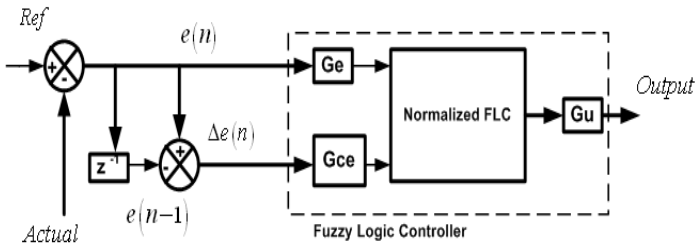

Figure 3.13 Block diagram of FLC with scaling factor

The design steps for fuzzy logic controller for speed and current control of PMSM are as follows –

1. Identify input and output variables.
2. Select membership functions (MFs) and define control rules./Fuzzification
3. Choose probable implication method./Inference
4. Translate fuzzy set into crisp set./Defuzzification
5. Tune the scaling factors for desired performance.

3.5.1 Identifying the Variables

Error in speed is defined as -

$$\Delta\omega_r(n) = \omega^*_r(n) - \omega_r(n) \tag{3.19}$$

Error in d-axis current is defined as -

$$\Delta i_d(n) = i^*_d(n) - i_d(n) \tag{3.20}$$

Error in q-axis current is defined as -

$$\Delta i_q(n) = i^*_q(n) - i_q(n) \tag{3.21}$$

Change in error for all three variables is defined as -

$$\Delta e(n) = e(n) - e(n-1) \tag{3.22}$$

the error for the speed and currents are defined by (3.19)-(3.21), three different expressions, now their own individuals will decide their respective 'e', the change in error expression is same for all three quantities as (3.22). One thing to be noted here is that the given expression for all three is one but all these three quantities speed, d-axis current, q-axis current will have their own three expressions.

3.5.2 Selection of Membership Functions

In the proposed FVC, the FCC has only five linguistic variables 1) negative medium (NM), 2) negative small (NS), 3) zero (Z), 4) positive small (PS), 5) positive medium (PM) and are shown in Figure 3.14(a). In case of FSC seven linguistic variables are chosen for input and output variables: 1) negative large (NL), 2) negative medium (NM), 3) negative

small (NS), 4) zero (Z), 5) positive small (PS), 6) positive medium (PM), 7) positive large (PL), as shown in Figure 3.14(b). First three linguistic variables were chosen for FCC but performance was not found suitable. When seven linguistic variables were chosen there was not significant difference between five and seven, so finally five linguistic variables were chosen, and same type of case happen with FSC as it was tries with five and nine.

Table 3-3 Properties of membership functions

	Type of MFs	Nos.	Interval
FSC	**Triangular**	**5**	**[-15 15]**
FCC	**Triangular**	**7**	**[-2 2]**

In case of speed controller more variables chosen because the variation and range of speed error is more as compared to current error.

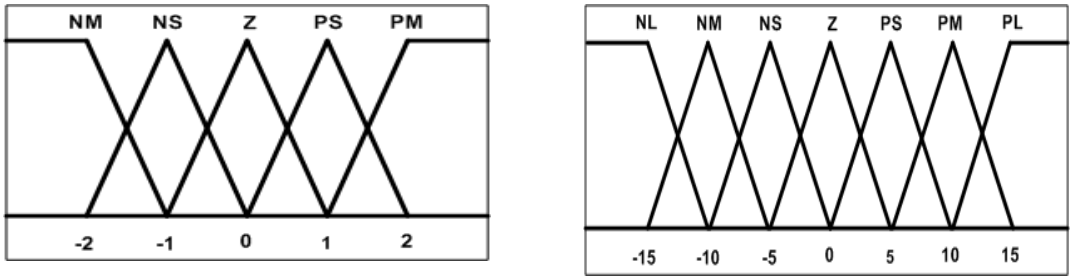

(a) Membership functions for current controller

(b) Membership functions for speed controller

Figure 3.14 Shape and boundaries of current and speed controllers

3.5.3 Constraints and Rules

Based on the experience and expertise of the system, membership functions are specified and fuzzy control rules are defined. These membership functions and control rules may require tuning to achieve high performance of drive under variable operating conditions. To obtain normalized inputs and output for FLC, gain blocks are used as scaling factors G_e, G_{ce} and G_u [65] as shown in Figure 3.13.

In the second stage of FLC, fuzzy variables E and CE are processed by an inference engine that executes a set of control rules contained in (7 × 7) rule base for speed controller and (5×5) rule base for both current controllers. The control rules are derived from experience or knowledge of experts. Each rule is expressed in form of -

Rule: IF $\Delta\omega_r(n)$'e' is A and 'ce' is B, THEN $\Delta i_{qs}^*(n)$'Output' is C

Where, 'e', 'ce', and 'Output' are fuzzy subsets.

The control rules for speed are formulated using behavior of PMSM. Derivation of control rules are based on following criteria for PMSM.

1. When speed error is more positive then to catch up the reference speed, current reference has to be more.
2. When speed error is small positive and change in speed error is large then current reference has to be kept constant to avoid overshoot.
3. At zero speed error current reference has to be unchanged.
4. At negative speed error current reference has to be negative.

Same way the control rules are formed for d-axis and q-axis currents. all 99 rules are processed be the inference engine.

3.5.4 Performance Optimization via Tuning

Design of a robust controller needs tuning of FLC parameters [11]. One method is to tune the rule base of FLC; other method is to tune scaling factors. As shown in block diagram of FLC, there are three (two input and one output) scaling factors G_e, G_{ce} and G_u used. The scaling factors are tuned depending upon the parameter of PMSM, inverter, load, and reference speed. The type, number and interval for each type of membership functions are given in Table 3-3.

The structure of current controllers is similar to speed controller as shown in Figure 3.13, but the scaling factors are different, because input and output requirements of each controller are different. Thus scaling factors are also different to bring them into same range specified by their corresponding membership functions. In this paper for the linguistic variable of current controller triangular membership functions are used between the interval [-2 2], for speed controller the interval is [-15 15] as given in

Table 3-3. To get the actual error and change in error in the range specified for corresponding controller, gains blocks are used. The control rules will be executed only when the inputs; e' and 'ce' are normalized using gain blocks, in the range specified for the corresponding controller. In work max-min algorithm is used to produce output fuzzy variable from inputs processed by control rules. The output variable from inference engine is converted to a crisp value in defuzzification stage.

3.6 Performance Evaluation of PMSM Drive

The FVC for PMSM is first implemented in MATLAB (version R2009a) on the PC having Intel core 2 duo CPU having 2.80 GHz processor and 4 GB RAM. In Simulation dc voltage for the inverter is kept 250 V. MAMDANI type inference engine is used for the realization of fuzzy controller. In the experimentation dSPACE version DS1104 is used for prototyping. The pulses to the inverter devices are given through digital I/O of dSPACE. Three phase inverter used here is an intelligent power module (PEC16DSM01) make Vi

Microsystems. Feedback signals are given to ADC channels for further processing and calculations. The parameters of PMSM are given in Table 3-4.

Table 3-4 Parameters of PMSM

Parameter	***Value***
Resistance (R_s)	2.0 ohm
d-axis inductance (L_d)	4.5 mH
q-axis inductance (L_q)	4.5 mH
Inertia (J)	0.8×10-3 kgm2
No of Poles (P)	8

The main feature of the drive system refers to its capability to operate within given speed and torque limits, and follow the reference command values. The performance of the proposed FVC is evaluated in terms of speed response, and torque response. The transient performance is also observed during change in reference speed and change in load. As explained earlier purpose of vector control is to control the speed and torque of machine independently. During the load change, motor, speed will also change, but is has to regain original value as fast as possible, it directly shows the effectiveness of controller.

Two controllers are used for d-axis and q-axis current control and one controller for speed control. Speed controller takes speed error as input and generates q-axis current reference. The voltage references for d-axis and q-axis are generated by two current controllers. Space vector pulse width modulated inverter is used to feed power to three-phase PMSM [66]. The FSC generates the torque component of stator current and the two FCC generate d-axis and q-axis voltage reference V_d and V_q for SVPWM inverter. These d-axis and q-axis reference voltages are then converted to V_α and V_β, which act as input to the SVM inverter, which feeds power to the motor. Here, the resolver is used for the position and speed measurement, which is attached to the motor assembly.

Figure 3.15−Figure 3.21 show the performance of vector controlled PMSM drive with different speed and current controllers. Figure 3.15 shows the speed response with conventional vector control with speed PI and current PI controller. The speed controller is replaced by a fuzzy controller as FSC; the performance of vector controlled PMSM drive with FSC and current PI controllers is shown in Figure 3.16. It is clear from the waveform that speed waveform has more ripples with PI controllers. To improve the performance FVC is applied and the speed response is shown in Figure 3.17. The application of FVC reduces the speed ripples as shown in Figure 3.15−Figure 3.17. With speed PI and current PI controller the speed waveform has ripples and more overshoot as compared to FVC.

The FVC shows the better performance, the three-phase stator currents at load change with FVC is shown in Figure 3.18. As shown in the stator currents waveform the change in load torque is independent of change in speed. Figure 3.19 and Figure 3.20 show the torque and speed response with change in load torque and speed response respectively. As shown in Figure 3.19 shows the torque response with change in load at 0.5s, 1.0s, and 1.5s, the result shows that the torque generated by PMSM is independent of change in reference speed as shown in Figure 3.20. Figure 3.21 shows the three-phase stator currents at load change during starting.

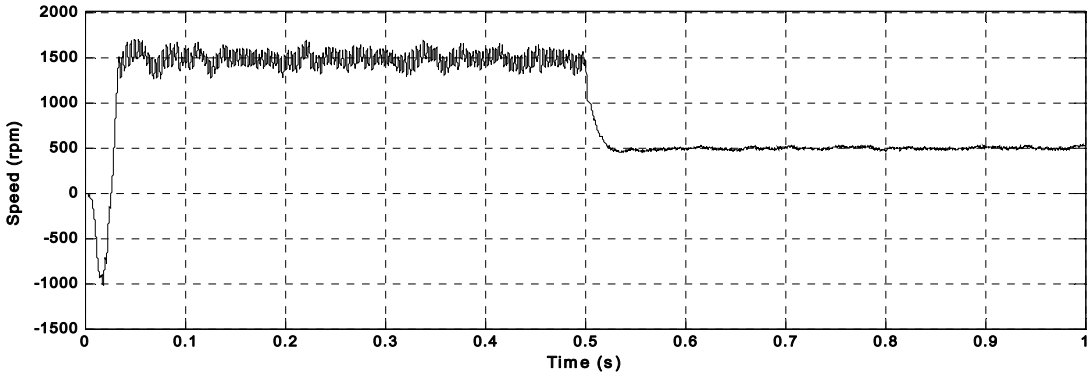

Figure 3.15 change in reference speed with speed PI and current PI controller

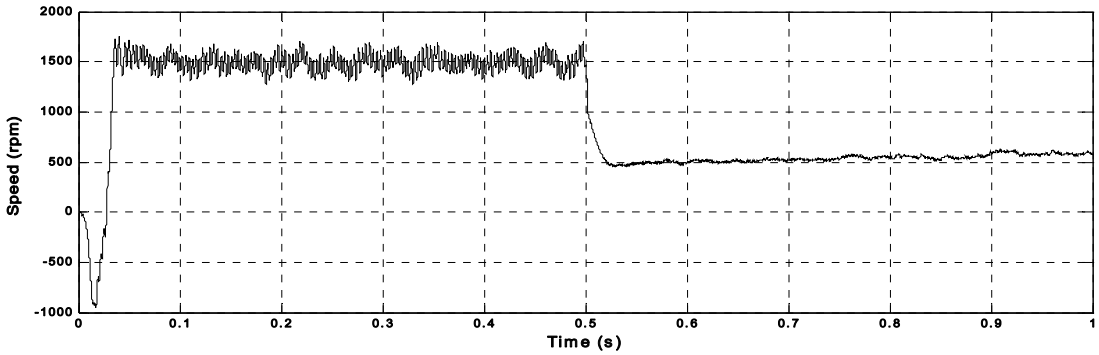

Figure 3.16 Speed performance with FSC and current PI controller

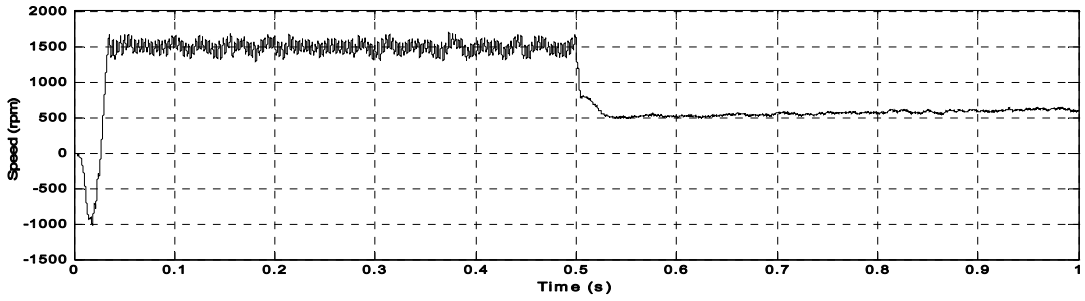

Figure 3.17 Speed performance with FVC

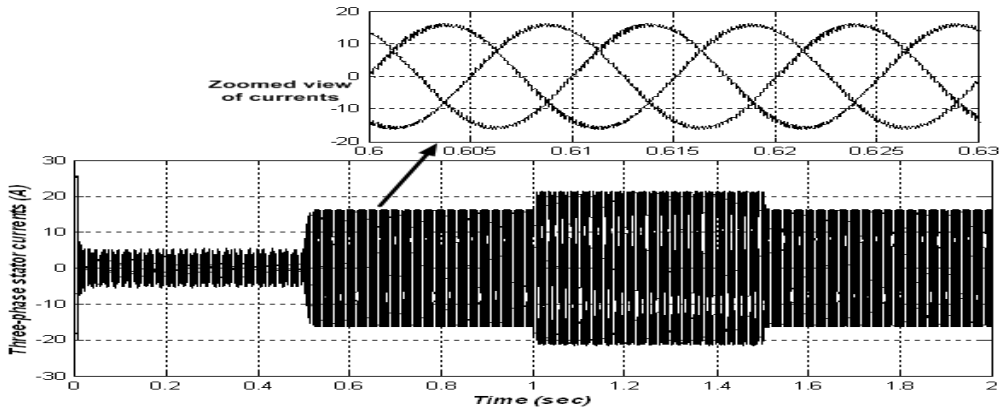

Figure 3.18 Three-phase stator currents at load change with FVC

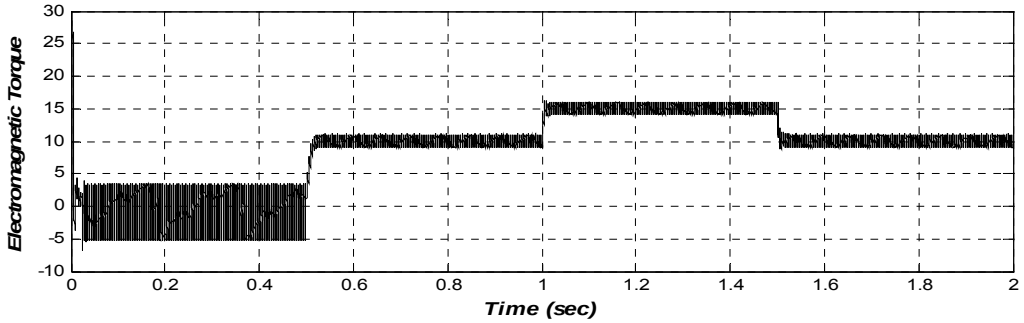

Figure 3.19 Torque performance with FVC

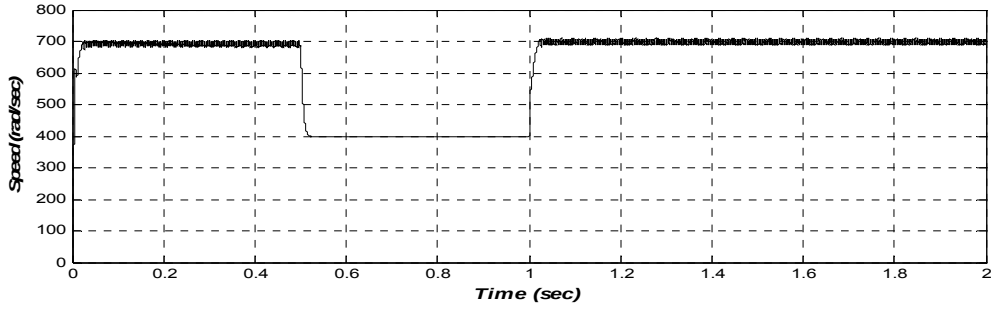

Figure 3.20 Speed change with FVC

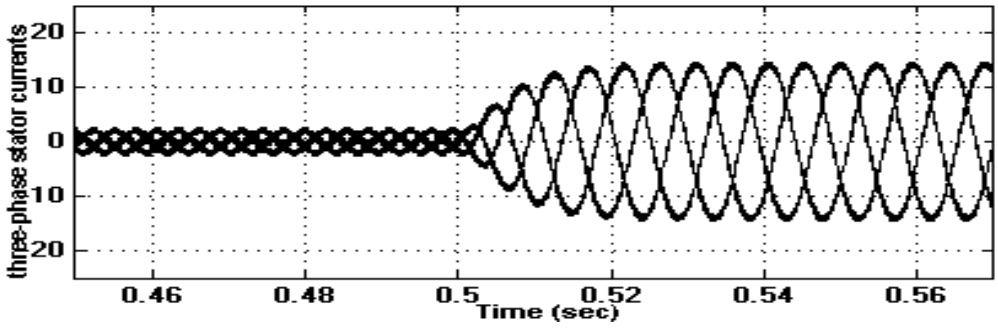

Figure 3.21 Three phase stator currents of PMSM with FVC

Table 3-5 Comparison of results for vector controlled PMSM drive with different controllers

Controller	Speed Response	Torque Response
PI Speed and PI Current	More ripples	More ripples
FSC and PI Current	Less ripples	More ripples
PI Speed and FCC	More ripples	Less ripples
FVC	Less ripples	Less ripples

Table 3-5 gives a summary of performance with different speed and current controllers. The comparison shows that the proposed FVC has better performance as compared to conventional PI controllers.

3.7 Conclusion

The PMSM with FVC shows an excellent performance under variable operating conditions. The vector control is applied to achieve the independent control of speed and torque in PMSM drive. The d-q model of PMSM is used for this purpose, as the quantities in d-q reference frame are independent and time invariant. The PI controller is generally used in drive applications, as speed controllers and as current controllers. A closed-loop PMSM drive has total three controller, one speed controller and two current controllers. Here in this work all these three controllers are replaced with fuzzy logic based controllers, and termed as fuzzy vector controller. The performance of FVC is investigated under various operating conditions, with different reference speed and load torque commands.

CHAPTER 4: POSITION SENSORLESS CONTROL OF PMSM DRIVE

[This chapter starts with requirements of a position sensor; drawbacks associated with use of these sensors and ways to operate the sensorless PMSM drive in close-loop are discussed. The cost of sensor is 10% of the cost of PMSM upto 10kW, but for the production units having large number of units, the sensors have to be eliminated. The importance of rotor position in implementation of vector control is highlighted. The advantages of sensorless drive are given and different position estimation methods are discussed in details with their significance and limitations. A sliding mode observer with adaptive feedback gains for sensorless PMSM without saliency is presented, the simulation results are shown to establish the feasibility of the observer.]

4.1 Introduction

In the closed-loop operation and control such as vector control, direct torque control of PMSM drive rotor position is required to achieve the proper commutation sequence between phases and properly align the stator current vector as discussed in chapter 3. The rotor position information is usually obtained by encoders or resolvers attached to rotor shaft. However, the use of these position sensors reduces the noise immunity, and increase the size, cost and weight of system. Elimination of these position sensors is highly encouraged to increase the reliability and robustness and reduce the cost of drive. In many applications, where no extra space is available for the mounting of additional sensors, methods developed to achieve the successful operation of drive without position/speed sensor is referred as “sensorless control”. Considering these shortcoming of using position sensors, sensorless PMSM drive is a topic of keen interest since last two decades in high performance drive application. The advantages of using sensorless control methods are lower cost, reduced size, reduced number of cables and connections, reduced complexity of hardware, better noise immunity, and increased reliability, and less maintenance requirement.

The rotor position is of critical importance for high precision control of PMSM, moreover speed feedback is also needed in the speed control-loop. Therefore, a suitable sensorless control strategy is to be developed depending on saliency present in the machine, precision required, and the cost which must be justified for required performance of drive application. The resolver is used for PMSM for position measurement, as compared to encoders the cost of resolver if higher. For the fractional-horsepower machines the percentage cost of sensors comes out to be more with respect to overall cost of drive. The signal flow between control circuit and sensors may be influenced by the electromagnetic interference (EMI) caused by external sources which leads to measurement error affecting the drive performance in feedback control [67].

Sensorless techniques for ac machines that rely to fundamental excitation are capable of providing high performance control in the medium to high-speed operation [68-70]. However, as the speed is lowered, the performance of these methods degrades and may fail at very low speed near zero.

A large number of methods are presented in the literature for low speed sensorless operation of PMSM with full load. The starting methods of sensorless PMSM are of three types; first one is to start from predetermined position, which can be obtained by applying the suitable stator current to align the stator magnetic field with rotor magnet flux. Performance of this method is affected by load torque. Second method is to start the machine in open-loop; it adjusts the acceleration to follow the stator magnetic field. This method also suffers in presence of load torque, as the time profile choice is a critical parameter. The third method is to obtain the position of rotor at standstill or at low speed by specific algorithms like, observers, Kalman filters, high frequency injection etc. The advantages of using a sensorless scheme are as follows.

- Compact drive with reduced maintenance,
- No cabling is required for transducers, easy implementation and reduced noise,
- Decreased cost of drive,
- Suitable for hostile operating environment; temperature and humidity etc.

There are a lot of sensorless control strategies in the literature, each of them having its own advantages, disadvantages and limitations. The term “sensorless control” does not mean that PMSM is being controlled without any sensor. It actually describes the position sensorless control which means that no position sensor will be used only voltage and current sensors are used in the entire control algorithm. These measured voltages and currents are used in different calculations and used to estimate the rotor position and or speed of PMSM. The sensorless methods can be categorized as open−loop methods, close−loop methods and the methods based on non ideal property of motor.

4.2 Open-Loop Methods

Open loop methods based on motor fundamental model are easy for implementation, and have quick dynamic response. But these methods are vulnerable to parameters uncertainty and stator current measurement noise. Some of the open-loop methods are presented here.

4.2.1 Direct calculation

In the steady state the voltage equations of PMSM in d−q reference frame are time−invariant and contain the speed information. The expression for the rotor position angle [71] is given by−

$$\theta_r = \tan^{-1}\left(\frac{A}{B}\right) \tag{4.1}$$

Where

$$A = v_b - v_c - r_s\left(i_b - i_c\right) - L_d p\left(i_b - i_c\right) - \sqrt{3}\omega_r\left(L_q - L_d\right)i_a$$

$$B = \sqrt{3}\left(v_a - r_s i_a - L_d p i_a\right) + \omega_r\left(L_q - L_d\right)\left(i_b - i_c\right)$$

The rotor position can be obtained in stator reference frame in terms of machine voltages and currents; provided ω_r is expressed in terms of available voltage and currents. The rotor speed is evaluated by assuming $L_d = L_q = L_s$ as given below.

$$\omega_r = \left(\frac{\sqrt{C}}{D}\right) \tag{4.2}$$

Where,

$$C = \left(v_a - r_s i_a - L_s p i_a\right)^2 + \frac{1}{3}\left[v_b - v_c - r_s\left(i_b - i_c\right) - L_s p\left(i_b - i_c\right)\right]^2$$

$$D = \lambda_m$$

Now the rotor position can be obtained in terms of stator quantities by putting the value of ω_r in equation(4.1). The initial rotor position is obtained by putting ω_r =0, in equation (4.1) and given by−

$$\theta_{r0} = \tan^{-1}\left(\frac{E}{F}\right) \tag{4.3}$$

Where,

$$E = \frac{1}{\sqrt{3}}\left[v_b - v_c - r_s\left(i_b - i_c\right) - L_s p\left(i_b - i_c\right)\right]$$

$$F = \left(v_a - r_s i_a - L_s p i_a\right)$$

The above equations are very easy to implement and gives good dynamic response. The measurement noise causes the error in calculation due to derivative terms. The uncertainty and parameter variations are the major problems in this method.

4.2.2 Estimation of Rotor Position by Integration of Back-EMF

For a balanced three-phase system, the back-emf space vector $\vec{e}_s$ is expressed as–

$$\vec{e}_s = \vec{v}_s - r_s \vec{i}_s = e_{s\alpha} + j e_{s\beta} = e_{sd} + j_{sq} \tag{4.4}$$

In the steady state stator and rotor flux vectors rotate synchronously, the angle between these two is load torque angle. If the stator flux vector is known, the rotor flux vector can be calculated which clearly specify the rotor position.

For the SMPMSM mathematical equations are symmetric in α–β reference frame. The stator flux in d–q reference frame can be easily obtained by simple integration.

$$\psi_{ds} = \int \left(v_{ds} - r_s i_{ds} \right) \tag{4.5}$$

$$\psi_{qs} = \int \left(v_{qs} - r_s i_{qs} \right) \tag{4.6}$$

The angle of stator flux vector is given by –

$$\theta_{\psi_s} = \arctan\left[\frac{\psi_{qs}}{\psi_{ds}} \right] \tag{4.7}$$

The rotor flux is difference of total flux and stator flux and the rotor flux vector can be calculated as–

$$\vec{\psi}_r = \vec{\psi}_s - r_s \vec{i}_s \tag{4.8}$$

The deceive parameter in this integration of stator resistance r_s, which increases with temperature. A small error in r_s affects $r_s \cdot i_s$, and it dominates when v_s reaches towards zero.

In back-emf, in terms of the phase voltage and currents, -

$$\begin{aligned} \vec{e}_s &= \left[v_a - \frac{j}{\sqrt{3}} \left(v_a + 2v_b \right) \right] - r_s \left[i_a + \frac{j}{\sqrt{3}} \left(i_a + 2i_b \right) \right] \\ &= v_a - r_s i_a + j \frac{1}{\sqrt{3}} \left[\left(v_a + 2v_b \right) - r_s \left(i_a + 2i_b \right) \right] \end{aligned} \tag{4.9}$$

Where,

v_a, i_a, v_b, i_b are the voltages and currents of phase “A” and “B” respectively;

$\vec{i}_s$ is the space vector of stator current;

$e_{s\alpha}$ and $e_{s\beta}$ are the components of back-emf space vector along stationary real and imaginary axis.

Theoretically it is assumed that the argument (inverse tangent or arctan) of the back-emf is the rotor position. The actual rotor position is difference of argument of $\vec{e}_s$ in stator reference frame, and the argument of the same vector in rotating reference frame. The expression of correct rotor position at steady state with $i_d = 0$ is given by–

$$\theta_r = \tan^{-1}\left(\frac{e_{s\alpha}}{e_{s\beta}} \right) - \tan^{-1}\left(\frac{\lambda_m}{L_q i_q} \right) \tag{4.10}$$

The first term in the above equation is phase of $\vec{e}_s$ vector in stationary reference frame and second term referred as "current–offset term" is the angle of $\vec{e}_s$ computed in rotor reference frame. Equation (4.10) presents two singularities when i_q or $e_{s\alpha}$ reaches zero crossings. As the arctan function converges to $\pm\pi/2$, so these singularities can be easily managed since at this point argument diverges to ∞. In the high-level languages these singularities can be easily eliminated in the pre-processor directives itself. The four–quadrant inverse–tangant function ("atan2") is suitable alternative to arctan function.

This method is satisfactory at medium and high-speed where back-emf is very low. There are two major deficiencies in the back-emf integration method at low speed are: pure integration problem and sensitivity to the stator resistance. The integrator has some advantage of reducing the switching losses. Since the back-emf varies with speed, the conduction period of inverter switches routinely adjusts inversely proportional to speed and the switching also adjusts automatically with change in speed. Similar to other back-emf based control schemes precision is a problem at low speed and the machine employing this method is not self starting. The high performance drives current control is important since it instantaneously controls the torque. The back-emf integration method can be used to have high quality current and instantaneous control of torque in all operating modes [72].

This method is not suitable for high performance applications bit it gives a way to use the measured back-emf to estimate speed by rotor flux, and to design sliding mode observer and other close loop estimation algorithm which uses back-emf of machine to estimate rotor position and speed of motor.

4.2.3 Estimation using Extended EMF

Among all available control methods of SMPMSM cannot directly be used for IPMSM. The position information is included not only in back-emf or flux, but also in the inductance profile due to saliency present in the rotor of IPMSM. The control method of SMPMSM can be used for IPMSM with utilization of extended emf as suggested [73, 74].

$$\begin{bmatrix} v_d \\ v_q \end{bmatrix} = \begin{bmatrix} R + pL_d & -\omega_r L_q \\ \omega_r L_q & R + pL_q \end{bmatrix} \begin{bmatrix} i_d \\ i_q \end{bmatrix} + \begin{bmatrix} 0 \\ \left(L_d - L_q\right)\left(\omega_r i_d - p i_q\right) + \omega_r K_E \end{bmatrix} \quad (4.11)$$

In this way the voltage equation of IPMSM will be identical to SMPMSM without any approximation. So in a symmetric form the extended is expressed as–

$$e_{ex} = \left(L_d - L_q\right)\left(\omega_r i_d - p i_q\right) + \omega_r K_E \quad (4.12)$$

The performance of estimation method based on this suffers during transient state of motor because the extended emf is subjective to motor currents. In the low-speed range the performance is not fine due to very small signal-to-noise ratio of extended emf.

4.2.4 Estimation using Inductance Variation

When the stator winding inductance is a function of rotor position then rotor position can be estimated from the measured winding currents and its rate of change [75]. This estimation method is applicable even when motor is at standstill and back-emf is zero. In case of IPMSM (with geometrical saliency; i.e. $L_d \neq L_q$) the stator winding phase inductance is function rotor position θ_r and varies twice of frequency of rotor speed [12]. In SMPMSM there is no geometrical saliency ($L_d = L_q$), the saliency is only due to saturation effect.

4.2.4.1 Saliency due to Saturation Effect: SMPMSM

In a PMSM, because of saturation effects, the stator inductances are a function of the rotor position. This variation can be used for the estimation of the rotor position. The variation arises even in a PMSM with surface-mounted magnets. In such a machine, due to saturation in the stator teeth the direct-axis synchronous inductance is smaller than the quadrature-axis synchronous inductance and these inductances are functions of the rotor position. It can be shown that, in general, these inductances depend on 2β, where β is the angle of the magnet flux (with respect to the stator-voltage space vector). It is possible to determine β even at standstill by applying test stator voltages with different directions (angles with respect to stator reference frame) and by measuring the resultant changes of stator current space vector. This can he proved by considering the stator voltage equation at standstill. Thus by neglecting the stator resistance, from the stator voltage equation we find that $di_s/dt = v_s/L$ holds, where v_s and i_s are the space vectors or the stator voltages and currents respectively, and L is a complex inductance, which depends on 2β. This technique can be used for the detection of the stator flux in the zero-speed region.

4.2.4.2 Saliency due to Geometrical Effect: IPMSM

A PMSM with interior magnets behaves like a salient-pole machine, and the inductances are different in the direct and quadrature axes, furthermore, it should he noted that $L_{sq} > L_{sd}$. The inductance variation can again be used for the estimation of the rotor position and the inductances can be obtained by using the monitored stator voltages and currents. In a PMSM with interior magnets, the inductances of d-axis and q-axis are different due to physical structure as the magnets are covered by iron, so the reluctance along d-axis is more as compared to q-axis. However, in the magnetic circuit on the quadrature-axis of the rotor there is only iron, and in the direct-axis of the rotor a part of the magnetic circuit consists of the magnet whose permeability is approximately equal to that of air. Thus the reluctance in the direct-axis is increased and the inductance is decreased, and since the reluctance in the direct axis is much larger than in the quadrature axis, $L_{sq} > L_{sd}$ arises.

In general, due to the saliency, all the stator inductances vary with ($2\theta_r$), where θ_r, is the rotor angle. For example, the phase "A" stator inductance can he expressed as–

$$L_a = \frac{\left[v_a - e_a - r_s i_a\right]}{di_a / d_t} \tag{4.13}$$

Where, $e_a = K\omega_r = K\dfrac{d\theta_r}{dt} = K\left[\dfrac{\theta_r(t_2) - \theta_r(t_1)}{t_2 - t_1}\right]$

Before performing the measurement of L_a first the variation of L_a with the rotor angle is obtained using the known values of L_d and L_q. The value of L_a, L_b and L_c are as given by–

$$L_a = \frac{L_q + L_d}{2}\left[\frac{L_q - L_d}{3}\right]\left[\cos 2\theta_r - \cos\left(2\theta_r - 2\pi/3\right)\right] \tag{4.14}$$

$$L_b = \frac{L_q + L_d}{2}\left[\frac{L_q - L_d}{3}\right]\left[\cos\left(2\theta_r - 2\pi/3\right) - \cos\left(2\theta_r - 4\pi/3\right)\right] \tag{4.15}$$

$$L_c = \frac{L_q + L_d}{2}\left[\frac{L_q - L_d}{3}\right]\left[\cos\left(2\theta_r - 4\pi/3\right) - \cos\left(2\theta_r - 2\pi\right)\right] \tag{4.16}$$

The variation of stator inductance with respect to rotor position is shown in A look-up table will be created containing corresponding inductances with rotor position using equations (4.14)–(4.16)

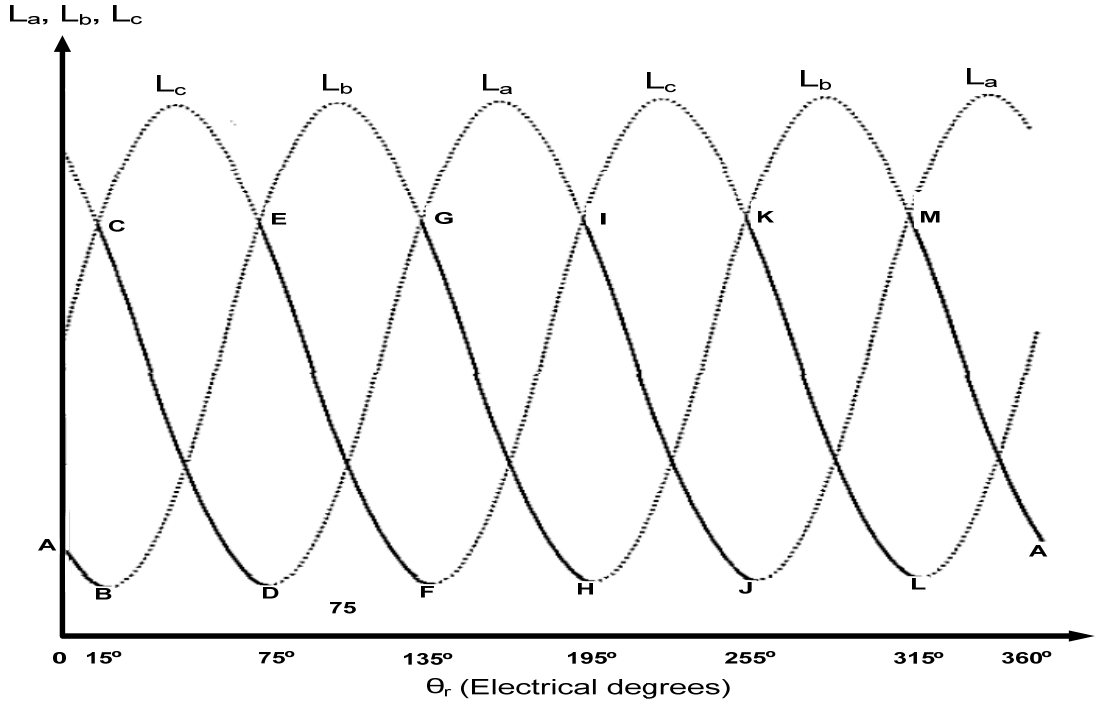

Figure 4.1 Stator phase stator phase inductance with rotor position

This table can then be used for the estimation of the rotor angle by using measured values of these inductances. Estimation of the accurate rotor position requires knowing the L_d and L_q very precisely. In theory the rotor position can be estimated from the measured inductance L_a only, but it must be considered that since it varies with twice the rotor angle, in every electrical cycle it goes through 2 cycles and a specific value of the inductance corresponds to four different rotor positions. For example, as shown in Figure 4.1, the value of L_a is the same at four points C, G, I, and M. Therefore, to obtain explicit rotor-position estimation for a specific value of the measured inductance, the information of all three inductances (L_a ,L_b and L_c) has to be used by calculating them during different intervals of each electrical cycle.

A simple way is that if the appropriate inductances are measured in advance, in the AB, CD, EF, GH, IJ, KL, and MA intervals shown in Figure 4.1. To accomplish this L_b is measured from point A to point B in Figure 4.1(0º to 15º electrical degrees interval), L_a is measured from point C to point D (15º to 75º), and L_c is measured from point E to point F (75º to 135º). Then L_b is then measured from point G to point H (135º to 195º), L_a is measured from point I to point J (195º to 255º), L_c is measured from point K to point L (255º to 315º), and finally L_b is measured from point M to point A (315º to 375º (360º plus 15º)). The measured inductance values are stored in the look-up table, e.g. for every 0.1º steps. However, since only parts of each inductance variation are utilized to estimate the rotor position, the look-up table has to be only 60 electrical degrees long and a position estimator using this scheme with an accuracy of 0.1 electrical degrees requires only 1200 stored elements (memory locations).

The estimations (calculated based on (4.14)–(4.16)) have inevitably some errors and leads to erroneous estimation. Another important point to be noted is that this is an open-loop method, so the exactness of estimation cannot be guaranteed under different variations like change in load, speed, or any other parameters. In case of stator flux saturation due to high current even then the estimation based on this look-up table.

The techniques based on the inductance saliency can estimate the rotor position at standstill and near zero speed, at medium and high speed the inductance saliency measurement is not possible due to back-emf.

The open-loop methods are simple for application, these methods are susceptible to motor parameter uncertainty, and these methods are not directly in use for high performance applications.

4.3 Closed-Loop Methods

Using measured voltages and or currents with a close-loop observer like Kalman Filter, Extended Kalman Filter (EKF), Luenberger Observer (LO), Sliding Mode Observer (SMO), Model Reference Adaptive System (MRAS) etc, high performance drive can be implemented without using position sensors. The performance of close-loop estimators (observers) is enhanced in contrast to the open-loop methods. Most of the close-loop methods use machine fundamental equations and measured back-emf, which has a lesser magnitude in low-speed range, so the estimation performance is not as fine as in high-speed range.

One of the techniques is to construct a state observer based on motor model including electrical and mechanical equations. Then stability of the observer is an important issue in providing accurate position information for motor drive system. In order to stabilize the system, a gain of the observers has to be optimized. As reported in literature the in state observer based methods (EKF, ELO, SMO) parameters are used as state and can be estimated along with position and speed [27, 76, 77].

4.3.1 MRAS based Estimation

In this the redundancy of two machine models of different structures are used to estimate the same state-variable. The model which is not dependent on state variable to be estimated is selected as reference model, and the second one is selected as adjustable model which involves the quantity to be estimated [15, 43-46]. The structure of MRAS for the estimation purpose shown in Figure 4.2, where quantity 'x' will be generated by both the models and error between two gives the error 'e'. The error signal is given to a self-adaptive organization which processes the error using a controller and drives reference model to estimate the desired quantity. In Figure 4.2, 'u' is the control input given to both reference model and adjustable model.

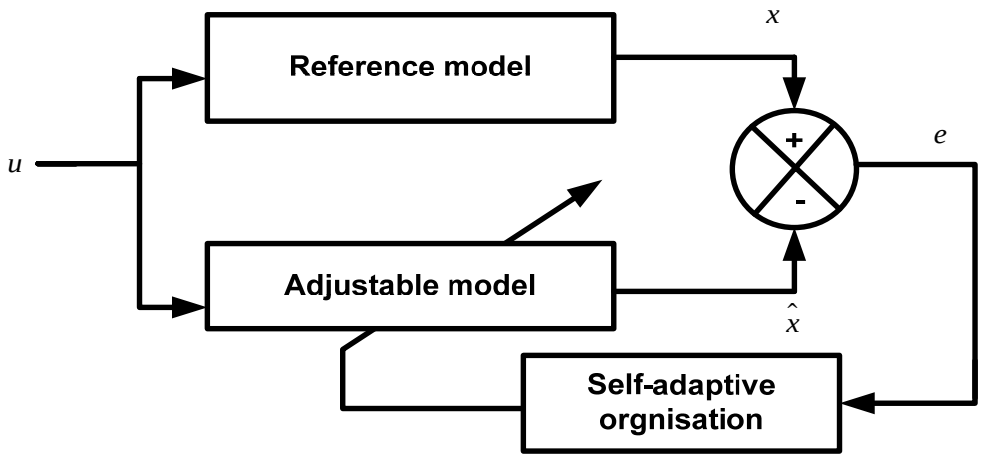

Figure 4.2 Structure of MRAS for estimation

In the literature various approaches are available to generate this error signal for adaptive mechanism. In [78] a flux model of PMSM is used to obtain the error, in [79] voltage model of PMSM with HF injection is used.

It does not matter that which quantity is being used for error generation, and which model is used, ultimately the rotor speed will be estimated because the every adjustable model has to be dependent on the speed. In order to achieve the sensorless operation of PMSM drive, an observer based on MRAS is designed for estimation of speed based on mathematical model of PMSM. The mathematical model of the any observers (SMO, ELO, etc.) is developed based on mathematical of system for which an unknown quantity has to be estimated. The speed estimation in PMSM a current model of PMSM is used as adjustable model the implementation block diagram of MRAS based speed estimation in sensorless PMSM drive is shown in Figure 4.3. In MRAS only adjustable model should depend on unknown parameter[47], the reference model is independent of speed. This method is simple and requires less computation.

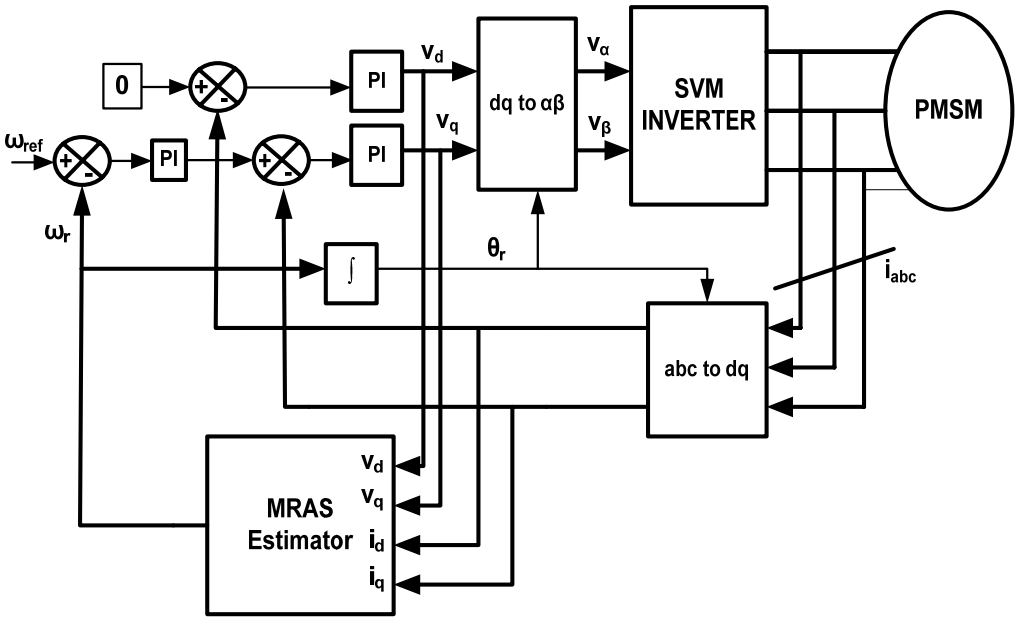

Figure 4.3 MRAS based implementation of sensorless PMSM drive

In the estimation of speed in sensorless PMSM drive using MRAS, the PMSM itself act as reference model and current model of PMSM in d–q reference frame selected as adjustable model. Both the models provides/estimates the rotor speed, the error between the estimated quantities generated by two models is used to tune the adjustable model with the help of an adaptive mechanism having a controller inside. In general the PI controller is used inside the adaptive mechanism to process the error and generate the tuning signal ω_r to tune adjustable model which is dependent on ω_r.

The sensorless vector controlled PMSM drive using MRAS based speed estimation is discussed, implemented, and analyzed in detail in chapter 5.

4.3.2 Sliding Mode Observer (SMO) based Estimation

For the estimation of rotor position and speed of PMSM, a large number of techniques are presented in literature; many of them has motor parameters (stator resistance, winding inductance, torque constant, inertia) dependency problem. The traditional linear estimators are not adaptive in nature for non-linear systems to change in the operating conditions. A non-linear observer/estimator is capable to operate with a non-linear system with adaptive nature.

A full state observer [80] is designed using dynamic machine model and voltage equations for the speed and position estimation. Its real-time implementation has many restrictions as, in operating conditions the parameters of dynamic equations like inertia, and viscosity friction coefficients are not well defined. In the high-speed region, an iterative sliding mode observer [81] used to estimate back-emf and further rotor position of PMSM. In a sapling period of PI current controller the conventional sliding mode observer was recursively iterated many times then chattering components superimposed on estimated back-emf and currents were decreased.

The sliding mode observers (SMO) exemplify a fancy way to design a speed observer based on the motor equations, but not only limited to basic structure. *Among the available sensorless methods* ***the SMO has been acknowledged as a successful control method due to its appealing features like; less sensitivity to motor parameter variations and disturbance rejection capability, for high performance electric drive applications.*** The SMO based estimation is applicable for both SMPMSM and IPMSM.

4.3.3 Extended Kalman Filter (EKF) based estimation.

In 1960 and 1961 Rudolf Emil Kalman worked and published many papers in the area of recursive predictive filtering that is based on recursive algorithms and state space equations. After that the field of estimation got revolutionized and Kalman filter has been a subject of extensive research. The state of a dynamic system can be estimated even when the accurate model of system in not known. This filter is found to be very powerful due to its estimation of past, present and even future states. The Kalman filter has two states prediction and correction, in the prediction the state is predicted with dynamic model and it is corrected by observation model. With these two steps the error covariance of estimator is minimized, so it an optimal estimator.

The Kalman filter is suitable to linear systems and for the non-linear systems extended Kalman filter discovered by Stanley F. Schmidt. The major problem of this Kalman filter for non-linear systems is more complex and time-consuming calculations, even this problem can

be solved by pre-computation of different matrices; dynamic matrix 'F', state transition matrix 'Φ' and the observation matrix 'H'. But in case of the non-linear systems, these matrices are the function of state and accordingly change with every time-step and can't be computed in advance.

The Kalman Filter is a mathematical model that runs in parallel to the actual system and gives estimations of the physical values of a linear system. The Extended Kalman Filter has been derived from the classic Kalman Filter to be used with non-linear systems. The extended Kalman filter is a generalized algorithm for the estimation in non-linear systems such as PMSM. An EKF is a recursive optimum state estimator and used for state and parameter estimation in dynamic non-linear system in real time by noisy monitored signals. The source of noise considered measured noise and modeling inaccuracies. In the PMSM, the EKF used to estimate the speed and rotor position, it is possible as the well known mathematical model of PMSM is available. The objective of EKF is to acquire the immeasurable states like position and speed of motor using measured states (voltage and current), and statistics of measurements and noise (i.e. covariance matrices 'Q', 'R', 'P' of system noise vector and the system state vector measurement noise vector). The computational inaccuracies, measurement error and modeling errors can be taken into account by proper noise inputs.

During the prediction stage next predicted value of state x(k+1) and previous values of estimated states by mathematical model. The predicted state covariance matrix 'P' is obtained before the new measurement by mathematical model and system covariance matrix 'Q'. In the second stage (filtering) the new estimated state $\hat{x}(k+1)$ is obtained from predicted state predicted state $x(k+1)$ by adding a correction term $K\left(y-\hat{y}\right)$ to predicted value; (y) is the actual output vector and $\left(\hat{y}\right)$ is the predicted output vector, K is the Kalman gain. The K is to be chosen to minimize estimation error and the computation is realized using recursive relations.

A decisive part of design is to correct the initial values of various covariance matrices, since they are usually not known. The EKF can be implemented in real-time using a significant fast processor. The design steps of discretized EKF based estimator for sensorless PMSM drive implementation are as given below -

1. Selection of time-domain model of PMSM
2. Discretization of motor model
3. Determination of state and noise covariance matrices **Q, R, P**
4. Implementation of discretized EKF based estimator and tuning.

4.3.3.1 Time-Domain Model of PMSM

The EKF can be implemented using time-domain model of PMSM expressed in stator reference frame or rotor reference frame. The selection of reference frame will affect the execution time of algorithm, as the EKF is already computationally intensive so it can be a basis of comparison with other techniques. The voltage equation of PMSM in stator reference frame and rotor reference frame is already given in mathematical modeling presented in chapter 2.

To obtain the state-space model of PMSM voltage equations are arranged into state-variable form, where i_d and i_q are selected as state-variables. The state-space form is–

$$\dot{x} = Ax + Bu \tag{4.17}$$

$$y = Cx \tag{4.18}$$

Where,

$$A = \begin{bmatrix} -R/L & \omega_r & 0 & 0 \\ \omega_r & -R/L & 0 & 0 \\ 0 & 0 & 0 & 0 \\ 0 & 0 & \omega_r & 0 \end{bmatrix}$$

$$B = \begin{bmatrix} \cos\theta_r/L & \sin\theta_r/L & 0 \\ -\sin\theta_r/L & \cos\theta_r/L & -1/L \\ 0 & 0 & 0 \\ 0 & 0 & 0 \end{bmatrix}$$

$$C = \begin{bmatrix} \cos\theta_r & -\sin\theta_r & 0 & 0 \\ \sin\theta_r & \cos\theta_r & 0 & 0 \end{bmatrix}$$

$x = \left[i_d, i_q, \omega_r, \theta_r \right]^T$; is the state vector,

$y = \left[i_D, i_Q \right]^T$; is the output vector,

$u = \left[v_D, v_Q, v_p \right]^T$; is the input vector,

In the rotor reference frame the voltage equations of PMSM are obtained by considering the transformed voltage and current space vectors expressed as–

$$v' = v_d + jv_q = v\exp(-j\theta_r) = (v_D + jv_Q)(\cos\theta_r - j\sin\theta_r) \tag{4.19}$$

$$i' = i_d + ji_q = i\exp(-j\theta_r) = (i_D + ji_Q)(\cos\theta_r - j\sin\theta_r) \tag{4.20}$$

The quantities (voltage and currents) with suffix ‘d’ represent the quantity expressed in rotor reference frame, and with suffix ‘D’ represent the quantity as expressed in stator

reference frame. These v_D, v_Q, i_D, i_Q are the stator d-q voltages and currents in stator reference frame means appears from stator side, $v_p = \omega_r \psi_m$ is the induced voltage in stator winding due to magnet flux and is constant, and i_d, i_q are the stator d-q currents in rotor reference frame or as seen from the observer on rotor. Only i_d, i_q not selected as state variable, and augmented with ω_r, θ_r which is to be estimated, for this instead of two voltage equations of PMSM two more equations will be required are $\omega_r = d\theta_r / dt$ and assuming $d\omega_r / dt = 0$. The equations (4.17)–(4.18) express the time-domain model of PMSM and can be visualize as shown in Figure 4.4. The obtained time-discrete model is of fourth order, non-linear, and time variant, it is used in EKF based estimation of state vector if the voltages and currents are sampled and measured.

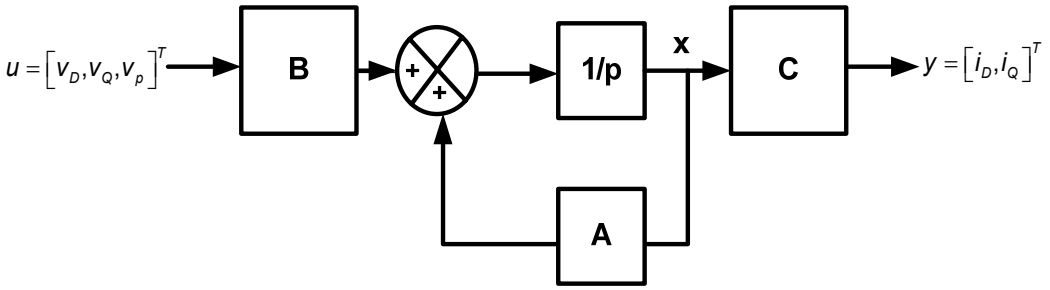

Figure 4.4 Block diagram of time-domain state-space model of PMSM

4.3.3.2 Time–Discrete Model of PMSM

The time-discrete model of PMSM is achieved by state-space equations (4.17)-(4.18) as given by–

$$x(k+1) = A_d x(k) + B_d(k) u(k) \tag{4.21}$$

$$y(k) = C_d(k) x(k) \tag{4.22}$$

The notation $x(t_k)$ is sampled value of x at t_k instant, in general $x(k)$ which strictly means $x(kT)$ which corresponds to value of x at k[th] sampling instant, where $T = (T_{k+1} - T_k)$ is sampling time. In above equations A_d and B_d are the discretized system matrix and noise matrix respectively and

$$A_d = \exp\left[A(k)\right] \approx I + A(k)T$$

$$B_d = B(k)T$$

I is the identity matrix and C_d is the discrete transformation matrix given by

$$C_d = C(k)$$

To achieve the satisfactory accuracy, sampling time should be significantly smaller than the characteristic time constant of drive. More clearly the sampling time should be based on the execution time of full EKF algorithm, acceptable accuracy and stability. The block-diagram of discretized state-space model of PMSM based on equation(4.21)–(4.22) is shown in Figure 4.5

The state vector is disturbed by noise vector 'v' (system noise vector) and the output vector 'y' is disturbed by noise vector 'w' (measurement noise vector) and are to be considered as–

$$x(k+1) = A_d x(k) + B_d(k) u(k) + v(k) \tag{4.23}$$

$$y(k) = C_d(k) x(k) + w(k) \tag{4.24}$$

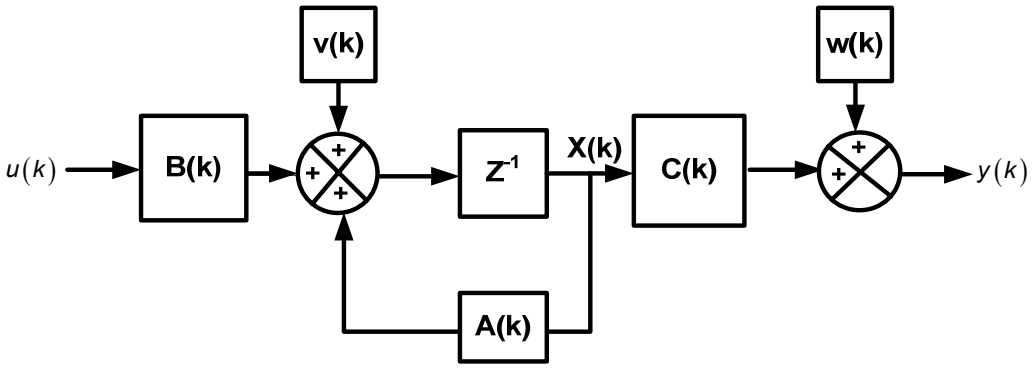

Figure 4.5 System model of EKF with time–discrete state–space model of PMSM

In general machine can't be perfectly modeled due to certain postulation, and measurement errors. It becomes possible to take into account of computational inaccuracies; measurement and modeling errors by adding a noise vector see Figure 4.5.

The noise vector v is zero–mean, white Gaussian noise and does not depend on initial state vector, and its covariance matrix is Q. the noise vector w is similar to w, and has covariance matrix R, these covariance matrices Q and R are assumed to be known.

4.3.3.3 Establishment of Noise and State Covariance Matrices

These covariance matrices have a significant influence on stability and convergence. The Q concerns for modeling error, system disturbances, and voltage measurement noise; R accounts for A/D quantization and current measurement noise. In general Q is a 4 by 4 matrix, P is 2 by 2, R is 4 by 4 matrix; total 36 covariance element is to be determined. though noise signals are not interrelated, so reduction of required element results; Q contain 4, R contain 2, and P contain 4 diagonal elements. The noise covariance matrices don't depend on d-q axes, so further reduction in elements is possible and first two element of Q are equal, first two element of P are equal and only two element of R are equal.

4.3.3.4 Implementation of Discrete EKF; Tuning

It is already discussed that during prediction stage next predicted state x(k+1) and covariance matrix P is obtained by using covariance matrix Q and state variables of PMSM. The estimated state $\left(\hat{x}\right)$ is obtained from predicted state during filtering stage by adding a correction term $K_e = K\left(y - \hat{y}\right)$ in predicted value$\left(x\right)$. The structure of EKF for PMSM is shown in Figure 4.6.

The tuning of filter is done by iterative modification to achieve the best estimate. The change in Q and R affect transient and steady state performance, if Q increases; the system noise increases or more parameter uncertainty and increased filter gain matrix leads to faster dynamic response and slower steady sate response. The increase in R means current measurements are subjected to stronger noise, therefore, it will be less weighted by filter and accordingly filter gain matrix will be reduced and transient performance becomes poorer.

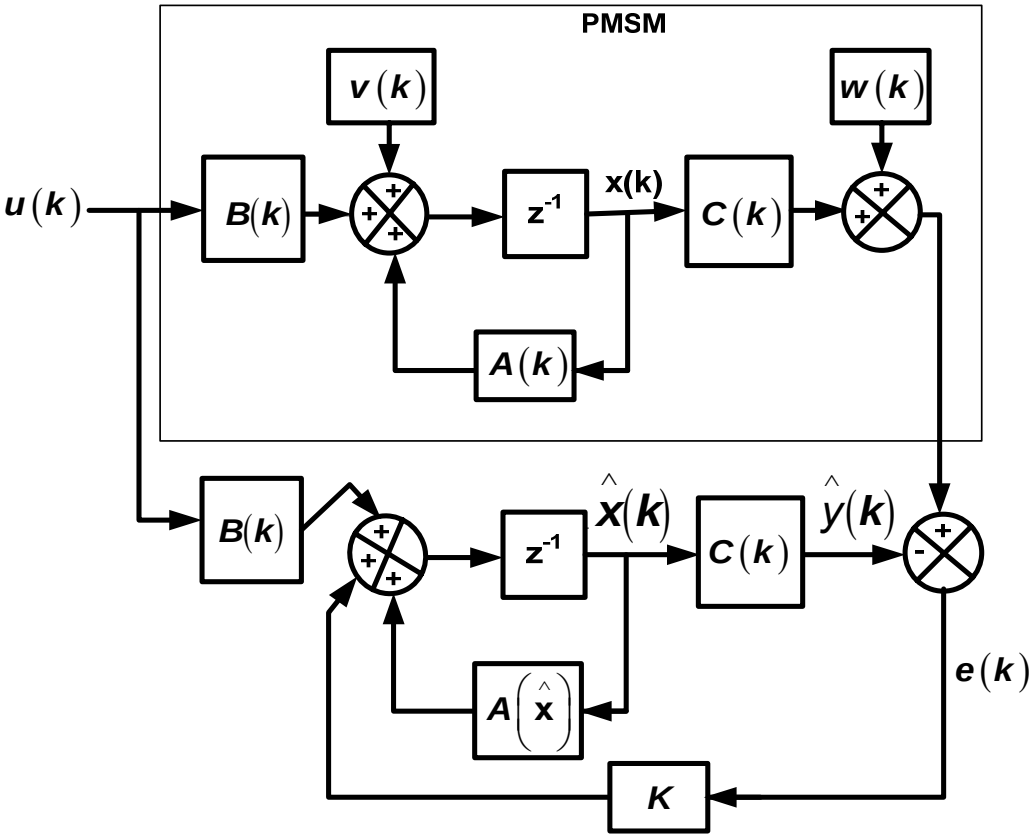

Figure 4.6 EKF Structure for PMSM

In general the tuning of covariance matrices is based on trial and error method. When the EKF is not tuned properly according to system, it is a non-optimal filter for which tuning is the one of major drawbacks of this algorithm. The EKF presented here is implemented in

rotor reference frame (d–q), if it will be implemented in stator reference frame (α–β), the filter may converge to incorrect estimation (for example –ω and or θ+π), and then special procedures can to be taken. The EKF algorithm for IPMSM undergo with another problem of complex motor dynamic voltage equation as EKF is already computationally intensive.

The EKF explained above can be used for speed and position estimation in both steady-state and transient conditions in a wide speed range but not at zero speed and insensitive to parameter variation.

However, the EKF method presents many drawbacks [13, 14, 33]:

- The EKF estimation is very sensitive to the PM flux linkage error.
- The EKF diverges at start-up and the direction of rotation can be incorrect.
- The gains of the EKF filters are difficult to tune.
- The EKF implies lots of matrix calculation, and thus computing time.
- Zero speed and low speed operation is extremely difficult.

The complexity of the EKF method, and its limitation towards low speeds, make this algorithm not suitable for low cost and high reliability applications.

The above discussed methods are suitable for medium and high-speed range. The methods based on signal injection for initial position estimation and estimation in low-speed is presented below.

4.4 Position Estimation Methods at Standstill and Low Speed

The above discussed open-loop and close-loop estimation methods are based on the motor fundamental equations, the major problem of these methods is that the estimation performance decisively depends on the magnitude of BEMF which varies with rotor speed. The magnitude of BEMF at very low-speed is very low and sometimes can't be measured then performance of the estimator is degraded. The initial rotor position detection is also having an important role in smooth start-up and drive operation in all speed-range. An estimator is said to be applicable and sufficient to all speed-range if it includes the zero-speed estimation. As a consequence the PMSM must be started in open-loop with random switching of inverter and brought-up to the speed at which the back-emf can be measured properly. The disadvantage of this method is that, if wrong switching is selected motor may run in wrong direction, it may be hazardous in applications like electric vehicle. So a initial position detection technique must be combined with a close-loop estimator for wide-speed range operation of drive. Some of the initial and very low-speed position detection techniques are discussed below. These methods depend on motor non-ideal properties like saliency ratio etc., not dependent on motor fundamental equations as the above methods do.

4.4.1 High frequency carrier injection

The scheme based on high frequency carrier injection use the saliency present in the machine for estimation of rotor position or flux. The saturation, slot harmonics, or the machine geometry causes the saliency. High frequency injection schemes bestow the high performance of drive in all speed range.

4.4.1.1 Rotating High-Frequency Carrier Injection

During 90s research in the area of sensorless control of induction machines, permanent magnet synchronous machines [32], switched reluctance motors and universal motors. The rotating high frequency carrier injection scheme was introduced by Professor R.D. Lorenz and his group. When a carrier signal of high frequency in injected on the fundamental excitation of a machine having saliency, response to this carrier signal contains the position information. As a carrier, voltage or current may be injected but the voltage injection is preferred because in case of current injection the required bandwidths for current regulators are very high even larger than carrier frequency.

Initially for the induction machines the saturation induced saliencies were basis of estimation, latter the slot harmonics, redesign of rotor slot opening, modifying the rotor bars, etc., based estimation were evaluate as the saturation based saliency was dependent on the operating conditions. In spite of the researches in the area of rotating carrier high frequency injection still there is no universal method for all type of induction machines. There is a limited number of the published work for rotating high frequency carrier injection based estimation for the PMSM. In [82] a rotating high frequency carrier was tested on an IPMSM, the bandwidth of position estimate exceeded 100 Hz.

4.4.1.2 Pulsating High-Frequency Carrier Injection

For the IPMSM [83] first pulsating high frequency carrier voltage was applied in estimated q-axis and the d-axis current response was demodulated and found proportional to the position error. The d-axis voltage injection for the position estimation was used in [84]. The response of carrier was transformed to a coordinate system π/4 displaced from estimated d-axis. In this coordinate system, the difference of squared components of current provides a term which is proportional to sine of twice angular displacement of estimated d-axis from real d-axis. The position estimate was by an alternative error: sine of carrier angle was multiplied to q-axis current and the resultant was low pass filtered similar to [83] but there injection is done in q-axis and the measurement is done in d-axis. The d-axis injection method was tested for PMSM, SRM and IM [83-87].

4.4.2 Low-Frequency Signal Injection

The online parameter estimation of rotor time constant based on pseudo random noise in the estimated d-axis of an IM, where acceleration of machine was given as input and position was measured for the rotor time constant. It was implemented by using a step-command in d-axis current and monitoring the acceleration of rotor, when applied pulses were smaller than time constant there was no torque response and estimated position equaled actual position. The sensorless control of IM by low frequency signal injection in d-axis is also realized in [88]. The operation of sensorless SMPMSM using low frequency injection was presented in [89], but the bandwidth performance was not clearly given. Due to the low frequency of injected signal, the sensorless schemes based on low frequency signal injection essentially have low bandwidth.

4.4.3 Transient excitation

In 1975 the rotor position was obtained by step voltages in field winding of a salient-pole synchronous machine [90]. The position dependent inductance of stator winding of PMSM which may be caused by saturation effect can be used to estimate rotor position at standstill and at low speed. One of the methods is INFORM (Indirect flux detection by online reactance measurement) [31], in which the current change were measured by applying the voltage pulse. The major drawback of this method was the operation of drive must be resumed during measurement, and the measurements were taking hundreds microseconds. Another drawback is that in steady-state the ripples cause in current by applied test voltage. In [91] the PWM modulator was reorganized to make all six vectors active for minimum time in every switching period, and derivative of current was measured at zero–speed. A further improvement to this was given in [92] by hardware sampling arrangement which increased the ADC resolution and tested for IPMSM, 300 ms settling time and 20rad/sec position response was obtained. The commercialization of INFORM was done in 2002 [93].

"All signal injection methods response on the same philosophy and the main difference among these are type of excitation signal and type & number of response signal measured. These, methods requires additional signals, extra hardware; cabling, sensors, ADCs. The replacement of one speed or position sensor by many other sensors observably limits the use of the injection based sensorless methods."

The discussed close-loop observers are superior to the open-loop methods. A feedback calibration is used and the convergence is assured. These methods are based on motor fundamental equations and back-emf, therefore the performance is underprivileged at low speed as compared to high-speed range.

4.5 Artificial Intelligence Based Estimation

The speed and rotor position of PMSM can be estimated by using a supervised feed forward multilayer ANN with back propagation training. The ANN (Artificial Neural Network) contains input layer, hidden layer and output layer, the number of input and output layers are known as per the inputs and required output for estimator however the number of hidden layers is not known in advance. This number of hidden layers and number of hidden nodes in hidden layers is determined by trial and error based on accuracy required; in general one or two hidden layers are used for estimation in drive application. The number of input nodes depends on input data (i_d and i_q) or the data used for training. When stator current is used as input, it uses present and past inputs $\left[i_d(k), i_d(k-1), i_q(k), i_q(k-1)\right]$ to avoid the dependency on mathematical model which is a greater advantage of ANN based estimator over other methods, since the well trained ANN is capable of estimating any non-linear system. Similar to EKF, ANN is also requires intensive calculations.

To overcome the limitations with ANN, a neural network with fuzzy features are used and so-called neural fuzzy estimator. The neural network with supervised learning uses a fixed inputs, outputs and structure based on the physical system (where estimation or control is to be done), however every time it may not be possible to match trained ANN with available system. The fuzzy-neural system combines the advantage of both fuzzy and neural and avoids the individual limitations of both, in this structure of network is based on the fuzzy logic and number of layer and number of nodes are known. In fuzzy number of membership functions, membership functions themselves, number of rules needs to be known. The adaptive fuzzy-neural network can be used for automated design and tuning of estimator.

The estimation methods of speed/position for PMSM are; open-loop methods, closed-loop methods and initial position estimation methods are presented above in detail. The outcome of this literature survey for the schemes suitable for the particular application needs to be summarized here as given in Table 4-1.

Any position/speed estimation method for PMSM drive has its own advantageous features and restrictions in form of cost, implementation complexity and feasibility.

Table 4-1 Summary of some position-sensorless methods for PM motor

Methods	constraints
Direct back-emf measurement	Sensitivity to switching transients Suffers at low speed Requires a starting method
Estimation of back-emf	Sensitivity to change in motor parameter
Special signal injection in the stator winding	Motor must have some degree of saliency
Monitoring switching states on inverter	Needs a starting method
Monitoring current/ calculation of phase inductance	Requires a start-up method from rest Limitation at high speed and high current Motor must have variable inductance profile
Observer based methods	Needs a starting method Requires d-q transformation Complexity is a major issue

For every controller application, it is always true that ***"there is always a compromise between cost, complexity and performance"***.

Although several methods are presented here for speed and position estimation of PMSM, numerous factors remain vital, to appraise their effectiveness for a high performance low cost drives. Some of the factors are as-

- Steady state error
- Dynamic performance
- Low speed operation
- Noise sensitivity
- Parameter sensitivity
- Implementation complexity
- Computation time
- Robustness

The open-loop methods are easy to implement, but they have poor dynamic performance, the closed-loop methods show low steady-state error and good dynamic performance, and needs a complex hardware as compare to open-loop methods. The artificial intelligence methods need a sufficient fast processor and large computing time. A performance wise comparison with their advantage and limitations are given here in Table 4-2.

Table 4-2 Comparison of schemes for sensorless PMSM drive

Method	Implementation	negative aspect	Parameter dependency	Earnings
Open- Loop	Easy	Poor dynamic performance	High	Low cost
MRAS	Less complex	at Low speed	Yes (except R_s)	Free from integration
Observer	Medium	Computation time	Yes	Good dynamic performance
EKF	Complex	Computation time	Low	Robust
Artificial intelligence	Medium	Need fast processor	Medium	Robust Good noise rejection
SMC	Medium	Chattering	Medium	No extra electronics

"Kalman filter and the other artificial intelligence and high frequency signal injection methods can be effective over a wide speed range, but their wide application range is handicapped by the complex/tedious computing algorithms. The major difference between a Luenberger observer and a sliding mode observer is just use of observer structure; SMO uses sign of the error whereas the Luenberger observer uses a linear feedback".

After going through the literature presented in this chapter, sliding mode controller is selected, as it has a major advantage that it does not need extra electronics for the implementation of algorithm. Furthermore, the variation of motor parameters has little impact on the results accuracy.

The SMC has following attractive features over other non-linear control.

- SM control offers large signal handling capability.
- It provides stability and provides better regulation over a wide operating range.
- Robustness of SM controller is better.
- It provides fast dynamic response because all control loops act concurrently.
- The actual system parameters have a little impact on the system response.
- Implementation of SM controller is simple as compared to other nonlinear controllers.

Therefore considering these advantages of sliding mode controller it is selected for the estimation of rotor position of PMSM drives. The sliding mode observer is implemented and analyzed in this thesis in detail in further section.

4.6 Sliding Mode Observer for Sensorless PMSM Drive

The sliding mode observer for the position estimation in PMSM drive is capable of estimate the rotor position in medium and high speed range with good response. As the back-emf is needed so it needs a starting method. In many industry applications, initial position sensing is not necessary, and an open-loop starting is used.

4.6.1 Sliding Mode control

To design a robust control system for a higher-order non-linear system, sliding mode control (SMC) is a proficient technique. The precise modeling is not essential due to the key features of SMC; less sensitivity to parameters deviations and external disturbances. The SMC shows easy design complexity as it has capability of decoupling the whole system motion into different small independent motions. The SMC is fundamentally a outcome of discontinuous control and can be easily implemented by general power converters with “on–off” feature. Due to these attractive features it has a wide application range in process control, electric drives, electric vehicles, motion control and robotics.

The term “*sliding mode*” first used in context to relay operation, the control as function of system state which switches at very high (theoretically infinite) speed, this motion is referred as sliding mode. In the real-time implementation, the imperfection in the switching devices causes the control switching at high frequency or take midway values for the continuous approximation of relay function.

The sliding mode in terms of state-space form for a second-order time-variant relay system with control input–

$$\ddot{x} + a_2 \dot{x} + a_1 x = u \tag{4.25}$$

Where

$u = -M\,\mathrm{sign}(s)$

$s = \dot{x} + cx$

and a_1, a_2, M, c are constant.

The behavior of system in state plane $\left(x, \dot{x}\right)$ is shown in Figure 4.7, for $a_1 = a_2 = 0$. At switching line s=0, u becomes discontinuous and state trajectories are constituted by two boundaries: the first is $s > 0$ and $u = -M$ (upper semi plane) and second is $s < 0$ and u=M, (lower semi plane). The state trajectories are oriented towards the switching line between m–n, for $t>t_1$ and this motion on the switching line is the sliding mode. Since the trajectories coincides to switching line s=0 in course of sliding mode and the equation is treated as motion equation–

$$\dot{x} + cx = 0 \tag{4.26}$$

And the solution for this–

$$x(t) = x(t_1)e^{-c(t-t_1)} \tag{4.27}$$

This is not depending on parameter and disturbances. It is the *invariance* property which is a promising feature for designing control system for a dynamic plant operating in environment with uncertainties.

The above is presented for an ideal model, for the real-time applications the trajectories are confined to some vicinity on the switching line as shown in Figure 4.8. The deviations of trajectories from the ideal model may be caused by imperfection in the switching devices, dead zones, delays and time-constants of sensors, and produce high frequency oscillations as shown in Figure 4.7 and Figure 4.7. These high frequency oscillations are referred as "*chattering*" and are obstacle in use of SMC for control applications and are being paid a serious attention to chattering suppression techniques in modern research.

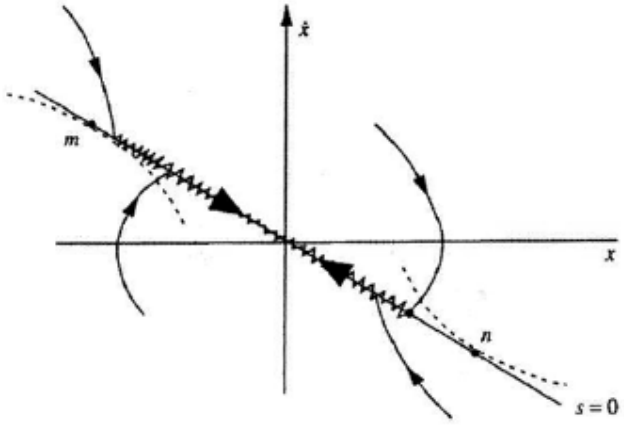

Figure 4.7 Behavior of second-order system in state plane

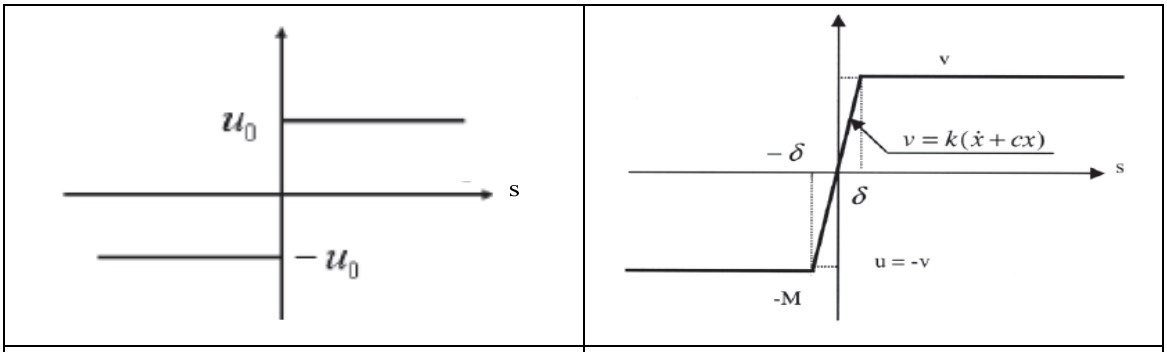

(a) Ideal system | (b) Practical system

Figure 4.8 Vicinity of switching line

At a δ-vicinity of line s=0, the control becomes a linear state function with gain k, and the eigenvalues are close to –k, and –c. It is clear that motions in the vicinity has fast components decaying and slow components solution of an ideal SMC. The equation (4.26) is ideal model of sliding mode. The main key points in use of SMC is as follows–

4.6.1.1 Chattering

The chattering phenomenon is already defined in above section; as the discontinuity in the feedback control causes a specific unwanted behaviour in the vicinity of surface as shown in Figure 4.9. Chattering is one of the major disadvantages of using SMC. It basically occurs between the theoretical recommendations and practical implementation. In the continuous control system the fast component of motion decays rapidly and the slow components depends on small time-constants, whereas in the discontinuous control the system performance also depends on a small parameter continuously. In the discontinuous control signal excite the system dynamics at fast rate which produces the oscillations in the state vector at higher frequency due to fast switching.

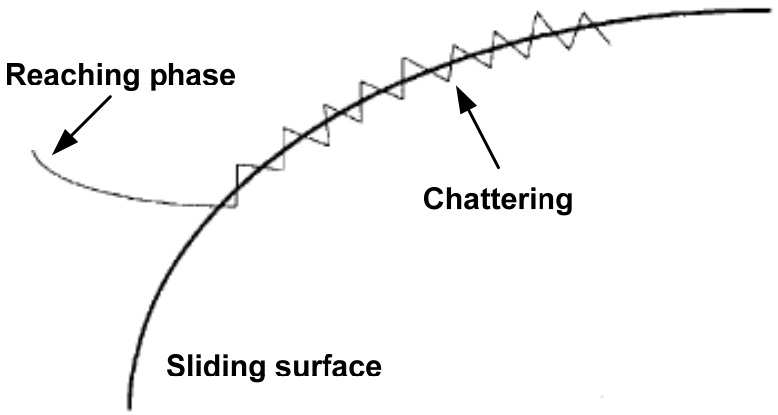

Figure 4.9 Chattering phenomenon

These oscillations are known as chattering problem and results low control accuracy, extra heat loss in the electrical power circuit and wear loss in the mechanical moving parts. The reduction or elimination of chattering phenomenon in SMC is an area of further research.

4.6.1.2 Robustness and Disturbance Rejection

It is a great advantage of insensitivity to system dynamics, which can be utilized for development of a robust control system for a plant operating in presence of external disturbances. This disturbance rejection capability of SMC can be explained in physical language. , since the sign of actuator signal varies, and may be either converging or diverging. The average output value is equal to disturbance with opposite sign due to high switching frequency in sliding mode. And then the disturbance to be rejected must be lie between diverging and converging exponential functions.

The design procedure of SMC has two sub-problems to be solved independently.

- Design of required dynamics for system of (n X m) order by properly selecting sliding manifold s = 0.
- Try continuously to enforce the sliding motion into this manifold equivalent to stability problem of m^{th} order system.

In principle the sliding mode can be achieved only in with discontinuous control and infinite switching frequency. As for as the implementation of SMO is concerned, no such sliding mode take place due to limited switching frequency and current sampling rate. The boundary solution is used to solve this problem by using saturation function in place of discontinuous control which transforms the sign function into a boundary layer of sliding mode manifold. By using this invariance property of sliding mode is fractionally preserved as the state trajectories motion and further convergence can't be guaranteed.

4.6.2 Sliding Mode Observer Design for PMSM

There are two critical issues in design of Sliding Mode Observer (SMO) design for PMSM; one is of less magnitude of Back-emf in low-speed range and other is in the high-speed range high switching gain to ensure the convergence of SMO. There is a compromise between estimation position and minimum operating speed, and it depends on quantization error of discrete –time controller. The other way to improve the low-speed performance of SMO by high switching gain but it will introduces the more ripples in high speed range which increase the estimation error.

The sensorless estimation method using a feedback observer combined with motor has promising features. The PMSMs (SMPMSM) have very low inductance variance as compared to back-emf influence over the rotor angle; in that case the SMO can be designed

in α–β reference frame. In case of IPMSM where inductance saliency is more, then the observer designed in d–q reference frame can be used.

In this work the sliding mode observer for rotor position estimation is based on the discontinuous control of stator currents. The sliding mode manifold s(x)=0 is selected on stator current trajectory, as the stator currents in PMSM drive can be directly measured. The advantage of selecting this sliding mode manifold or sliding surface is that when stator currents ('state') reaches the sliding surface the sliding mode occurs and being enforced, estimated currents track the real currents and current estimation error forced to zero even in the presence of some external disturbances.

The PMSM model in α–β reference frame is given by-

$$\dot{i}_{\alpha\beta s} = -L_{\alpha\beta s}^{-1} r_{\alpha\beta s} \cdot i_{\alpha\beta s} + L_{\alpha\beta s}^{-1}\left(v_{\alpha\beta s} - e_{\alpha\beta s}\right) \tag{4.28}$$

And can be written in matrix form as-

$$\begin{bmatrix} \dot{i}_{\alpha s} \\ \dot{i}_{\beta s} \end{bmatrix} = \begin{bmatrix} -R_s/L_s & 0 \\ 0 & -R_s/L_s \end{bmatrix} \begin{bmatrix} i_{\alpha s} \\ i_{\beta s} \end{bmatrix} + \begin{bmatrix} 1/L_s & 0 \\ 0 & 1/L_s \end{bmatrix} \left(\begin{bmatrix} v_{\alpha s} \\ v_{\beta s} \end{bmatrix} - \begin{bmatrix} e_{\alpha s} \\ e_{\beta s} \end{bmatrix} \right) \tag{4.29}$$

As explained above for the PMSM without saliency (SMPMSM), the current estimator will be designed in same α–β reference frame.

$$\dot{\hat{i}}_{\alpha\beta s} = -L_{\alpha\beta s}^{-1} r_{\alpha\beta s} \cdot \hat{i}_{\alpha\beta s} + L_{\alpha\beta s}^{-1}\left(v_s^* + I \cdot Z_{eq} + Z\right) \tag{4.30}$$

The above equation (4.30) can be written in a simplified form as-

$$\dot{\hat{i}}_s = A \cdot \hat{i}_s + B\left(v_s^* + I \cdot Z_{eq} + Z\right) \tag{4.31}$$

Where,.

$$A = \begin{bmatrix} -R_s/L_s & 0 \\ 0 & -R_s/L_s \end{bmatrix}, \quad B = \begin{bmatrix} 1/L_s & 0 \\ 0 & 1/L_s \end{bmatrix}, \quad \hat{i}_s = \begin{bmatrix} \hat{i}_{\alpha s} \\ \hat{i}_{\beta s} \end{bmatrix}$$

$$v_s^* = \begin{bmatrix} v_{\alpha s}^* \\ v_{\beta s}^* \end{bmatrix}, \quad i_s = \begin{bmatrix} i_{\alpha s} \\ i_{\beta s} \end{bmatrix}, \quad Z_{eq} = \begin{bmatrix} Z_{eq\alpha} \\ Z_{eq\beta} \end{bmatrix}, \quad k = \begin{bmatrix} k & 0 \\ 0 & k \end{bmatrix}$$

$$Z = \begin{bmatrix} Z_{\alpha s} \\ Z_{\beta s} \end{bmatrix} = -K \cdot sign\left(\hat{i}_s - i_s\right) = -k \begin{bmatrix} sign\left(\hat{i}_{\alpha s} - i_{\alpha s}\right) \\ sign\left(\hat{i}_{\beta s} - i_{\beta s}\right) \end{bmatrix}$$

The equation (4.31) in matrix form becomes-

$$\begin{bmatrix} \dot{\hat{i}}_{\alpha s} \\ \dot{\hat{i}}_{\beta s} \end{bmatrix} = \begin{bmatrix} -R_s/L_s & 0 \\ 0 & -R_s/L_s \end{bmatrix} \begin{bmatrix} \hat{i}_{\alpha s} \\ \hat{i}_{\beta s} \end{bmatrix} + \begin{bmatrix} 1/L_s & 0 \\ 0 & 1/L_s \end{bmatrix} \left(\begin{bmatrix} v^*_{\alpha s} \\ v^*_{\beta s} \end{bmatrix} + I \cdot \begin{bmatrix} Z_{eq\alpha} \\ Z_{eq\beta} \end{bmatrix} + \begin{bmatrix} Z_{\alpha s} \\ Z_{\beta s} \end{bmatrix} \right) \quad (4.32)$$

Here, the Z_{eq} is the equivalent control vector, I is the feedback gain of Z_{eq}, k is switching gain of discontinuous control Z and k>0, '*' denotes command value, '^' represent estimated value. The equivalent control vector Z_{eq} is achieved by using a low-pass filter as-

$$Z_{eq} = \begin{bmatrix} Z_{eq\alpha} \\ Z_{eq\beta} \end{bmatrix} = -k \begin{bmatrix} sign\left(\hat{i}_{\alpha s} - i_{\alpha s} \right) \cdot \dfrac{\omega_c}{s + \omega_c} \\ sign\left(\hat{i}_{\beta s} - i_{\beta s} \right) \cdot \dfrac{\omega_c}{s + \omega_c} \end{bmatrix} \quad (4.33)$$

ω_c is the cut-off frequency of LPF, the time-constant of LPF should be selected small enough to conserve the low-frequency component (equivalent control) and large enough to eradicate high-frequency component. To ensure the actual motion close to ideal mode, the width of vicinity of sliding surface Δ should be small. With the reduction of Δ, the switching gain will be reduced and switching frequency will be increased or else 'state' may go beyond boundary layer which is undesirable. The cut-off frequency ω_c of LPF must be selected based on fundamental frequency of tracked phase currents.

Assuming $v_{\alpha\beta s} = v^*_s$, the sliding mode motion equation is obtained as-

$$\dot{S} = A \cdot S + B \cdot \left(e_{\alpha\beta s} + I \cdot Z_{eq} + Z \right) \quad (4.34)$$

Where S is the error vector and $S = \left(\hat{i}_s - i_s \right)$, if the switching gain 'k' of Z is large enough to ensure –

$$S^T \cdot S < 0 \quad (4.35)$$

then sliding mode occurs and it is obtained that

$$e_{\alpha\beta s} = \begin{bmatrix} e\alpha s \\ e\beta s \end{bmatrix} = -\left(1 + I \right) Z_{eq} \quad (4.36)$$

Using this back-emf equation(4.36), the rotor position is estimated as-

$$\hat{\theta}_r = -\tan^{-1}\left(\frac{e_{\alpha s}}{e_{\beta s}} \right) = -\tan^{-1}\left(\frac{Z_{eq\alpha}}{Z_{eq\beta}} \right) \quad (4.37)$$

In the digital control system with finite switching frequency, the discontinuous control is replaced by a saturation function similar to Figure 4.8 as shown in Figure 4.10. The block diagram of SMO for position estimation of PMSM is shown in Figure 4.11.

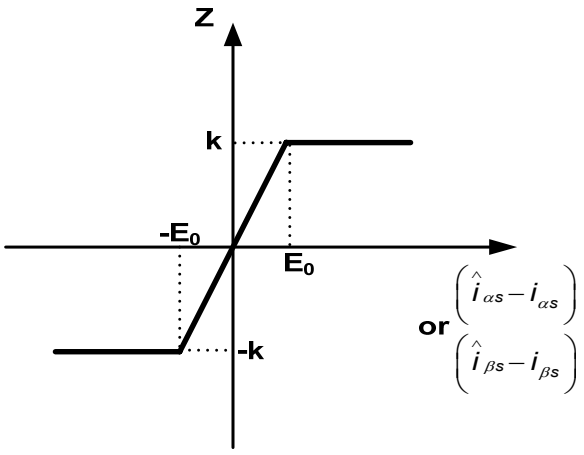

Figure 4.10 Saturation function

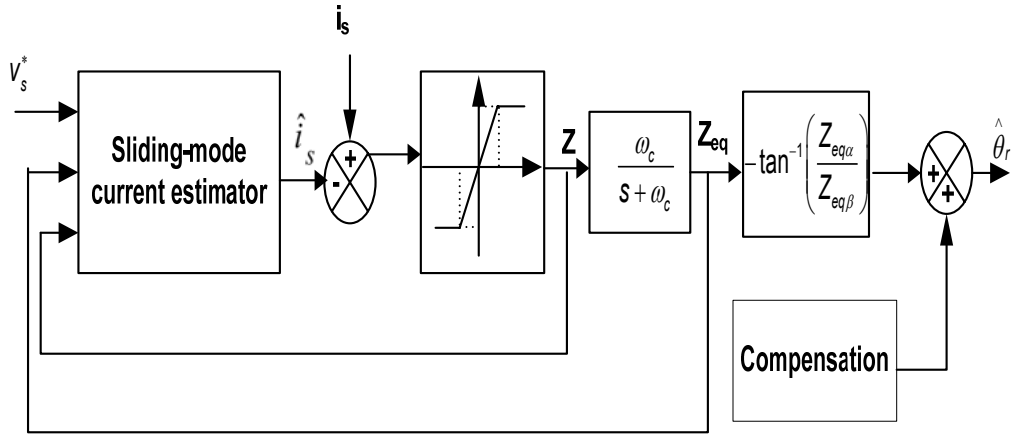

Figure 4.11 SMO for rotor position estimation of PMSM

4.6.2.1 Stability Analysis of the Observer

The stability analysis of the designed SMO is done using Lyapunov function. The Lyapunov function can be defined as-

$$V = \frac{1}{2} S^T \cdot S > 0 \tag{4.38}$$

The derivative of this positive definite Lyapunov function along the system trajectories will be-

$$\dot{V} = S^T \cdot \dot{S} = S^T AS + S^T B \cdot \left(e_{\alpha\beta s} + I \cdot Z_{eq} + Z \right) \tag{4.39}$$

Putting the value of Z_{eq} from equation (4.33) and the time-constant of LPF, $\mu = 1/\omega_c$ in equation (4.39), it comes-

$$\dot{V} = S^T AS + S^T B \cdot e_{\alpha\beta s} - k\left(1 + \frac{I}{\mu s + 1}\right) S^T B \cdot sign(S) \qquad (4.40)$$
$$= f_1 + f_2$$

Where

$f_1 = S^T AS$ and

$$f_2 = \frac{1}{L_s}\left[i_{\alpha s}\left\{ e_{\alpha s} - k \cdot \frac{\mu s + 1 + I}{\mu s + 1} sign\left(i_{\alpha s}\right)\right\} + i_{\beta s}\left\{ e_{\beta s} - k \cdot \frac{\mu s + 1 + I}{\mu s + 1} sign\left(i_{\beta s}\right)\right\}\right]$$

As the SMO is designed in the $\alpha-\beta$ reference frame, the value in the above expression changes based on the sign of the stator currents $i_{\alpha s}$ and $i_{\beta s}$, in same stator reference frame.

$$f_2 = \frac{1}{L_s}\left[i_{\alpha s}\left\{ e_{\alpha s} - k \cdot \frac{\mu s + 1 + I}{\mu s + 1} sign\left(i_{\alpha s}\right)\right\} + i_{\beta s}\left\{ e_{\beta s} - k \cdot \frac{\mu s + 1 + I}{\mu s + 1} sign\left(i_{\beta s}\right)\right\}\right], \begin{matrix} i_{\alpha s} > 0, \\ i_{\beta s} > 0 \end{matrix}$$

$$f_2 = \frac{1}{L_s}\left[i_{\alpha s}\left\{ e_{\alpha s} - k \cdot \frac{\mu s + 1 + I}{\mu s + 1} sign\left(i_{\alpha s}\right)\right\} + i_{\beta s}\left\{ e_{\beta s} + k \cdot \frac{\mu s + 1 + I}{\mu s + 1} sign\left(i_{\beta s}\right)\right\}\right], \begin{matrix} i_{\alpha s} > 0, \\ i_{\beta s} < 0 \end{matrix}$$

$$f_2 = \frac{1}{L_s}\left[i_{\alpha s}\left\{ e_{\alpha s} + k \cdot \frac{\mu s + 1 + I}{\mu s + 1} sign\left(i_{\alpha s}\right)\right\} + i_{\beta s}\left\{ e_{\beta s} - k \cdot \frac{\mu s + 1 + I}{\mu s + 1} sign\left(i_{\beta s}\right)\right\}\right], \begin{matrix} i_{\alpha s} < 0, \\ i_{\beta s} > 0 \end{matrix}$$

$$f_2 = \frac{1}{L_s}\left[i_{\alpha s}\left\{ e_{\alpha s} + k \cdot \frac{\mu s + 1 + I}{\mu s + 1} sign\left(i_{\alpha s}\right)\right\} + i_{\beta s}\left\{ e_{\beta s} + k \cdot \frac{\mu s + 1 + I}{\mu s + 1} sign\left(i_{\beta s}\right)\right\}\right], \begin{matrix} i_{\alpha s} < 0, \\ i_{\beta s} < 0 \end{matrix}$$

It is clear from equation (4.31) that A is negative definite and B is positive definite as the R_s>0, and L_s>0, then $f_1 = S^T AS$ is a negative function. If the LPF is assumed to have very high cut-off frequency then time-constant $\mu \ll 1$, f_2 will be negative only if-

$k \cdot \frac{\mu s + 1 + I}{\mu s + 1} > \left|e_{\alpha s}\right|$, and

$k \cdot \frac{\mu s + 1 + I}{\mu s + 1} > \left|e_{\beta s}\right|$

Then, the boundary limit for f_2 to be negative for a stable operation is-

$$k \cdot (1 + I) > \left|e_{\alpha\beta s}\right|_{\max} \qquad (4.41)$$

The above equation (4.41) gives a selection criterion for the switching gain 'k' for the discontinuous control and sliding mode to occur. The feedback gain of equivalent control 'I' must be more than -1, to satisfy the criteria defined by equation(4.41).

Therefore as per the Lyapunov stability criteria, the time derivative of defined Lyapunov function must be negative, here the derivative of Lyapunov function is negative as (4.41) with a high switching gain and testify the convergence to $S(t) = 0$ in fine time and shows occurrence of sliding mode. The discontinuous control is replaced by saturation function as

shown in Figure 4.10, approximate $sign(s)$, in E_0 vicinity of sliding mode manifold $S(t)=0$. Beyond vicinity $|S(t)|>E_0$, it is considered that $sat(S)=sign(S)$. In case of saturation the Z becomes saturation function as shown in Figure 4.10 and defined by-

$$Z=-k_s\left(\hat{i}_s-i_s\right) \tag{4.42}$$

Where $k_s=k/E_0$, putting this value of Z in (4.34), instead of using sign function it becomes-

$$\dot{S}=\left[A-(I+1)\cdot k_s\cdot B\right]\cdot S+B\cdot e_{\alpha\beta s} \tag{4.43}$$

Within the boundary layer the system is continuous and linear so the first convergence to boundary layer is guaranteed. To enforce the convergence during high-speed operation, the eigenvalues placement for linear system can be implemented.

4.6.2.2 Selection of Feedback Gain and Switching Gain

As discussed in the previous section that proper selection of feedback gain '*I*' accelerates the convergence rate and enforces the further convergence in the boundary. Selection the value of I (*I*>-1 once, provides the flexibility for selection of switching gain k to improve the tracking performance of currents and thereafter accuracy of rotor position estimation. The selection procedure for these gains below and above base speed is given as under -

- *Below the base speed,* $-1<I<0$

When the feedback gain I is in the range $-1<I<0$, the magnitude of equivalent control is always greater than magnitude of back-emf from the equation(4.36), by selecting the feedback gain in this range the Z_{eq} is amplified even at the low-speed where magnitude of back-emf is very low. By using proposed sliding mode observer with equivalent control, the extended minimum operating speed is achieved.

- Above base speed (field-weakening), $I>0$

The eigenvalues of $A-(I+1)\cdot k_s\cdot B$ goes smaller with increase in I, moving away from imaginary axis means faster convergence. This is a key characteristic for high-speed operation of any observer based estimation.

As compare to traditional sliding mode control here the switching gain k has to be smaller, to satisfy the same sliding mode condition defined in equation(4.41). Without changing the cut-off frequency of LPF with this method the oscillations can be reduced to get a smother estimated rotor position.

4.6.3 Implementation of SMO for Sensorless PMSM Drive

The implementation block diagram of sliding mode observer based sensorless vector-controlled PMSM drive is given in Figure 4.12. The vector control drive includes one speed controller and two current controllers, reference frame transformation blocks, space vector pulse width modulation based pulse generation and an inverter.

Speed controller takes speed error as input and generates q-axis current reference. The voltage reference for d-axis and q-axis are generated by two current controllers. Space vector pulse width modulated inverter is used to feed power to three-phase PMSM [66]. Measured voltage and currents are converted to two-phase stationary reference frame, and then these $v_\alpha, v_\beta, i_\alpha, i_\beta$ are given as input to the observer which estimates the rotor position using discontinuous current control. Here d-axis and q-axis reference voltages are then converted to V_α and V_β, which act as input to the SVM inverter, which feeds power to the motor.

The estimated speed is calculated by using PLL (Phase-locked-loop) with the rotor position provided by observer [94]. A PLL system is a closed-loop electronic circuit that controls an oscillator so that it provides an output signal that maintains a constant phase angle with respect to a reference signal, which can range from a fraction of Hz to many GHz. Vector control decouples the currents and including the current feedback loop. In the present work Lyapunov algorithm is used in the stability analysis and proper convergence of the observer. The compensation in θ_r is required and required compensation changes with speed.

In this work the sliding mode observer for rotor position estimation is based on the discontinuous control of stator currents. The SMO is designed in stationary reference frame as the motor is surface mounted type. In this approach the flexibility of selecting is discussed. The observer internal structure is as per Figure 4.11.

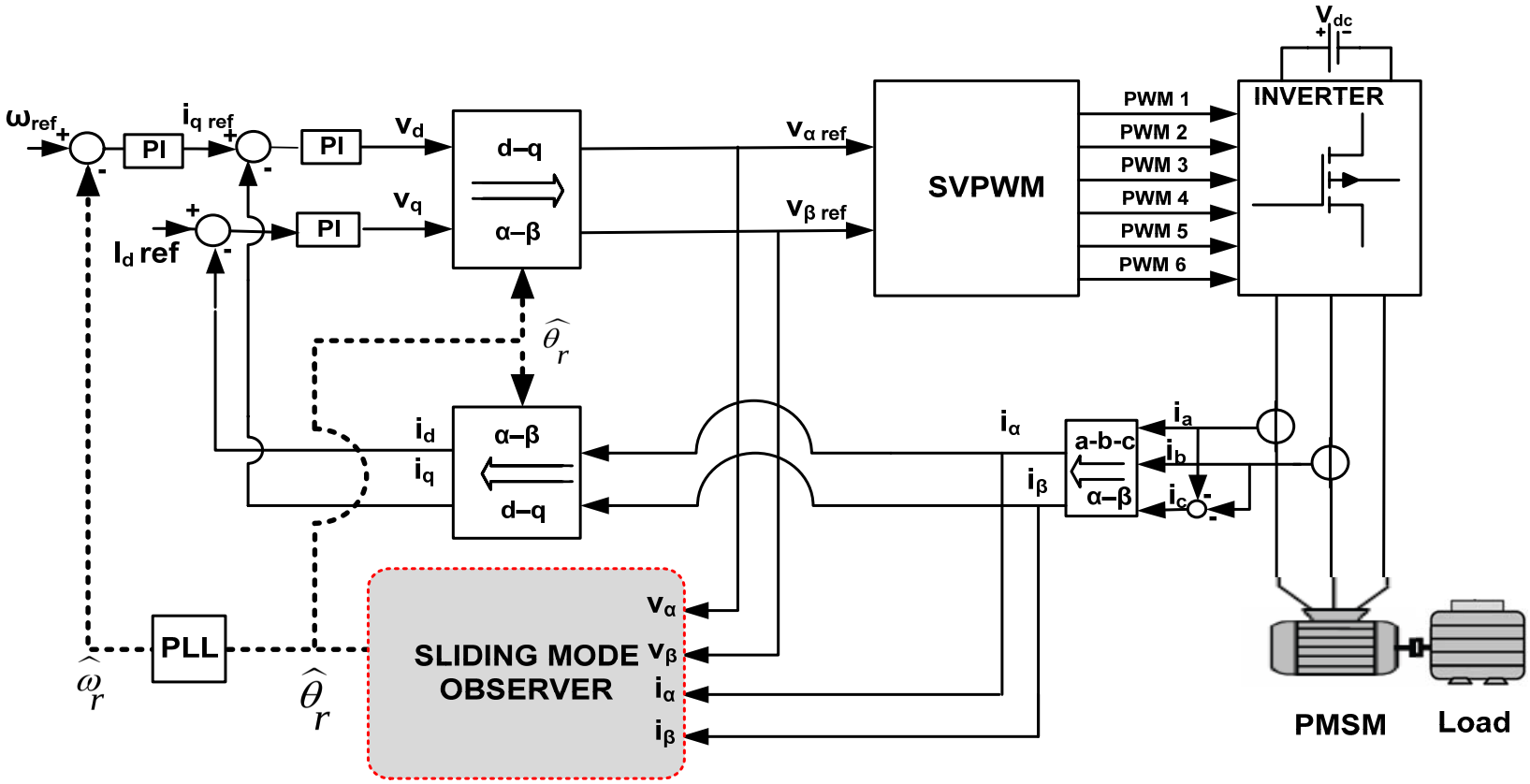

Figure 4.12 SMO based implementation of sensorless PMSM drive

4.6.4 Simulation Performance

The complete sensorless PMSM drive with siding mode observer is implemented in MATLAB (version R2009a) on the PC having Intel core 2 duo CPU having 2.80 GHz processor and 4 GB RAM. Two controllers are used for d-axis and q-axis current control and one controller for speed control all these are the PI controllers.

The output switching frequency of PWM is kept 5 kHz; the inverter dc voltage is kept 100 V for the SMO switching gain k is kept 70, the cut-off frequency of low-pass filter to achieve equivalent control is 20 kHz, the feedback gain is being changed for different values of reference speed and load torque. The overall system is sampled at every 20 μs. The feedback gain *l* is -0.7, and the Z has been sampled at very fast rate as compared to the system sampling time which is 20 μs. The space vector pulse width modulation technique is used for pulse generation.

Figure 4.13 shows the simulation performance of SMO based PMSM drive running at 50rpm. The Figure 4.13(a) shows the rotor position, Figure 4.13 (b), shows the estimated back-emf, and Figure 4.13 (c) shows the control Z_a.

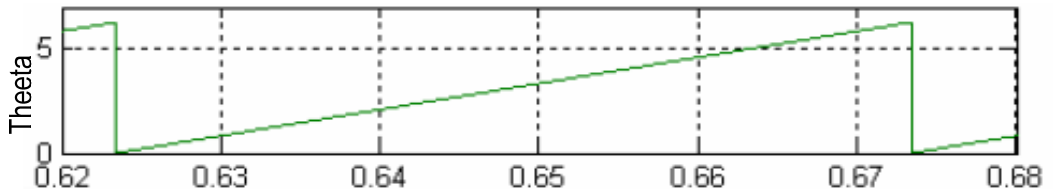

(a) rotor position

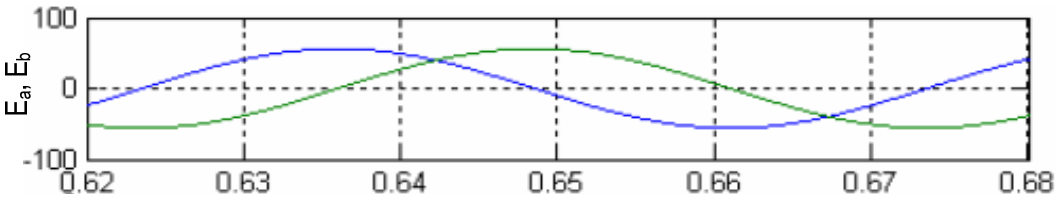

(b) estimated Back-emf

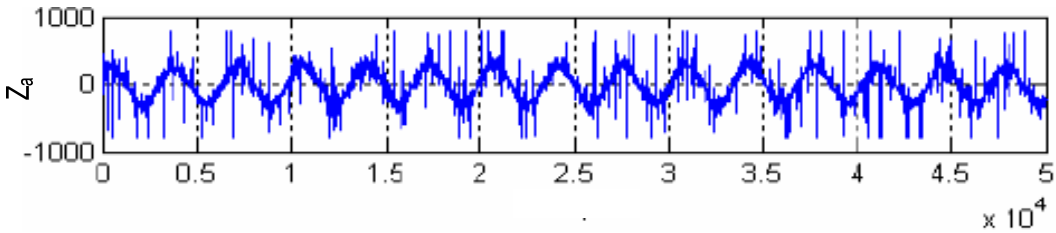

(c) Sliding mode control Z_a at *l*=-0.7 for 1000 rpm

Figure 4.13 Simulation performance for SMO

The simulation results with adaptive feedback gain are shown in Figure 4.14. The measured and estimated rotor position (rad) is shown in Figure 4.14 (a), the estimation error is 0.8 electrical degrees. The equivalent control Z_{eq} is shown in Figure 4.14 (b), the error in theta is shown in Figure 4.14 (c). The estimated stator currents i_α, and i_β are shown in Figure 4.14 (d).

To show the variation of the gain the machine is accelerated constantly as shown in Figure 4.14 (e). It is observer that the equivalent control Z_{eq} does not change, and the feedback gain is changing with rotor speed.

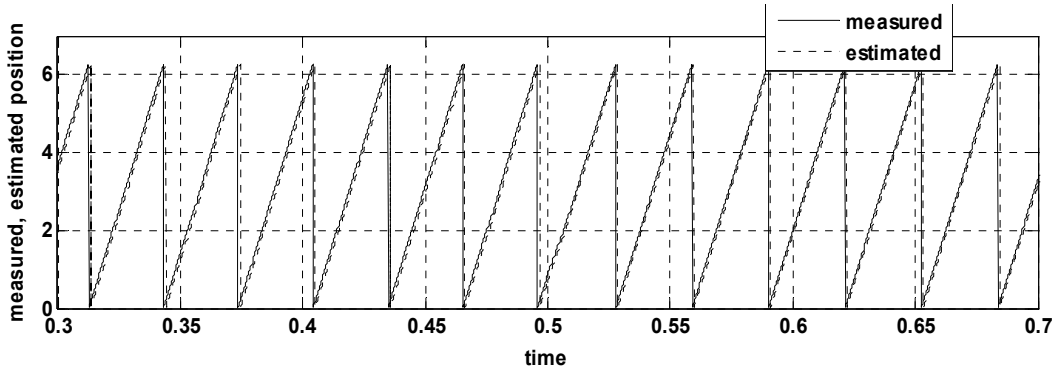

(a) Measured and estimated rotor position

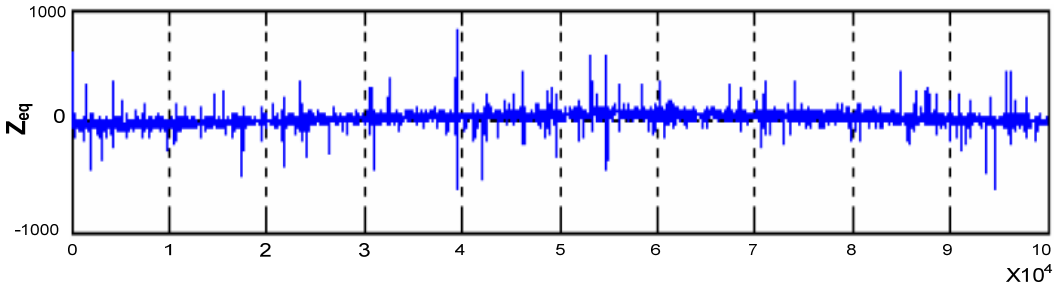

(b) Equivalent control, $Z_{eq,}$ (x-axis: samples),

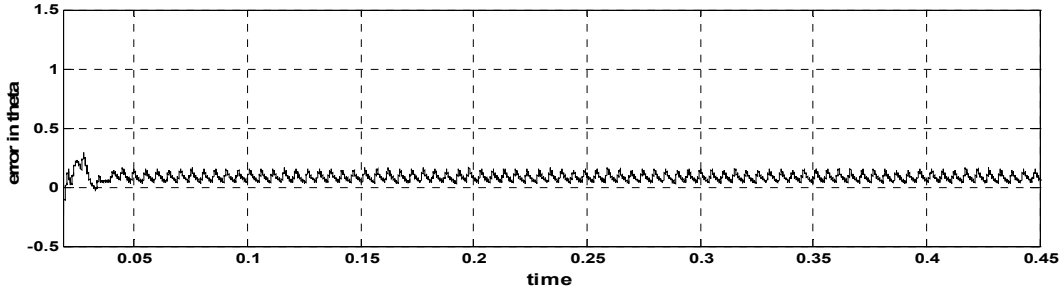

(c) Position error

Figure 4.14 Simulation performance of SMO with adaptive gain

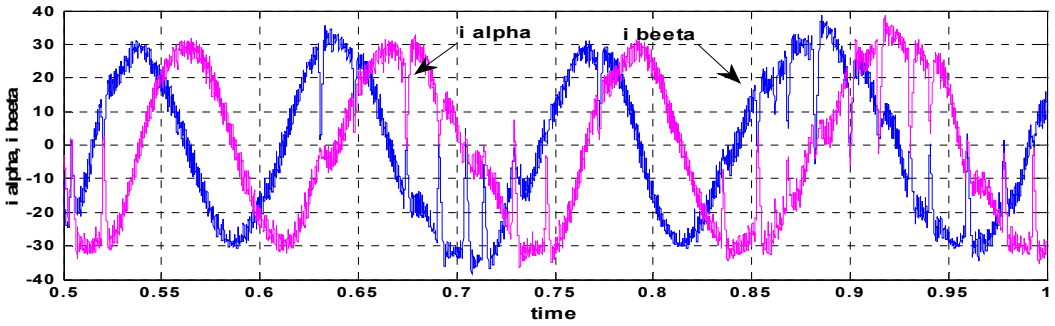

(d) Estimated i_α and i_β currents

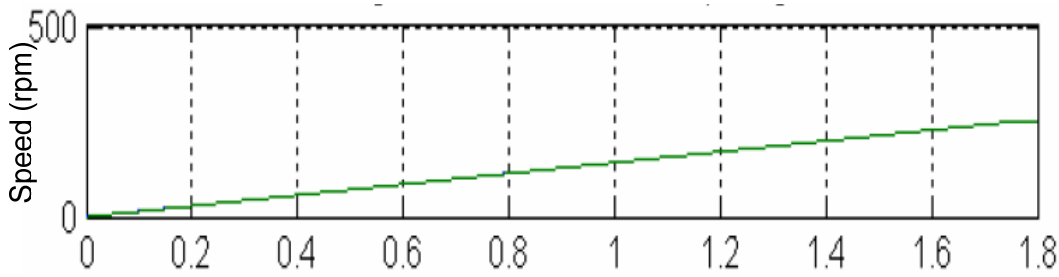

(e) speed

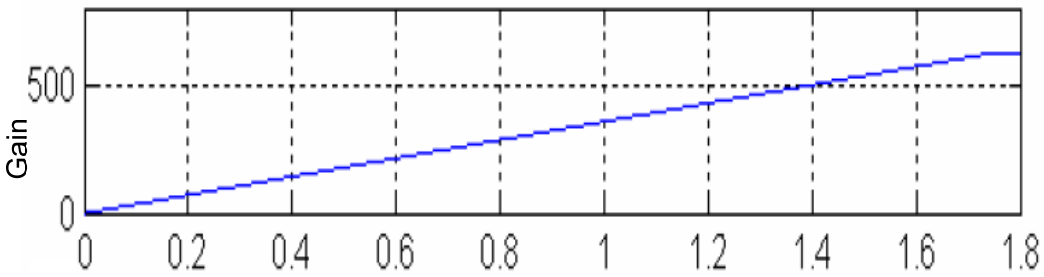

(f) estimated Back-emf

Figure 5.14 (cont'd) Simulation results for SMO with adaptive gain

To compare the performance of different estimation methods in various operating conditions, the simulation is conducted for BEMF, SMO, and MRAS based algorithm. The obtained results are compared and tabulated in Table 4-3. The performance of different estimation methods are compared in different operating conditions, starting, speed change, load change. In general SMO performance is found better in most of the operating conditions. The MRAS is showing comparable performance to SMO, as both are the closed-loop methods and better than open-loop method; BEMF as discussed here.

Following are the highlights of this chapter.

- The SMO is a method that uses measured back-emf, therefore has parameter dependency.
- SMO has a disturbance rejection property.
- The implementation of SMO is simple as compared to other non-linear adaptive controllers.
- The closed loop methods gives superior performance in all operating condition.

Table 4-3 Comparison of results of different estimation methods for sensorless PMSM drive

Operating Condition	Parameter	BEMF	MRAS	SMO
During starting	Overshoot	3.2%	1.8%	1.2%
	Settling Time	1.2s	0.8s	0.8s
Change in reference speed (200-500) rpm	Overshoot	2.6%	1.5%	1.1%
	Settling Time	0.8s	0.5s	0.4s
Change in reference speed (500 to 200) rpm	Undershoot	2.8%	1.9	0.9%
	Settling Time	1.2s	0.8s	0.9s
Load change (0-5) Nm	Overshoot	2.7%	1.1%	0.9%
	Settling time	0.9s	0.7s	0.8s

4.7 Conclusion

In the back-emf integration method based schemes the motor must rotate in order to have a position dependent term in the voltage equation of PMSM. The voltage drop in the resistance, dead-time of the inverter, effects the integration of back-emf.

The signal injection based methods to avoid calculation of back-emf; here the specific signals are used to produce extra response which includes the rotor position information. The performance of these methods suit at zero and low-speed, yet even after initial position estimation at medium and high speeds, where the injection based method is not necessarily to be used; the excitation signal is still needed. In steady-state this injected signal causes the transient which affects the dynamic response of drive and increase or decrease the inverter

voltage fed to the motor. The signal processing and use of various filters degrades the overall dynamic response and reduces the reliability of drive.

Of all the carrier injection based schemes for sensorless control, those based on high frequency carrier injection were on highest activity during the 90-ties. These schemes use saliency in the machine as the basis for the flux or position estimate. The saliency may be present due to saturation, slot variations, slot harmonics or inherent saliency due to machine geometry. The goal for this type of schemes is to enable high performance control at all speeds including zero speed.

Extended Kalman Filter (EKF) is computationally complex, needs initial conditions, which degrade the superiority of this method [13, 33, 34, 95-97]. The sliding mode observer based techniques are simple and robust against variation of machine parameter but it suffers from chattering problem.

Therefore, to achieve a high performance estimation algorithm for wide speed range different methods can be combined for operation of drive during specific range of speeds (start from initial position detection method at standstill; then switch to algorithm suitable at low-speed; then at medium and high speed any advance close loop estimator can be used). All sensorless schemes, based on stator flux estimate, suffer from limitations at low speed and needs an alternative. Separation of all schemes, based on their properties (advantages and restrictions) as reported in literature, is very difficult. A summary of some indirect position-sensorless methods are given with its applicability and limitations in Table 4-1.

In this chapter a sliding mode observer for sensorless vector control of PMSM is developed. Using feedback gain the observer is able to operate over wide-speed range. There two gains; switching gain k and feedback gain l, and the flexibility in selection of these gains are discussed. The stability analysis of observer is done on basis of Lyapunov algorithm.

A sliding mode observer with adaptive feedback gain to speed is implemented; this observer is able to estimate the rotor flux and rotor position. This method first uses a sliding mode observer to estimate the winding current in a stationary reference frame, then using a LPF and feedback the rotor position is estimated. Further, a PLL calculates the estimated speed. The role of cut-off frequency of LPF is also discussed in the convergence of observer. The validity of observer is validated by computer simulations and verified experimentally in chapter 6.

CHAPTER 5: SPEED ESTIMATION USING AI BASED MRAS FOR PMSM

[*In this chapter the estimation method based on model reference adaptive system is presented with space vector modulation for sensorless operation of PMSM drive. The performance of drive with traditional MRAS estimator using PI controller is improved using application of fuzzy logic in adaptation mechanism of MRAS. The estimation algorithm used is independent of stator resistance, computationally less complex, free from integrator problem, as the back-emf estimation is not required and provides stable operation of drive system. This proposed control methodology solves the problem of nonlinearity and parameter deviations of PMSM drive with application of Fuzzy logic. The estimation algorithm with FLC is implemented in MATLAB/Simulink to prove the effectiveness of proposed FMRAS as compared with PI controller and performance of drive under various operating condition is demonstrated.*]

5.1 Introduction

There are a wide range of applications of vector controlled PMSM drive in high performance drive applications. The implementation of vector control for PMSM requires speed and position information. However, the sensor requires additional mounting space, reduces reliability and increases the cost of drive. A large variety of algorithms are reported in the literature for the elimination of sensors: estimators based on state equations, Kalman filters, sliding mode observers, artificial intelligence based observers and so on [98-104].

Back-emf based method offers satisfactory performance at higher speed, but at low or zero speed the magnitude of back-emf becomes negligible and difficult to measure. This makes speed estimation at low speed difficult and this method is also highly sensitive to machine parameters. Signal injection methods exploit the saliency of machine to extract the position information. Due to saliency present in machine the phase inductance varies with the rotor position. A high frequency signal is injected in motor phases to extract the rotor position. This method is reliable at zero speed but there is adverse effect of signal injection on motor dynamics and requirement of extra hardware. As reported in literature the in state observer based methods [105, 106] (extended kalman filter, extended luenburger observer, sliding mode observer) parameters are used as state and can be estimated along with position and speed [27, 76, 77]. Extended Kalman Filter (EKF) is computationally complex, needs initial conditions, which degrade the superiority of this method [13, 33, 34, 95-97]. The sliding mode observer (SMO) based techniques are simple and robust against variation of machine parameter but it suffers from chattering problem.

In [107, 108], the performance of MRAS based estimation is compared with EKF method for rotor position estimation and the obtained results shows that the MRAS method is easy and quicker than EKF.

Among the various available computational intelligence techniques such as ANN, Fuzzy, Genetic Algorithm, the fuzzy logic is found less complicated and easy to implement as compared to others to achieve the same performance. The neural network control is a good choice for control applications. In ANN controller the selection of size of network structure, number of neurons, number of hidden layers, weight coefficients are the major challenges [29]. Moreover the complexity of the ANN controller increases while achieving the robustness in overall system performance, and its real time implementation becomes difficult on given hardware platform where sampling time and processing speed is limited. Similarly in GA the mutation and selecting the new chromosomes are computationally complex and time consuming. In order to overcome the above limitations fuzzy based controllers are employed for motor control which eliminates the controller parameter dependency on the system mathematical model and load disturbances. A fuzzy logic controller (FLC) is basically a non linear and an adaptive controller which gives robust performance for a linear or non linear plant with parameter variation. Use of fuzzy logic algorithm, to reduce the torque ripples, has been proposed, it refines the voltage vectors [48]. Use of space vector modulation (SVM) significantly reduces the torque and flux ripples.

The MRAS algorithm is well-known for the sensorless control of induction machines. The MRAS based estimation for sensorless control of induction motor has been proved to be effective [108]. The MRAS is one of the best available sensorless algorithms for PMSM in high performance application similar to induction motor due to its parameter independency [109, 110]. The performance of most of the observers depends on motor parameters which vary with temperature. In MRAS based estimator the estimation algorithm used is independent of stator resistance, computationally less complex, free from integrator problem because back-emf estimation is not required and provides stable operation of drive system [111].

In [112] instantaneous reactive power based speed estimation is presented. The benefit of this method is that it is independent of stator resistance and less sensitive to parameters. Most of the observer's performance depends on temperature which varies according to temperature. To conquer this an adaptive algorithm with on-line parameter identification is used in [47].

5.2 MRAS based Estimation of Speed

The Model Reference Adaptive System (MRAS) based estimators provide the desired state from two different models, one is reference model and another one is adjustable model [15, 43-46]. The error between two models is used to estimate the unknown parameter (speed in this case). In MRAS only adjustable model should depend on unknown parameter [47], the reference model is independent of speed [113, 114]. The error signal is fed into

adaptation mechanism that provides the estimated quantity which is used to tune the adjustable model. This method is simple and requires less computation.

MRAS is an effective method in sensorless AC drives for position and speed estimation. In the adaptation mechanism of conventional MRAS the PI controller is used in the adjustable model.

5.2.1 Structure of MRAS

The structure of MRAS is shown in Figure 5.1. The given performance x is generated by reference model and estimated performance $\hat{x}$ is generated by adjustable model and the same input u is given to both the models. x and $\hat{x}$ are the state variables of reference and adjustable model. The given and estimated performance is compared and generated error y is given to self-adaptive organization which draws the state variable $\hat{x}$ near to x and the error signal y approaches zero.

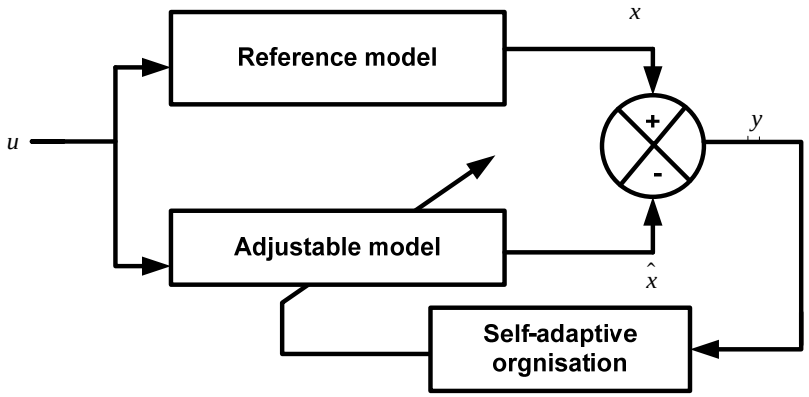

Figure 5.1 Structure of MRAS

5.2.2 Estimator Synthesis for speed estimation of PMSM

The design of sensorless algorithm for PMSM drive uses PMSM itself as reference model, and the current equations of PMSM in d-q reference frame as adjustable model [115], and an adaptation mechanism. A sensorless control algorithm is shown in Figure 5.2.

The current model of surface mounted PMSM is obtained by mathematical model presented in chapter 2, is given by-

$$v_d = R_s i_d + L_s \frac{di_d}{dt} - w_r L_s i_q \tag{5.1}$$

$$v_q = R_s i_q + L_s \frac{di_q}{dt} - \omega_r L_s i_d + \omega_r \psi_f \tag{5.2}$$

The above equations (5.1) and (5.2) can be re-written in form of-

$$\frac{di_d}{dt} = -\frac{R_s}{L_s} i_d + \omega_r i_q + \frac{v_d}{L_s} \tag{5.3}$$

$$\frac{di_q}{dt} = -\frac{R_s}{L_s} i_q - \omega_r i_d - \frac{\psi_r}{L_s} \omega_r + \frac{v_q}{L_s} \tag{5.4}$$

Where v_d, v_q, i_d, i_q are the stator voltages and currents in d-q components; R_s is stator resistance; L_s is stator inductance; ω_r is rotor speed; and ψ_f is rotor flux.

The equations (5.3) and (5.4) can be rearranged and written in matrix form as-

$$p\begin{bmatrix} i_d + \frac{\psi_f}{L_s} \\ i_q \end{bmatrix} = \begin{bmatrix} -\frac{R_s}{L_s} & \omega_r \\ -\omega_r & -\frac{R_s}{L_s} \end{bmatrix} \begin{bmatrix} i_d + \frac{\psi_f}{L_s} \\ i_q \end{bmatrix} + \frac{1}{L_s} \begin{bmatrix} v_d + \frac{R_s \psi_f}{L_s} \\ v_q \end{bmatrix} \tag{5.5}$$

The above equation can be written be written in simplified form, suppose;

$$i_d^{'} = i_d + \frac{\psi_f}{L_s}$$

$$i_q^{'} = i_q$$

$$v_d^{'} = v_d + \frac{R_s \psi_f}{L_s}$$

$$v_q^{'} = v_q$$

Now with these assumptions equation (5.5) becomes in form of-

$$p\begin{bmatrix} i_d^{'} \\ i_q^{'} \end{bmatrix} = \begin{bmatrix} -\frac{R_s}{L_s} & \omega_r \\ -\omega_r & -\frac{R_s}{L_s} \end{bmatrix} \begin{bmatrix} i_d^{'} \\ i_q^{'} \end{bmatrix} + \frac{1}{L_s} \begin{bmatrix} v_d^{'} \\ v_q^{'} \end{bmatrix} \tag{5.6}$$

The equation (5.6) can be written in form of a state equation as-

$$pi^{'} = Ai^{'} + Bv^{'} \tag{5.7}$$

Where

$$A = \begin{bmatrix} -\frac{R_s}{L_s} & \omega_r \\ -\omega_r & -\frac{R_s}{L_s} \end{bmatrix}$$

$$B = \frac{1}{L_s}$$

It is clear that only matrix A contains the speed information, which is to be estimated, and the PMSM is reference model. In the same way the expression for estimated values to be obtained by adjustable model is expressed as–

$$p\begin{bmatrix}\hat{i}'_d\\ \hat{i}'_q\end{bmatrix}=\begin{bmatrix}-\frac{R_s}{L_s} & \hat{\omega}_r\\ -\hat{\omega}_r & -\frac{R_s}{L_s}\end{bmatrix}\begin{bmatrix}\hat{i}'_d\\ \hat{i}'_q\end{bmatrix}+\frac{1}{L_s}\begin{bmatrix}\hat{v}'_d\\ \hat{v}'_q\end{bmatrix} \tag{5.8}$$

The equation (5.8) also can be written in state equation form as–

$$p\hat{i}' = \hat{A}\hat{i}' + B\hat{v}' \tag{5.9}$$

Now subtracting equation (5.8) from equation (5.6)

$$\begin{bmatrix}\frac{de_d}{dt}\\ \frac{de_q}{dt}\end{bmatrix}=\begin{bmatrix}-\frac{R_s}{L_s} & \omega_r\\ -\omega_r & -\frac{R_s}{L_s}\end{bmatrix}\begin{bmatrix}e_d\\ e_q\end{bmatrix}-J\left(\omega_r-\hat{\omega}_r\right)\begin{bmatrix}\hat{i}'_d\\ \hat{i}'_q\end{bmatrix} \tag{5.10}$$

where

$$e_d = i'_d - \hat{i}'_d$$

$$e_q = i'_q - \hat{i}'_q$$

$$J=\begin{bmatrix}0 & -1\\ 1 & 0\end{bmatrix}$$

In the short form it can be written as–

$$\frac{de}{dt} = A_e e - W \tag{5.11}$$

Where

$$A_e=\begin{bmatrix}-\frac{R_s}{L_s} & \omega_r\\ -\omega_r & -\frac{R_s}{L_s}\end{bmatrix}$$

$$w = J\left(\omega_r-\hat{\omega}_r\right)\hat{i}'_s$$

The adaptation mechanism uses PI controller to process the error and to tune the adjustable model so as to achieve the estimated value of rotor speed.

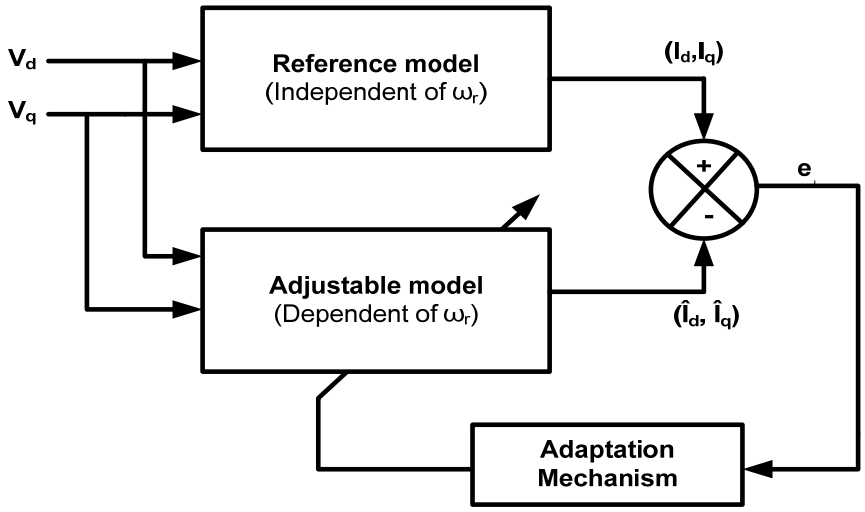

Figure 5.2 Structure of MRAS for PMSM

Using the PI controller the estimated speed using MRAS algorithm is obtained as–

$$\hat{\omega}_r = \left(K_p + \frac{1}{s}K_i\right)\left[i_d \hat{i}_q - i_q \hat{i}_d - \frac{\psi_f}{L_s}\left(i_q - \hat{i}_q\right)\right] \tag{5.12}$$

5.3 Proposed FMRAS based Speed Estimation for PMSM

The traditional MRAS uses the PI control in adaptation mechanism to process the error. The use of PI control makes the estimation performance affected by change in motor parameter and variation in load. To improve the system rapidity, robustness and stability, the intelligent control is incorporated. The application of fuzzy logic controller in the estimation algorithm improves the system anti-disturbance ability and dynamic-static performances.

Fuzzy control with good robustness is independent of mathematical model of system [116, 117] and the algorithm is very practical and easy to design. It has very low steady state error and precision. A fuzzy controller is proposed to process the error between reference model and adjustable model in the adaptation mechanism of MRAS. It provides the robustness in the drive. The estimation algorithm used is independent of stator resistance, computationally less complex, free from integrator problem because back-emf estimation is not required and provides stable operation of drive system. This control methodology solves the problem of nonlinearity and parameter deviations of PMSM drive with application of Fuzzy logic. Moreover, it achieves high dynamic performance and accurate speed tracking and torque control with superior steady state characteristics.

5.3.1 Design Consideration of FLC

In the design of a fuzzy logic controller for any application certain criteria has to be followed. These design criterion are different for different applications [118]. As for as the controller parameters are concerned, these are the range of membership functions, type of

membership function, implication methods, rules and number of rules. These controller parameters vary with motor parameters and load variations. The principal factors that are considered prior to implementation of the fuzzy control algorithm are the as follows.

5.3.1.1 Shape of the Fuzzy Sets

In the design of a fuzzy controller the shape of fuzzy sets has been the subject of research and it can be stated that there is no theory which can guide the designer for selection of best shape for particular application. Simple computation and the hands on to the controllers are basis for selection of shape for the membership functions, whereas triangular and trapezoidal functions are generally used. In this work triangular membership functions are used.

5.3.1.2 Coarseness of Fuzzy Sets

The number of fuzzy sets that are required to specify a variable is termed as the coarseness of the controller and which determines the controller accuracy. A large number of fuzzy sets are required to achieve the high accuracy. The coarse control is applied using few fuzzy sets, when the process variables are far from the desired operating point. The number of fuzzy sets is increased near operating point, which provides finer control and high accuracy. An example of coarse-fine control with a pair of fuzzy sets is shown in Figure 5.3

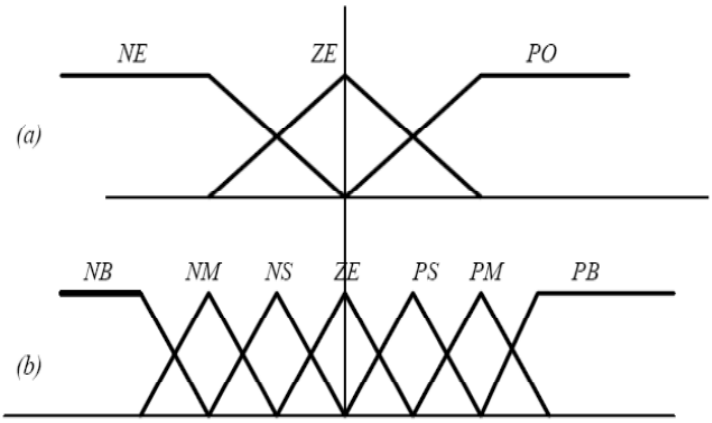

Figure 5.3 (a) Coarse, (b) fine fuzzy sets

Here three fuzzy sets are used for coarse control and seven for fine control. In the present work seven fuzzy sets are used in adaptive mechanism of MRAS for estimation of speed. This technique has been successfully applied in a number of applications requires high accuracy.

5.3.1.3 Completeness of Fuzzy Sets

The control algorithm of FLC must lead to a unique control action for any selected inputs. This property is termed as completeness and depends on the contents of the

knowledge-base as well as the number and shape of the fuzzy sets used to describe the inputs and outputs of the controller. The manner in which the fuzzy sets are defined on the universe of discourse, as well as the degree with which they overlap specifies the integrity of the controller. In the example of above Figure 5.3, the intersection is at least 50%. In this case there will always be a dominant rule which has membership in excess of 0.5 so that an outcome will always be forthcoming. In the worst case, two rules at most will fire with an equal membership of 0.5 but still there will be no ambiguity as to the final result. The fuzzy sets shown in Figure 5.4 possess points on the universe of discourse where the intersection is less than 0.5. This leads to highly uneven control surfaces and irregular control actions.

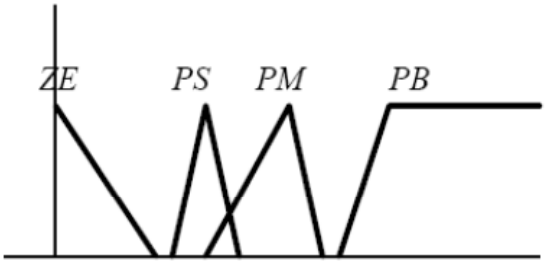

Figure 5.4 Fuzzy sets overlap

There are regions on universe of discourse where membership is zero whereupon if the instantaneous value of the input falls in these regions no rule can be fired with the result that the controller is unable to infer any control action. This is clearly undesirable and indicates that fuzzy sets must overlap in order to obtain a continuous output.

5.3.1.4 Rule Conflict

The set of linguistic rules used to control a plant or process is normally elicited from expert human operators or domain experts. It is an undisputed fact that the knowledge elicited from two human operators is rarely the same. Though they may have been trained with the same rules, with experience and time they have learned to modify them, believing that in this manner they can control the process better. Of course “better” is clearly a subjective criterion, since it may imply increased productivity, reduced energy costs or even less trouble to the operator. Many of these criteria are conflicting.

Thus in eliciting the knowledge for a controller it is advisable to restrict interviews to one human operator, e.g., the supervisor whose knowledge on how to control the plant efficiently and effectively is undisputed. If this is not possible, then there is little recourse but for the plant engineer to state the rules that he wishes to be followed. Dispite, rule conflict is a common phenomenon and some means must be found for resolving this conflict.

5.3.2 Design of Proposed FMRAS Estimator

The design of FLC is based on the experience and intuition of human plant operator. A typical FLC consist of fuzzifier, knowledge rule base, and defuzzifier. The fuzzifier converts actual crisp values to fuzzy values, which are then processed by defined rules in certain conditions. These rules are in rule base, and defined by an expert of system. After the implementation of rules output fuzzy values will be converted to crisp values by defuzzifier and used as output of controller. Figure 5.5 shows the structure of FLC for PMSM as controller where error 'ε' and change in speed error 'cε' are input to FLC and the estimated speed $\hat{\omega}$ is the output.

Based on the experience and expertise in the system membership functions are specified and fuzzy control rules are defined. These membership functions and control rules may require tuning to achieve high performance of drive under variable operating conditions. To obtain normalized inputs and output for fuzzy logic controller, gain blocks are used as scaling factors G_e, G_{ce} and G_u [119] as shown in Figure 5.5.

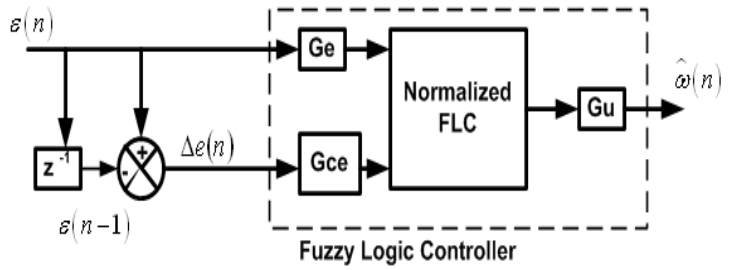

Figure 5.5 Structure of FLC in MRAS for speed estimation

Fuzzy logic is an approximate interpretation of multiple & diverse data sets and decisions by using linguistic variables similar to human analysis. Scaling factors at the input and output side of FLC are used to tune the controller with system parameter variation to achieve the high performance. As for as the controller parameters are concerned, these are the range of membership functions, type of membership function, implication methods, rules and number of rules.

It is observed that if the large numbers of membership functions are taken then the output is more near to exact but it increases the computational requirement. When very less number of membership functions is taken the computation decreases but the performance may not be satisfactory in a high performance application. So a compromise is to be made between number of membership functions and the output performance of controller. This compromise depends on the level of performance required and complexity of control action to be performed. In this work first three membership functions are taken but the performance was not found satisfactory, because here FLC is used in the estimation process to get speed and position information. This position information is used in the various transformations in

control of PMSM; as these transformations are trigonometric mathematical calculations, so a small error in position information produces a large gap in the performance.

The FLC consist of three stages: the fuzzification, rule execution and defuzzification are shown in Figure 5.6. In this work seven linguistic variable are chosen for input and output variables: 1) negative large (NL); 2) negative medium (NM); 3) negative small (NS); 4) zero (Z); 5) positive small (PS); 6) positive medium (PM); 7) positive large (PL). The fuzzy variables are processed by an inference engine that executes a set of control rules contained in (7 × 7) rule base. The control rules are derived from experience or knowledge of experts.

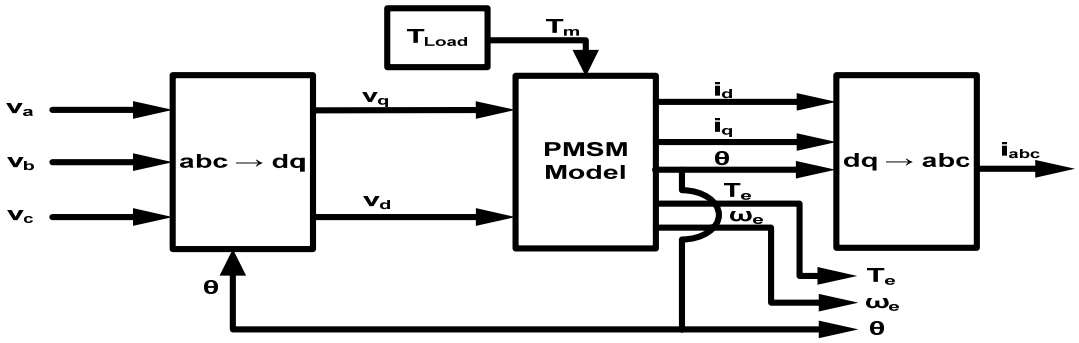

Figure 5.6 Internal structure of FLC

It is clear from the literature survey in the area of fuzzy logic control for drive applications, that in general triangular and trapezoidal membership functions are used [120]. Here for all the linguistic variables triangular membership function is used. Another important thing about selection of membership function is the range of membership function which is taken [2 -2] here. This range may be changed; accordingly scaling factors will be changed. Fuzzy rules will be executed only when it will receive the input in the interval [-2 2]. There is no strict rules to decide the interval for variables, it may be chosen based on own requirement of user for particular application.

In the second stage of FLC, fuzzy variables E and CE are processed by an inference engine that executes a set of control rules contained in (7 × 7) rule base. The control rules are derived from experience or knowledge of experts. The 3D- plots of these control rules of FLC is given in Figure 5.7 and Figure 5.8.

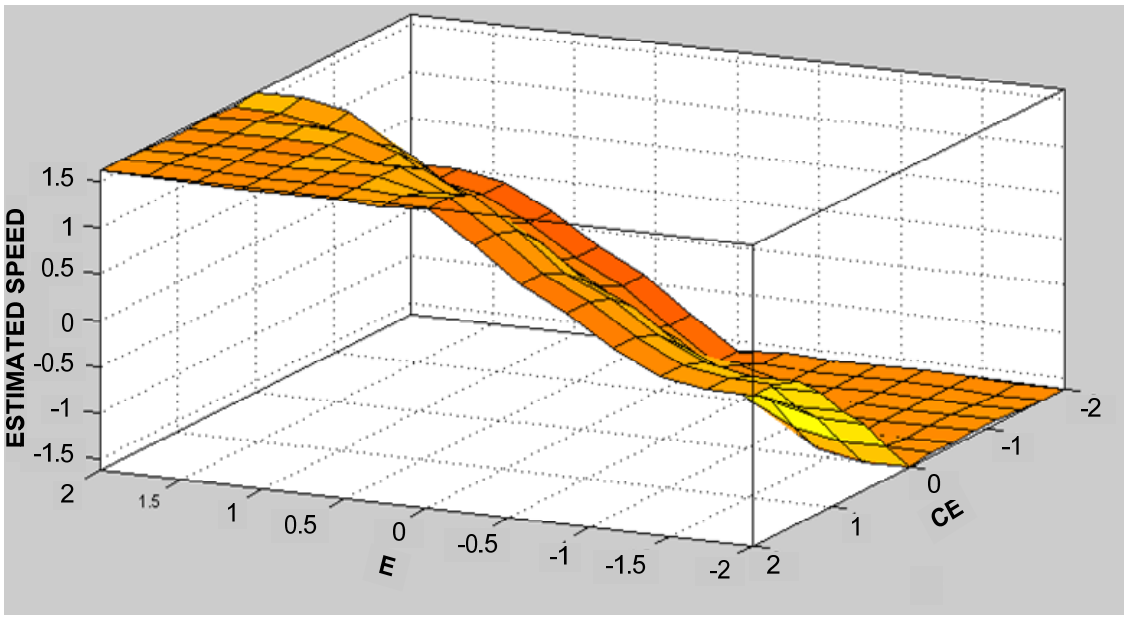

Figure 5.7 Surface view of rules

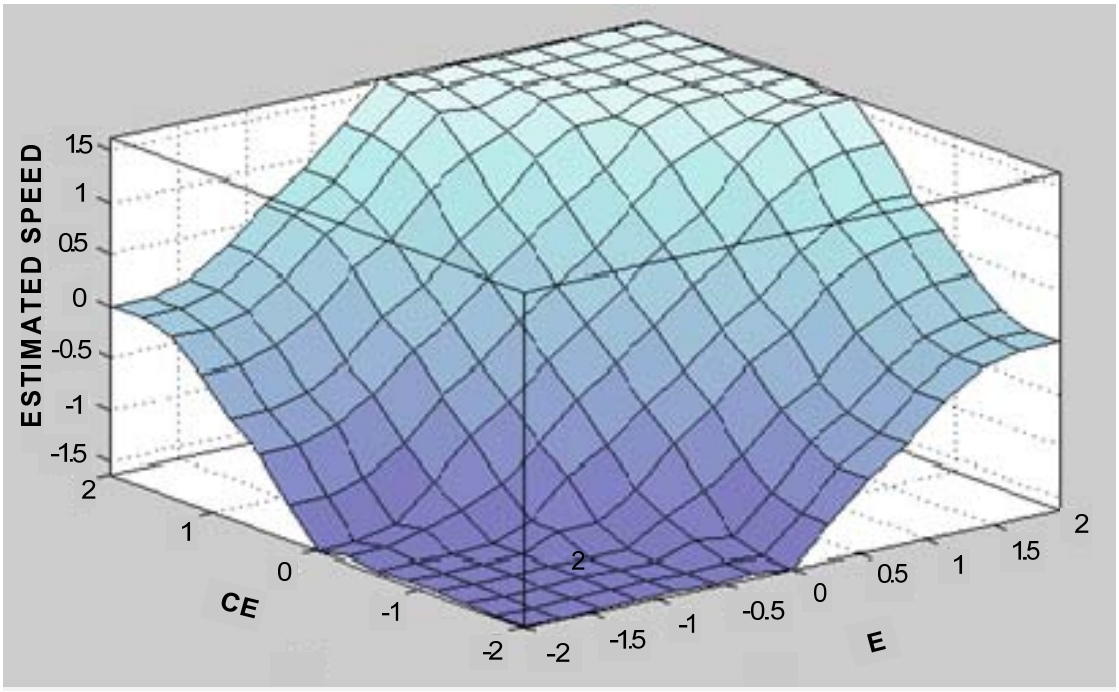

Figure 5.8 Plot of control rules of FLC in adaptive mechanism of MRAS

The width and symmetry of membership functions are generally a compromise between dynamic and steady state performance. If one is not using the gain blocks the interval may be as per actual error. To design a robust controller FLC parameter has to be tuned [11]. One method is to tune the rule base of FLC; other method is to tune scaling factors. As

shown in fig.6 two inputs scaling factors 'G_e' and 'G_{ce}', and one output scaling factor 'G_u' is used.

In this work max-min algorithm is used to produce output fuzzy variable from inputs processed by control rules. The output variable from inference engine is converted to a crisp value in defuzzification stage. Various defuzzification algorithms have been reported in literature, in this work centroid defuzzification algorithm is used. In centroid defuzzification algorithm the crisp value is calculated from center of gravity of membership functions. The fuzzy based adaptive mechanism for speed estimation is shown in Figure 5.9. The schematic block diagram of implementation of FMRAS based speed estimation for PMSM is shown in Figure 5.10.

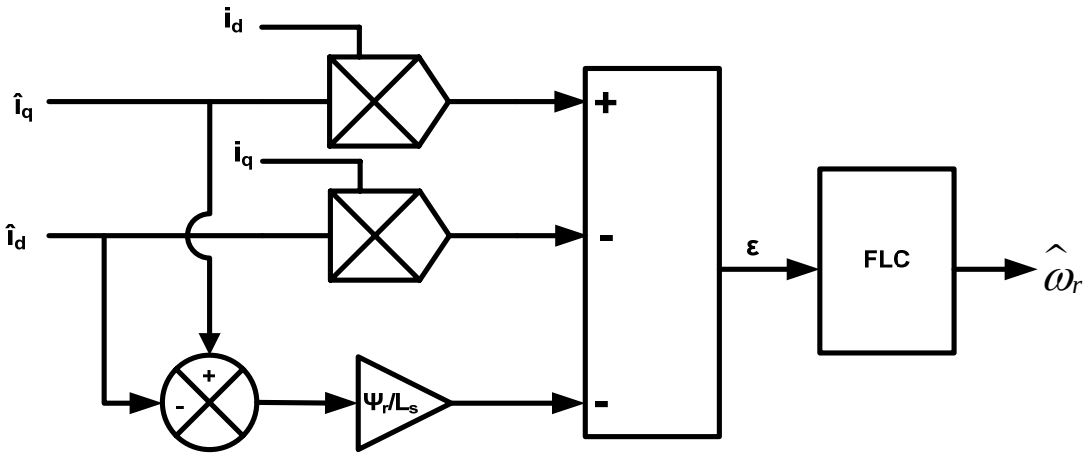

Figure 5.9 FMRAS adaptive mechanism based on equation (5.12)

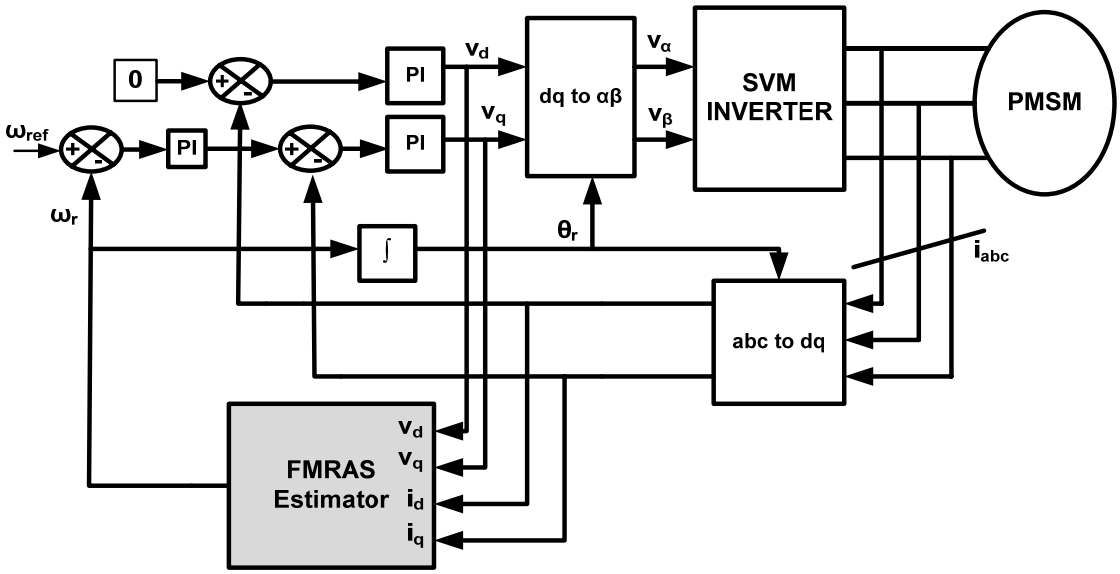

Figure 5.10 Schematic block diagram of FMRAS based estimation for PMSM

5.4 Implementation of FMRAS based Sensorless Algorithm

A model reference adaptive system technique has been used for speed and position estimation in sensorless vector control of the PMSM with space vector pulse width modulated inverter. A fuzzy based model reference adaptive system (FMRAS) for speed estimator of PMSM drive has been proposed. A fuzzy controller is used to process the error between reference model and adjustable model in the adaptation mechanism of MRAS. It provides the robustness in the drive. The estimation algorithm used is independent of stator resistance, computationally less complex, free from integrator problem because back-emf estimation is not required and it provides stable operation of drive. This control methodology solves the problem of nonlinearity and parameter deviations of PMSM drive with application of fuzzy logic. Moreover, it achieves high dynamic performance and accurate speed tracking and torque control with superior steady state characteristics.

The proposed FMRAS based speed estimator is implemented for PMSM drive in MATLAB/Simulink. MRAS used in this system is designed based on the current model of PMSM and uses FLC. The block diagram of PMSM employing FMRAS as speed estimator is shown in Figure 5.11. Here the voltages and currents are measured in a−b−c reference and converted to d−q reference frame and given as input to FMRAS estimator, which generates the estimated speed. The estimated d−q currents are generated from adjustable model, which is also controlled by output of adaptation mechanism as clearly shown in Figure 5.11. In the adjustable model the estimated output is function of (v_s, i_s, ω_{est}).

The Simulink diagram of sensorless PMSM drive based on MRAS is shown in Figure 5.13. The measured rotor position is used to compare the estimated value and find out the estimation error. The estimation error is the key point in defining the performance of a sensorless algorithm. Figure 5.14 shows the simulink diagram to achieve the intermediate values $i_d^{'}$ and $i_q^{'}$ of current as obtained in equation (5.6). The estimation of speed using PI controller is given in equation (5.12) is shown in Figure 5.15. The internal processing of estimation algorithm is shown separately in Figure 5.14 and Figure 5.15, which take v_d, v_q, i_d, i_q as combined inputs and gives estimated speed as output as shown in block diagram (Figure 5.11) and simulink diagram (Figure 5.13). Here the controller which processes the error to estimate the speed plays a very important role in performance of sensorless algorithm.

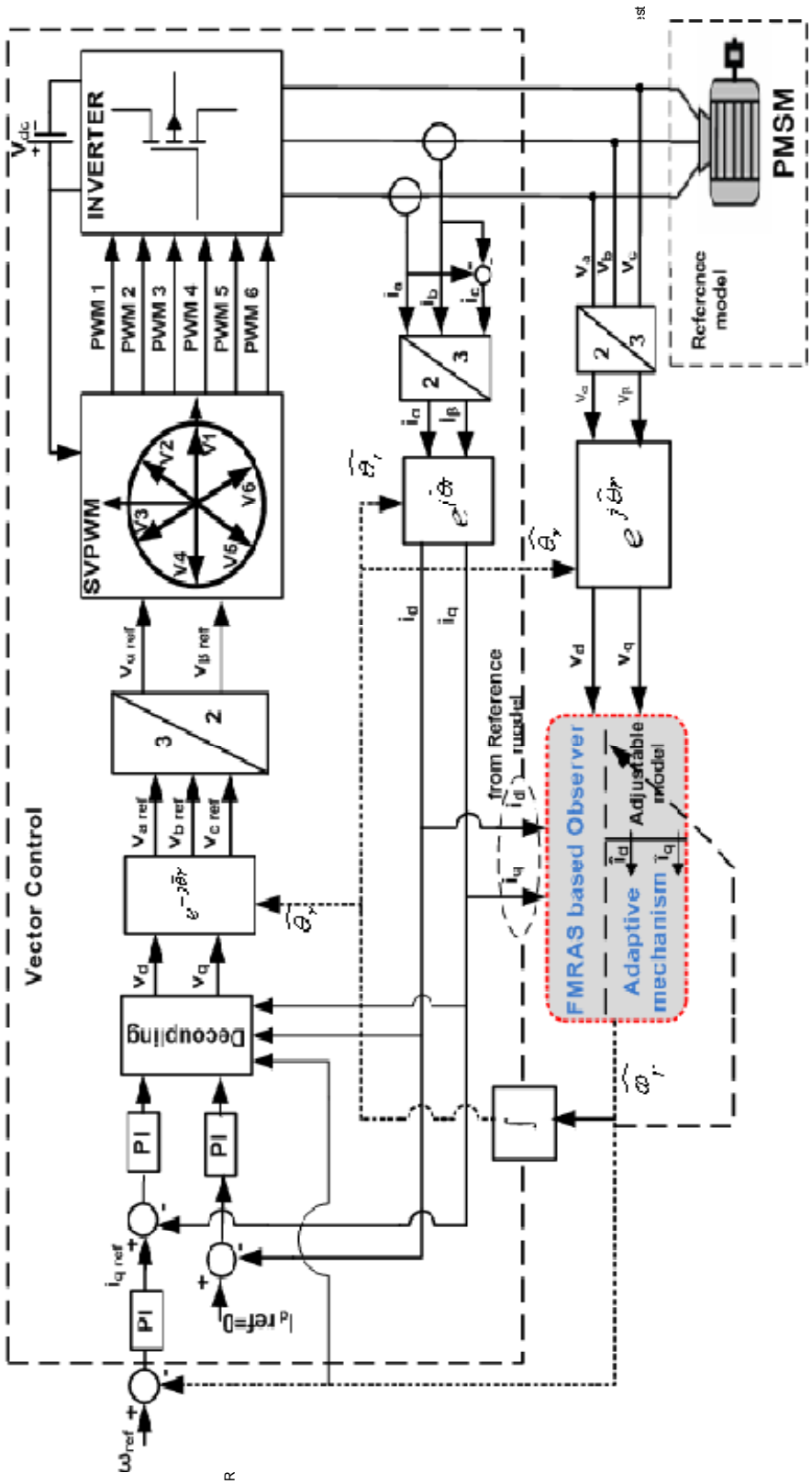

Figure 5.12 Block diagram of sensorless PMSM drive with FMRAS

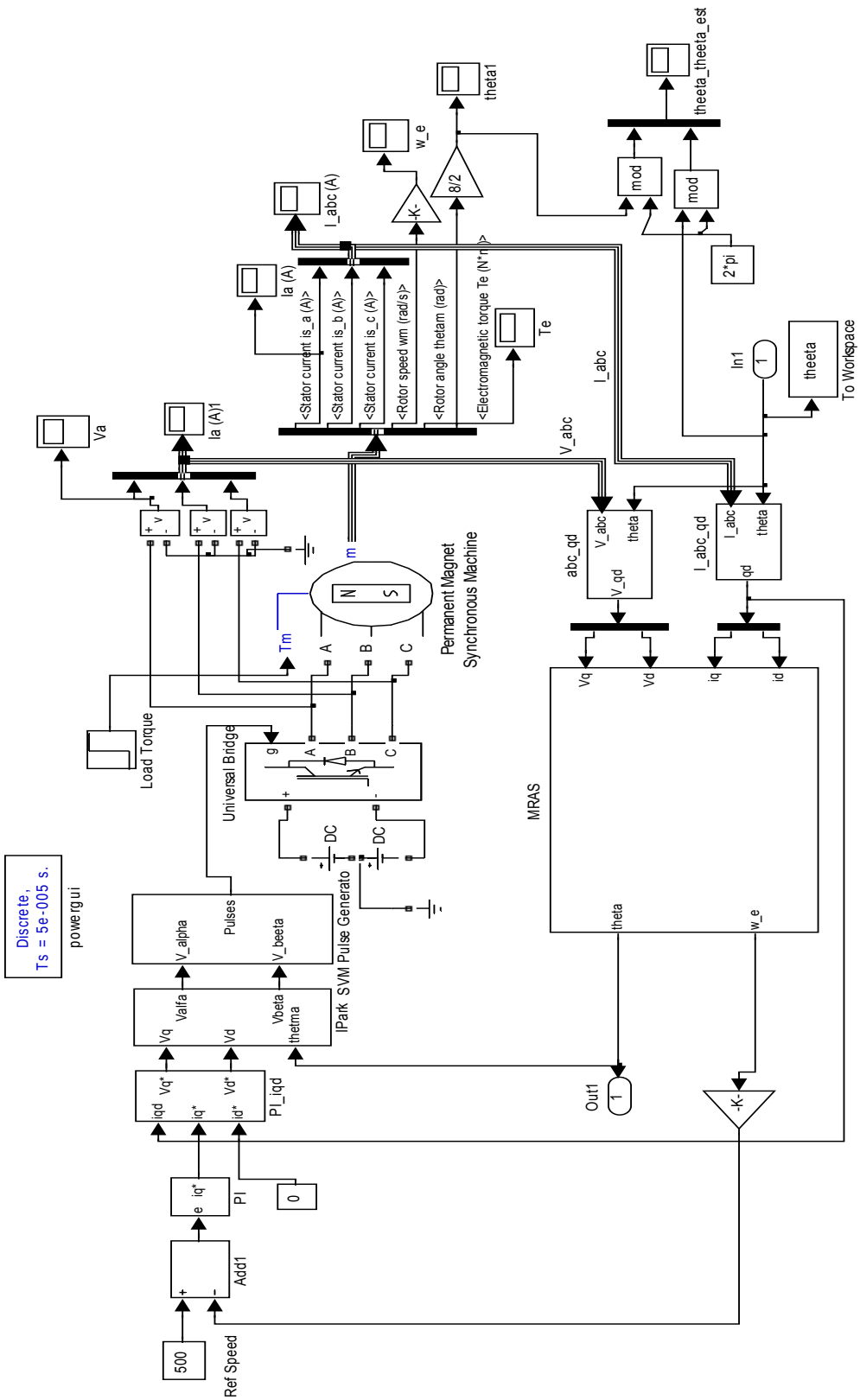

Figure 5.13 Simulink diagram of MRAS based PMSM Drive

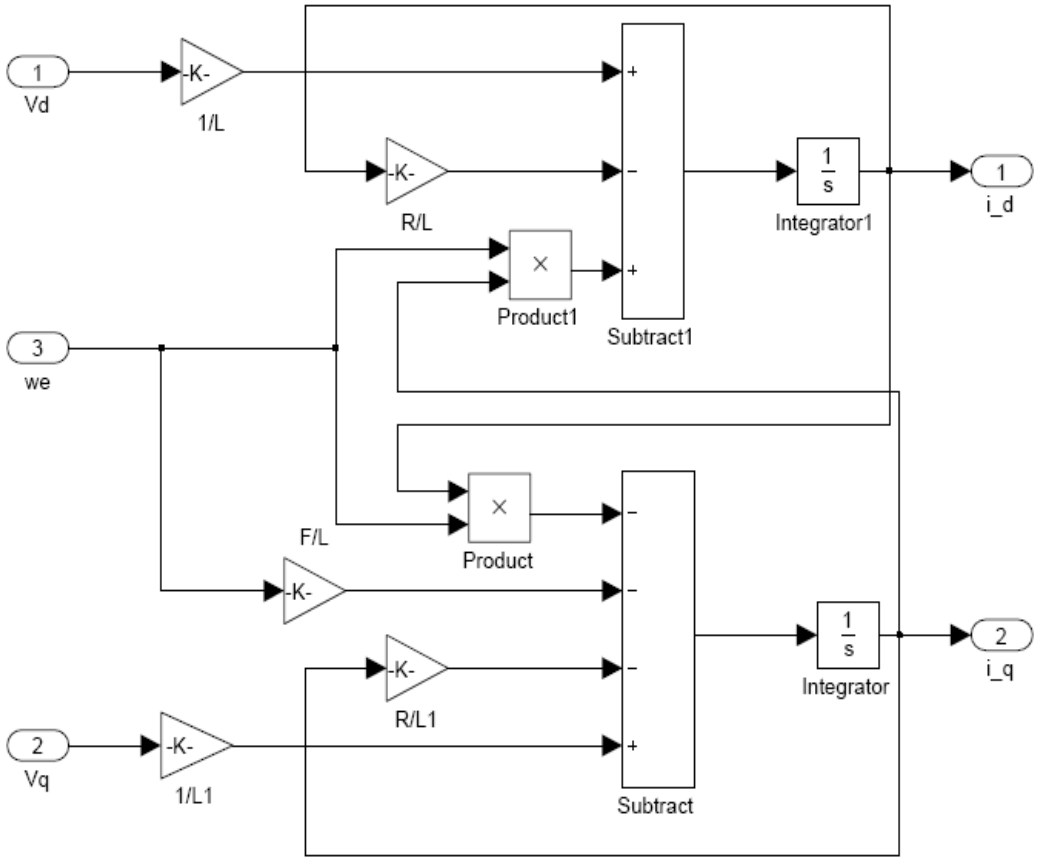

Figure 5.14 Simulink diagram for equation (5.6)

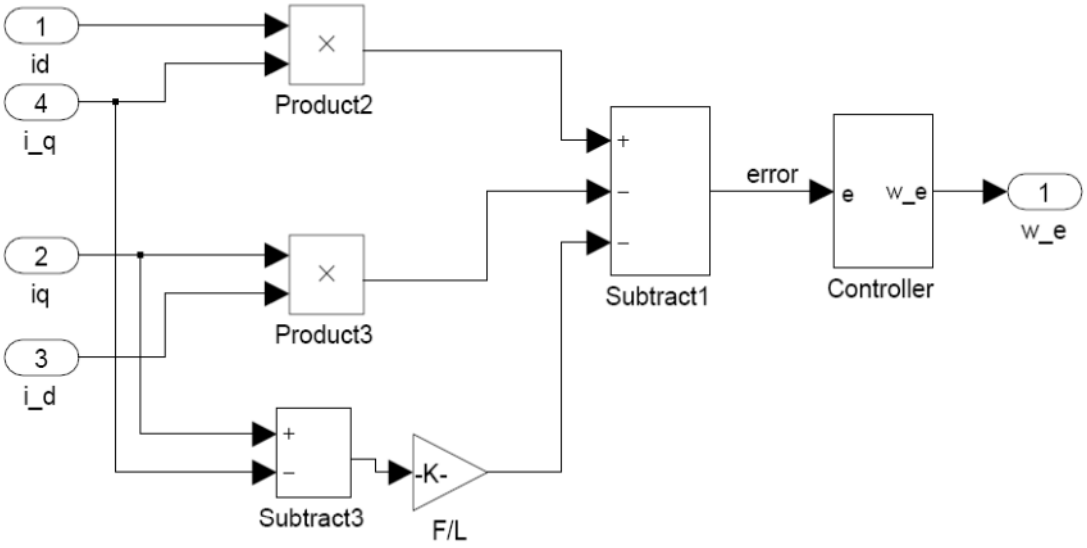

Figure 5.15 Estimation of speed using MRAS

5.5 Simulation Results

In the drive system three PI controllers are used; one as speed controller and two as current controllers (d-axis current and q-axis current) to achieve the vector control. The space vector pulse-width modulated inverter is used to feed the three-phase power to the PMSM. V_α and V_β are the control inputs to SVM inverter, modulation index is kept 0.9. For the estimation voltages and currents are obtained in d– q reference frame using measured ones. As clearly shown in the block diagram (Figure 5.11), that the adjustable model generates intermediate values of currents (only for internal calculations) using v_d and v_q as shown in Figure 5.14. These intermediate current values $i_d^{'}$, $i_q^{'}$ and the,i_d, i_q obtained from reference model (PMSM itself) are used to obtain the estimated speed using a controller as shown in Figure 5.15. Accuracy of this controller decides the error in the estimated speed. Using PI controller mathematical equation for estimation is given in (5.12). The estimation performance of MRAS is improved by application of FLC in the adaptive mechanism. The performance of the complete FMRAS based estimation algorithm is observed using speed PI controller for various operating conditions, the input voltage of inverter is kept 100V.

The performance of controller has been investigated with computer simulation studies performed in MATLAB/Simulink environment. Simulation studies have been carried out for with parameter changes and are presented here. Figure 5.16 shows the measured and estimated rotor position at 500 rpm with no load, the position error is 0.03 rad means 1.71°.

The measured and estimated rotor speed at 1000 rom with no load is shown in Figure 5.17 and the α and β components of stator currents at no load condition is shown in Figure 5.18. The measured q-axis and d-axis current components i_q and i_d intermediate current values $i_q^{'}$ and $i_d^{'}$ of stator current are shown in Figure 5.19 and Figure 5.20 respectively.

Figure 5.21 shows the measured and estimated rotor speed using FMRAS based sensorless algorithm with 750 rpm reference speed. Figure 5.22 shows the speed response with step change in the reference speed 750 rpm-500rpm at 0.5 sec. The stator phase current response with step change in load torque 0-5.0 Nm at 0.5 sec is shown in Figure 5.23, and the three-phase current response with step change in load torque is shown in Figure 5.24.

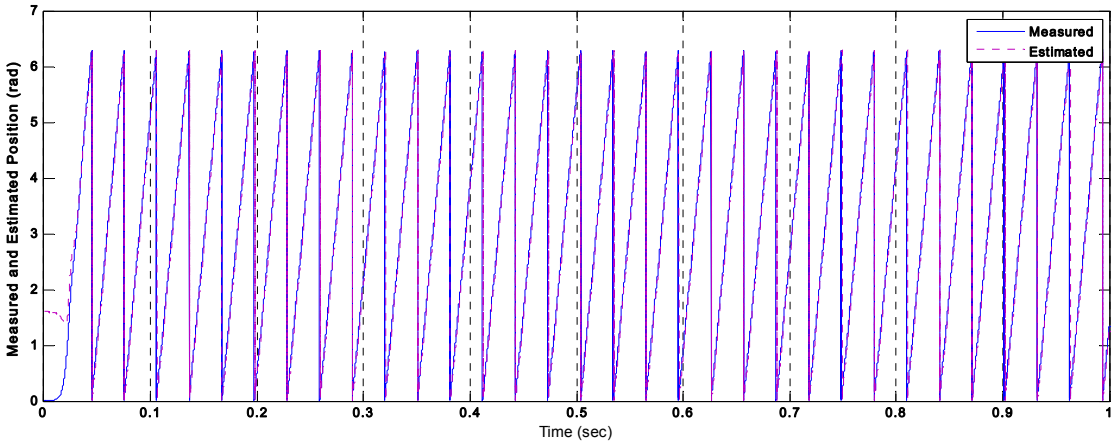

Figure 5.16 Measured and estimated rotor position at 500 rpm on no load

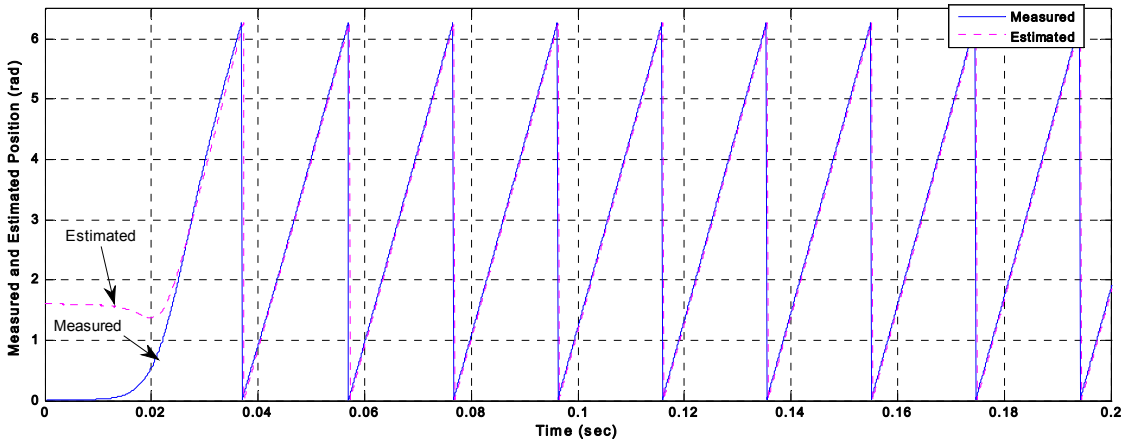

Figure 5.17 Measured and estimated rotor position at 1000 rpm on no load

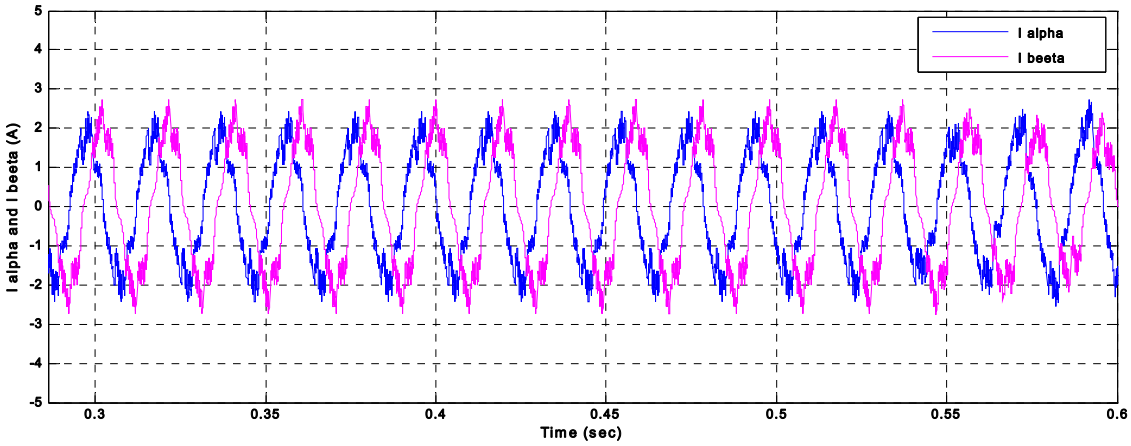

Figure 5.18 Stator I_α and I_β currents for 1000 rpm at no load

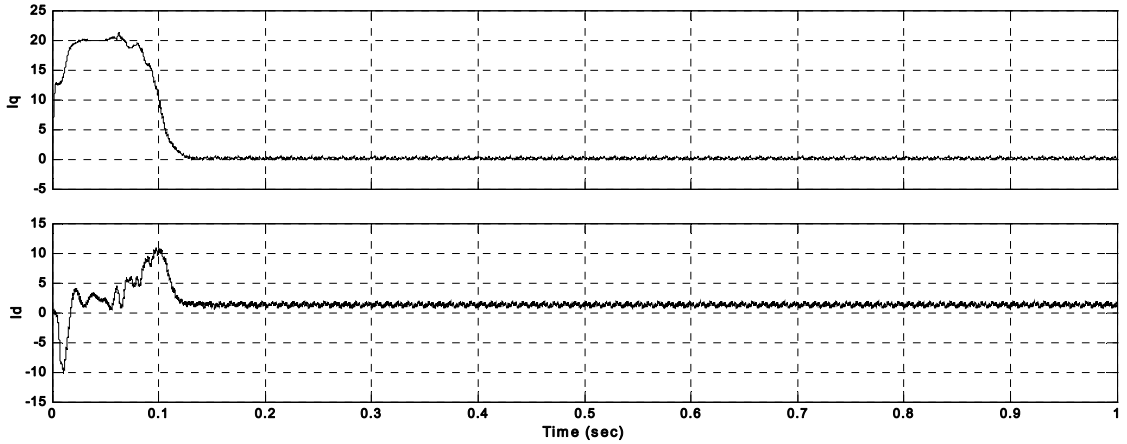

Figure 5.19 Currents I_q and I_d for 1000 rpm at no load

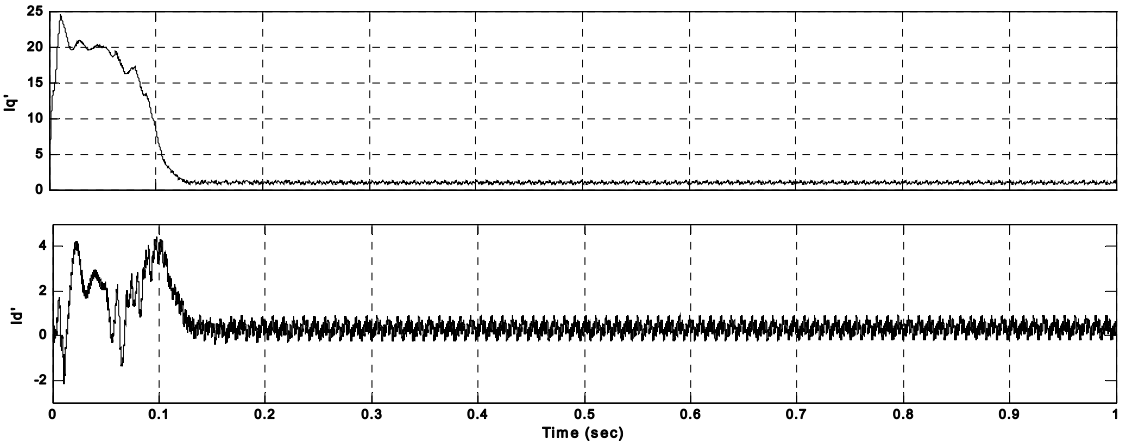

Figure 5.20 Currents I_q' and I_d' for 1000 rpm at no load

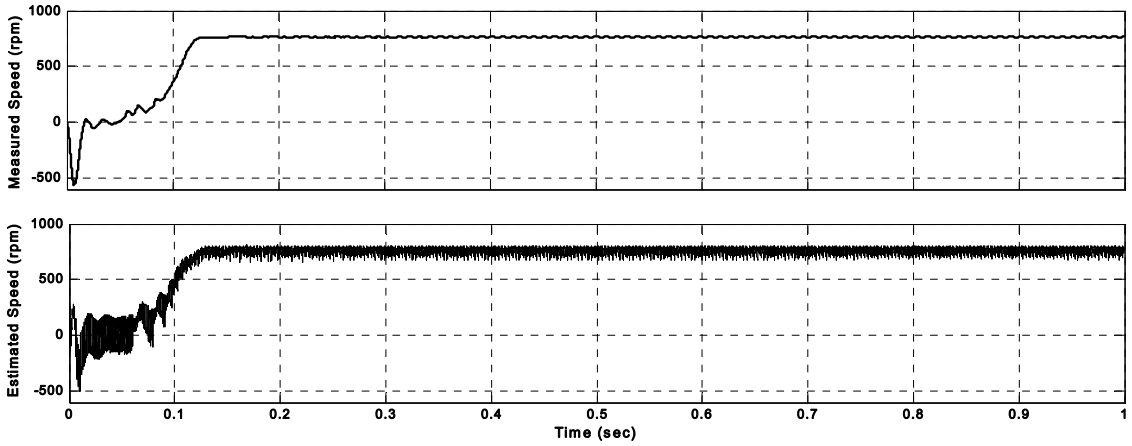

Figure 5.21 Measured and estimated rotor speed with 750 rpm ref. speed

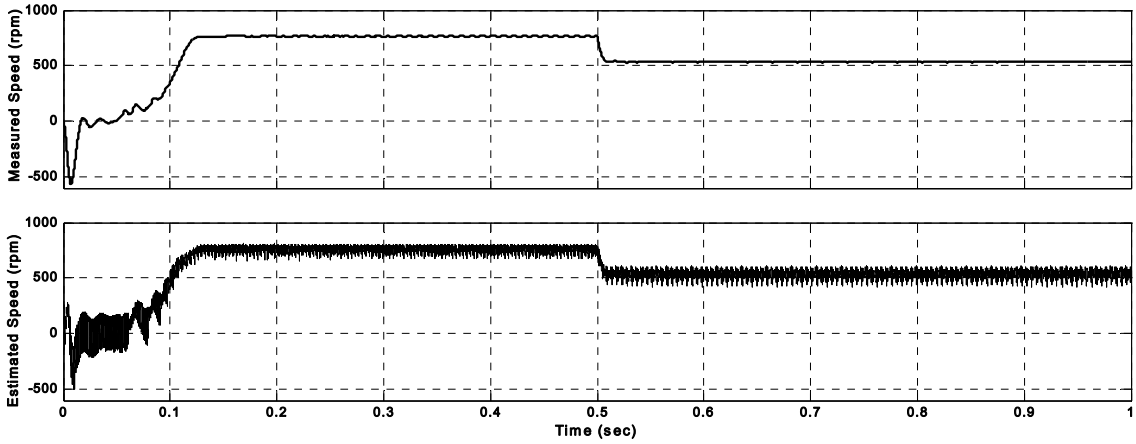

Figure 5.22 Measured and estimated rotor speed for step change 750-500 rpm at 0.5 sec

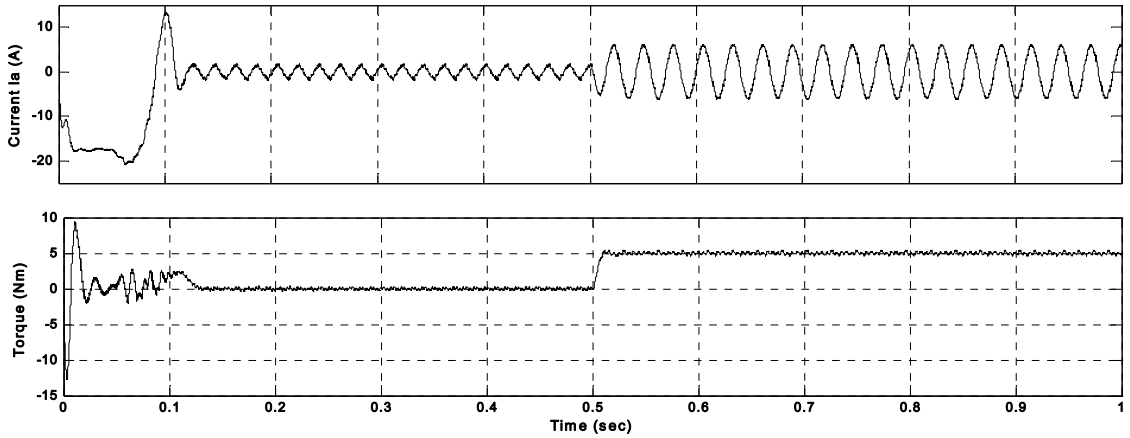

Figure 5.23 Stator current response with step change in load torque 0-5 Nm at 0.5 sec

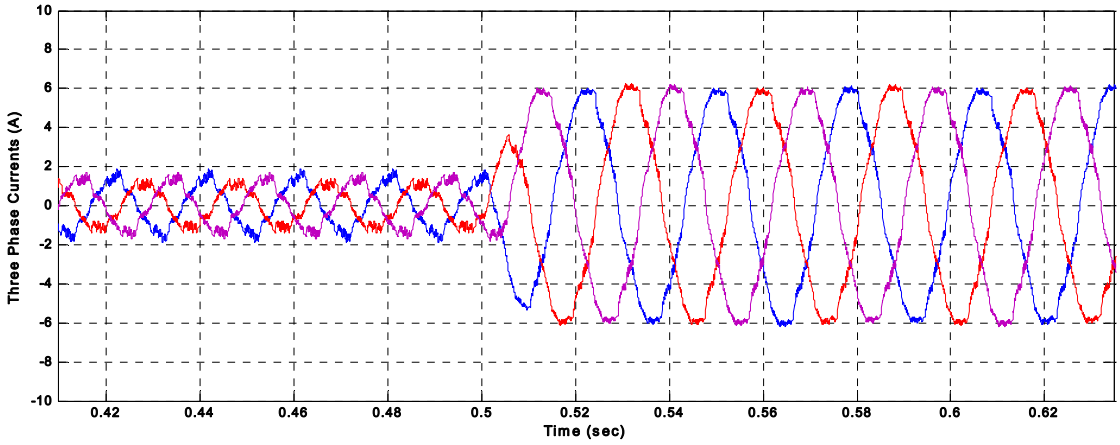

Figure 5.24 Three-phase stator currents at step change in load torque 0-5 Nm at 0.5 sec

The highlights of the chapter is as follows

- While the motor is running with variable load, the parameters will change and the performance do not remains good, the adaptive methods have capability to deal with this problem.
- The adaptive mechanism can be designed in two ways; either by using gradient method or by using stability theory.
- The error between adjustable model and reference model is given to adaptive mechanism, which commands the adjustable model, this approach allow the estimated currents to follow the measured currents.
- MRAS with some advanced controller in adaptive mechanism is one of the methods that can be used for the wide range of sensorless PMSM drive applications.
- The MRAS based sensorless PMSM drive [121] with MPTA and field weakening capability is suitable for low cost high performance applications.

5.6 Conclusion

A model reference adaptive system has been investigated to estimate the rotor speed and position, by using PMSM as reference model, PMSM current equations in d-q reference frame as adjustable model and an adaptation mechanism. The estimation algorithm used is independent of stator resistance, computationally less complex, free from integrator problem because back-emf estimation is not required and provides stable operation of drive system. Traditionally a PI controller is used in the adaptation mechanism to process the error and to tune the adjustable model to achieve the estimated value of rotor speed.

The MRAS is simple and easier implementation as compared to the observer based sensorless schemes with reduced mathematical computation time. In the proposed FMRAS a FLC is designed for the adaptive mechanism processing. With the application of FLC for the error processing in adaptive mechanism, the estimator shows the robustness against the small variations in operating condition, parameters. The system anti-robustness behaviour is improved and the dynamic and static performance of drive is improved. The simulation results verified the effectiveness and feasibility of the FMRAS based estimator.

[*The system hardware, dSPACE–DS1004 interfacing and experimentation for the laboratory prototype models of the complete PMSM drive, with and without sensors are described in detail to validate the simulation results presented in previous chapters. The resolvers attached to the PMSM are used just to compare the measured and estimated rotor position with different algorithms for the development of sensorless PMSM drive. Further, these experimental studies are validated with simulation results using the experimental parameters.*].

6.1 Introduction

To validate the viability and effectiveness of the different algorithms used for sensorless PMSM drive are−

1. The PMSM drive with fuzzy speed controller.
2. The PMSM drive with fuzzy speed controller and PI current controller.
3. The PMSM drive with fuzzy speed controller and fuzzy current controller.
4. Sensorless PMSM drive with sliding mode observer based estimation of rotor position.
5. Sensorless PMSM drive with AI based MRAS for estimation of rotor position.

In the experimentation dSPACE version DS1104 is used for prototyping. The pulses to the inverter devices are given through digital I/O of dSPACE. Three phase inverter, used here, is an intelligent power module (PEC16DSM01) make Vi Microsystems. Feedback signals are given to ADC channels for further processing and calculations. This rapid control prototyping system consists of both, hardware and software. The hardware is composed of the CPL1104 controller board with analogue and digital I/O. The analogue I/O can send or receive signals within the range of ±10 V and the digital I/Os operate within TTL (Transistor-transistor logic) range. All signals in CPL1104 can be monitored by status LEDs. The software consists of real time interface (RTI) blocks that connect the software-implemented controller to the hardware controller boards. Moreover, Control Desk is software that allows the user to run experiments, modify the parameters and operating points online and to visualize the chosen signals involved during the experiment.

The power circuit consists of an auto-transformer, and a two-level IGBT based inverter module, two mechanically coupled PMSM with resolver. As its clear from the diagram that one PMSM is working as motor and other as generator. The power capability of used PMSM in experimentation is 1 KW. Both the motors have 24 volt DC brake and resolvers. The IPM used takes three-phase supply as input and internally first converts is into DC. Through DC-link it is connected to inverter which receives gate pulses externally from user by analogue channel of dSPACE.

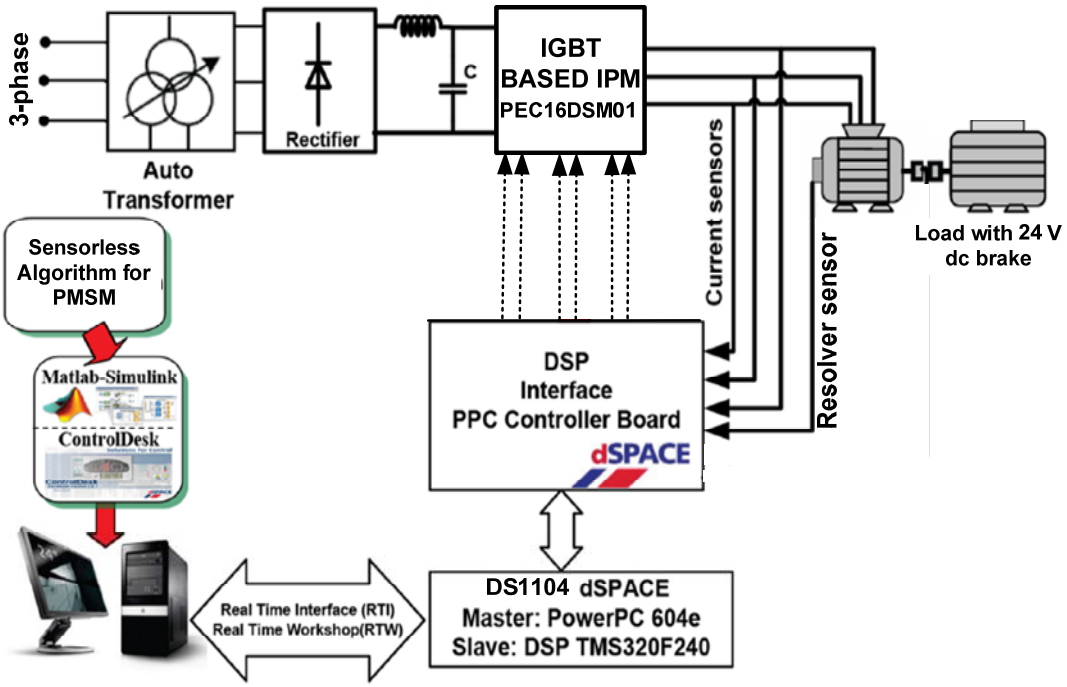

Figure 6.1 Experimental schematic diagram of setup

6.2 Development of System Hardware

In the development of hardware prototype following sub parts are designed/assembled.

1) Power module as inverter
2) Interfacing circuits
3) Measurement circuits
   - Position measurement by resolver
   - Voltage measurement
   - Current measurement

6.2.1 Inverter Power Module

The intelligent power module (IPM) works as converter (rectifier or inverter) and have advanced hybrid power devices [122]. The IPM has high speed, low loss IGBTs with optimized gate drive and inbuilt protection circuit. It has the IGBT based power module of rating 1200V, 25A and operates by receiving the pulses from DSP or dSPACE. The internal diagram of the power module is shown in Figure 6.2.

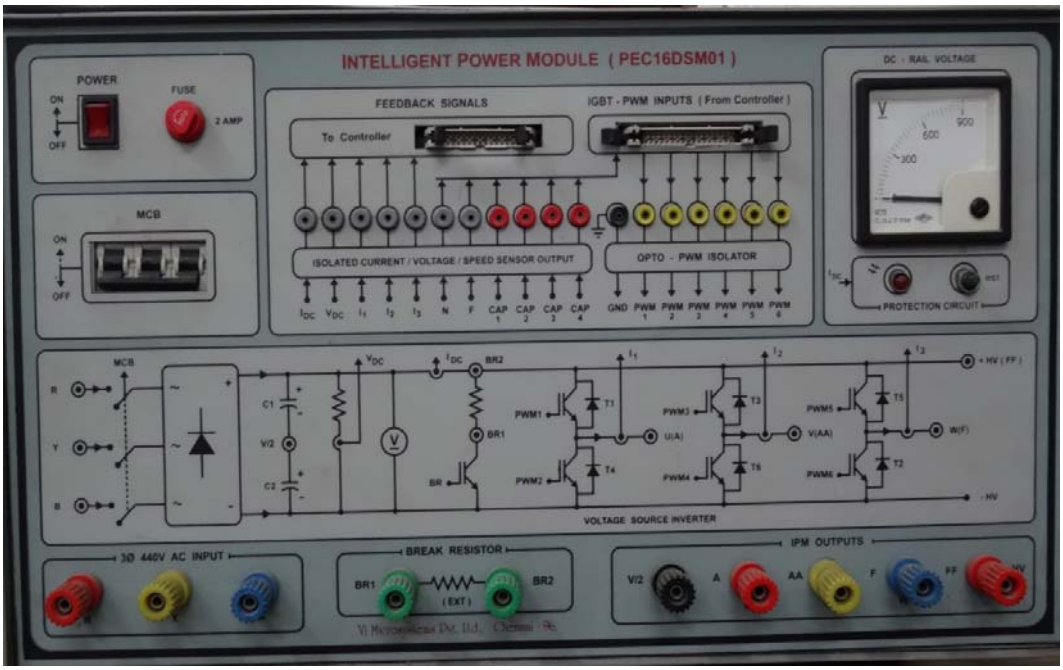

Figure 6.2 Front pannel of IPM

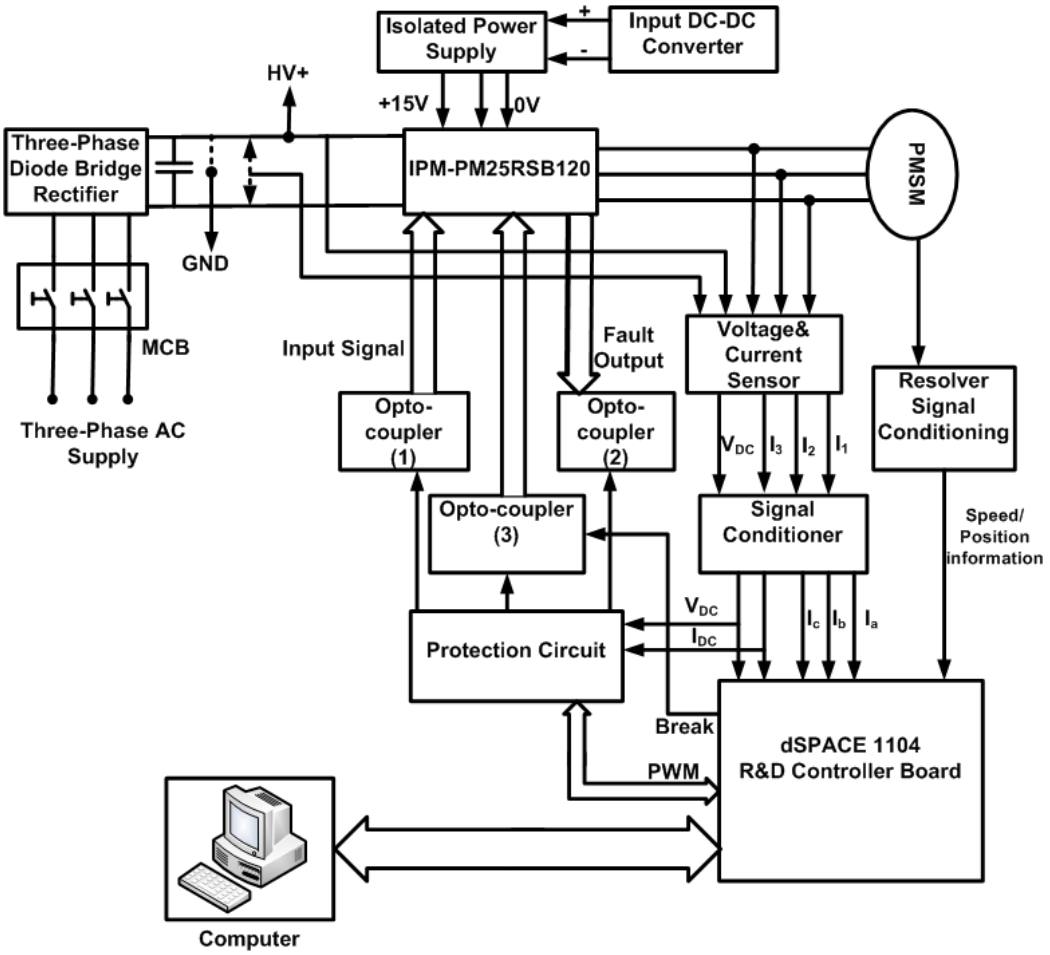

Figure 6.3 IPM internal diagram and connections

. The over-current and short-circuit protection is realized using advance current sense IGBT chips, which allows the regular monitoring of the power device current. The integrated over-temperature and under voltage protection makes the system more reliable, the temperature sensors are mounted on the isolating base near to the IGBT. When the temperature of base plate goes beyond over temperature trip level (OT), the power devices are protected by disabling the gate drive internally and ignoring the control input signals. The IPM is optimized to minimum switching losses to meet the industrial demand for acoustically noiseless inverters with carrier frequencies upto 20 kHz. The in-built gate drive and protection circuit has been designed in such a way that it requires the minimum components for user interface circuit. ML57120L is a non-isolated DC-DC converter with a built-in transformer with wide range of input voltage (DC 113V-400V), which enable the direct connection to rectified 120V and 240V AC.

The IPM output current and voltage are directly not fed to protection circuits, as the output voltage of IPM is very high, so using transducers voltage is sensed and converted in the range of ±5V. The opto-coupler in the IPM isolates the power circuit from control circuit and protects the control circuitry in case of fault in the power circuit. The gate pulse signals to IGBTs (PWM1-PWM6) are given from the dSPACE depending on control circuit designed in MATLAB using the computer.

The IPM used in the experimentation of PMSM drive is Vi Microsystems made, model no. PEC16DSMO-1. This IPM is specially designed for motor control applications upto 3 HP, using 3rd generation IGBT and DIODE technology. The feature and rating of the IPM is given here.

- Input: single phase/three-phase AC 50 Hz.
- Output: 400V/10A AC/DC on each leg of three-phase bridge
- 1200V, 25A Three-phase IGBT inverter bridge
- 1200V, 10A IGBT for over voltage braking
- Built-in over voltage, under voltage, over current and over temperature protection

The additional features of the IPM used in this work is as follows-

- SPM (Smart Power Module) based IGBT power circuit is used
- 1200V, 25A AC-DC power conversion
- 4 no. of hall-effect current sensors for DC-link current and output currents three-phase inverter bridge
- 1 hall-effect voltage sensor for DC-link voltage and a analogue
- voltmeter on the front panel
- 1 no. of diode-bridge rectifier with filter capacitor for DC-rail
- All PWM signals (PWM1-PWM6) are isolated using Opto-isolator

- Protection against over current with LED indication
- Optically isolated fault signal to dSPACE for protection
- All circuits have independent isolated power supplies
- A voltmeter 0-900V for DC-link voltage on front panel
- All PWM signals, feedback signals, and currents are terminated at front panel
- A FRC connector is provided to interface with other controller (DSP or embedded controller) if required
- 1 no. of protection circuit with indication and a reset switch is provided
- All inputs/outputs are terminated at banana sockets

6.2.2 dSPACE DS1104

The dSPACE system based on DS1104 R&D controller board comprises both hardware and software. It is specifically designed for the high speed multivariable digital control applications and real-time simulation. It is a standard board that can be easily fitted into PCI port of a computer. It is 603 PowerPC floating point processor based real-time controller. The board has a TMS320F240 DSP based slave-DSP subsystem for the advanced I/O purposes. The Rapid Control Prototyping (RCP) is accomplished by available specific connectors on board, where access to all input and output signals is possible. For the development of cost-sensitive RCP application, DS1104 is the ideal hardware.

This rapid control prototyping system consists of both, hardware and software. The hardware is composed of the CPL1104 controller board with analogue and digital I/O. The analogue I/O can send or receive signals within the range of ±10 V and the digital I/Os operate within TTL (Transistor-transistor logic) range. All signals in CPL1104 can be monitored by status LEDs.

The software consists of real time interface (RTI) blocks that connect the software-implemented controller to the hardware controller boards. Moreover, Control Desk is software that allows the user to run experiments, modify the parameters and operating points online and to visualize the chosen signals involved during the experiment.

6.2.2.1 Hardware

The DS1104 has ADCs, DACs and other type of input and output connectors, indication LEDs on the board. The parameter characteristics of DS1104 R & D controller board is given in Table 6-1.

Table 6-1 Parameters of DS1104 R&D Controller Board

Parameter	Characteristics/Values
Processor	➢ MPC8240 with PPC603e core and on-chip peripherals ➢ Floating point processor ➢ 250 MHz CPU ➢ On-chip 2X16 KB cache ➢ On-chip PCI bridge (33MHz)
Memory	➢ Global memory: 32 MB SDRAM ➢ Flash memory: 8 MB
Interrupt Controller	➢ 5 Timer interrupts ➢ 2 Incremental encoder index line interrupts ➢ 1 UART interrupt ➢ 1 Slave DSP interrupt ➢ 1 Slave DSP PWM interrupt ➢ 05 ADC end of conversion interrupts ➢ 1 host interrupt ➢ 4 user interrupts from the I/O connector
ADC 1 X 16 bit ADC with MUX	➢ 4 Muxed channels with one 16-bit sample and hold ADC [05 ADCs (1X16-bit+ 4X12-bit)] ➢ 16-bit resolution ➢ Input voltage range ±10V ➢ 2μs conversion time ➢ ±5 mV off-set error ➢ ±0.25% gain error ➢ >80 db signal-to-noise ratio
ADC 4 X 12-bit	➢ 4 channels with one 12-bit sample and hold ADC ➢ 12-bit resolution ➢ Input voltage range ±10V ➢ 8 ns conversion time ➢ ±5 mV off-set error ➢ ±0.25% gain error

	➢ >65 db signal-to-noise ratio
DAC 8 X 16-bit DAC	➢ 16-bit resolution ➢ Output voltage range ±10V ➢ ±5 mA maximum output current ➢ ±1 mV off-set error ➢ ±0.1% gain error ➢ >80 db signal-to-noise ratio
Digital I/O	➢ 20-bit parallel I/O ➢ Single bit selectable from input or output ➢ ±5 mA maximum output current ➢ TTL output/input levels
Digital Incremental Encoder Interface 2 X 24 bit	➢ 2 channels ➢ Selectable single-ended(TTL) or differential (RS422) input ➢ Max 1.65 MHz input frequency ➢ 24-bit loadable position counter ➢ Reset on index ➢ 5V/0.5A sensor supply voltage
Serial Interface	➢ 1 UART ➢ Selectable transceiver mode RS232/RS422/RS485 ➢ Max baud rate (RS232): 115.2 kBaud ➢ Max baud rate (RS422/RS485): 1 MBaud
Slave DSP system	➢ TI TMS320F240 DSP ➢ 16-bit fixed point processor ➢ 20 MHz clock-frequency ➢ 64k X 16 external program memory ➢ 28k X 16 external data memory ➢ 4k X 16 dual port memory for communication ➢ 16k X 16 flash memory ➢ 1 X 3-phase PWM outputs ➢ 4 X 1-phase PWM outputs ➢ 4 Capture inputs

	➢ SPI (Serial peripheral interface) ➢ Max 14-bit digital I/O ➢ TTL output/input levels for all digital I/O pins ➢ ±13 mA maximum output current
Host Interface	➢ 32-bit PCI host interface ➢ 5V PCI slot ➢ 33 MHz ± 5%
Physical size	➢ PCI 185 X 106.68 mm
Ambient Temperature	➢ 0….55 ºC
Cooling	➢ Air cooled by fan
Power Supply	➢ +5 V± 5 %, 2.5 A ➢ +12 V± 5 %, 0.3 A ➢ -12 V± 5 %, 0.2 A
Power Consumption	➢ 18.5 W

6.2.2.2 Software

Historically, control softwares were developed using assembly language. In recent years, industry began to adopt MATLAB/SIMULINK and Real-Time Workshop (RTW) platform based method, which provides a systematic approach to develop control software. Figure 6.4 shows the Total Development Environment (TDE) of dSPACE and its major component blocks.

- MATLAB is widely used as an interactive tool for modelling, simulations and visualization of real-time systems, which contains more than 600 mathematical functions and supports additional toolboxes to make it more inclusive.
- SIMULINK is a MATLAB add-on software that enables block diagram based modelling and analysis of linear, non-linear, and hybrid systems.
- RTW is SIMULINK add-on software that enables automatic C or ADA code generation from the SIMULINK model. The optimized code, so generated can be executed on computer, microcontrollers, DSP, etc.
- Real Time Interface (RTI) is add-on software of dSPACE provides the libraries for I/O hardware integration of DS1104 R&D controller board and generates optimized code for master and slave processors of board.
- dSPACE's control desk is a software tool for interfacing with real-time experimental setup and provides easy and flexible analysis, visualization, control, data acquisition and automation of the experimental work. The main feature of real-time simulation is that the simulation has to be carried out as

quickly as real system would actually run, thus allowing to combine the simulation and the inverter (real plant).

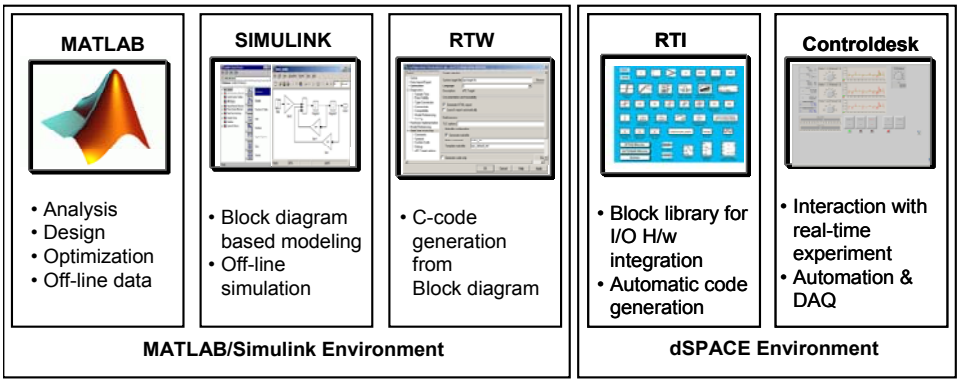

Figure 6.4 Environment of dSPACE for real-time applications

The sensed voltages and currents are fed to the dSPACE via ADC channels of connector panel. In order to add an I/O block (such as ADCs or master bit I/Os in this case) to the SIMULINK model, the required block is dragged from the dSPACE I/O library and dropped into the SIMULINK model of the PMSM drive. In fact, adding a dSPACE I/O block to a SIMULINK model is similar to adding any SIMULINK block to the simulation model. In this case, six master bit I/Os, configured in the output mode, are connected to the model for issuing six gating signals o the IGBT based IPM. In addition, eight ADCs are connected to the model for giving the motor phase current, input voltage, and resolver secondary signals as input to the DSP.

Since a balanced three-phase system has been considered, hardware requirement can be minimized by adding electrical quantities of two separate phases and from the resulting quantity, the corresponding value for the third phase is obtained. For example, the source line currents i_{Sa} and i_{Sb} are measured and the remaining line current i_{Sc} has been obtained by $i_{sc} = -\left(i_{sa} + i_{sb}\right)$. Similarly to sense three phase supply voltages and three input currents, two sensors are used in each case. These sensed signals are used for processing in control algorithm. Because real-time simulation is a major aspect for control system applications, the same is true for the automatic generation of real-time code, which can be implemented on the system hardware. For dSPACE based systems, Real-Time Interface (RTI) carries out the link function. Together with RTW from the Mathworks®, it automatically generates the real-time code from SIMULINK models and implements this code on dSPACE real-time prototype hardware. It saves the time and effort significantly as there is no need to manually convert the MATLAB SIMULINK model to other language such as 'C'. RTI carries out necessary steps needing only addition of the mandatory dSPACE blocks (I/O interfaces, etc.) to the SIMULINK model. The RTI is an interface between SIMULINK and various dSPACE based

platforms. It is implementation software for single-board hardware and connects the simulation control models to the I/O of the board. In this case, the optimized C-code of the SIMULINK model of the control algorithm is automatically generated by the RTW of MATLAB in combination with RTI of dSPACE DS.1104.

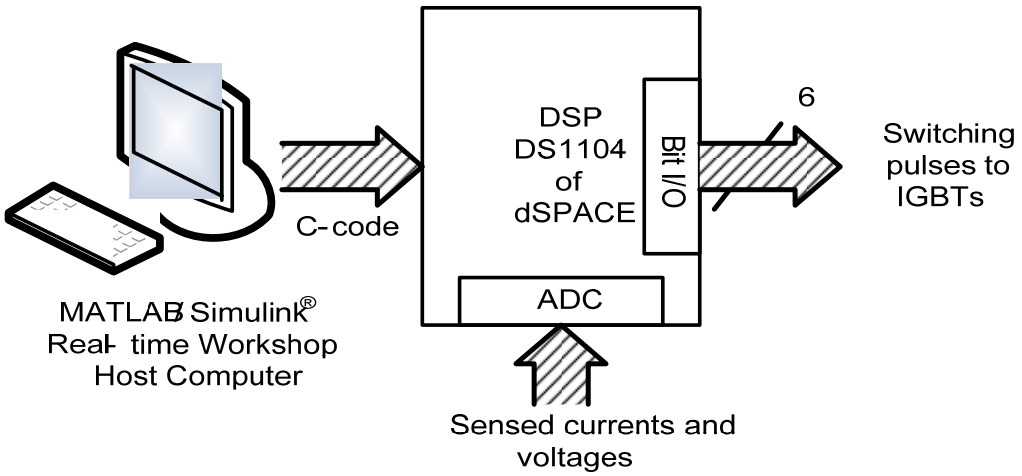

Figure 6.5 dSPACE-DS1104 circuit interfacing

The generated code is then automatically downloaded into the dSPACE hardware where it is implemented in real-time and the gating signals are generated. The gating pulses for the power switches of converter are issued via the Master-bit I/Os available on the dSPACE board. The CLP1104 Connector/LED combo panel provides easy-to-use connections between DS1104 board and the devices to be connected to it. The panel also provides an array of LEDs indicating the states of digital signals.

6.2.3 Measurement Circuit

The accurate and reliable operation of drive in close-loop requires the measurement of different parameters, like input AC voltage to motor, winding currents and rotor position information provided by resolver in-built with motor. The measurement circuit must be accurate, have the galvanic isolation from power circuit and must provide the linear response to its input (voltage or current). The hall-effect sensors and isolation amplifiers used to accomplish the above requirement of sensing circuits.

6.2.3.1 Voltage Sensing

As the motor is fed three-phase AC power from the inverter power module, the input voltage to the PMSM is measured at output terminal of inverter using three voltage sensors. These voltage sensors use the isolation amplifier AD202; it is a general purpose transformer coupled isolation amplifier and capable of measuring both AC and DC voltages. This AD202 has small physical size with wide bandwidth and high accuracy.

The voltage sensor based on AD202 can be used for the voltage measurement in range of ±1 kV (peak). It needs additional power supply of ±12V to ±15V to operate the devices in the sensing circuit. The voltage to be sensed (ac or dc) is applied between the terminals 1 and 2 (across a voltage divider circuit comprising of 100 kΩ and 1 kΩ) and the voltage input to the sensor is available at the pins 1 and 2 of AD202 via a resistance of 2.2 kΩ. The isolated sensed voltage is available at the output terminal 19 of AD202. The voltage sensing circuit is shown in Figure 6.6.

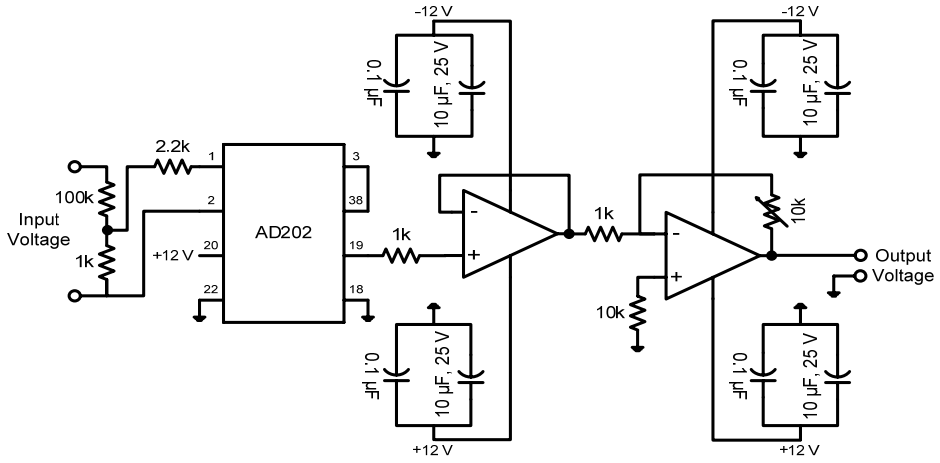

Figure 6.6 AC/DC voltage sensing circuit using AD202

The output voltage of sensor is scaled down to meet the control requirement of PMSM, and its control algorithm, and this sensed and scaled voltage is fed in the close-loop control algorithm through the ADC channel of dSPACE.

6.2.3.2 Current Sensing

The phase currents of motor are sensed by using hall-effect current sensors (TELCON HTP25). The HTP25 is a closed loop Hall-effect current transformer suitable for measuring AC currents up to 25 A. The current sensing circuit diagram is shown in Figure 6.7.

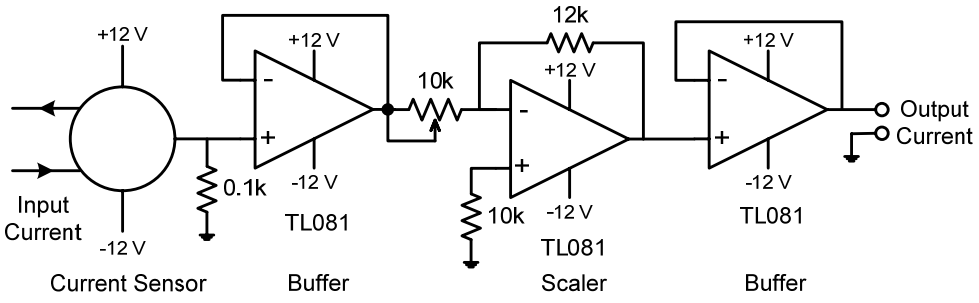

Figure 6.7 Sensing circuit for AC current

These current sensors provide the galvanic isolation between the high voltage power circuit and the low voltage control circuit and require a nominal supply voltage of the range ±12V to ±15V. It has a transformation ratio of 1000:1 and thus, its output is scaled properly to obtain the desired value of measurement.

6.2.3.3 Position Sensing using Resolver

The PMSM used in this work is in-built with the resolver mounted on the motor shaft.

Figure 6.8 Outer view of PMSM with Resolver

A resolver is used to obtain the rotor position of the PMSM. The resolver is mounted on the rotor of the PMSM. The stator of the resolver consists of three windings i.e. one primary winding and two secondary windings. The secondary windings are placed in quadrature to each other in space. A two pole permanent magnet is mounted on the rotor of the resolver. It induces sinusoidal emfs in the stator windings. Since the two secondary windings are in quadrature to each other, if the voltage induced in one is sinusoidal, then the voltage induced in the other will be co-sinusoidal. The signal conditioning circuit for the primary is shown in Figure 6.9, and for two-secondaries is shown in Figure 6.10.

A zero to 3V, 5kHz square pulse obtained from the dSPACE is amplified using a comparator and driver circuit to +5V to -5V square pulse to excite the primary winding of the resolver. A large resistance is connected across all the windings to dissipate the magnetic energy stored in these windings when the polarity of the voltages across them varies. The peak voltage induced in the secondary windings is +2.5 V to -2.5 V. The square pulse excitation of the primary winding induces emfs in the secondary windings having sharp peaks. The integrators reduce the amplitude of the sharp peaks .the signals are amplified by requisite amplification circuits. The dSPACE has an ADC input range of ± 10V, hence the output signals from the secondaries are then amplified and a requisite DC shift is added to each of the signals to make them compatible with the ADC voltage range of ADC.

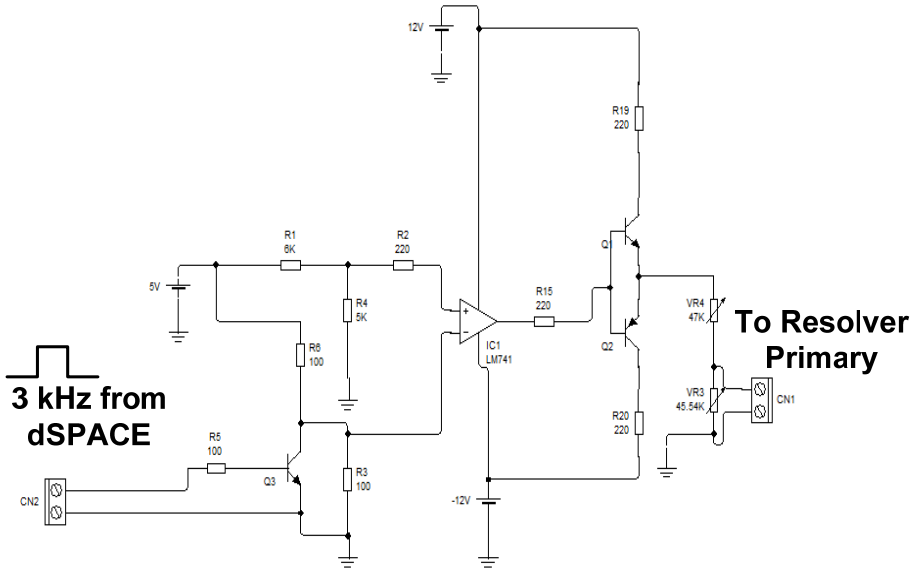

Figure 6.9 Resolver Primary Signal conditioning circuit

The resolver is basically a rotary transformer with one rotating reference winding (V_{ref}) and two stator windings. The reference winding is fixed on the rotor, and therefore, it rotates jointly with the shaft passing the output windings [21]. Two stator windings are placed in quadrature (shifted by 90°) with one another and generate the sine and cosine voltages (V_{sin}, V_{cos}) respectively. Both the windings will be further referred to as output windings. In consequence of the excitement applied on the reference winding V_{ref} and along with the angular movement of the motor shaft θ, the respective voltages are generated by resolver output windings V_{sin} , V_{cos}. The frequency of the generated voltages is identical to the reference voltage and their amplitudes vary according to the sine and cosine of the shaft angle θ as shown in figure 6. The resolver algorithm and the relevant equations are presented in chapter 2. The block diagram of resolver algorithm is shown in Figure 6.11. The ±5 V square wave signal is generated from dSPACE and given to the primary winding of resolver through DAC channel available on board and generated voltage of both secondaries are given to dSPACE through ADC channel. The input and output of the resolver is shown in Figure 6.12.

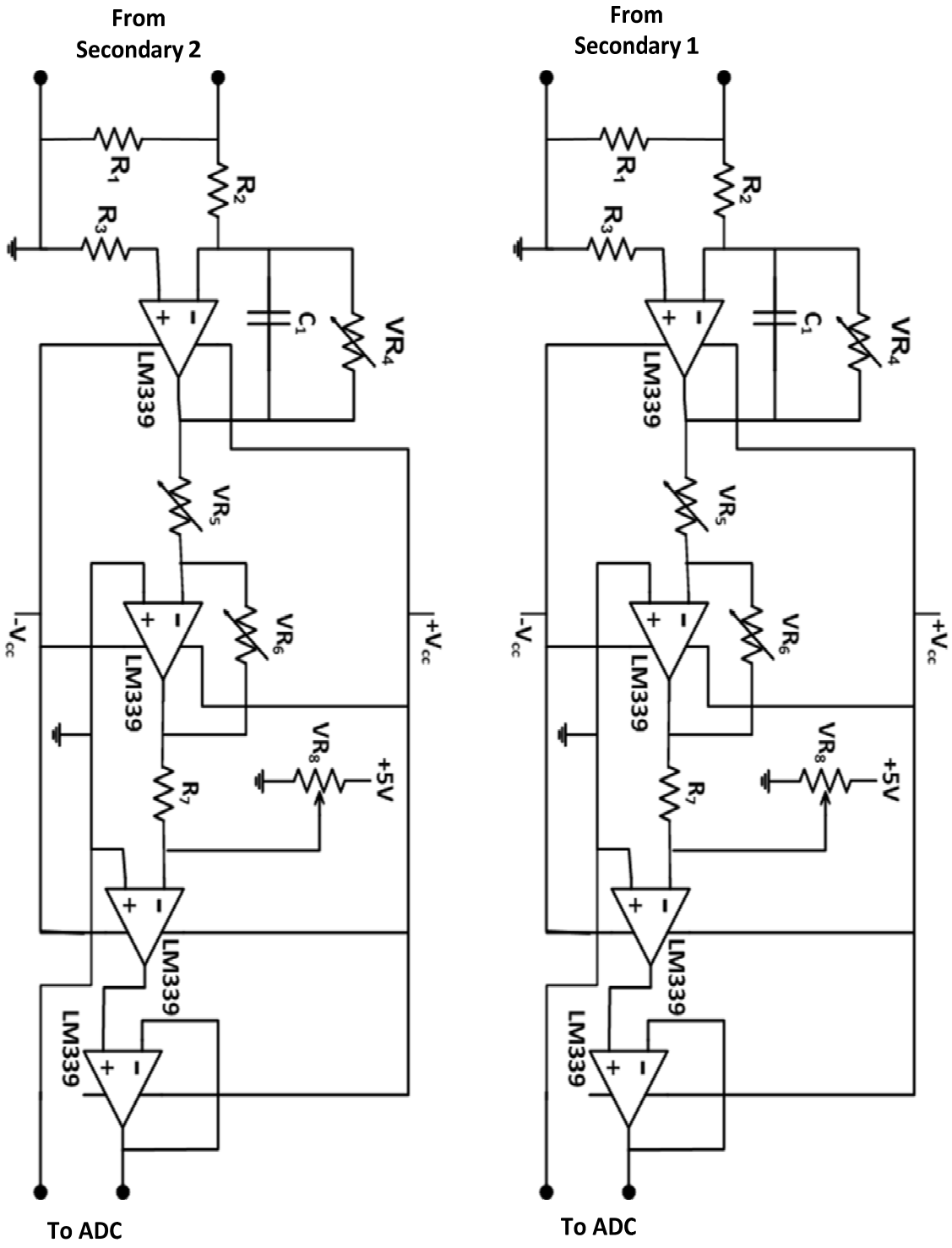

R_1=R_2=R_7=1kΩ, R_3=220Ω, VR_4=4kΩ, VR_5=1.98kΩ, VR_6=330Ω, VR_8=2kΩ (50%), C_1=0.01μF

Figure 6.10 Resolver Secondary 1 and Secondary 2 conditioning circuit

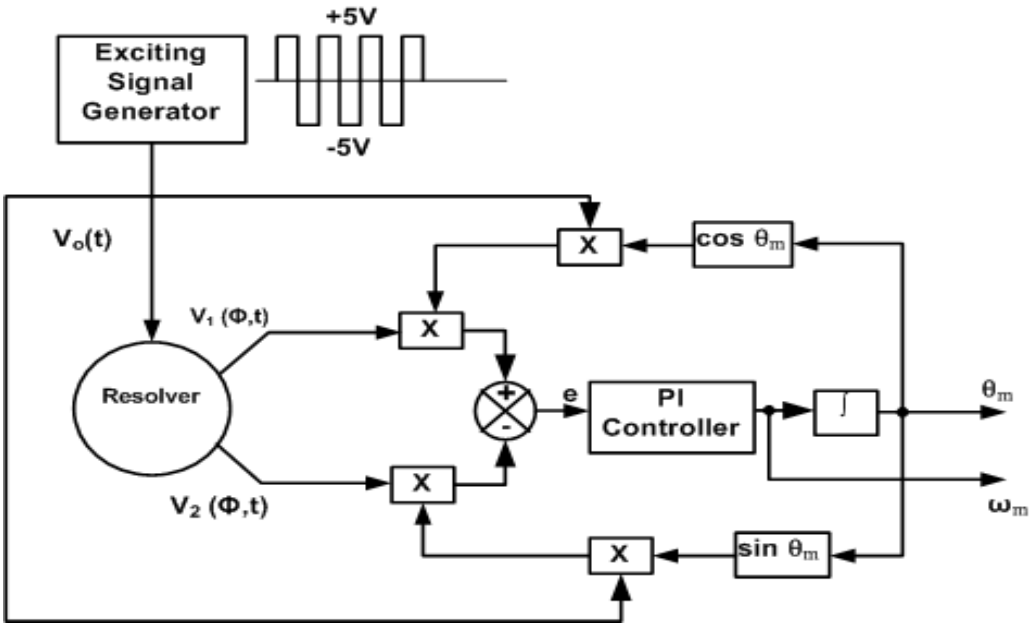

Figure 6.11 Resolver algorithm

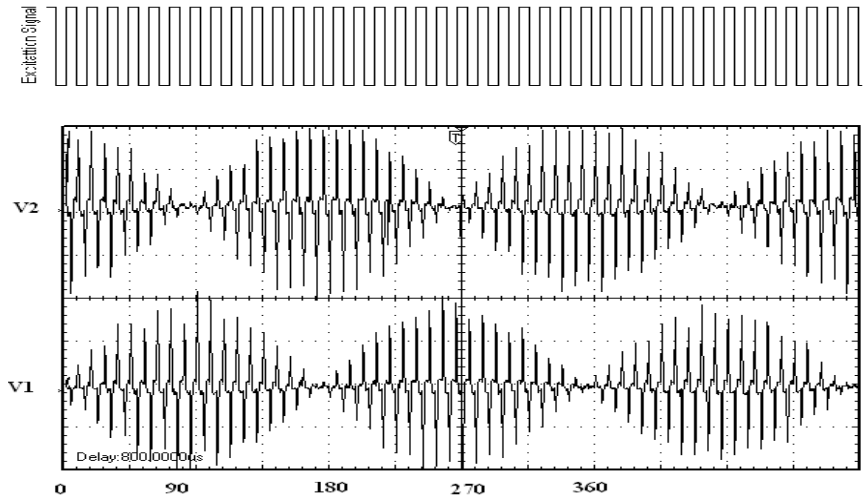

Figure 6.12 Measured rotor winding (excitation) signal and stator winding signals (V1: sine; V2: cosine) of Resolver

6.3 Experimental Results

The prototype is developed in the laboratory using a three-phase auto transformer, an IGBT based IPM (as inverter), DS 1104, voltage and current sensors, PMSM with load. The test motor is mechanically coupled to another PMSM acting as motor, three three-phase winding of load motor generates AC voltage which is given to a three-phase diode bridge rectifier which is connected to a lamp load as shown in the experimental set-up. The system parameter is given in Table 6-2. The control schemes discussed in the simulation is implemented on prototype.

Table 6-2 System Parameters

PMSM Parameter	Value
Make	MOOG G400 series brushless servo motor (MOOG GmbH D-71034 Boblingen)
Model No.	G423-814
Type	G3L40 BRAKE 1.5 Nm
BRAKE	24 V_{DC} (release)
M_0	3.7
I_{max}	4.2 A_{rms}
$V_{DC\ max}$	325 V
Power	1.4 kW
Torque Constant	0.75Nm/A
Phase Resistance (terminal to terminal)	4.1 ohm
Phase Inductance	5.15 mH
No. of Poles	08
Moment of Inertia 'J'	1.04 $kgcm^2$
Total Load Inertia	0.002 kgm^2
Damping Friction	0.0041Kgm^2
Normal Speed	3900 rpm
Maximum Speed	4500 rpm
Resolver Parameters	
Input Voltage	5V
Carrier Frequency	3 kHz
Transformation Ratio	0.5

The dSPACE ADC has a gain of 10/1, and the DAC has a gain of 1/10. The measured signal given to ADC of dSPACE divided by 10, this is the internal feature of the ADC channel, so we have to multiply the signal by 10 in SIMULINK file of control algorithm, and same is the opposite case with DAC.

The pulses for the inverter (IPM) is generated in MATLAB/Simulink, the RTI carries out the linking function for dSPACE. Together with RTW of MATLAB, it generates the real-time code for simulink model and sends this code to real-time hardware through dSPACE. The RTI performs the necessary steps after adding the required dSPACE blocks (I/O interface) to simulink models, it considerably saves the time and efforts as there is no need of manual conversion of simulink model to other language like C. The connection of simulink model and I/O of controller board is made by RTI. The optimized C code of desired control algorithms is

generated by RTW of MTLAB and RTI of dSPACE. The RTI is used to build and execute the generated code at DS1104 R&D controller board and the output signals are obtained at CP1104. The control desk is used to visualize, store and modify the parameters of a running system in real-time. The required sensed voltages, currents, speed, and rotor position is fed to ADCs and the generated gating pulses are given through master bit I/Os of dSPACE.

6.3.1 Performance Evaluation of FVC based PMSM Drive

In the experimentation dSPACE version DS1104 is used for prototyping. The pulses to the inverter devices are given through digital I/O of dSPACE. Three−phase inverter used here is an intelligent power module (PEC16DSM01) make Vi Microsystems. Feedback signals are given to ADC channels for further processing and calculations. The resolver used for position measurement required for vector control.

Figure 6.13 - Figure 6.25 shows the speed and torque response of the vector controlled PMSM drive for the various operating conditions of load and speed reference.

Figure 6.13 shows the speed and torque response of FSC and PI current controlled PMSM drive with step change in load torque at zero speed. Figure 6.14 shows the speed and torque response with step change in load torque 5-0 Nm with zero speed.

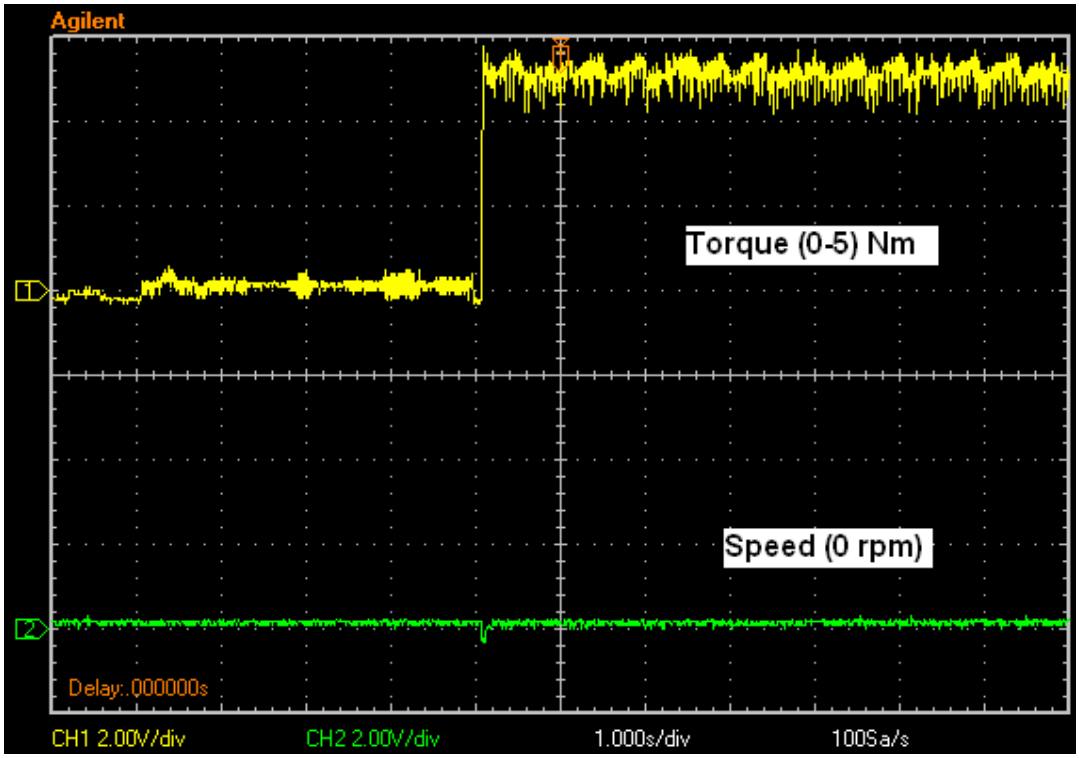

Figure 6.13 Speed (0) and Torque (0-5 Nm) response with FVC

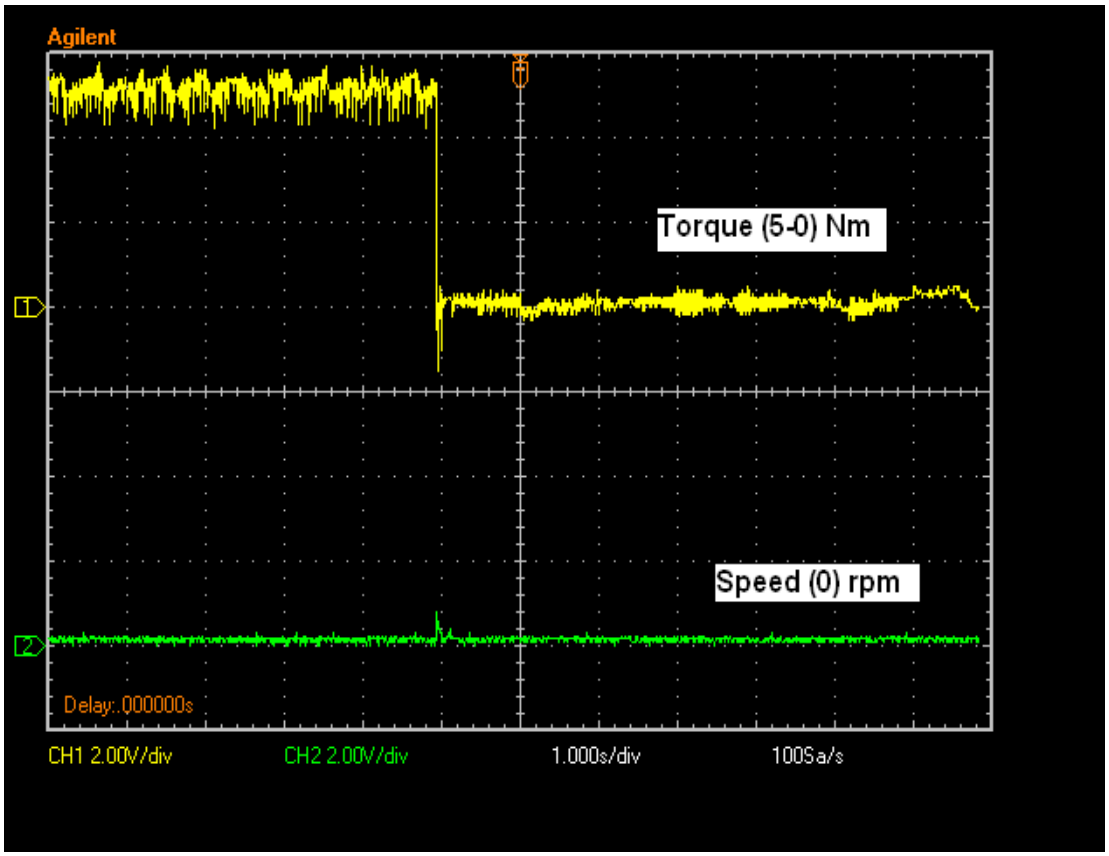

Figure 6.14 Speed (0) and Torque (5-0 Nm) response with FVC

Figure 6.15 shows the response with step change in speed (0-200-500) rpm with all PI controllers zero load torque, and Figure 6.16 shows the response with 0-200 rpm step change in speed with PI current controller and FCC.

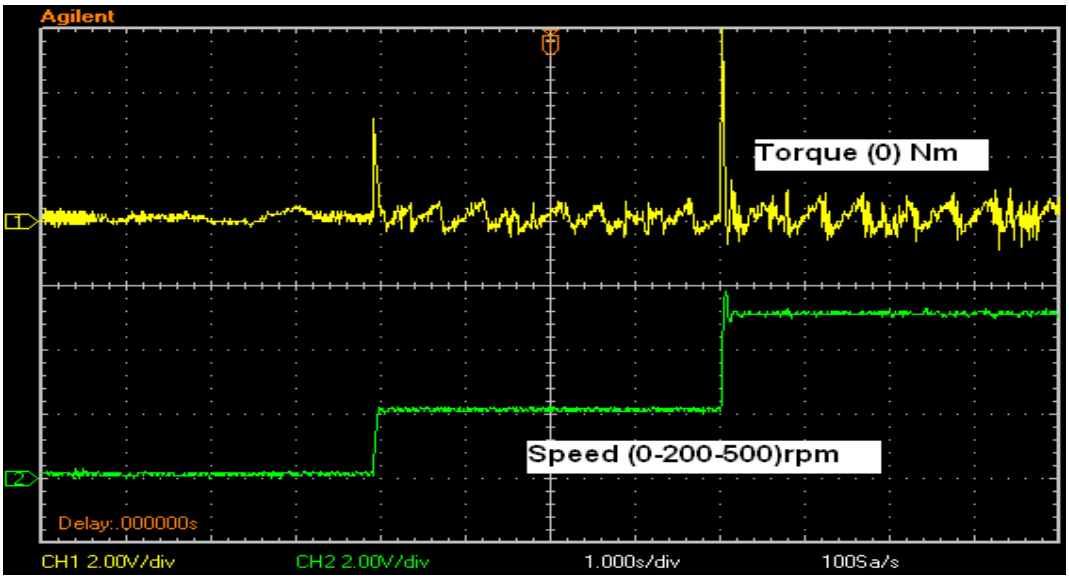

Figure 6.15 Speed (0-200-500), Torque (0) Response

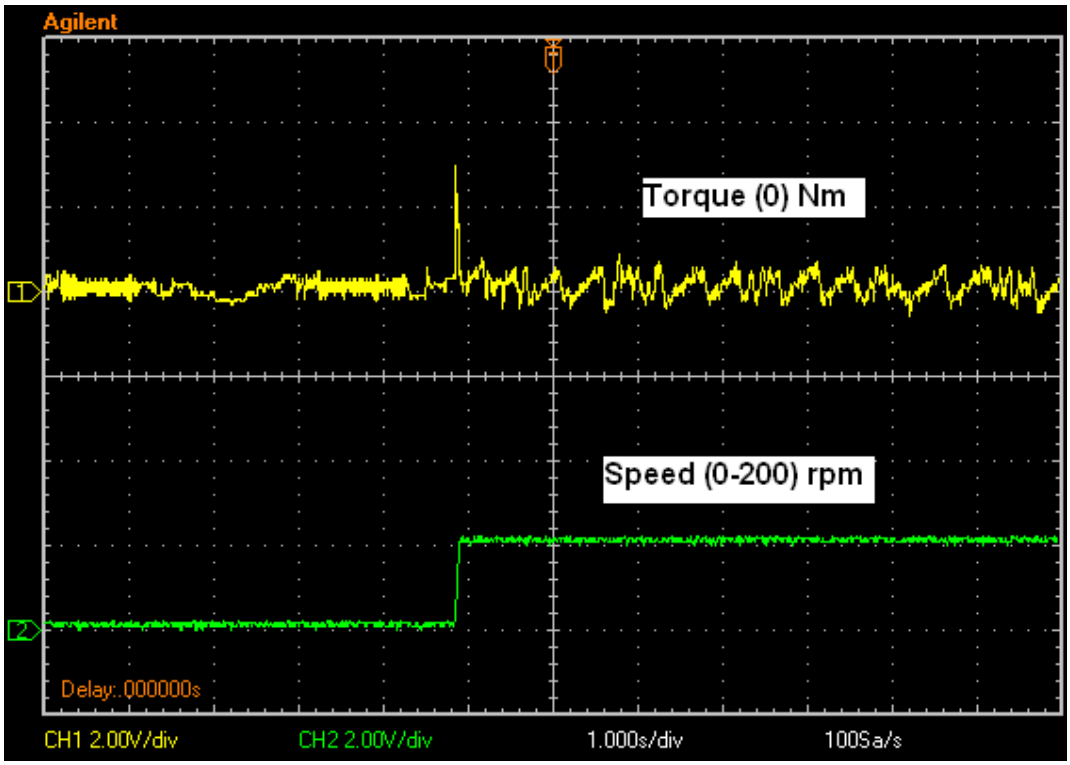

Figure 6.16 Speed (0-200), Torque (0) Nm response

Figure 6.17 shows the response with step change in speed command (0-500) rpm and load torque (0-4) Nm with PI controllers. As shown in waveform it has more ripples in speed due to PI controller. Figure 6.18 gives the response with FVC at step change in speed (0-500) rpm and zero load torque. It has less ripples as compared to Figure 6.16 and Figure 6.17.

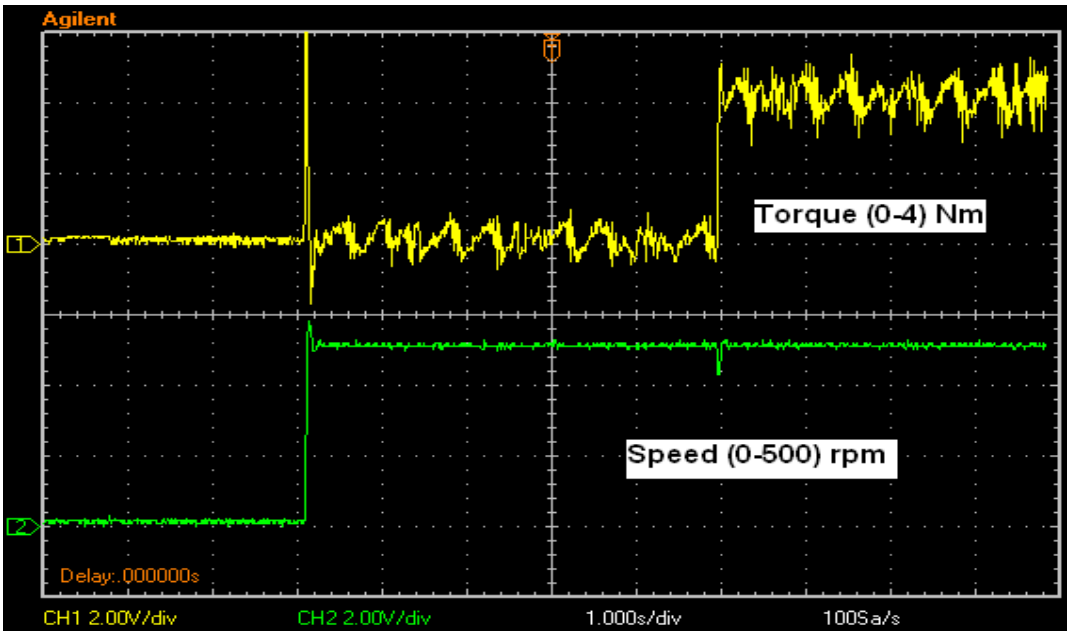

Figure 6.17 Speed (0-500), Torque (0-4) response

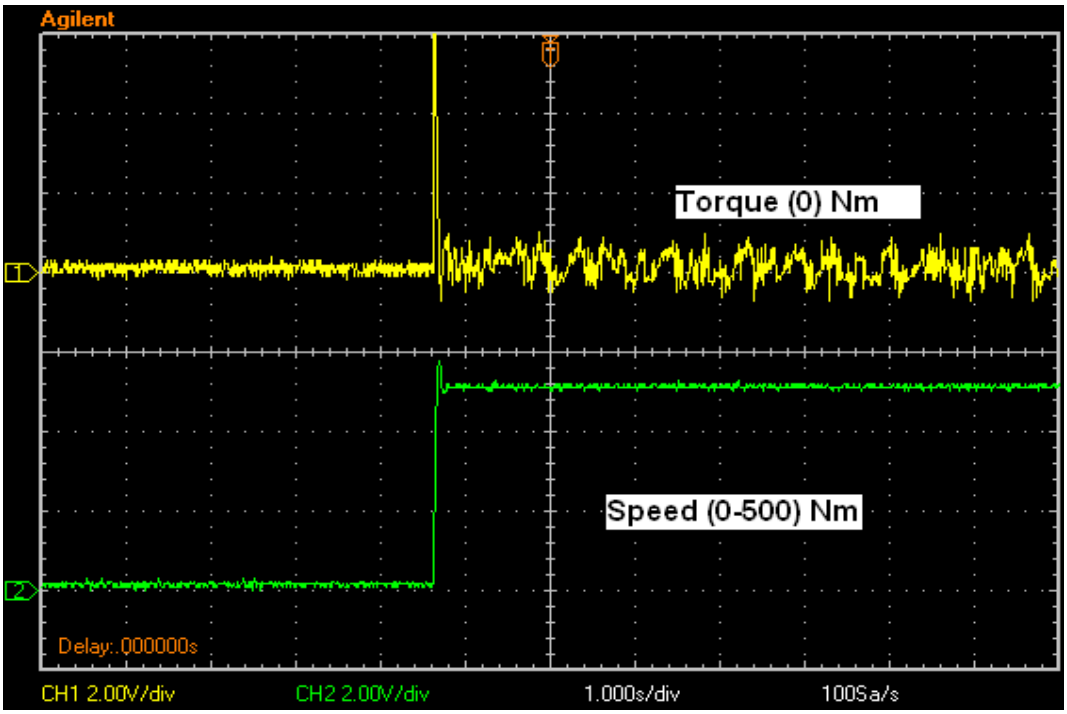

Figure 6.18 Speed (0-500), Torque (0) response

Figure 6.19 shows the response with step change in speed command (200-500) rpm and zero load torque with FVC. And Figure 6.20 gives the response with step change in speed (500-0) rpm and constant load torque of 5 Nm with FSC and PI current controllers. It has less ripples and more overshoot.

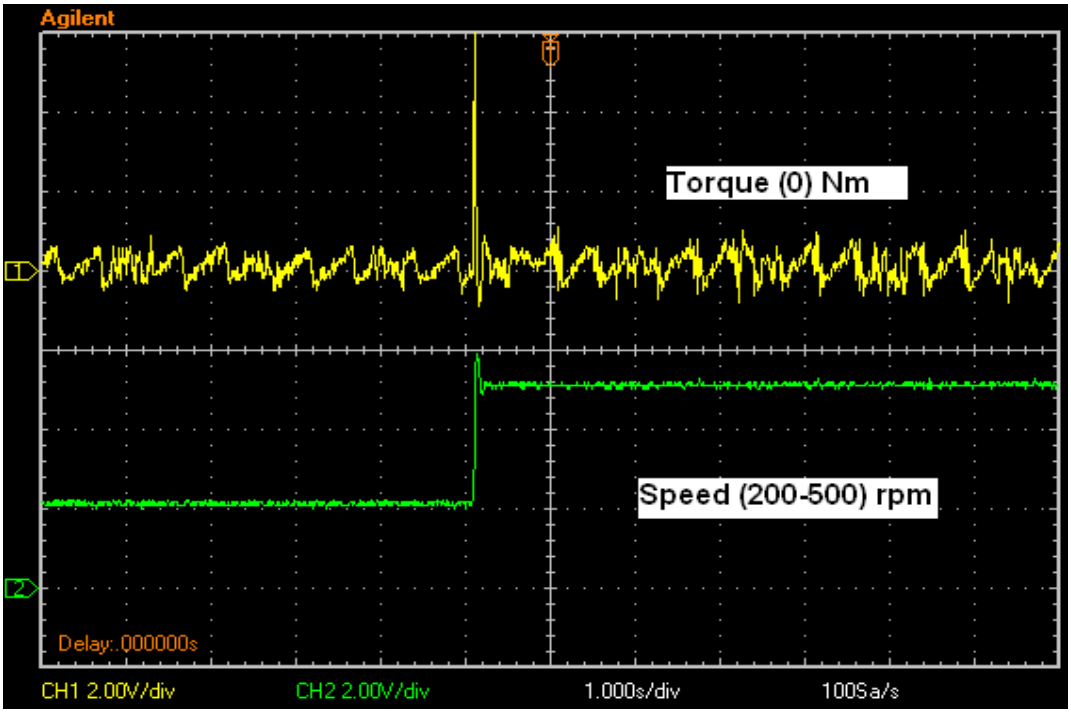

Figure 6.19 Speed (200-500), Torque (0) response

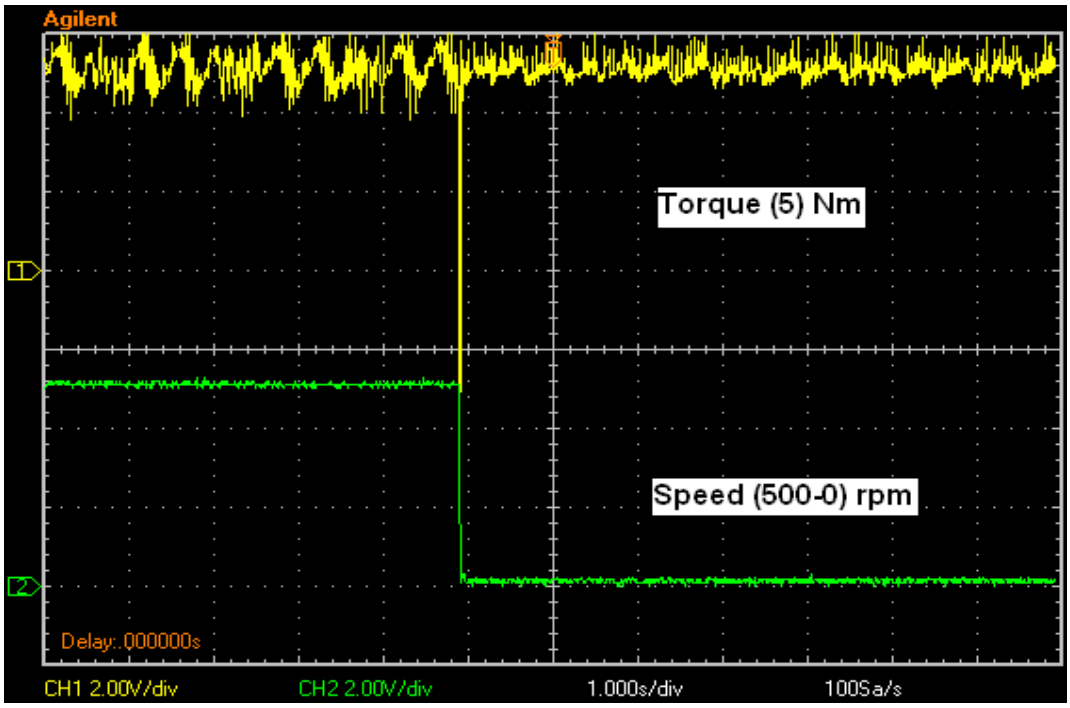

Figure 6.20 Speed (500-0), Torque (5), Nm

Figure 6.21 gives speed and torque response with step change in the reference speed (500-0) rpm with zero load torque. It has low ripples and less overshoot. The response with (500-200-0) rpm reference speed with FVC is shown in Figure 6.22; it also has low ripples and low overshoot. At transition to zero speed the torque has more overshoot.

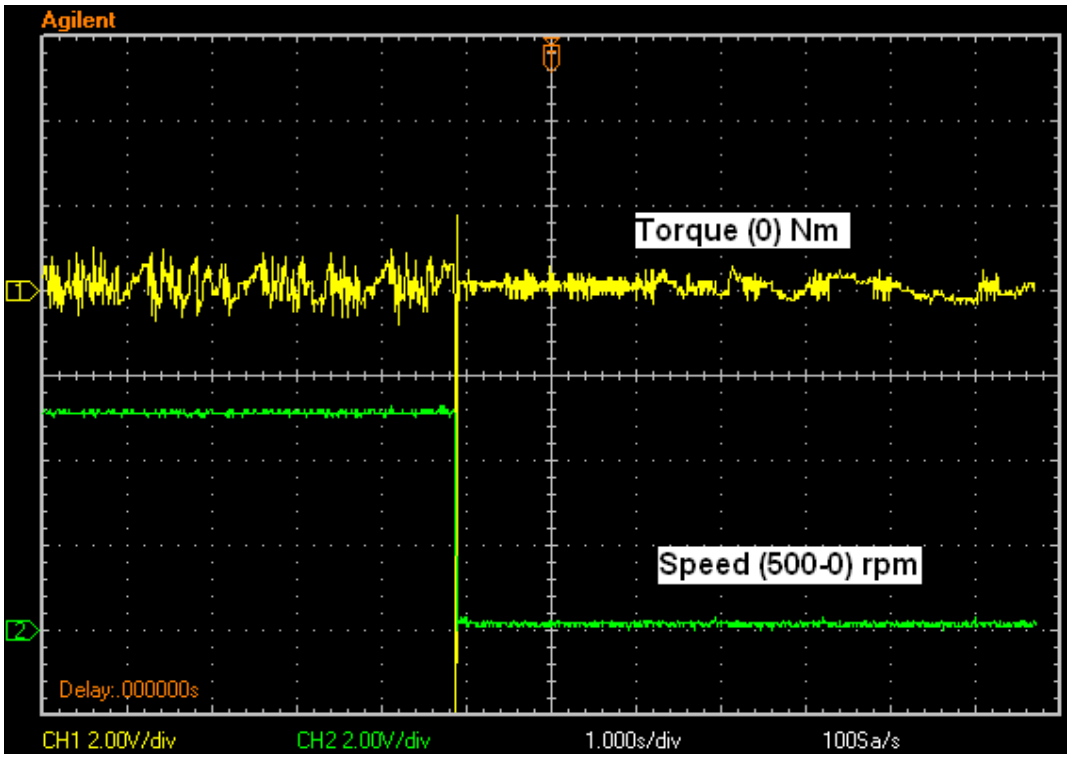

Figure 6.21 Speed (500-0), Torque (0) response

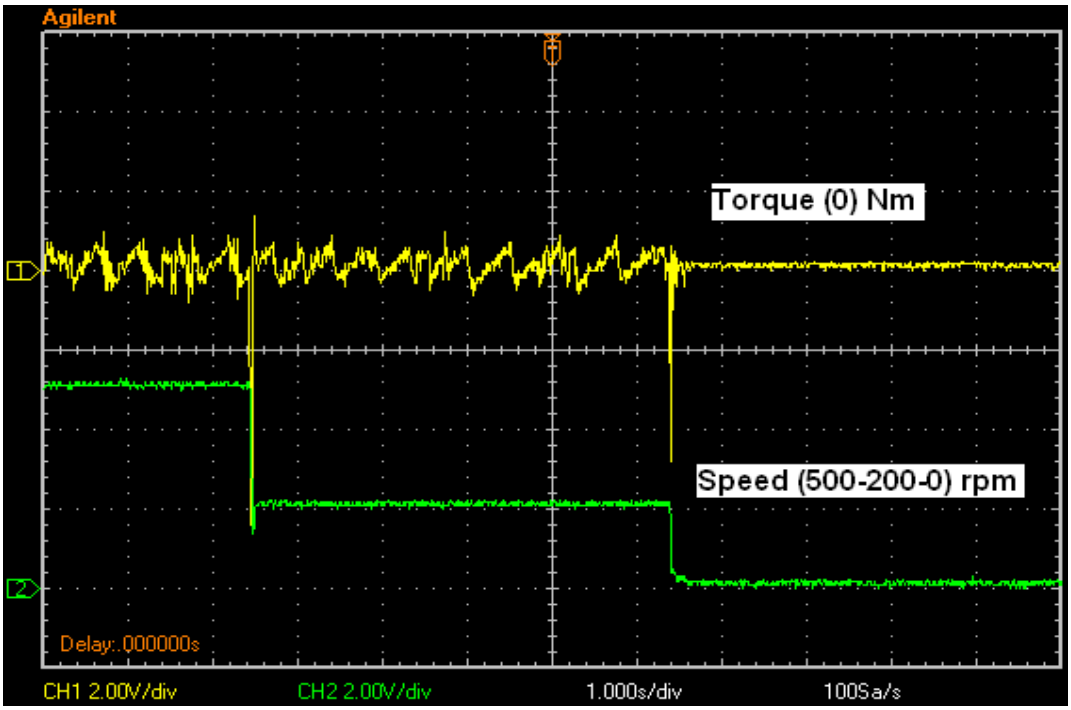

Figure 6.22 Speed (500-200-0), Torque (0) response

The speed and torque response with constant load torque of 3 Nm and step change in speed (500-200) rpm is shown in Figure 6.23, it show the very low ripples and very low overshoot in speed and torque. Figure 6.24 shows the response at constant speed of 500 rpm and the step change in load (0-5) Nm. At constant speed with FSC and current PI controller, the speed waveforms is good in terms of both ripples and overshoot, while the torque waveform has less overshoot and more ripples.

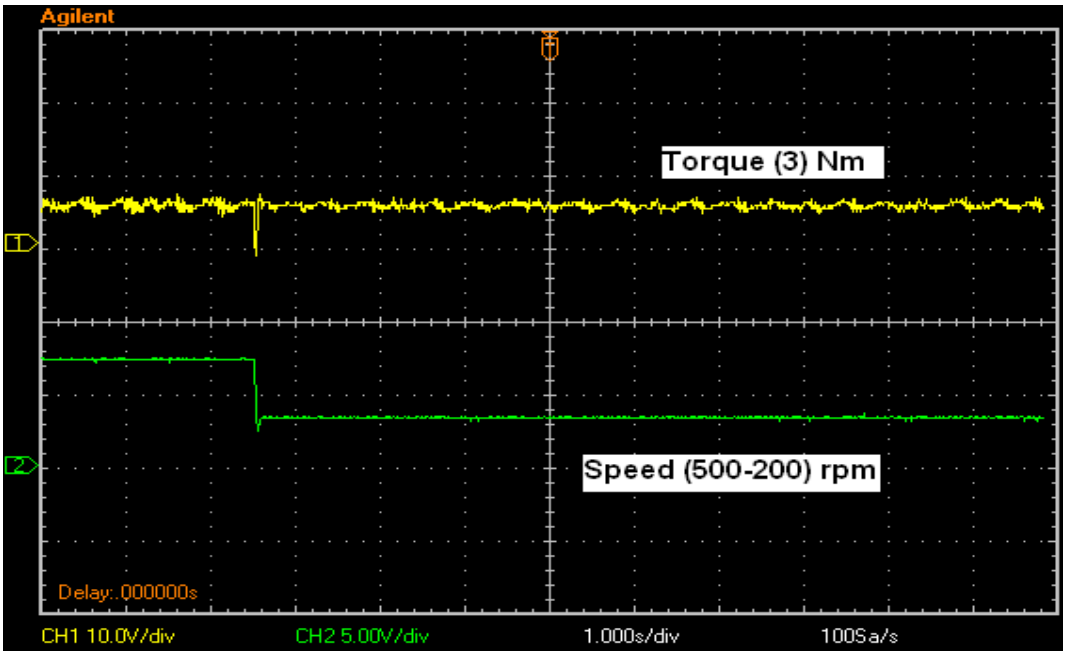

Figure 6.23 Speed (500-200), Torque (3) response

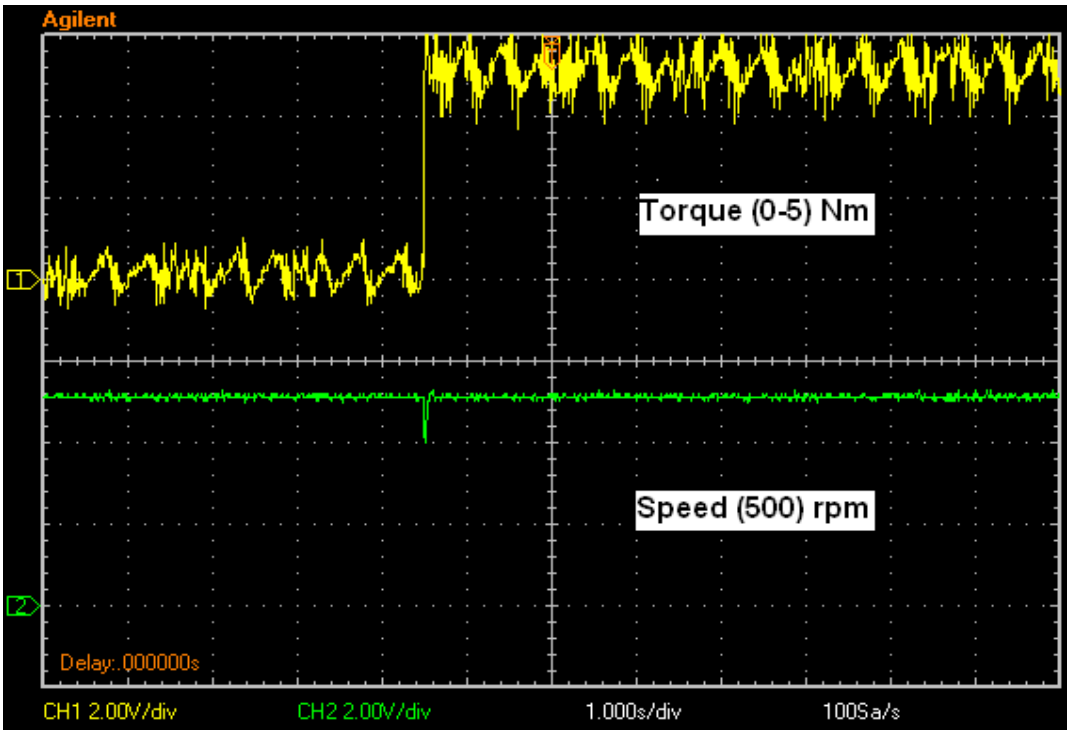

Figure 6.24 Speed (500), Torque (0-5) response

Figure 6.25 shows the response at constant speed of 500 rpm and the step change in load (5-0) Nm.

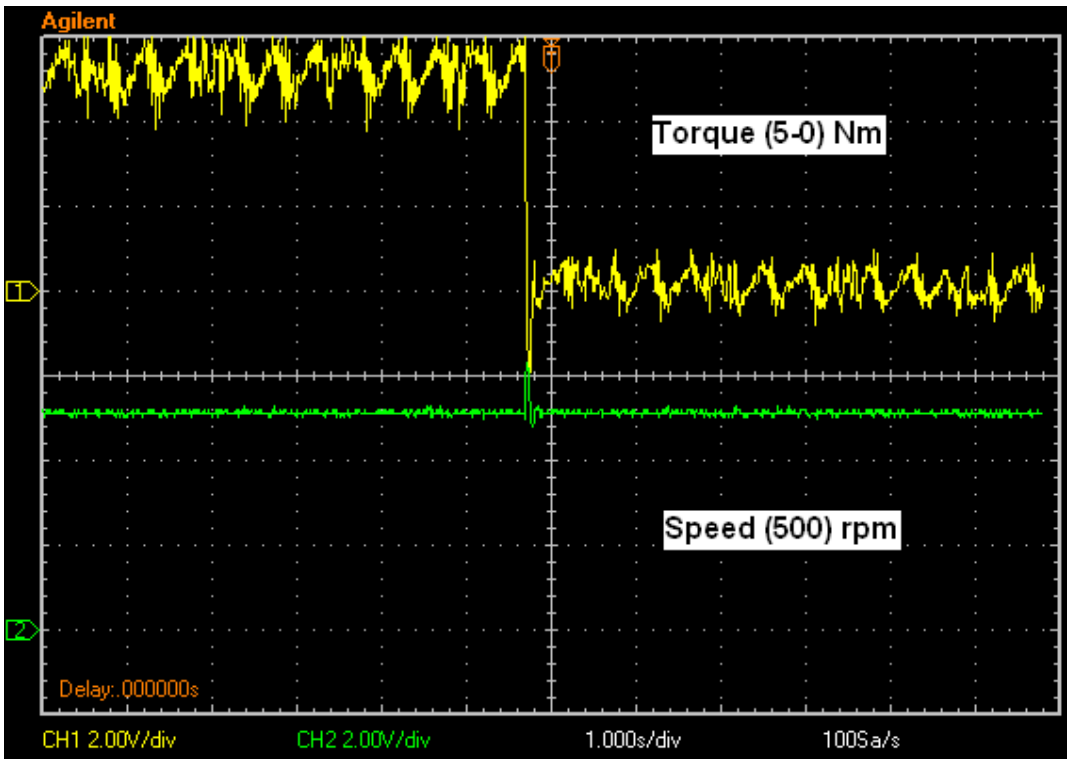

Figure 6.25 Speed (500), Torque (5-0) response

Table 6-3 Comparison of results for different current and speed controllers for vector controlled PMSM drive

Controllers	Parameter	At starting		Step change in load		Step change in speed	
		Exp.	Sim.	Exp.	Sim.	Exp.	Sim.
PI+PI	Overshoot %	4	2.8	2.0	1.3	2.8	1.7
FSC+PI	Overshoot %	2.0	2.2	1.5	1.7	1.9	1.3
PI+FCC	Overshoot %	1.2	1.1	0.9	0.8	0.9	1.2
FVC	Overshoot %	0.9	1.1	0.7	0.65	0.5	0.4

The highlights of the vector control implementation for PMSM drive obtained from the simulation and experimental results are as follows−

- The drive with speed PI and current PI controllers has more ripples in speed and torque both.
- The drive with FSC and current PI controller has fewer ripples in speed and more ripples in torque especially at load change. As the current controllers directly affect the quality of current fed to the motor.
- The drive with speed PI and FCC show the good torque response with change in loading conditions.
- The transient and steady-state performance of drive is improved by application of FVC in terms of overshoot and ripples as given in Table 6-3.
- The anti-disturbance ability is improved by application of fuzzy logic to improve the transient performance.
- At the constant speed when there is change in load, the torque has more ripples as shown in Figure 6.17.
- At no load when there is change in speed it generates high peaks in torque waveform as shown in Figure 6.15.

The signals generated at the secondary of resolver are processed in the resolver conditioning circuit and then given to ADC of dSPACE. These signals appear in the control desk as shown in Figure 6.27 and Figure 6.28 at two different positions. Figure 6.29 shows

the resolver secondary signals when the motor is at stop. Figure 6.26 shows the measured rotor position of PMSM running in reverse direction as theta is of decreasing in nature.

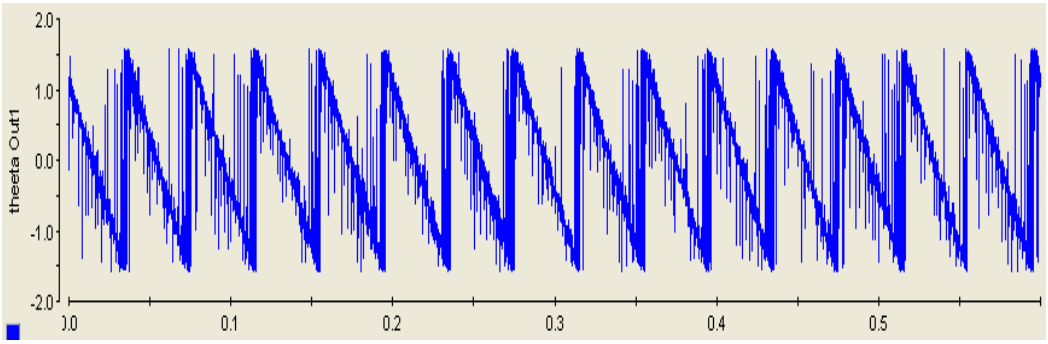

Figure 6.26 Measured Position using resolver

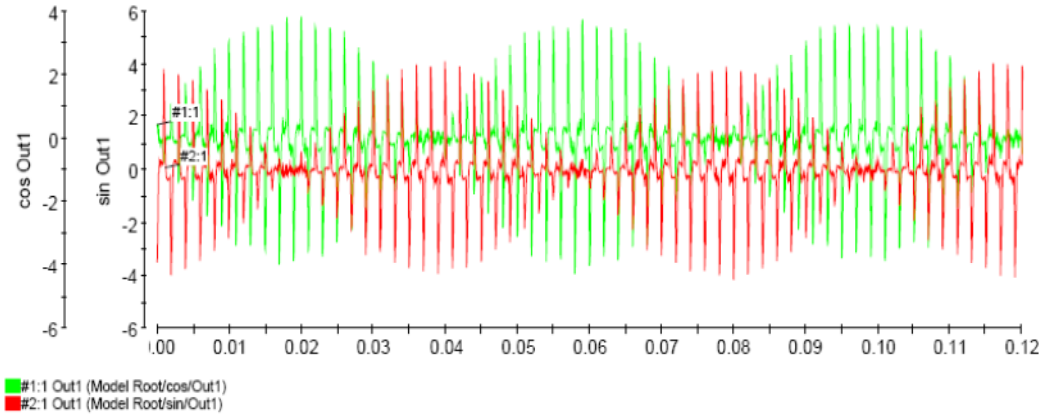

Figure 6.27 Resolver output (cosine and sine) signals in running conditions

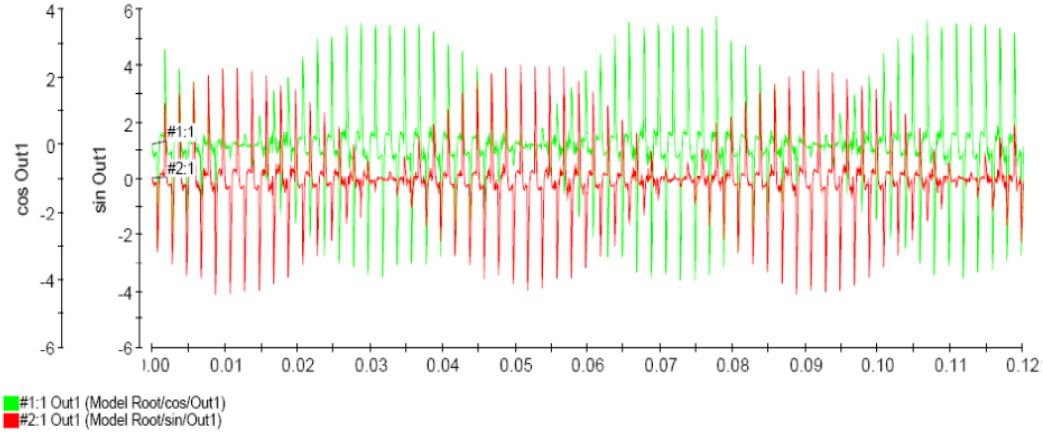

Figure 6.28 Resolver output (cosine and sine) signals in running conditions 1

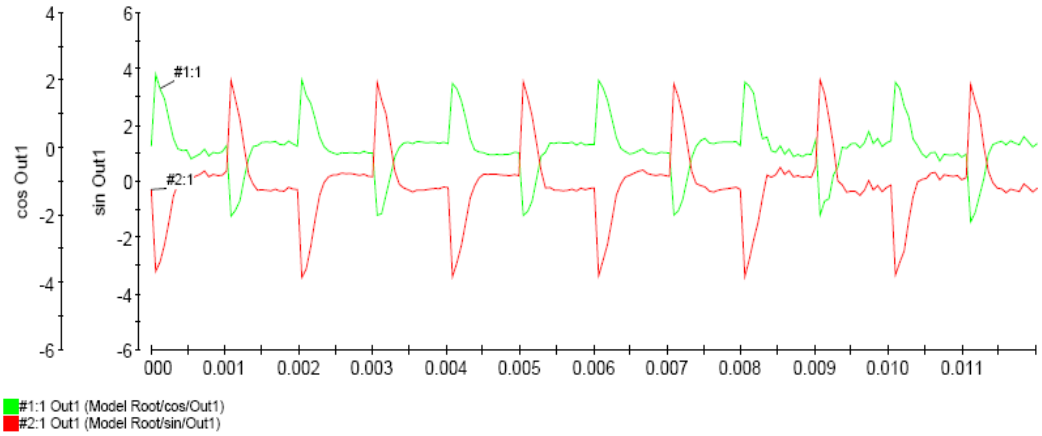

Figure 6.29 Resolver output (cosine and sine) signals while motor is at rest

6.3.2 Performance Evaluation of SMO based Sensorless Algorithm for PMSM Drive

The SMO based sensorless algorithm is implemented on the prototype with system parameter as given in Table 6-2. The performance of proposed algorithm is investigated in various operating conditions to prove the effectiveness of the controller. The experimental performance and simulation performance is compared for sensorless PMSM drive. The comparison data is tabulated in Table 6-4. This Table gives a comparative analysis of sensorless algorithms discussed and presented in this thesis.

The three-phase stator currents with SMO are shown in Figure 6.30. The speed and rotor position with step change in speed is shown in Figure 6.31 and Figure 6.32. The estimation error of rotor position with SMO is shown in Figure 6.33.

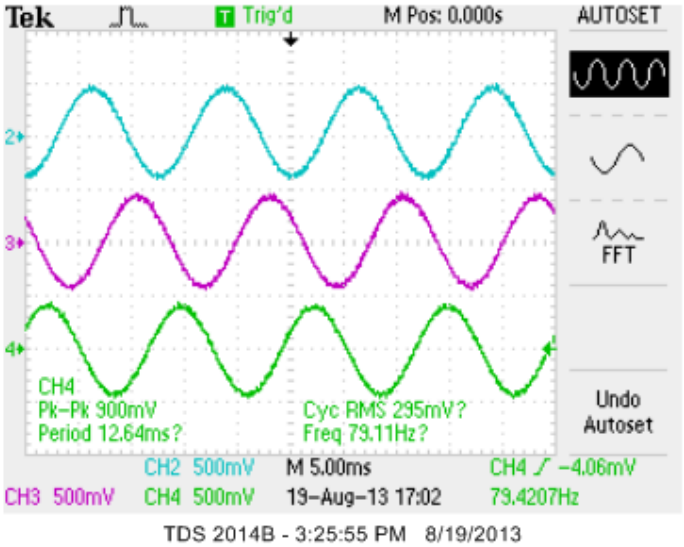

Figure 6.30 Three-phase stator current of PMSM with SMO

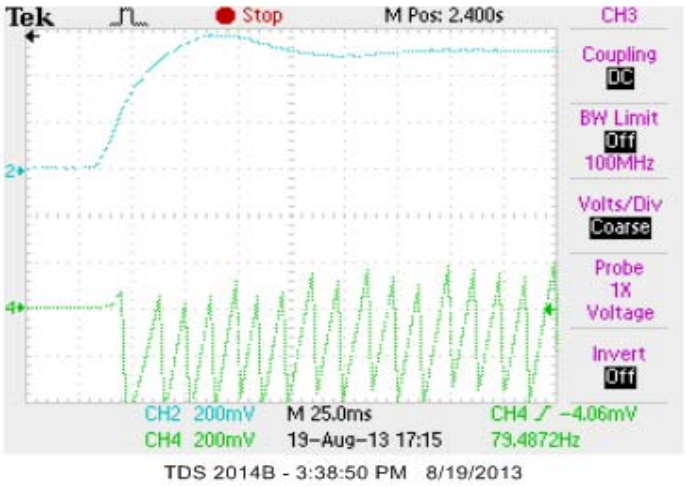

Figure 6.31 Speed and rotor position with step change (0-100) rpm in speed with SMO

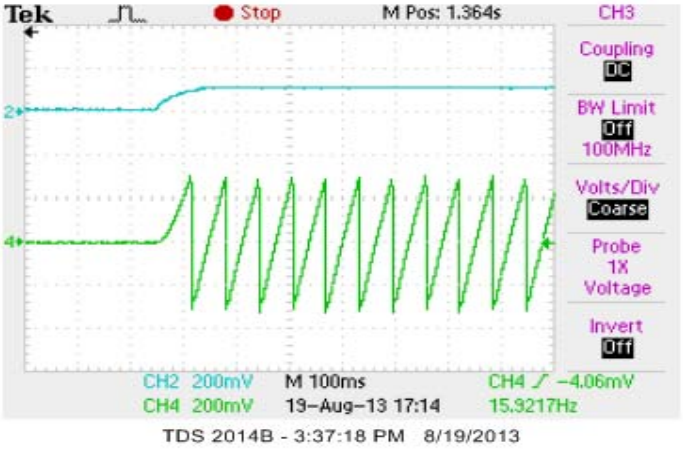

Figure 6.32 Speed (0-500 rpm) and estimated rotor position with sliding mode observer with feedback gain

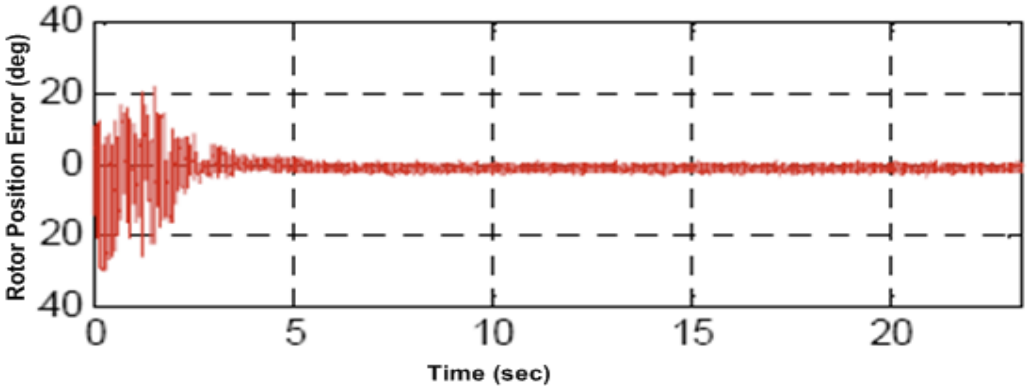

Figure 6.33 Estimation error for SMO with feedback gain

The simulation results to prove the effectiveness is shown in

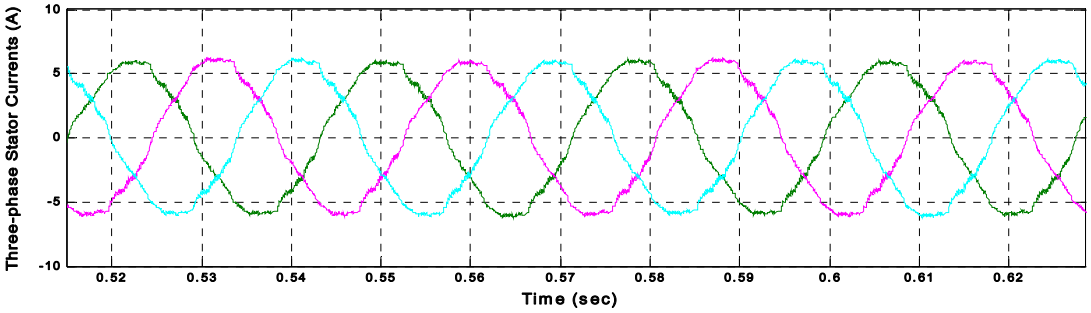

Figure 6.34 Simulation performance with SMO-Three-phase stator currents

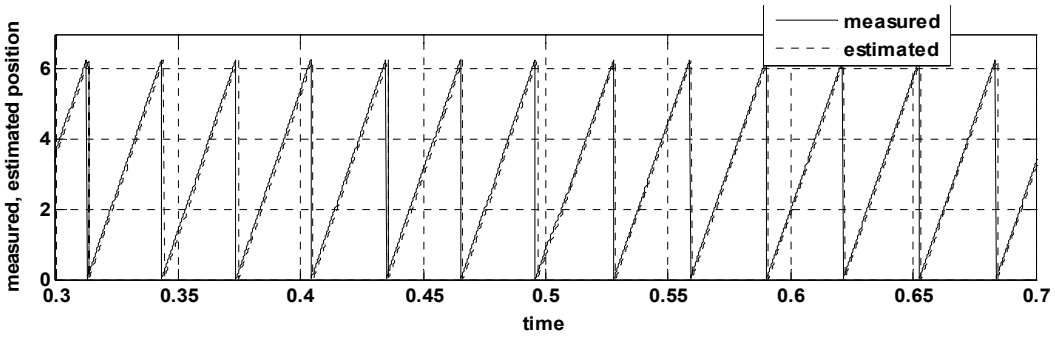

Figure 6.35 Simulation performance with SMO

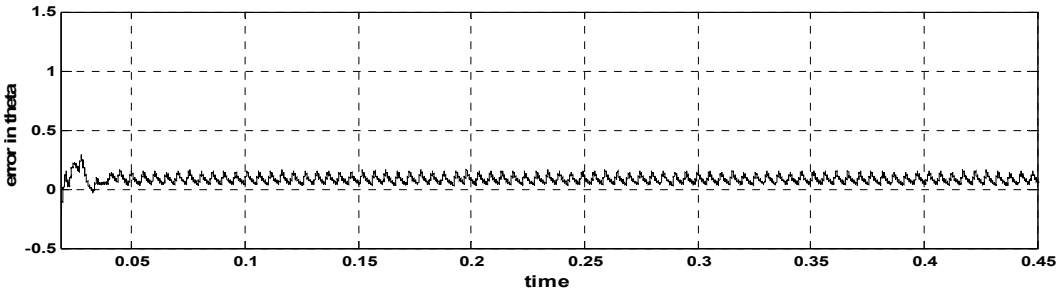

Figure 6.36 Simulation performance in position error with SMO

The experimental results shown here clearly reflect the efficacy of simulation results presented. The comparison on simulation and experimental results are given in Table 6-4 for the verification.

The highlights of the implementation of SMO based sensorless PMSM drive are as follows−

- The SMO is able to handle more signals at a time.
- The SMO show good stability in wide speed range of speed.
- The proposed SMO with equivalent feedback gain show a good robustness.
- Provides good dynamic response due to concurrent actions of every loops.
- The system performance merely depends on system parameters.
- The hardware implementation does not need extra electronics.

6.3.3 Performance Evaluation of FMARS based Sensorless Algorithm for PMSM Drive

The MRAS based sensorless algorithm for PMSM is implemented as per Figure 6.1. To verify the viability and effectiveness of proposed FMRAS for the speed estimation of PMSM, experimental investigations are carried out. Voltage and current sensors are used for sensing of stator terminal voltages and winding currents.

Experimental studies are carried out in different operating conditions to investigate the performance of drive with proposed sensorless algorithm. First the conventional MRAS is implemented with PI controller in the adaptive mechanism. The proposed FMRAS implemented on the same setup, the FLC is incorporated in simulink model of adaptive mechanism. The motor parameters are given in Table 6-2.

Figure 6.37 shows the three-phase stator current of PMSM in the close-loop operation with MRAS estimation algorithm. Figure 6.38 shows the speed, torque and rotor position at step change in load torque.

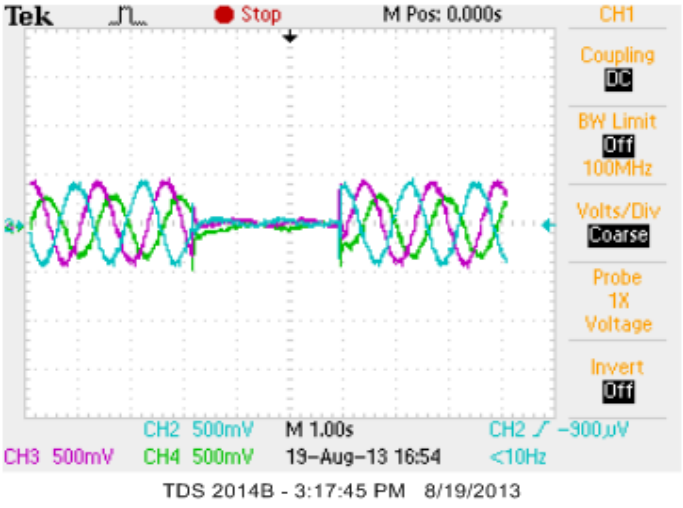

Figure 6.37 Three-phase stator current in close-loop operation with MARS

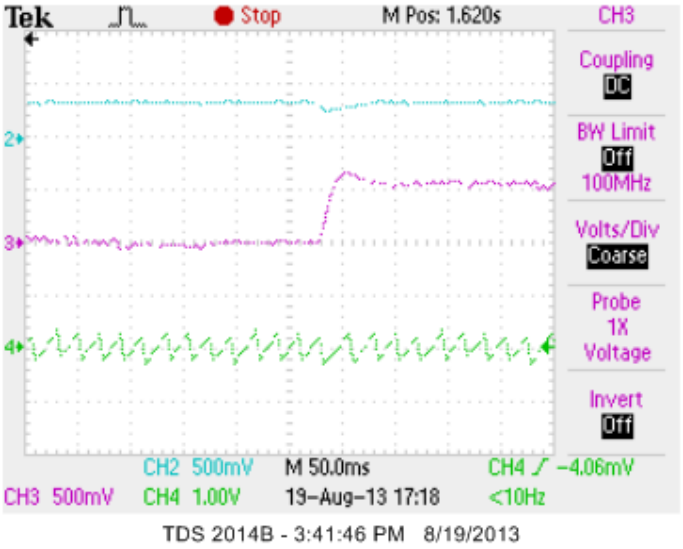

Figure 6.38 Speed, Torque and estimated rotor position with MRAS

Trace 1: Speed 500 rpm

Trace 2: Torque 0-5 Nm step change

Trace 3: Estimated rotor position

Figure 6.39 shows the reference speed, actual speed and estimated rotor speed with MRAS with PI controller. The estimated, actual and reference speed with FMRAS is shown in Figure 6.40.

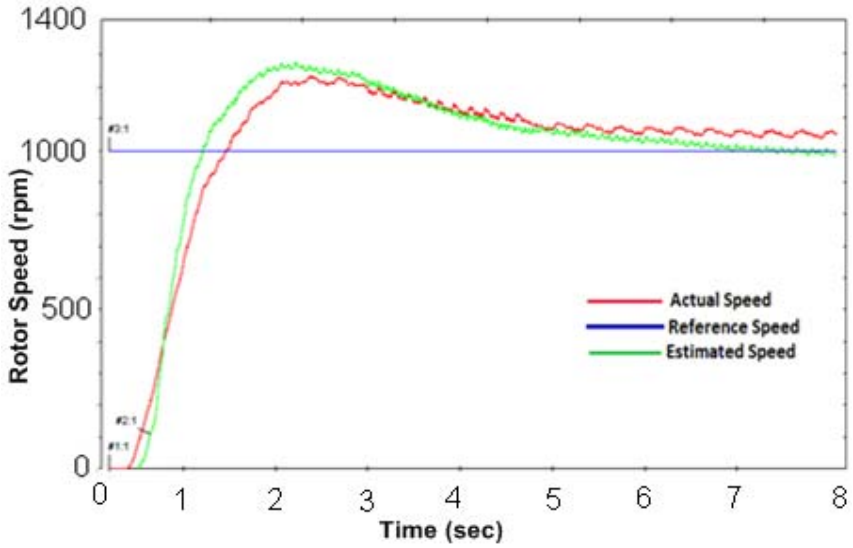

Figure 6.39 Reference, estimated and actual speed of motor with conventional MRAS

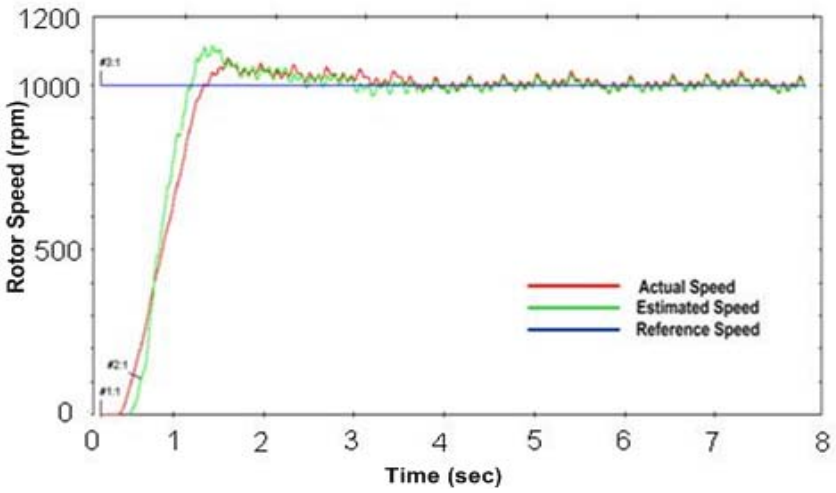

Figure 6.40 Reference, estimated and actual speed of motor with FMRAS

The simulation performance of drive with FMRAS is shown here again to prove the efficacy of the algorithm.

The stator current with change with FMRAS in load is shown in Figure 6.41, which is matching with experimental results. The measured and estimated speed using FMRAS is shown in Figure 6.42. The comparison of simulation and experimental results are given in Table 6-4.

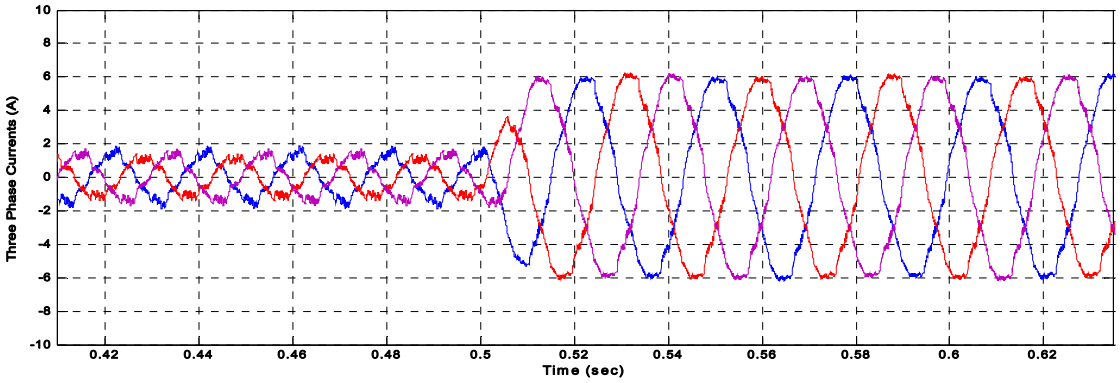

Figure 6.41 Simulation performance with FMRAS during load change

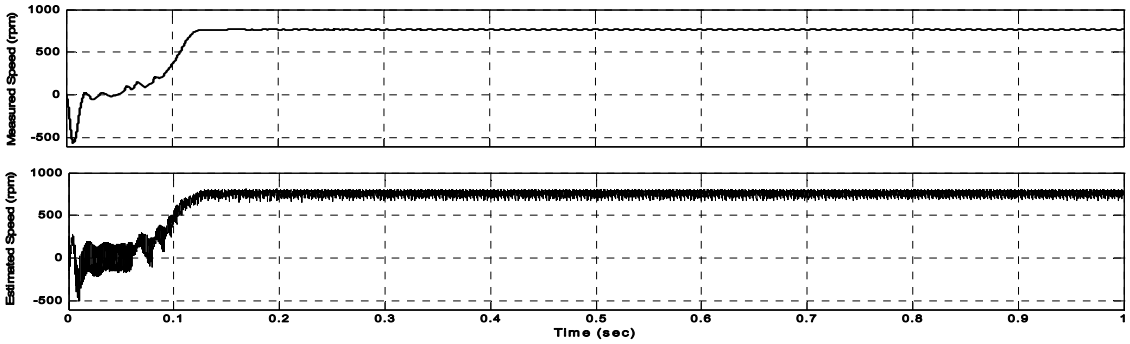

Figure 6.42 Simulation performance of measured and estimated speed with FMRAS

The highlights of the implementation of FMRAS for PMSM drive are as follows−

- The estimation algorithm used is independent of stator resistance, computationally less complex, free from integrator problem because back-emf estimation is not required and provides stable operation of drive system.
- the performance at low and zero speed is also good.
- Adaptation mechanism uses a PI controller to process the error and to tune the adjustable model to achieve the estimated value of rotor speed.
- The enhanced performance is achieved through designing and tuning of FLC for each controller separately.
- This control methodology solves the problem of nonlinearity and parameter deviations of PMSM drive.
- Moreover, it achieves high dynamic performance and accurate speed tracking and torque control with superior steady state characteristics.

Table 6-4 Comparison of results for different sensorless algorithms

Operating Condition	Parameters	SMO		MRAS	
		Exp.	Simulation	Exp.	Simulation
During Starting	Settling Time (s)	1.4	0.6	1.7	0.6
	Overshoot (%)	1.7	0.6	1.4	0.4
	Estimation Error (º)	1.0	0.8	1.1	1.7
Change in Speed	Settling Time (s)	0.8	0.56	0.7	0.45
	Overshoot (%)	0.8	0.7	0.7	0.6
	Estimation Error (º)	1.2	1.5	1.7	1.6
Change Loading	Settling Time (s)	0.6	0.7	0.7	0.5
	Overshoot (%)	0.5	0.3	0.4	0.7
	Estimation Error (º)	0.9	0.7	0.7	0.8

6.4 Conclusion

The detailed descriptions of design, control and development of laboratory prototype sensorless PMSM drive including hardware and software are given in this chapter. A DSP DS1104 of dSPACE is used to implement the control algorithms developed in MATLAB/Simulink in the real-time. The various different components such as input three-phase autotransformer, IPM based three-phase inverter (IGBT based), a PMSM with load, inbuilt resolver, voltage and current sensing circuit, resolver conditioning circuit, and interface circuits are developed in the laboratory and implemented using dSPACE.

The IGBT based power module used as inverter, takes three-phase ac power and use a diode bridge rectifier and provides a dc-link for the inverter. The dSPACE generates the required gating signals for inverter, and given through DAC channel. First this inverter was tested with lamp load, and then connected to PMSM. The measured voltages and currents of PMSM stator winding sensed through isolation amplifier AD202 and TELCON HTP25 based current sensor.

The resolver inbuilt with PMSM generates sine and cosine signal of rotor position, which is further processed and used as measured rotor position and compared with rotor position estimated by SMO and MRAS in different operating conditions.

The control algorithms FVC, SMO, and MRAS are implemented on the prototype using DS1104 in the laboratory for various operating conditions.

[The research work carried out in this thesis focuses on the modeling analysis and control of PMSM drive. The fuzzy logic based vector controlled PMSM was investigated. The centre of attention for the work presented here is the estimation of rotor speed/position for sensorless vector controlled PMSM drive. The laboratory prototype of sensorless PMSM drive is developed using DS1104. This chapter gives a detailed discussion on conclusion and prospects for future work in this area.]

7.1 Conclusion

EMDS (Electrical Motor Driven Systems) are the largest consumer of electric energy including domestic and commercial applications which is 46% of global energy consumption according to the IEA (International Energy Agency) statistic. The adjustable speed drives (ASD) used to match the speed and torque of the drive to the process requirements, and energy saving. The application demand of electric motors is increasing rapidly with increasing technological advancement. Due to increasing demands of electric motors, researchers have been continuing their efforts to develop new machines like the brushless dc (BLDC) machine, the switched reluctance machine (SRM), the permanent magnet hysteresis machine and the permanent magnet synchronous machine (PMSM). After developing these new types of special machines, researchers are working on the control of these motors to optimize the design performance and cost. These developmental activities are now in a revolutionary stage due to the recent development of semiconductor and microprocessor technologies. Permanent magnets are the vital components of PM machines. Characteristics of permanent magnet materials provide a basis for appreciating the potential and limitation of PM machines.

The ASDs are used to reduce the utility demands; electricity and cost. It increases the life of equipments and reduces the stress on the motor. There was a transition from single speed to variable speed drives; there was another transition within the field of variable speed drive. The dc motor and induction motor drives were replaced by PMSM and BLDC due to their advantages in the low power applications. The high efficiency and compact size are the promising advantages of PMSM over dc and induction motors. The vector control requires instantaneous control of stator currents, which decreases the torque ripples. The objective of vector control is to control the flux and torque of motor separately to follow the reference command values irrespective of change in load and machine parameters.

Rapid development of microprocessors and controllers (μC) and digital signal processors (DSP) has facilitated the vector control in becoming a common technique for PMSM drive systems, especially in low-cost applications such as home appliance and machine tools. The vector control of PMSM is widely used due to its excellent torque

response. The implementation of vector control requires the knowledge of rotor position for the reference frame transformations to regulate the corresponding current component. In high performance drive current controller plays a vital role as it directly affects the quality of current fed to motor and indirectly affects the performance of motor in terms of efficiency, dynamic response. In vector controlled PMSM drive system the proportional integral (PI) controller is widely used for speed control due to its simple implementation. However, tuning of gains of PI controller, when there is a change in system parameter or change in load torque or speed command values, is a challenging task. Usually the rotor position is measured by using encoders, resolvers or Hall Effect sensors.

The motor used in this work is inbuilt with resolver. The presence of these sensors increases not only the cost of drive system, but also reduces the reliability and robustness. It is desirable to eliminate such sensors in PMSM drives to reduce system costs and total hardware complexity, to increase the mechanical robustness and reliability, to reduce the maintenance requirements, to ensure that the inertia of the system is not increased, and to have noise immunity. Back-emf based method offers satisfactory performance at higher speed, but at low or zero speed the magnitude of back-emf becomes negligible and difficult to measure. This makes speed estimation at low speed difficult and this method is also highly sensitive to machine parameters. In INFORM, a high frequency signal is injected to motor phases to extract the rotor position. This method is reliable at zero speed but there is adverse effect of signal injection on motor dynamics and requirement of extra hardware.

Adaptive control seems to be the most promising one of various modern control strategies reported in the literature. In this work the MRAS based speed estimation was considered due to simple structure and less computational requirements. The major promising issues of MRAS based methods are parameter sensitivity and integration problem. The artificial intelligent techniques are used in this work to improve the performance of MRAS based estimation methods.

Among the existing sensorless approaches, sliding mode has been recognized as the prospective control methodology for electric machines. Sliding mode observers (SMO) have attractive advantages of robustness to disturbances and low sensitivity to parameter variations. The main advantage of this method is that it does not need extra electronics. Furthermore, the variation of motor parameters has little impact on the results accuracy.

The fuzzy controller has time varying gains for speed control according to system responses invoked by its different control rules. Therefore, fuzzy speed controller can overcome the demerits of conventional PI controller. Moreover, the FLC system, in essence, is based on the experience and intuition of a human plant operator. Therefore, for a linear or a nonlinear plant with severe parameter variations, a robust control system can be designed and implemented. The major contributions derived from this work are summarized as–

- The mathematical model of PMSM in different reference frames, resolver is presented. The changes in controller parameters are obtained for the given load variations. A developed model of PMSM in MATLAB is studied and simulation performance is analyzed. The developed PMSM drive has a PI controller and PWM inverter. The performance of the drive for different reference speed with step change in the load torque is presented.
- In order to overcome the inherent coupling effect and the sluggish response of scalar control and to achieve the high performance the vector control is employed. In order to overcome the problems associated with PI controllers, fuzzy based current controllers are employed for motor control which eliminates the controller parameter dependency on the system's mathematical model and load disturbances. The designed vector controlled PMSM drive has three fuzzy logic controllers (FLC); one FSC, and other two FCCs, which is unique in its application while, speed is controlled by using fuzzy logic in vector control. This complete fuzzy based vector controller is termed here as Fuzzy Vector Controller (FVC). The FVC is implemented on the prototype using DS1104.

- The importance of rotor position in implementation of vector control is highlighted. The advantages of sensorless drive are given and different position estimation methods are discussed in details with their significance and limitations. The sliding mode observer with adaptive feedback gains for sensorless PMSM without saliency is presented, the simulation results are shown to establish the feasibility of the observer. The SMO is selected, as it has a major advantage that it does not need extra electronics for the implementation of algorithm. Furthermore, the variation of motor parameters has little impact on the results accuracy. It provides fast dynamic response because all control loops act concurrently. Implementation of SM controller is simple as compared to other nonlinear controllers. The effectiveness is proposed SMO with adaptive feedback gain is validated on the prototype.
- An estimation method based on model reference adaptive system is presented with space vector modulation for sensorless operation of PMSM drive. The performance of drive with traditional MRAS estimator using PI controller is improved using application of fuzzy logic in adaptation mechanism of MRAS. The estimation algorithm used is independent of stator resistance, computationally less complex, free from integrator problem, as the back-emf estimation is not required and provides stable operation of drive system. The system anti-robustness behavior is improved and the dynamic and static performance of drive

is improved. The simulation results verified the effectiveness and feasibility of the FMRAS based estimator, and validated on the prototype.

7.2 Future Prospects

The research work presented in this thesis reveals some issues that could be a future consideration and to be investigated further.

- The full-digital implementation of a high performance vector controlled PMSM drive is an active area of research. As needs a number of controllers and transformations equations. The applications of SPWM, SVM are implemented in this work, other modulations techniques for inverter is a potential area of research for high performance applications.
- The artificial intelligence based techniques like NN, GA, PSO can be used directly as controller or to be used for tuning of classical PI controller.
- In the sensorless PMSM drives for low cost application, like fans, compressors, the techniques could be based on digital implementation for compact size of drives.
- The SMO can be optimized by application of artificial intelligence techniques for high performance digital implementation.
- The NN based stator resistance estimator can be used with MRAS speed estimator to achieve the high performance drive with high robustness.
- The performance of sensorless PMSM drive can be achieved by applications of multilevel inverters for high power application.
- In general, the PMSM drive is useful for low and medium power applications. The applications of low cost converter and sensorless algorithms can make the low cost high reliability applications.

PUBLICATIONS FROM THE WORK

Journals

[1] **A comprehensive analysis and implementation of vector control of permanent magnet synchronous motor,"** *International Journal of Power and Energy Conversion,* vol. 5, pp. 1-23.

[2] **"A Complete Fuzzy Logic Based Vector Control of PMSM Drive"** *International Review of Electrical Engineering,* accepted for Publication.

[3] **"Brief Analysis and Field Oriented Control of Permanent Magnet Synchronous Motor Drive,"** *Vivechan International Journal of Research* vol.3, pp. 53-69, 2012.

[4] **"MRAS Based Speed Estimation in PMSM Drives"** selected and submitted after revision in *IEEE Transaction on Industrial Applications*, after presented in the conference PICONF 2012.

International conferences

[5] **"Modeling and implementation of vector control for PM synchronous motor drive,"** *International Conference on Advances in Engineering, Science and Management* (ICAESM),Nagapattinam India 2012, pp. 582-585.

[6] **"Mathematical Modeling and Fuzzy Based Speed Control of Permanent Magnet Synchronous Motor Drive,"** *The 7th IEEE Conference on Industrial Electronics and Applications (ICIEA 2012)* Singapore, pp. 2034-2038.

[7] **"Fuzzy Logic Based Speed and Current Control of Vector Controlled PMSM Drive,"** *2nd International Conference on Power, Control and Embedded Systems (ICPCES-2012)*, pp1-6.

[8] **"MRAS Based Estimation of Speed in Sensorless PMSM Drive,"** *2012 IEEE Fifth POWER INDIA Conference, DCRUSTM Haryana*, pp. 1-5.

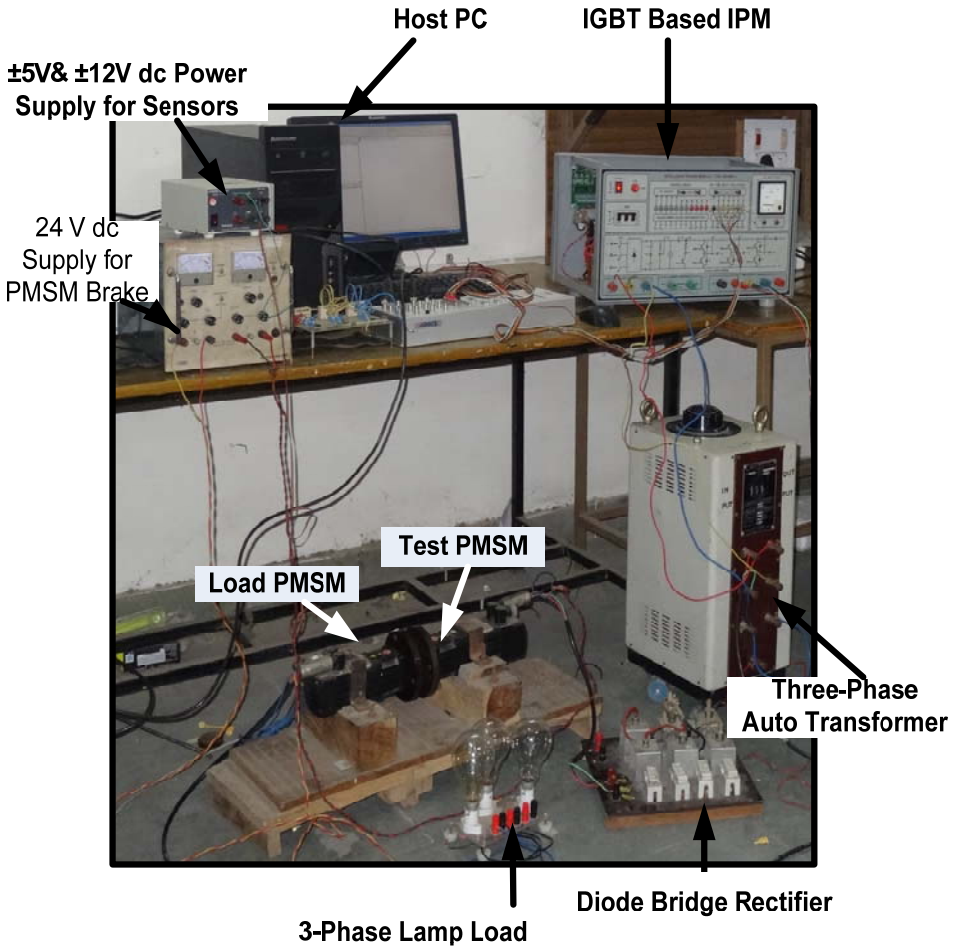

Experimental Setup of PMSM drive using dSPACE DS1104 R&D controller board

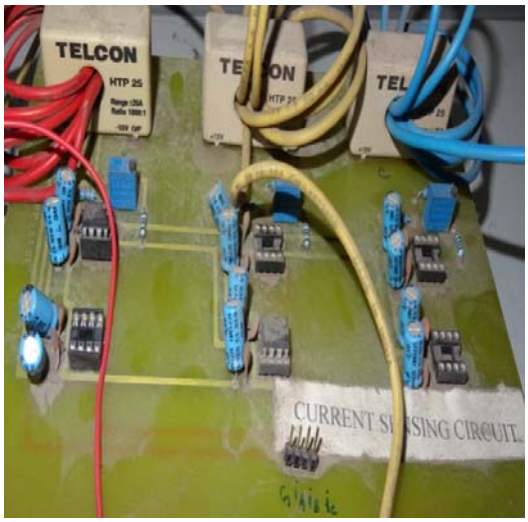

Current Sensor

Voltage sensor

CP1104 Connector board

8 Pole, 1.4 kW PMSM

BIBLIOGRAPHY

[1] **B. K. Chaudhari and B. G. Fernandes**, "Synchronous motor using ferrite magnets for general purpose energy efficient drive," *TENCON 99. Proceedings of the IEEE Region 10 Conference*, pp. 371-374 vol.1, 1999.

[2] **B. K. Chaudhari, S. K. Pillai, and B. G. Fernandes**, "Energy efficient line start permanent magnet synchronous motor," *TENCON '98. 1998 IEEE Region 10 International Conference on Global Connectivity in Energy, Computer, Communication and Control*, pp. 379-382 vol.2, 1998.

[3] **S. P. Nikam, V. Rallabandi, and B. G. Fernandes**, "A High-Torque-Density Permanent-Magnet Free Motor for in-Wheel Electric Vehicle Application," *IEEE Transactions on Industry Applications,,* vol. 48, no. 6, pp. 2287-2295, (2012)

[4] **Y. Liao and T. A. Lipo**, "A new doubly salient permanent magnet motor for adjustable speed drives," *Electric Machines and Power Systems,* vol. 22, no. 2, pp. 259-270, (1994)

[5] **B. A. Welchko, T. M. Jahns, and T. A. Lipo**, "Fault interrupting methods and topologies for interior PM machine drives," *Power Electronics Letters, IEEE,* vol. 2, no. 4, pp. 139-143, (2004)

[6] **A. Emadi**, *Handbook of automotive power electronics and motor drives*: CRC press, 2005.

[7] **R. C. Bansal**, "Closure of' "Bibliography on the fuzzy set theory applications in power systems (1994-2001)"," *IEEE Transactions on Power Systems,,* vol. 19, no. 4, pp. 2118-2119, (2004)

[8] **P. G. Kini, R. C. Bansal, and R. S. Aithal**, "Performance Analysis of Centrifugal Pumps Subjected to Voltage Variation and Unbalance," *IEEE Transactions on Industrial Electronics,,* vol. 55, no. 2, pp. 562-569, (2008)

[9] **P. Pillay and R. Krishnan**, "Modeling of permanent magnet motor drives," *IEEE Transactions on Control Systems Technology,* vol. 35, no. 4, pp. 537-541, (1988)

[10] **A. Mishra, J. A. Makwana, P. Agarwal, and S. P. Srivastava**, "Modeling and implementation of vector control for PM synchronous motor drive," *International Conference on Advances in Engineering, Science and Management (ICAESM), 2012*, pp. 582-585.

[11] **M. N. Uddin and R. S. Rebeiro**, "Online Efficiency Optimization of a Fuzzy-Logic-Controller-Based IPMSM Drive," *IEEE Transactions on Control Systems Technology,* vol. 47, no. 2, pp. 1043-1050, (2011)

[12] **P. Vas**, *Sensorless vector and direct torque control* vol. 729: Oxford university press Oxford, UK, 1998.

[13] **S. Bolognani, L. Tubiana, and M. Zigliotto**, "Extended Kalman filter tuning in sensorless PMSM drives," *IEEE Transactions on Industry Application,* vol. 39, no. 6, pp. 1741-1747, (2003)

[14] **S. Bolognani, M. Zigliotto, and M. Zordan**, "Extended-range PMSM sensorless speed drive based on stochastic filtering," *IEEE Transactions on Power Electronics,* vol. 16, no. 1, pp. 110-117, (2001)

[15] **G. Wu and X. Xiao**, "Speed controller of servo system based on MRAS method," *IEEE International Conference on Industrial Technology ICIT*, pp. 1-5, 2009.

[16] **L. Yen-Shin**, "Machine modeling and universal controller for vector-controlled induction motor drives," *IEEE Transactions on Energy Conversion,* vol. 18, no. 1, pp. 23-32, (2003)

[17] **B. K. Bose**, *Modern power electronics and AC drives*: Prentice Hall PTR USA, 2002.

[18] **M. Kadjoudj, M. E. H. Benbouzid, C. Ghennai, and D. Diallo**, "A robust hybrid current control for permanent-magnet synchronous motor drive," *IEEE Transactions on Energy Conversion,* vol. 19, no. 1, pp. 109-115, (2004)

[19] **Z. Ibrahim and E. Levi**, "A comparative analysis of fuzzy logic and PI speed control in high-performance AC drives using experimental approach," *IEEE Transactions on Control Systems Technology,* vol. 38, no. 5, pp. 1210-1218, (2002)

[20] **Y. Baudon, D. Jouve, and J. P. Ferrieux**, "Current control of permanent magnet synchronous machines. Experimental and simulation study," *IEEE Transactions on Power Electronics,* vol. 7, no. 3, pp. 560-567, (1992)

[21] **W. Kaewjindam and M. Konghirun**, "A DSP - Based Vector Control of PMSM Servo Drive Using Resolver Sensor," *IEEE Region 10 Conference TENCON*, pp. 1-4, 2006.

[22] **Z. Q. Zhu and D. Howe**, "Influence of design parameters on cogging torque in permanent magnet machines," *IEEE Transactions on Energy Conversion,* vol. 15, no. 4, pp. 407-412, (2000)

[23] **Z. Bin, L. Yaohua, and Z. Yansheng**, "A DSP-based fully digital PMSM servo drive using on-line self-tuning PI controller," *The Third International Power Electronics and Motion Control Conference, IPEMC 2000.* , pp. 1012-1017 vol.2, 2000.

[24] **R. Guclu and K. Gulez**, "Neural network control of seat vibrations of a non-linear full vehicle model using PMSM," *Mathematical and Computer Modelling,* vol. 47, no. 11â€“12, pp. 1356-1371, (2008)

[25] **M. Rashed, P. F. A. MacConnell, A. F. Stronach, and P. Acarnley**, "Sensorless Indirect-Rotor-Field-Orientation Speed Control of a Permanent-Magnet Synchronous Motor With Stator-Resistance Estimation," *Industrial Electronics, IEEE Transactions on,* vol. 54, no. 3, pp. 1664-1675, (2007)

[26] **S. Maiti, C. Chakraborty, and S. Sengupta**, "Simulation studies on model reference adaptive controller based speed estimation technique for the vector controlled permanent magnet synchronous motor drive," *Simulation Modelling Practice and Theory,* vol. 17, no. 4, pp. 585-596, (2009)

[27] **C. Song, Z. Zheng, and X. Longya**, "Sliding-Mode Sensorless Control of Direct-Drive PM Synchronous Motors for Washing Machine Applications," *Industry Applications, IEEE Transactions on,* vol. 45, no. 2, pp. 582-590, (2009)

[28] **X. Jian-Xin, S. K. Panda, P. Ya-Jun, L. Tong Heng, and B. H. Lam**, "A modular control scheme for PMSM speed control with pulsating torque minimization," *IEEE Transactions on Industrial Electronics,* vol. 51, no. 3, pp. 526-536, (2004)

[29] **T. D. Batzel and K. Y. Lee**, "An approach to sensorless operation of the permanent-magnet synchronous motor using diagonally recurrent neural networks," *Energy Conversion, IEEE Transactions on,* vol. 18, no. 1, pp. 100-106, (2003)

[30] **K. Jezernik and R. Horvat**, "High performance control of PMSM," *First Symposium on Sensorless Control for Electrical Drives (SLED)* pp. 72-77, 2010.

[31] **M. Schroedl**, "Sensorless control of AC machines at low speed and standstill based on the "INFORM" method," *Conference Record of the IEEE Industry Applications Conference, Thirty-First IAS Annual Meeting, IAS'96*, pp. 270-277, 1996.

[32] **M. J. Corley and R. D. Lorenz**, "Rotor position and velocity estimation for a salient-pole permanent magnet synchronous machine at standstill and high speeds," *IEEE Transactions on Industry Applications,* vol. 34, no. 4, pp. 784-789, (1998)

[33] **S. Bolognani, R. Oboe, and M. Zigliotto**, "Sensorless full-digital PMSM drive with EKF estimation of speed and rotor position," *IEEE Transactions on Industrial Electronics,* vol. 46, no. 1, pp. 184-191, (1999)

[34] **M. Boussak**, "Implementation and experimental investigation of sensorless speed control with initial rotor position estimation for interior permanent magnet synchronous motor drive," *Power Electronics, IEEE Transactions on,* vol. 20, no. 6, pp. 1413-1422, (2005)

[35] **B. Jiang**, "A Novel Algorithm Based on EKF to Estimate Rotor Position and Speed for Sensorless PMSM Drivers," *Information Engineering and Computer Science, 2009. ICIECS 2009. International Conference on*, pp. 1-4, 2009.

[36] **B. K. Bose**, *Power electronics and motor drives: advances and trends*: Access Online via Elsevier, 2006.

[37] **M. Naidu and B. K. Bose**, "Rotor position estimation of a permanent magnet synchronous-machine for high performance drive," Google Patents, 1992.

[38] **R. Raute, C. Caruana, J. Cilia, C. S. Staines, and M. Sumner**, "A zero speed operation sensorless PMSM drive without additional test signal injection," *European Conference on Power Electronics and Applications, 2007* pp. 1-10, 2007.

[39] **A. Girolkar and G. Bhuvaneswari**, "Control of PMBLDC motor using back EMF sensing with adaptive filtering," *Computer Communication and Informatics (ICCCI), 2013 International Conference on*, pp. 1-5, 2013.

[40] **S. Madishetti, G. Bhuvaneswari, and B. Singh**, "Improved power quality converter for direct torque control-based induction motor drives," *Power Electronics, IET,* vol. 6, no. 2, (2013)

[41] **B. Singh, G. Bhuvaneswari, V. Garg, and S. Gairola**, "Pulse multiplication in AC-DC converters for harmonic mitigation in vector-controlled induction motor drives," *Energy Conversion, IEEE Transactions on,* vol. 21, no. 2, pp. 342-352, (2006)

[42] **E. Robeischl, M. Schroedl, and M. Krammer**, "Position-sensorless biaxial position control with industrial PM motor drives based on INFORM- and back EMF model," *IEEE 28th Annual Conference of the Industrial Electronics Society, IECON 02*, pp. 668-673 vol.1, 2002.

[43] **P. Vaclavek and P. Blaha**, "Synchronous machine drive observability analysis and sensorless control design," *Power and Energy Conference, 2008. PECon 2008. IEEE 2nd International*, pp. 265-270, 2008.

[44] **W. Maogang, Z. Rongxiang, and W. Junwei**, "Sensorless estimation and convergence analysis based on MRAS for PMSM," *Intelligent Control and Automation (WCICA), 2010 8th World Congress on*, pp. 1641-1644.

[45] **H. M. Kojabadi and M. Ghribi**, "MRAS-based adaptive speed estimator in PMSM drives," *9th IEEE International Workshop on Advanced Motion Control*, pp. 569-572, 2006.

[46] **K. Jinsong, Z. Xiangyun, W. Ying, and H. Dabing**, "Study of position sensorless control of PMSM based on MRAS," *Industrial Technology, 2009. ICIT 2009. IEEE International Conference on*, pp. 1-4, 2009.

[47] **A. Quntao and S. Li**, "On-line parameter identification for vector controlled PMSM drives using adaptive algorithm," *Vehicle Power and Propulsion Conference, 2008. VPPC '08. IEEE*, pp. 1-6, 2008.

[48] **D. Sun, Y. He, and J. G. Zhu**, "Fuzzy logic direct torque control for permanent magnet synchronous motors," *Fifth World Congress on Intelligent Control and Automation*, pp. 4401-4405, 2004.

[49] **B. N. Chaudhari and B. G. Fernandes**, "Steady state performance of polyphase permanent magnet synchronous motor fed from single phase supply system," *Power Engineering Society Winter Meeting, 2001. IEEE*, pp. 1382-1387, 2001.

[50] **M. Aydin, S. Huang, and T. A. Lipo**, "Design, analysis, and control of a hybrid field-controlled axial-flux permanent-magnet motor," *Industrial Electronics, IEEE Transactions on,* vol. 57, no. 1, pp. 78-87, (2010)

[51] **V. Nedic and T. A. Lipo**, "Low-cost current-fed PMSM drive system with sinusoidal input currents," *Industry Applications, IEEE Transactions on,* vol. 42, no. 3, pp. 753-762, (2006)

[52] **S. Q. A. Shah, T. A. Lipo, and B. I. Kwon**, "Modeling of Novel Permanent Magnet Pole Shape SPM Motor for Reducing Torque Pulsation," *Magnetics, IEEE Transactions on,* vol. 48, no. 11, pp. 4626-4629, (2012)

[53] **B. K. Bose**, "A high-performance inverter-fed drive system of an interior permanent magnet synchronous machine," *IEEE Transactions on Industry Applications,* vol. 24, no. 6, pp. 987-997, (1988)

[54] **J. Qian and M. A. Rahman**, "Analysis of field oriented control for permanent magnet hysteresis synchronous motors," *IEEE Transactions on Industry Applications,* vol. 29, no. 6, pp. 1156-1163, (1993)

[55] **J. Rodriguez, J. Pontt, C. Silva, R. Huerta, and H. Miranda**, "Simple direct torque control of induction machine using space vector modulation," *Electronics Letters,* vol. 40, no. 7, pp. 412-413, (2004)

[56] **J. L. Chen, T. H. Liu, and C. L. Chen**, "Design and implementation of a novel high-performance sensorless control system for interior permanent magnet synchronous motors," *IET Electric Power Applications,* vol. 4, no. 4, pp. 226-240, (2010)

[57] **R. C. Panaitescu and N. Mohan**, "A simple space-vector PWM algorithm for VSI-fed AC motor drives," *Seventeenth Annual IEEE Applied Power Electronics Conference and Exposition, 2002. APEC 2002,*, pp. 72-75 vol.1, 2002.

[58] **R. Dhaouadi and N. Mohan**, "Analysis of current-regulated voltage-source inverters for permanent magnet synchronous motor drives in normal and extended speed ranges," *IEEE Transactions on Energy Conversion,,* vol. 5, no. 1, pp. 137-144, (1990)

[59] **A. Mishra, J. Makwana, P. Agarwal, and S. P. Srivastava**, "Mathematical modeling and fuzzy based speed control of permanent magnet synchronous motor drive," *7th IEEE Conference on Industrial Electronics and Applications (ICIEA), 2012*, pp. 2034-2038.

[60] **N. Mohan and T. M. Undeland**, *Power electronics: converters, applications, and design*: Wiley. com, 2007.

[61] **M. S. S. Srinivas and K. R. Rajagopal**, "Fuzzy Logic Based Gain Scheduled PI Speed Controller for PMBLDC Motor," *Annual IEEE India Conference (INDICON)*, pp. 1-4, 2009.

[62] **A. V. Sant and K. R. Rajagopal**, "PM Synchronous Motor Speed Control Using Hybrid Fuzzy-PI With Novel Switching Functions," *IEEE Transactions on Magnetics,* vol. 45, no. 10, pp. 4672-4675, (2009)

[63] **A. Mishra, V. Mahajan, P. Agarwal, and S. P. Srivastava**, "Fuzzy logic based speed and current control of vector controlled PMSM drive," *2nd International Conference on Power, Control and Embedded Systems (ICPCES), 2012* pp. 1-6.

[64] **L. Zhen and L. Xu**, "Fuzzy learning enhanced speed control of an indirect field-oriented induction machine drive," *IEEE Transactions on Control Systems Technology,* vol. 8, no. 2, pp. 270-278, (2000)

[65] **K. Hakiki, A. Meroufel, V. Cocquempot, and M. Chenafa**, "A new adaptive fuzzy vector control for permanent magnet synchronous motor drive," *18th Mediterranean Conference on Control & Automation (MED)* pp. 922-927, 2010.

[66] **A. Lidozzi, L. Solero, F. Crescimbini, and A. Di Napoli**, "SVM PMSM Drive With Low Resolution Hall-Effect Sensors," *Power Electronics, IEEE Transactions on,* vol. 22, no. 1, pp. 282-290, (2007)

[67] **F. Genduso, R. Miceli, C. Rando, and G. R. Galluzzo**, "Back EMF Sensorless-Control Algorithm for High-Dynamic Performance PMSM," *IEEE Transactions on Industrial Electronics,,* vol. 57, no. 6, pp. 2092-2100, (2010)

[68] **S. Morimoto, K. Kawamoto, M. Sanada, and Y. Takeda**, "Sensorless control strategy for salient-pole PMSM based on extended EMF in rotating reference frame," *Industry Applications, IEEE Transactions on,* vol. 38, no. 4, pp. 1054-1061, (2002)

[69] **B. Nahid-Mobarakeh, F. Meibody-Tabar, and F. M. Sargos**, "Back EMF Estimation-Based Sensorless Control of PMSM: Robustness With Respect to Measurement Errors and Inverter Irregularities," *Industry Applications, IEEE Transactions on,* vol. 43, no. 2, pp. 485-494, (2007)

[70] **O. Wallmark and L. Harnefors**, "Sensorless Control of Salient PMSM Drives in the Transition Region," *Industrial Electronics, IEEE Transactions on,* vol. 53, no. 4, pp. 1179-1187, (2006)

[71] **M. A. Hoque and M. A. Rahman**, "Speed and position sensorless permanent magnet synchronous motor drives," *Electrical and Computer Engineering, 1994. Conference Proceedings. 1994 Canadian Conference on*, pp. 689-692 vol.2, 1994.

[72] **R. C. Becerra, T. M. Jahns, and M. Ehsani**, "Four-quadrant sensorless brushless ECM drive," *Sixth Annual Applied Power Electronics Conference and Exposition, APEC'91.*, pp. 202-209, 1991.

[73] **A. Eilenberger and M. Schroedl**, "Extended back EMF model for PM synchronous machines with different inductances in d- and q-axis," *Power Electronics and Motion Control Conference, 2008. EPE-PEMC 2008. 13th*, pp. 945-948, 2008.

[74] **M. Schrodl, M. Hofer, and W. Staffler**, "Extended EMF- and parameter observer for sensorless controlled PMSM-machines at low speed," *Power Electronics and Applications, 2007 European Conference on*, pp. 1-8, 2007.

[75] **A. V. Stankovic, E. L. Benedict, V. John, and T. A. Lipo**, "A novel method for measuring induction machine magnetizing inductance," *IEEE Transactions on Industry Applications,* vol. 39, no. 5, pp. 1257-1263, (2003)

[76] **K. Hongryel, S. Jubum, and L. Jangmyung**, "A High-Speed Sliding-Mode Observer for the Sensorless Speed Control of a PMSM," *Industrial Electronics, IEEE Transactions on,* vol. 58, no. 9, pp. 4069-4077,

[77] **H. Yoon-Seok, C. Jung-Soo, and K. Young-Seok**, "Sensorless PMSM drive with a sliding mode control based adaptive speed and stator resistance estimator," *Magnetics, IEEE Transactions on,* vol. 36, no. 5, pp. 3588-3591, (2000)

[78] **A. Piippo and J. Luomi**, "Adaptive observer combined with HF signal injection for sensorless control of PMSM drives," *Electric Machines and Drives, 2005 IEEE International Conference on*, pp. 674-681, 2005.

[79] **A. Piippo, M. Hinkkanen, and J. Luomi**, "Sensorless control of PMSM drives using a combination of voltage model and HF signal injection," *Industry Applications Conference, 2004. 39th IAS Annual Meeting. Conference Record of the 2004 IEEE*, pp. 964-970 vol.2, 2004.

[80] **R. B. Sepe and J. H. Lang**, "Real-time observer-based (adaptive) control of a permanent-magnet synchronous motor without mechanical sensors," *Industry Applications, IEEE Transactions on,* vol. 28, no. 6, pp. 1345-1352, (1992)

[81] **K. Kye-Lyong, K. Jang-Mok, H. Keun-Bae, and K. Kyung-Hoon**, "Sensorless control of PMSM in high speed range with iterative sliding mode observer," *Applied Power Electronics Conference and Exposition, 2004. APEC '04. Nineteenth Annual IEEE*, pp. 1111-1116 vol.2, 2004.

[82] **C. M. Jansen PL, Lorenz RD**, "Flux position, and velocity estimation in AC machines at zero and low speed via tarcking of high frequency saliencies.," *EPE,* vol. Sevilla, (1995)

[83] **M. J. Corley and R. D. Lorenz**, "Rotor position and velocity estimation for a permanent magnet synchronous machine at standstill and high speeds," *IEEE Industry Application conference,*, pp. 36-41, 1996.

[84] **J.-I. Ha and S.-K. Sul**, "Sensorless field-orientation control of an induction machine by high-frequency signal injection," *IEEE Transactions on Industry Applications, ,* vol. 35, no. 1, pp. 45-51, (1999)

[85] **F. Briz, M. W. Degner, J. M. Guerrero, A. ZamarrÃ³n, and R. D. Lorenz**, "Implementation issues affecting the performance of carrier signal injection based

sensorless controlled AC drives," *Conference Record of the IEEE Industry Applications Conference, 2001. Thirty-Sixth IAS Annual Meeting.* , pp. 2645-2652, 2001.

[86] **J.-H. Jang, S.-K. Sul, J.-I. Ha, K. Ide, and M. Sawamura**, "Sensorless drive of SMPM motor by high frequency signal injection," *Seventeenth Annual IEEE, Applied Power Electronics Conference and Exposition, APEC 2002.* , pp. 279-285, 2002.

[87] **J.-I. Ha, S.-J. Kang, and S.-K. Sul**, "Position-controlled synchronous reluctance motor without rotational transducer," *IEEE Transactions on Industry Applications, ,* vol. 35, no. 6, pp. 1393-1398, (1999)

[88] **E. K. K. Sng, A.-C. Liew, and T. A. Lipo**, "New observer-based DFO scheme for speed sensorless field-oriented drives for Low-Zero-Speed operation," *IEEE Transactions on Power Electronics,,* vol. 13, no. 5, pp. 959-968, (1998)

[89] **T. Kereszty, V. M. Leppanen, and J. Luomi**, "Sensorless control of surface magnet synchronous motors at low speeds using low-frequency signal injection," *The 29th Annual Conference of the IEEE Industrial Electronics Society, IECON'03.*, pp. 1239-1243, 2003.

[90] **F. Blaschke and W. Dreiseitl**, "Method and apparatus for determining the initial rotor angle in a rotating field machine," US Patent 3,909,688, 1975.

[91] **S. Ogasawara and H. Akagi**, "An approach to real-time position estimation at zero and low speed for a PM motor based on saliency," *IEEE Transactions on Industry Applications,,* vol. 34, no. 1, pp. 163-168, (1998)

[92] **S. Ogasawara and H. Akagi**, "Implementation and position control performance of a position-sensorless IPM motor drive system based on magnetic saliency," *IEEE Transactions on Industry Applications,,* vol. 34, no. 4, pp. 806-812, (1998)

[93] **M. Schroedl**, "Method for regulating a three-phase machine without a mechanical rotary transducer," US Patent 6,479,971, 2002.

[94] **S. Shinnaka**, "New "D-State-Observer"-based vector control for sensorless drive of permanent-magnet synchronous motors," *IEEE Transactions on Industry Applications,* vol. 41, no. 3, pp. 825-833, (2005)

[95] **Z. Zhengfang and F. Jianghua**, "Sensorless control of salient PMSM with EKF of speed and rotor position," *Electrical Machines and Systems, 2008. ICEMS 2008. International Conference on*, pp. 1625-1628, 2008.

[96] **L. Yingpei, W. Jianru, S. Hong, L. Guangye, and Y. Chenhu**, "PMSM speed sensorless direct torque control based on EKF," *Industrial Electronics and Applications, 2009. ICIEA 2009. 4th IEEE Conference on*, pp. 3581-3584, 2009.

[97] **A. Qiu, W. Bin, and H. Kojori**, "Sensorless control of permanent magnet synchronous motor using extended Kalman filter," *Electrical and Computer Engineering, 2004. Canadian Conference on*, pp. 1557-1562 Vol.3, 2004.

[98] **A. Qiu, W. Bin, and H. Kojori**, "Sensorless control of permanent magnet synchronous motor using extended Kalman filter," *Canadian Conference on Electrical and Computer Engineering*, pp. 1557-1562 Vol.3, 2004.

[99] **K. Hyunbae, M. C. Harke, and R. D. Lorenz**, "Sensorless control of interior permanent-magnet machine drives with zero-phase lag position estimation," *IEEE Transactions on Industry Applications,* vol. 39, no. 6, pp. 1726-1733, (2003)

[100] **P. C. Krause, O. Wasynczuk, S. D. Sudhoff, and I. P. E. Society**, *Analysis of electric machinery and drive systems* vol. 2: IEEE press Piscataway, NJ, 2002.

[101] **L. Changsheng and M. Elbuluk**, "A sliding mode observer for sensorless control of permanent magnet synchronous motors," *Thirty-Sixth IAS Annual Meeting. Conference Record of the IEEE Industry Applications Conference, 2001.*, pp. 1273-1278 vol.2, 2001.

[102] **H. Jun and W. Bin**, "New integration algorithms for estimating motor flux over a wide speed range," *IEEE Transactions on Power Electronics,* vol. 13, no. 5, pp. 969-977, (1998)

[103] **S. Chi, Z. Zhang, and L. Xu**, "Sliding-mode sensorless control of direct-drive PM synchronous motors for washing machine applications," *IEEE Transactions on Industry Applications, ,* vol. 45, no. 2, pp. 582-590, (2009)

[104] **H. Lee and J. Lee**, "Design of iterative sliding mode observer for sensorless PMSM control," *IEEE Transactions on Control Systems Technology, ,* vol. 21, no. 4, pp. 1394-1399, (2013)

[105] **Q. Gao, G. M. Asher, M. Sumner, and P. Makys**, "Position Estimation of AC Machines Over a Wide Frequency Range Based on Space Vector PWM Excitation," *IEEE Transactions on Industry Applications,,* vol. 43, no. 4, pp. 1001-1011, (2007)

[106] **C. Silva, G. M. Asher, and M. Sumner**, "Hybrid rotor position observer for wide speed-range sensorless PM motor drives including zero speed," *IEEE Transactions on Industrial Electronics,,* vol. 53, no. 2, pp. 373-378, (2006)

[107] **N. Bianchi, S. Bolognani, J. Jang, and S. Sul**, "Comparison of PM motor structures and sensorless control techniques for zero-speed motor position detection," *IEEE Transactions on Power Electronics,* vol. 22, pp. 2466-2475, (2007)

[108] **F. Z. Peng and T. Fukao**, "Adaptive Speed Identification for Vector Control of Induction Motors without Rotational Transducers," *IEEE Transactions on Industry Applications,* vol. 28, no. 5, pp. 1054-1061, (1994)

[109] **S. Maiti and C. Chakraborty**, "An adaptive stator resistance estimation technique for sensorless permanent magnet synchronous motor drive," *International Journal of Automation and Control,* vol. 3, no. 2, pp. 189-201, (2009)

[110] **S. Maiti and C. Chakraborty**, "A new instantaneous reactive power based MRAS for sensorless induction motor drive," *Simulation Modelling Practice and Theory,* vol. 18, no. 9, pp. 1314-1326, (2010)

[111] **A. Mishra, V. Mahajan, P. Agarwal, and S. P. Srivastava**, "MRAS based estimation of speed in sensorless PMSM drive," *IEEE Fifth Power India Conference, 2012* pp. 1-5.

[112] **S. Maiti and C. Chakraborty**, "Reactive Power Based Speed Sensorless Controller for Permanent Magnet Synchronous Motor Drive," *Industrial Technology, 2006. ICIT 2006. IEEE International Conference on*, pp. 247-252, 2006.

[113] **R. Cardenas, R. Pena, J. Proboste, G. Asher, and J. Clare**, "MRAS observer for sensorless control of standalone doubly fed induction generators," *IEEE Transactions on Energy Conversion,,* vol. 20, no. 4, pp. 710-718, (2005)

[114] **Q. Gao, G. M. Asher, M. Sumner, and L. Empringham**, "Position Estimation of a Matrix-Converter-Fed AC PM Machine From Zero to High Speed Using PWM Excitation," *IEEE Transactions on Industrial Electronics,,* vol. 56, no. 6, pp. 2030-2038, (2009)

[115] **B. Bon-Ho, S. Seung-Ki, K. Jeong-Hyeck, and B. Ji-Seob**, "Implementation of sensorless vector control for super-high-speed PMSM of turbo-compressor," *Industry Applications, IEEE Transactions on,* vol. 39, no. 3, pp. 811-818, (2003)

[116] **K. Ying-Shieh, W. Ming-Shyan, and H. Chung-Chun**, "DSP-based adaptive fuzzy control for a sensorless PMSM drive," *Control and Decision Conference, 2009. CCDC '09. Chinese*, pp. 2379-2384, 2009.

[117] **X.-l. Yuan and H.-h. Wang**, "Intelligent Sensorless Control of Permanent Magnet Synchronous Motor Drive," *Intelligent Computation Technology and Automation, 2009. ICICTA '09. Second International Conference on*, pp. 454-457, 2009.

[118] **R. C. Bansal**, "Bibliography on the fuzzy set theory applications in power systems (1994-2001)," *Power Systems, IEEE Transactions on,* vol. 18, no. 4, pp. 1291-1299, (2003)

[119] **K. Hakiki, A. Meroufel, V. Cocquempot, and M. Chenafa**, "A new adaptive fuzzy vector control for permanent magnet synchronous motor drive," pp. 922-927, 2010.

[120] **Y. Jae-Sung, K. Sang-Hoon, L. Byoung-kuk, W. Chung-Yuen, and H. Jin**, "Fuzzy-Logic-Based Vector Control Scheme for Permanent-Magnet Synchronous Motors in Elevator Drive Applications," *Industrial Electronics, IEEE Transactions on,* vol. 54, no. 4, pp. 2190-2200, (2007)

[121] **S. Kai, L. Kui, and H. Lipei**, "Control strategy of PMSM drive in high speed operation for air-condition compressor," *Industrial Electronics, 2008. IECON 2008. 34th Annual Conference of IEEE*, pp. 1137-1142, 2008.

[122] **A. Consoli, F. Gennaro, V. John, and T. A. Lipo**, "Effects of the internal layout on the performance of IGBT power modules," *Brazilian Power Electronics Conference (COBEP), Iguasu, Brazil*, 1999.